Characterisation of Invadolysin, a Novel Essential Metalloprotease in *Drosophila melanogaster*

Bin Yu

A thesis submitted to the University of Edinburgh in conformity with the requirements of examination for a Ph.D.

2007

Declaration

I hereby declare that this thesis is entirely my own composition and the experimental work described within was performed entirely by me unless otherwise stated. Any contributing work by collaborators has been clearly indicated as such.

I also declare that the contents of this thesis have not been submitted for any other degree or professional qualification.

In have also included a copy of a research paper in which I am one of the authors.

Bin Yu

12th of July 2006

This thesis is gratefully dedicated to my parents Yu Bo Hai and Wu Yu Lan, to my wife Han Xu and my eight-month-old son, Yu Chao Ran for their love and support.

Acknowledgements

First of all, I would like to thank my supervisor Dr. Margarete Heck for her patience, support and guidance during the years of my Ph.D. As a medical student, I knew very little about biology at the beginning, I had received enormous help and advice on both techniques and biology knowledge from Margarete and other member of the Heck laboratory, past and present. Dr. Brian McHugh brought me to the real cell biology world during my first four months of the Ph.D. Dr. Neville Cobbe and Dr. Sharron Vass instructed my lab work hand by hand with big patience in my first year. Also, they both checked my grammar from "10 week report" to my final thesis. They kept giving me help and advice throughout my Ph.D. Marie-Louise Loupart helped me in the first year of my Ph.D. and kindly checked my first lab meeting. Dr. Ellada Savvidou, Dr. Kate Marshall, Dr. Bryce Nelson, Shubha Gururaja Rao, Ching-Wen Chang all gave me great support during my research. I was really lucky to work with them. Members of Prof. William Earnshaw's lab, Dr. Eric Schirmer's and Dr. Andreas Merdes' lab all gave me all kinds of good suggestions during my lab meetings.

I also would like to thank the School of Biology Studentship to partly support my Ph.D. financially and thank my Parents Yu Bo Hai and Wu Yu Lan to support the other part, besides the love and support they gave me from the day I was born.

The last, but definitely not the least, I should thank is my wife Han Xu for her kind company. She gave up her promising job and came to Edinburgh to help me, support me and love me during my Ph.D. What's more, thank her to bring me a son, Chao Ran Yu, at the end of my Ph.D.

Abstract

The *IX-14* mutant was first found as a mutation affecting neuroblasts and imaginal discs and later characterised as a mutant affecting chromosome condensation. Base on its sequence, IX-14 may be classified as a metalloprotease that is a homologue of leishmanolysin. IX-14 have a wide range of functions in cell cycle and cell migration, probably through its alternative spliced forms or its diverse substrates.

In this study, I have showed that *IX-14* mutants have a chromosome structure defect besides a length-wise chromosome hyper-condensation phenotype. The turnover of three nuclear envelope proteins (lamin Dm0, otefin and lamin A/C) was affected in *IX-14* mutants. One of them, lamin Dm0, has been shown to be cleaved by IX-14 *in vitro*, which suggests it is a substrate of IX-14.

I have also shown *Drosophila IX-14* mutant embryos have a germ cell migration defect, germ cells failing to form gonads at stage 13 after passing through the midgut. This was consistent with the suggestion that IX-14 might play a migration role based on the observation that IX-14 localized to the leading edge of macrophages and as invadopodia-like structures in some HeLa cells.

Due to the presence of a signal sequence at the N-terminus and a GPI anchor sequence at the C-terminus of DmIX-14, I could not purify DmIX-14 since it keeps losing its tags on both the N-terminus and the C-terminus in the baculovirus system. Methods to express large scale active IX-14 still need to be found.

Chapter 1: Introduction

1.1 Cell cycle and chromosome condensation

The cell cycle is made up of four phases. S phase refers to the period of DNA replication. Mitosis is when a somatic cell divides into two daughter cells. The two gaps between them are called the G1 and the G2 phases, which with S phase are referred to as interphase. Mitosis involves a dramatic reorganization of both the nucleus and cytoplasm brought about by activation of a number of protein kinases, including Cdk1-cyclin B and can be further divided into six phases, among which are prophase, prometaphase, metaphase, anaphase, telophase and cytokinesis. Besides cyclins and cyclin-dependent kinase, chromosome passengers, anaphase-promoting complex and polo like kinase are all contribute to the process of mitosis (Pollard and Earnshaw 2002).

People are interested in chromosome condensation since the DNA will face such catastrophes as sister-chromatid entanglement and cleavage of trailing chromatin during cytokinesis, which may result in loss of or damage to vital genes without proper condensation. At the first level of organization, two tight superhelical turns of DNA are wrapped around a histone octamer consisting of two copies each of the four histone proteins (H2A, H2B, H3 and H4), generating fibers of ~10 nm diameter. Association of histone H1 with the 10 nm fiber causes the fiber to shorten and thicken to ~30 nm in diameter, forming the so-called "30 nm" fiber, which gives the chromosome its next level of folding. However, this degree of condensation can not meet the required chromatin

structure in mitosis, higher-order levels of chromatin folding are required for mitotic chromosome. Topoisomerase II, condensin complex, AKAP95 (A Kinase-Anchoring Protein 95) and titin were reported to involved in this higer-order of chromosome condensation (Heck 1997).

1.2 Background of Invadolysin (IX-14)

The advantage of using *Drosophila melanogaster* as a model organism

Drosophila melanogaster is a fruit fly, a little insect about 3 mm long for adult, of the kind that accumulates around spoiled fruit. It is one of the most valuable organisms in biology research and has been used as a model organism for research for almost a century.

Drosophila has extensive advantages as a research model. There is a high level of conservation of genes, pathways and cellular processes between *Drosophila* and other higher metazoa. Although *Drosophila* has a lower number of genes (14,392) and a small genome (180 Mb) compared to human (23,758 genes and 3069 Mb respectively), 68% of 2746 human disease gene entries in OMIM (www.ncbi.nlm.nih.gov/entrez/query.fcgi?db=OMIM, Online Mendelian Inheritance in Man, a catalog of human genes and genetic disorders with links to literature references, sequence records, maps, and related databases) have strong matches to one or more sequences in the *Drosophila* database (Homophila, www.superfly.ucsd.edu/homophila, the human disease to *Drosophila* gene database). *Drosophila* also displays advantages in

its short life cycle (only 10 days or so), affordability and ease to keep in large numbers, simplicity of manipulating genetics, availability of its entire genome and mutant flies which have defects in any of several thousand genes. Its four relatively large and easily identifiable mitotic chromosomes are easier for studying mitosis and chromosome structure than those of yeast. In addition, many cell lines are available (mainly from *Drosophila* embryonic tissues) and the advent of techniques such as dsRNA-mediated interference facilitates the study of protein function at the level of single cells.

Drosophila melanogaster has a life cycle about 10 days (Figure 1.2A). Starting from the fertilisation of an egg, the embryo goes through 16 morphologically distinct stages until it hatches into a fist instar larva. This takes approximately 24 hours. During the first four stages, fertilized eggs go through 13 rapid and synchronous cycles of nuclear divisions consisting of only S and M phase. This is known as the syncytial divisions. These are completed within two hours. The details of the 16 embryonic stages will be introduced in Chapter 4. The first instar larva eats its way though food for 24 hours until it moults into a second instar larva. The second instar larva eats similarly and moults after 24 hours into a third instar larva. The third instar larva eats for two days and then emerges from the food medium and wanders on the vial wall until it pupates when the body is completed remodelled. Four days later, an adult fly encloses from the pupal case. Larval tissue growth occurs mostly by endo-replication and increase in cell size (e.g., in the salivary glands). Mitotic activity only occurs in tissues that will be used to form the adult fly, e.g. the brain and imaginal disc, and histoblasts.

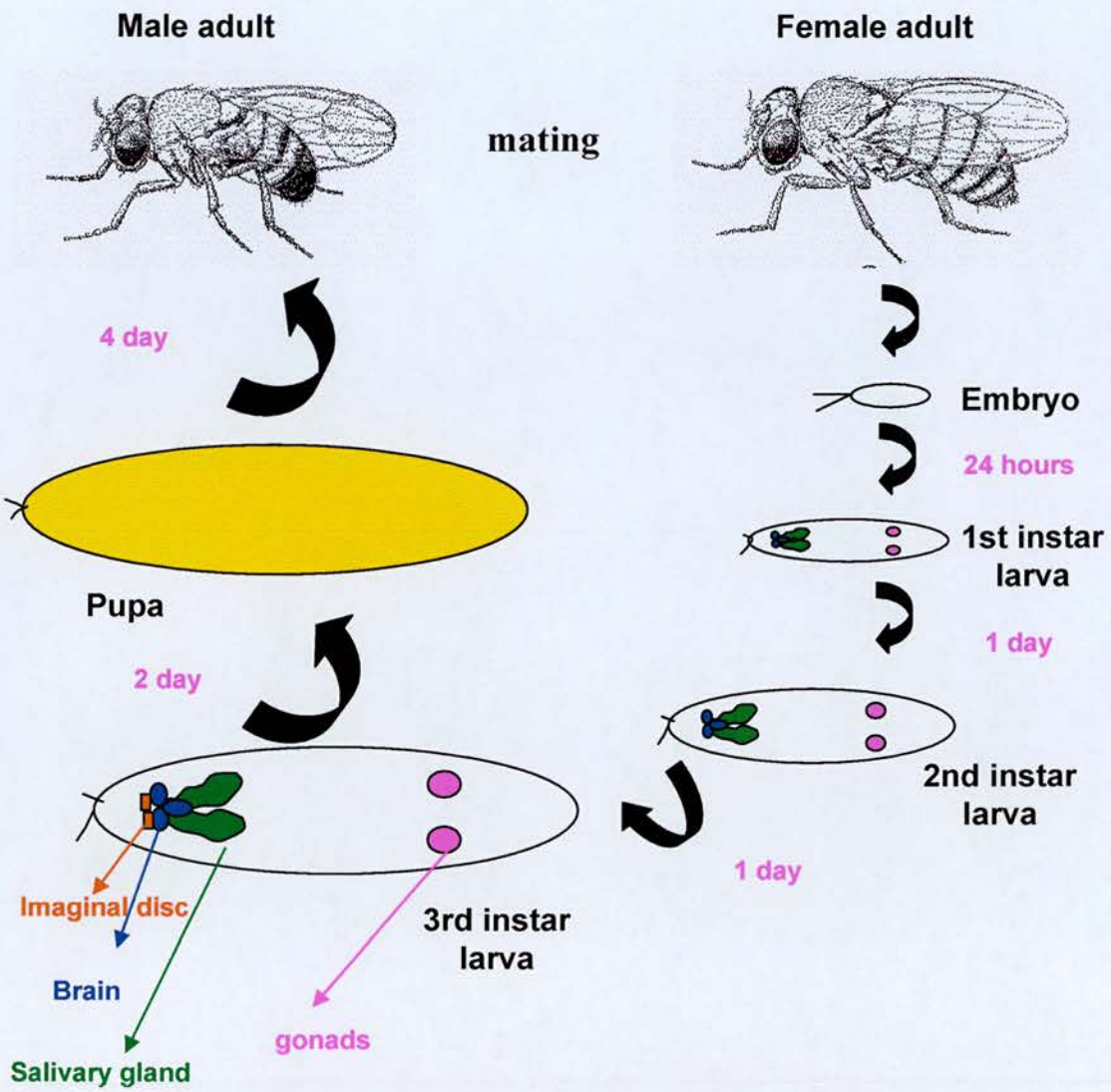

Figure 1.2A: The life cycle of *Drosophila melanogaster*.

After the *Drosophila* egg is laid, it takes approximately one day to develop and hatch into a worm-like larva. There are three larval moults at one day, two days and four days after hatching for 1st, 2nd and 3rd instar larva. The third instar larvae moult to form an immobile pupal case, inside which the body is completely remodelled. Four days later, an adult fly (male or female) encloses from the pupal case. Difference in body features help distinguish between male and female adult. Females are slightly larger and have a light-colored, pointed abdomen. The abdomen of males will be dark and blunt. The male adult also has sex combs, dark bristles on the upper portion of the forelegs.

Introduction to proteases

Proteases (peptidases) are enzymes that break peptide bonds between amino acids of proteins. They appear naturally in all organisms and constitute 1-5% of the gene content (Beynon and Bond 2001). Proteases play roles in digestion, growth, maturation, aging and death of all organisms. Proteases regulate most physiological processes by controlling the activation, synthesis and turnover of proteins. Proteases are also essential in viruses, bacteria and parasites for their replication and the spread of infectious diseases. Single amino acid changes in some proteases, over or under abundance of a particular crucial protease or abnormal levels of natural inhibitors/ activators of proteases can lead to abnormal physiology and disease. There are two groups of proteases: the endopeptidases and the exopeptidases. Endopeptidases are enzymes that split peptides and polypeptides into smaller peptides by targeting peptide bonds near the centre of the molecule while exopeptidases are enzymes that cleave di- and tri- peptides into their constituent amino acids by targeting terminal peptide bonds. Based on its catalytically active centre, proteases can also be classified as serine proteases, cysteine proteases, aspartic acid proteases, glutamic acid proteases, threonine proteases and metalloproteases. Metalloproteases bind a metal ion such as zinc or calcium in their active site. The ion usually serves to coordinate two to four side chains and it is indispensable for the activity of the enzyme. The ion itself is also coordinated by a water molecule, which is also crucial for catalytic activity.

The first MMP (matrix metalloprotease) was found 40 yeas ago, when researchers described an 'activity' that was present during metamorphosis in tadpoles and had the ability to degrade rigid rods of collagen (Gross and Lapiere 1962). This activity turned

out to be due to interstitial collagenase (MMP-1). Currently 24 members have been found in the families of human MMPs, all of which share a basic structural organization comprising a signal peptide that targets them for secretion, a propeptide domain and catalytic domain. A subfamily of MMPs associated with the cell membrane has also been identified and categorized as the membrane-type MMPs (MT-MMPs). The MT-MMPs can be divided into 2 subgroups, the transmembrane MT-MMPs and the glycosylphosphatidyl inositol (GPI)-anchored MT-MMPs (Handsley and Edwards 2005). The catalytic domain of MMPs contains a catalytic zinc, bound in the sequence HEXXHXXGXXH by three histidine residues. Glutamic acid is believed to transfer hydrogen atoms and to polarize a zinc-bound water molecule for nucleophilic attack on the scissile peptide bond of bound substrate (Stocker and Bode 1995).

The structure of MMP catalytic domains are highly similar. These consist of a five stranded β sheet and three α helices (Figure 1.2B, panel A). MMPs are normally inactive because a prodomain cysteine coordinates the zinc. Activation occurs when the prodomain is removed by proteolytic cleavage. The mechanism of replacing the cysteine with bound water has been denoted the "Cysteine switch" (Figure 1.2C) (Wasserman 2005). Tissue inhibitors of metalloproteinases (TIMPs) are endogenous MMP inhibitors produced by the same cells which produce MMPs. They act by forming a 1:1 complex with the activated catalytic zinc in MMPs (Pender and MacDonald 2004). MMPs have traditionally been thought to cleave various components of the ECM (Extra Cellular Matrix), a complex structural entity surrounding and supporting cells found within metazoan tissues. ECM is composed of three major classes of biomolecules: 1) Structural proteins: collagen and elastin, 2) Specialized proteins: fibrillin, fibronectin,

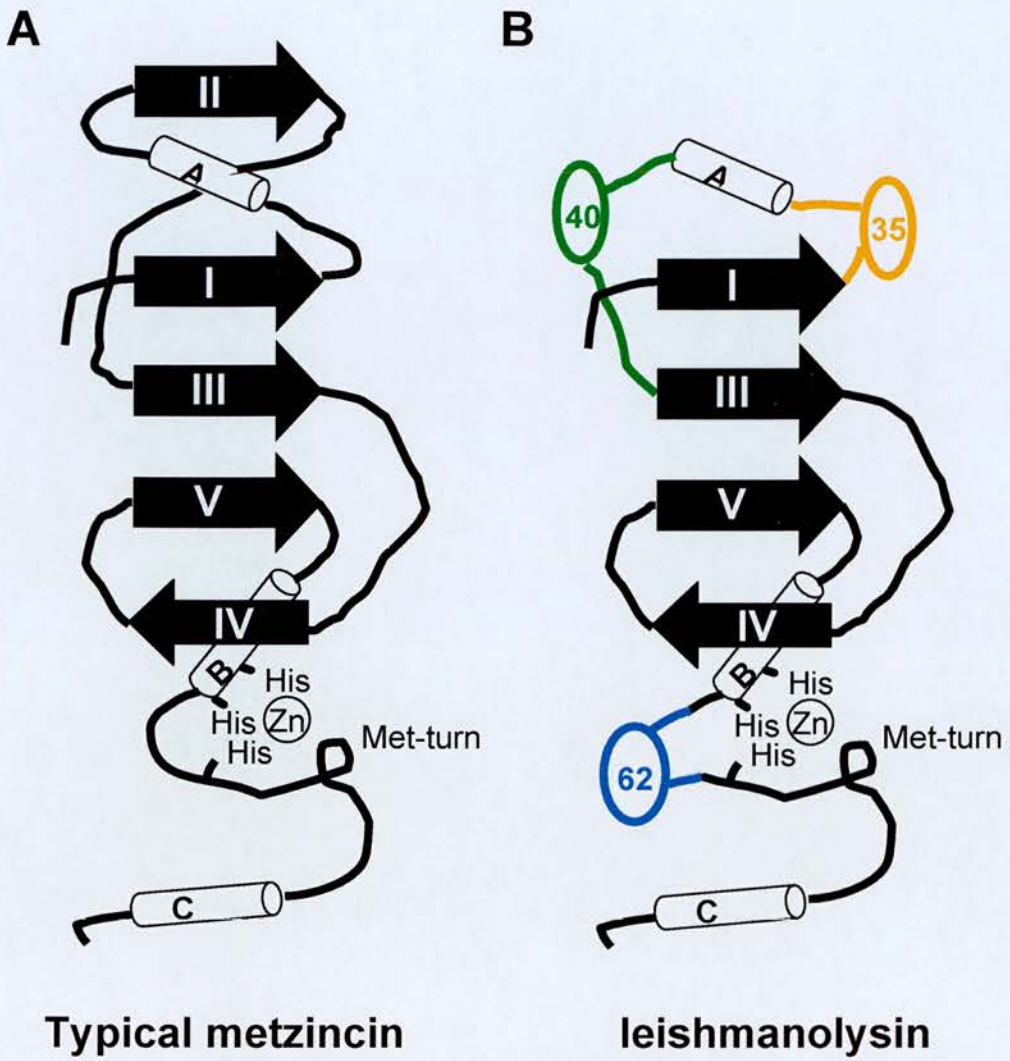

Figure 1.2B: Secondary structure of catalytic domain of typical metzincin and leishmanolysin.

A: The catalytic domain of metzincin family share conserved structure of three a helices and five stranded b sheet. Three histidines are bound to the catalytic zinc iron and a met-turn methionine follows. B: Leishmanolysin lacks the strand II b sheet and includes three insertions (coloured circles with number of inserted residues). The arrangement of three zinc binding histidine and underlying met-turn methionine are present in leishmanolysin as well. All these similarities classify leishmanolysin into metzincin class zinc protease.

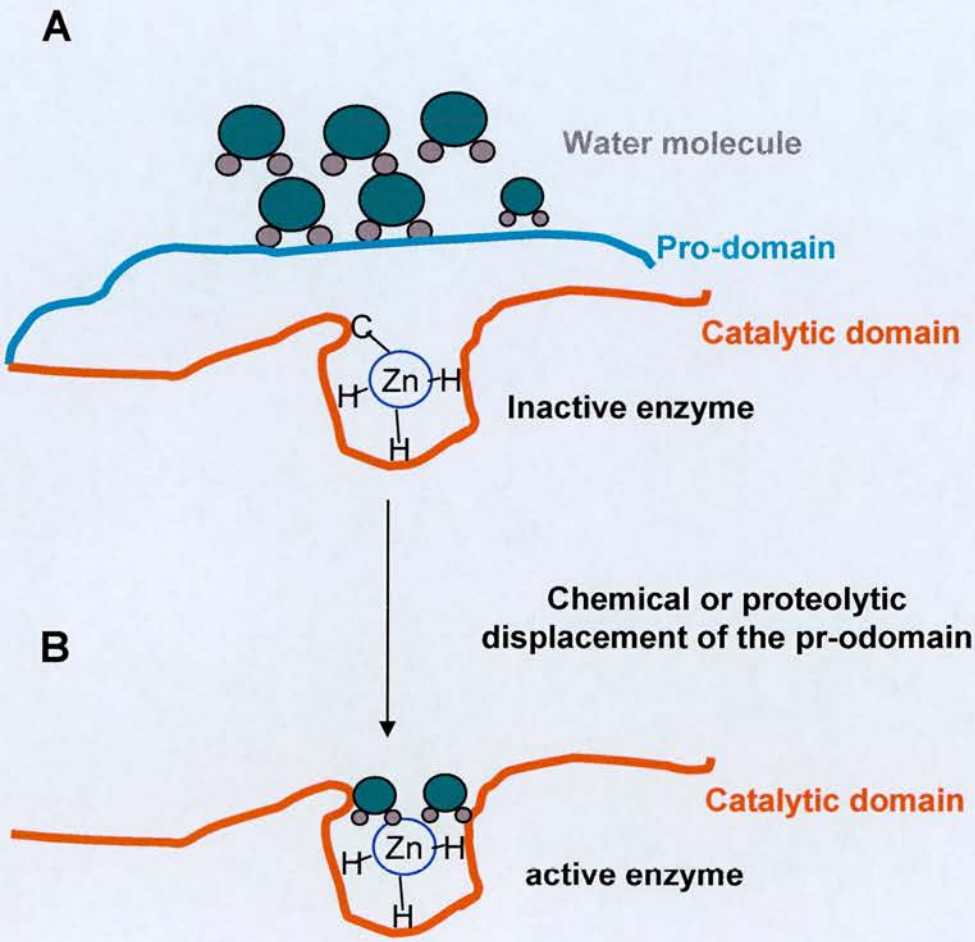

Figure 1.2C: The mechanism of Cysteine switch.

A: Zinc ion is blocked from associating with water molecule by a cysteine in pro-domain of GP63. This results in an inactive form of this protease. B: Pro-domain is removed by chemical or proteolytic factor which release the blockage of zinc ion. This make the zinc associate with water molecular and allow nucleophilic attacks to the substrate.

laminin etc, 3) proteoglycans. MMPs may be divided into subclasses according to their primary matrix substrate specificities: the collagenase (MMP-1, -8, -13, -18), the gelatinises (MMP-2 and –9), the stromelysins (MMP-3, -7, -10 and –11), elastase (MMP-12), membrane type (MMP-14, -15, -16, -17, -24, -25) and others (MMP-19, -20, -23, 26, -27 and –28) (Pender and MacDonald 2004). However, with the discovery of a number of non-matrix substrates, MMPs have also been shown to be involved in the cleavage of cell surface receptors, the release of apoptotic ligands, cell behaviors such as cell proliferation, migration, differentiation, angiogenesis, apoptosis and host defence (McCawley and Matrisian 2001). MMPs are present at low levels under normal conditions when they are responsible for normal physiological tissue turnover. However, under pathology conditions, MMPs are related to a wide range of diseases such as rheumatoid arthritis, cancer, degenerative eye disease, inflammation, bone disease, etc. (Brinckerhoff and Matrisian 2002). In *Drosophila*, two MMPs was found, Dm-MMP1 (others MMPs type in vertebrate) is expressed more specifically during embryonic stages (Llano, Pendas et al. 2000) and Dm-MMP2 (membrane bound type) apparently through out development (Llano, Adam et al. 2002). Tissue remodelling is disrupted in single Dm-MMP mutants. Larval tracheal growth and pupal head eversion defects are seen in Dm1-MMP mutants and larval tissue histolysis and epithelial fusion defects are observed during metamorphosis in Dm2-MMP mutants. Double mutants of the two *Drosophila* MMPs have shown no defects in embryonic development, larval mitosis and cell migration (Page-McCaw, Serano et al. 2003).

Leishmanolysin (GP63)

Leishmania sp. are a kind of protozoa causing leishmaniasis (black fever) in humans which is characterized by persistent fever, enlarged liver and spleen, dark and scaly skin, etc (Murray, Berman et al. 2005). Its life cycle requires a sandfly vector and a mammalian host (e.g. human). Leishmaniasis is transmitted by the bite of sandflies. The sandflies inject promastigotes into the human body during their blood meals. Promastigotes are then phagocytosed by macrophages and transform into aflagellated amastigotes. Amastigotes multiply in infected cells and affect different tissues, causing the clinical manifestations of leishmaniasis as describe above. Sandflies could be infected by ingesting macrophages containing amastigotes from a infected human during blood meal. In the sandfly's midgut, the amastigotes differentiate into promastigotes, which migrate to the proboscis of sandflies (Yao, Donelson et al. 2003). The major surface glycoprotein, leishmanolysin (GP63, derived from glycoprotein of 63 kDa), contributes to *Leishmania* sp.'s virulence and pathogenicity. It is involved in the interaction of the promastigotes with the host's macrophages and the resistance of promastigotes to be lysed by the defensive system (Russell and Wilhelm 1986). Although an unexpected 62 amino acid was inserted between the glycine and third histidine residue of the metzincin (a family of proteins share topologically similar structure, of which MMPs are also members, Figure 1.2B panel B) motif (HEXXHXXGXXH), GP63 is clearly a metzincin according to the similar arrangement of the three zinc ligand histidine side chains and the underlying met-turn methionine to metzincin class zinc proteinases (Schlagenhauf, Etges et al. 1998). However, GP63 could not be categorised within an MMP family because the 62 amino acid insertion diverts the

catalytic domain of it from that of MMPs. The protein is synthesised in the endoplasmic reticulum where the signal sequence is cleaved post-translationally and the C-terminal residues are replaced with a GPI membrane anchor structure. GP63 may be activated by means of a cysteine switch in the same manner as MMPs (Schlagenhauf, Etges et al. 1995). GP63 is also post-translationally modified by N-glycosylation which contributes to *Leishmania*'s virulence (Kink and Chang 1988). GP63 degrades many protein substrates including casein, hemoglobin, gelatin, fibrinogen and CD4 molecules on human T cells (Yao, Donelson et al. 2003).

MRP (MARCKS-related protein) was reported as a substrate for GP63, with a predominant cleavage site between Ser^{92} and Phe^{93} within ED (Effector Domain). MARCKS (Myristoylated alanine-rich C kinase substrate) and MRP are major protein kinase C substrates expressed in diverse cell types, including macrophages. They are implicated in coordination of membrane-cytoskeletal signalling events, such as cell adhesion, migration, secretion, and phagocytosis in a variety of cell types. A highly basic sequence in MRP or MARCKS known as ED binds with high affinity to actin, calmodulin and acidic phopholipids. The ED also contains the serine residues that are subject to PKC-dependent phosphorylation. PKC-dependent phosphorylation of ED serine residues prevented MRP degradation by GP63 in a cell-free assay (Corradin, Ransijn et al. 1999; Ramsden 2000; Sundaram, Cook et al. 2004).

Background of IX-14 (Invadolysin)

l(3)IX-14^{1} is a late larval lethal mutation that was generated by abdominal injection of the acridine compound ICR-170 (which preferentially cause frame-shift mutations),

when Shearn and Garen searched for mutants affecting the imaginal discs (which contain the cells that will form the epidermal structures such as the legs and wings of the adult fly during pupation) of *Drosophila* (Shearn, Rice et al. 1971). It was subsequently characterised not as a developmental defect, but as a mutation affecting chromosome condensation (Gatti and Baker 1989). The protein, IX-14, was latter named invadolysin by the Heck laboratory to take into account leishmanolysin and invadopodia.

Further work on the *l(3)IX-14^{1}* mutation was initiated by Sue Ann Kruase, a former Ph.D. student in the Heck laboratory who was able to generate a P element insertion allele of *l(3)IX-14^{1}* by local hopping of a nearby P element. This allele was termed *l(3)IX-14^{4Y7}*. Both *l(3)IX-14^{1}* and *l(3)IX-14^{4Y7}* have defects in mitotic and polytene chromosome architecture. In third instar *l(3)IX-14^{1}* mutant neuroblasts, metaphase chromosomes are hypercondensed in length and some loosely condensed chromatin was found surrounding the hypercondensed chromosomes. In salivary glands from third instar *l(3)IX-14^{1}* mutant, polytene chromosomes lose the distinctive banding pattern along the chromosome arms and the chromosome arms seem to be twisted and frayed instead. The chromocenter which contains the clustered centromeres of the endoreduplicated chromosomes could not be distinguished in the *l(3)IX-14^{1}* mutant polytene chromosomes. *l(3)IX-14^{1}* heterozygous flies also have redder eyes in a PEV (position effect variagation) assay compared to the control w^{m4} allele. Thus *l(3)IX-14^{1}* acts as a Suppressor of Variagation (Su(var)) which indicates an effect on gene expression, possibly through chromatin structure.

l(3)IX-14^{1} also shows spindle and centrosome abnormalities. The spindle defects include monopolar spindles, asymmetric bipolar spindles and completely disorganised

spindles. It was not surprising then to see the checkpoint component BubR1 on the mitotic chromosomes of this mutant because of the aberrant mitotic spindles attachment has never been assessed (Hoyt, Totis et al. 1991). In addition, most mutant mitotic cells have only one centrosome, or dumbbell-shaped centrosomes which suggested replicated, but unseparated centrosomes, close to one another.

l(3)IX-14^{1} also has replication defects, as shown by low levels of BrdU incorporation which suggest the cell cycle was blocked or delayed earlier than mitosis. There is no anaphase observed in *l(3)IX-14*^{1} and more cells entered to apoptosis, as indicated by TUNEL (Terminal deoxynucleotidyl transferase biotin-dUTP Nick End Labeling) staining.

The *l(3)IX-14*^{1} allele was mapped to the 85E10-F16 region by crossing to deficiency lines with known breakpoints. The responsible gene was identified by inverse PCR cloning of DNA flanking the *l(3)IX-14*^{4Y7} allele P element. A 3.6 kb cDNA was identified in *Drosophila* adult head library EST. The *Drosophila IX-14* gene has 9 exons, spread over 15 kb of genomic DNA with the first intron about 9 kb. It contains an ORF of 2052 nucleotides encoding a protein of 683 amino acids. The insertion site of the P element was 40 base pairs upstream of the start of transcription (Figure 1.2D, panelA). In human, there are at least two splice variants that have been found while only one has been found in *Drosophila* so far. Some conserved motifs were found in the homologous sequences. Besides the HEXXH catalytic motif, there is a signal sequence in the N-terminus of 2 human variants and the *Drosophila* IX-14 which targets proteins to the ER (endoplasmic reticulum) through docking with the signal recognition particle. In addition, there is a C-terminal GPI (Glycosylphosphatidylinisotol) anchor recognised site

that helps to insert proteins in the plasma membrane. The sequence also have some destruction motifs (D-box and KEN box) which direct protein turnover by ubiquitin. Invadolysin also have SUMO-ylation signal just upstream the HEXXH motife (Figure 1.2D, panel B). There are fours variants of Invadolysin exist in human. HsINV variant 1 and 1Δ37 differ from variant 2 and 2Δ37 in their longer N-terminal regions. Variant 1 and 2 differ from variant 1Δ37 and 2Δ37 in the presence (variant 1 and 2) or absence (variant 1Δ37 and 2Δ37) of a 37 amino acid (aa) insertion that was encoded by a separate exon. As a result, variant 2 and 2Δ37 would not target to ER nor become GPI anchored to the membrane. Variant 1 EST was appeared in testis and brain while the variant 1Δ37 EST was appear in embryonic stem cells, colon and melanoma. Variant 2 EST was appear in testis and placenta. There was no EST found for variant 2Δ37, but there are expected size band for it shown in RT-PCR on HeLa cells done by Dr. Neville Cobbe. The IX-14 gene has homologues in *Homo sapiens, Mus musculus, Caenorhabditis elegans, Oryza sativa, Arabidopsis thaliana, Dictyostelium discoideum* and *Leishmania* (leishmanolysin, also called GP63), which share a HEXXH catalytic motif, and surprisingly 14 conserved cysteines (Figure 1.2E, panel A). Nine region of sequence were shared among higher eukaryotic orthologues but absent in leishmanolysin/gp63. These map to the surface of the leishmanolysin structure and may likely mediate interactions with substrates, regulators, or binding other partners and could potentially be used for tagging and antigen for antibody injection (Figure 1.2E, panel B). Based on its sequence homology to the active motif of GP63, the protein that the *IX-14* gene encodes was identified as a novel zinc-metalloprotease whose substrates are still

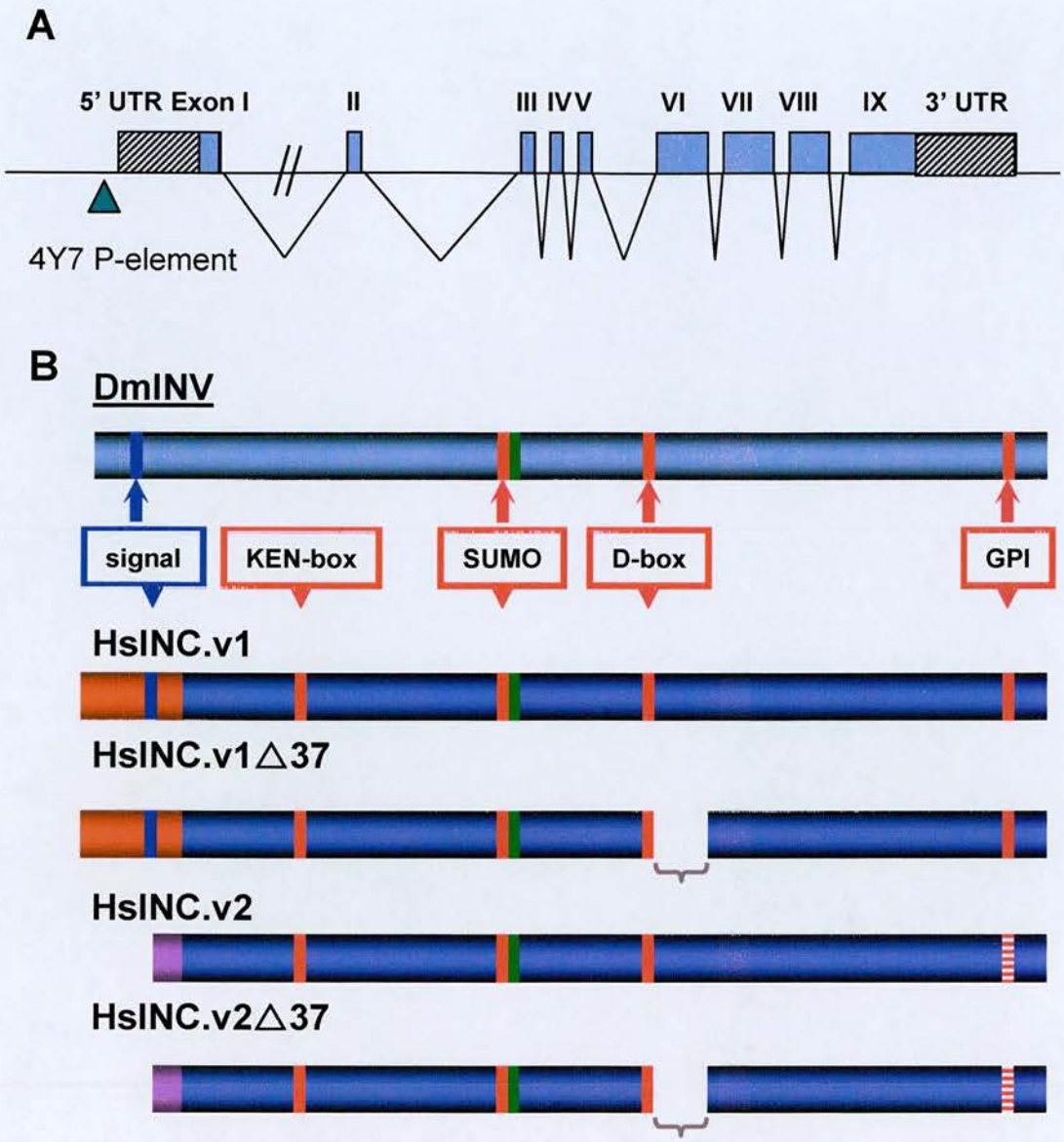

Figure 1.2D: *Drosophila invadolysin* gene and invadolysin variants in *Drosophila* and human.

A: *DmINV* cDNA has 9 exons and the P-element insertion is 40 bp upstream of the starting point of transcription in the 4Y7 allele. The first intron is 8.6kb and not shown to scale. B: DmINV has only one variant while four splice variants of Invadolyisn have been found in human. They share some common motifs like signal sequences in N-terminal region, GPI anchor site near the C-terminus, an HEXXH catalytic motif, SUMO-ylation signal, KEN-Box and D-Box. In human, variant 1 and v1△37 contains the signal sequence which was missing in v2 and v2△37. V1△37 and v2△37 miss a 37 amino acid insertion which is encoded by a separate exon compare to v1 and v2 sequentially.

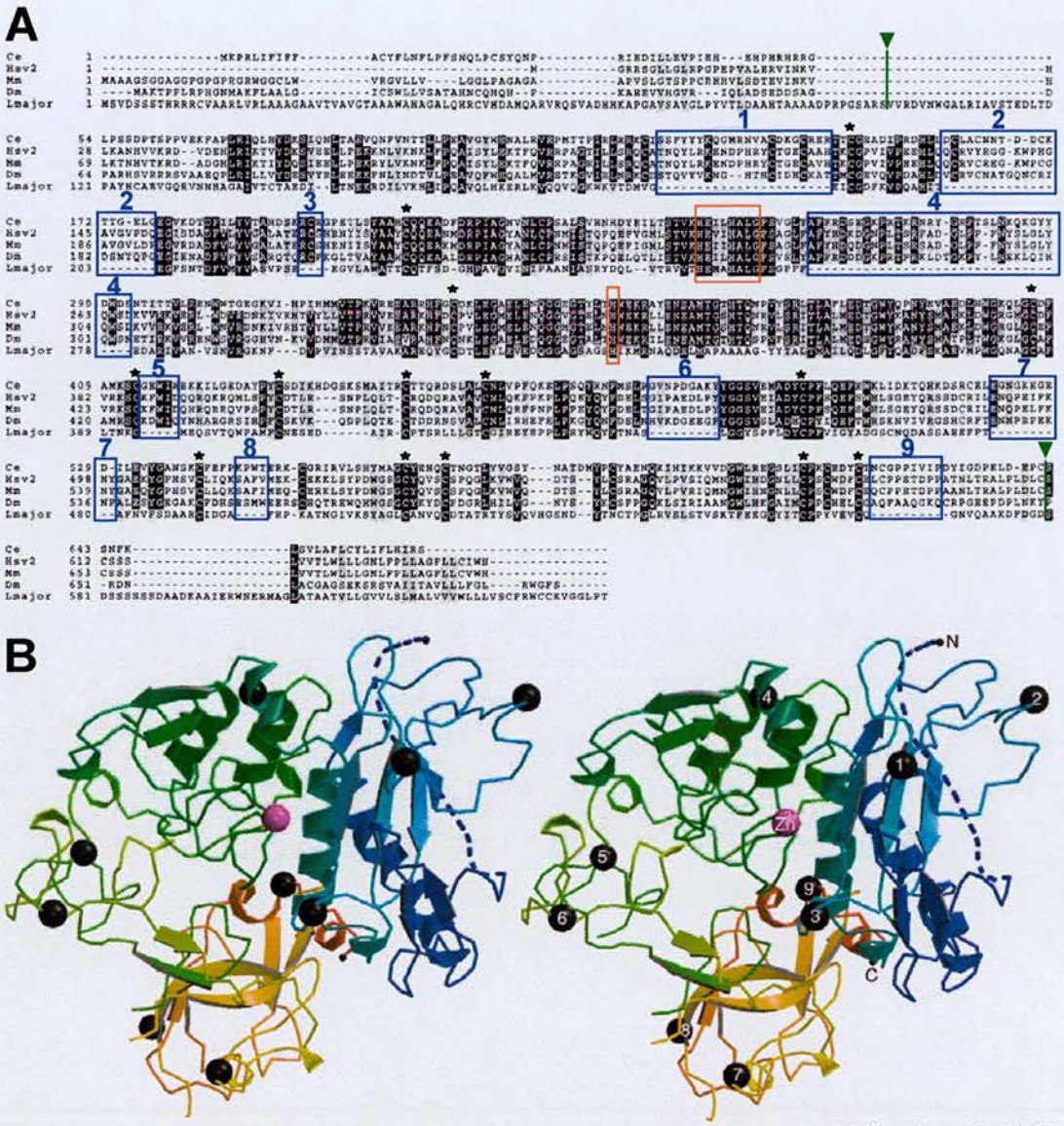

Figure 1.2E: Homologues of invadolysin and structure of leishmanolysin.

A: T-COFFEE alignment showing homologues of invadolysin conserved between *Caenorhabditis elegans* (Ce), *Homo sapiens* variant 2 (HsV2), *Mus musculus* (Mm), *Drosophila melanogaster* (Dm) and *Leishmania major* (Lmajor) with the conserved HEXXHXXG (and third required H) zinc-metalloprotease motif (red box). Although the homology between leishmanolysin and the other proteins appears to be largely limited to regions surrounding the metalloprotease motif, the placement of 14 cysteines (asterisks) is strikingly conserved. Nine regions (insertions relative to leishmanolysin) shared among the higher eukaryotic orthologues (absent from leishmanolysin) are indicated by blue boxes with the numbers above them. The green line and triangles delimit the region of the leishmanolysin protein that is shown in B. B: Stereo pair of the three-dimentional structure of leishmanolysin. The black numbered spheres represent the insertions that map to the surface of the leishmanolysin structure. The internal magenta sphere represents the zinc ion required for catalysis.

unknown. Although the appearance of the common sequence of HEXXH is conserved between MMPs, the IX-14 productor GP63, does not seems to belong to MMPs base on its distinct catalytic domain. The Heck laboratory is currently using bioinformatics way to ascertain relationship between MMPs and IX-14.

Three lines of evidence indicate that mutation of *IX-14* is responsible for the cellular phenotypes observed in *IX-14* mutant flies. 1) An expected 3.6 kb mRNA was absent in the two alleles of Invadolysin homozygous mutants, *l(3) IX-14*^{1} and *l(3) IX-14*^{4Y7}, but was present in wild type and heterozygous extracts of the two alleles (larval extracts in all case). 2) The phenotype of *IX-14* RNAi in *Drosophila* S2 cells, are similar to that of the two *IX-14* mutant alleles with regard to centrosome and spindle morphology. 3) A proteolytic activity was missing in *l(3)IX-14*^{1} larval brains which is consistent with the assumption that IX-14 was a protease based on its sequence (McHugh, Krause et al. 2004). The band which was missed in homozygous mutant could be certified as IX-14 by in gel proteolysis followed by mass spectrometry. IX-14 has a cytoplasmic localisation pattern in both *Drosophila* S2 cells and human HeLa cells (Figure 1.2F, panel A and B). Strikingly, HsIX-14 shows a distinct ring-like structure in the cytoplasm of HeLa cells. These ring-like structures are not specific to HeLa cells as they are also observed in Jurkat (T cell derived) and CF-PAC cells (pancreas carcinoma cell line). However the ring-like structures are specific to interphase cells since they seem to be dispersed in mitosis. These structures resemble invadopodia, in which a protrusion of 200-nm-wide and up to 3-μm-long extends into the extracellulas matrix. Invadopodia is an actin rich structure that contain actin associate protein (WASp, Arp2/3 etc), MMPs (MMP2, MMP9, MT-MMP1 etc), adhesion molecules (Integrin etc), signal protein (RhoA etc)

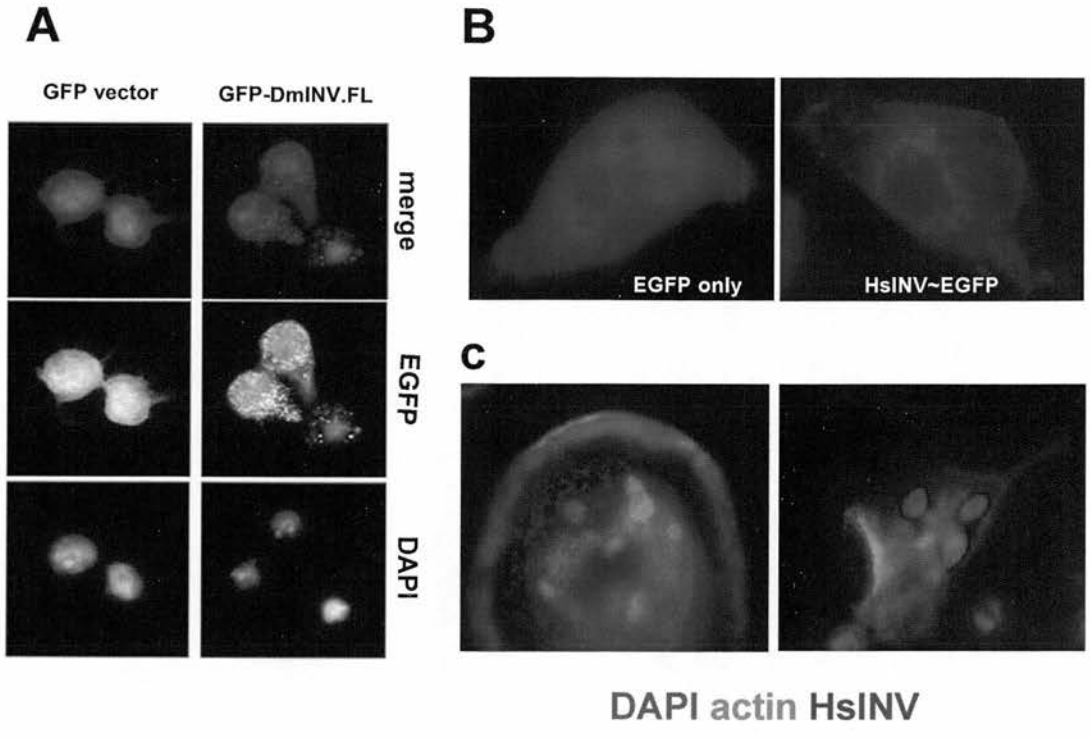

Figure 1.2F: Localisation of invadolysin in human and *Drosophila* cells.

A: GFP-DmINV was localized to the cytoplasm of *Drosophila* S2 cells compared to the whole cell localization of GFP alone. B: HsINV-EGFP was localized to the cytoplasm in HeLa cells and shown as distinct ring-like structures compared to the whole cell localization of EGFP vector. C: HsINV showed the punctate staining in the cytoplasm of stationary macrophages but was localised to the leading edge of migrating macrophages.

(Gimona and Buccione 2006). These are prominent in invasive cells and function in degrading the ECM (Baldassarre, Pompeo et al. 2003). Like invadopodia, the ring-like structures containing Invadolysin are localized to the lower third of the cell close to the substratum. Invadolysin staining on stationary macrophage cells was performed and a punctate staining in the cytoplasm was observed. Surprisingly, all the Invadolysin localized to the leading edge of migrating macrophages which suggest a role for Invadolysin in cell migration (Figure 1.2F, panel C).

l(3)IX-14^{1} neuroblasts have abnormally high levels of lamin Dm_O, a nuclear envelope protein, during mitosis (McHugh, Krause et al. 2004). Therefore, lamin is a good candidate substrate for Invadolysin, based on its accumulation in *IX-14* mutant brains. Beside its proteolysis by caspase during apoptosis, *Drosophila* lamin has not reported to be proteolysed by any other protein or at any stage in the cell cycle. Thus invadolysin might shed new light on *Drosophila* lamin turnover. More details about nuclear envelope proteins will be introduced in Chapter 3. Interestingly, the mouse Zmpste24 metalloprotease plays an important role in the processing of prelamin A (Pendas, Zhou et al. 2002). There is no Zmpste24 homologe in *Drosophila* has been identified, so it is possible that invadolysin process lamin Dm0 in a different way. Moreover, there is growing evidence that lamins are implicated in DNA replication, chromatin organization, regulation of transcription and cell division (Wilson and Zastrow 2001). Invadolysin mutants have similar defects. Given the mitotic phenotype, it is also plausible that molecules important for chromosome condensation or spindle assembly may be substrates of Invadolysin.

In Drosophila, 27 proteins were reported as potential interactors of Invadolysin through a genome-wide yeast two-hybrid screen (Giot, Bader et al. 2003). Among these, CG6268 (mask) and CG4719 are annotated as structural constituents of the cytoskeleton, which might indicate links to the observed spindle defects of the Invadolysin mutant and forming the invadopodia structure in human cell lines. CG12789 and CG3212 are involved in a defence response which might provide a link to the observed leading edge localization of Invadolysin in macrophages. Thus there are many potential interactors which may play a role in Invadolysin localization or activity in mitotic and cell migration. It was at this point that I began my Ph.D. in the Heck laboratory with the aim of further characterising the role of this novel, essential metalloprotease and discerning potential substrates of Invadolysin.

Chapter 2 Materials and Methods

2.1 Abbreviations

BrdU	Bromodeoxyuridine
BSA	Bovine Serum Albumin
C-terminus	Carboxyl terminus
CLAP	Chymostatin, Leupeptin, Antipain, Pepstatin A
DAPI	4', 6-diamidino-2-phenylindole
DTT	Dithiothreitol
dsRNA	Double stranded RNA
EBR	Ephrussi Beadle Ringer's Solution
E. coli	*Escherichia coli*
ECL	Enhanced Chemiluminescence
EDTA	Ethylenediaminetetraacetic acid
EGTA	Ethyleneglycol-bis-(aminoethylether)-tetraacetic acid
EM	Electron Microscopy
EST	Expressed Sequenced Tag
FBS	Fetal Bovine Serum
GFP	Green Fluorescent Protein
HEPES	N-(2-hydroxyethyl) piperazine-N'-(2-ethanesulfonic acide)
HPR	Horseradish Peroxidase

IPTG	Isopropyl-β-D-thiogalactopyranoside
LB	Luria-Bertrani broth
N-terminus	Amino terminus
OD	Optical Density
ORF	Open Reading Frame
PAGE	Polyacrylamide Gel Eletrophoresis
PBS	Phosphate Buffered Saline
PCR	Polymerase Chain Reaction
P-H3	Phosphorylated Histone H3
PMSF	Phenyl Methyl Sulfonyl Fluoride
PFA	Paraformaldehyde
RT-PCR	Reverse Transcriptase- Polymerase Chain Reaction
SDS	Sodium Dodecyl Sulfate
SMC	Structure maintenance of Chromosomes
TAE	Tris acetate buffer with EDTA
TBE	Tris borate buffer with EDTA
TE	Tris buffer with EDTA
UAS	Upstream Activating Sequence
UTR	Untranslated Region
UV	Ultraviolet

2.2 Materials

Drosophila melanogaster stocks

Strain	Source
Canton S	Bloomington Stock Center
l(3)IX-14^{1}/TM6B (Antp^{Hu} e^{1} Tb^{1})	(Chemical induction) M. Gatti, Rome
l(3)IX-14^{4Y7}/TM6B (Antp^{Hu} e^{1} Tb^{1})	(P-element insertion) S.A.Krause Heck Laboratory
L(3)IX-14^{1}/TM3, KrGFP (y1 w; D* gl3/TM3, P{GAL4-Kr.C}DC2, P{UAS-GFP.S65T}DC10, Sb1)*	Bin Yu, Heck laboratory
l(3)IX-14^{4Y7}/TM3 (y1 w; D* gl3/TM3, P{GAL4-Kr.C}DC2, P{UAS-GFP.S65T}DC10, Sb1)*	Bin Yu Heck laboratory
D/TM3, Kr-GFP (y1 w; D* gl3/TM3, P{GAL4-Kr.C}DC2, P{UAS-GFP.S65T}DC10, Sb1)*	Bloomington stock center

Bacterial strains

Escherichia coli XL1 Blue (Stratagene)

RecA endA1 gyrA96 thi-1 hsdR17 supE44 relA1 lac [F'proAB lacIqZDM15 Tn10]

Escherichia coli BL21 (Stratagene)

B F' dcm opm T hsdS (r_8^- m_8^-) gal

Escherichia coli MAX Efficiency DH10Bac™ (Invitrogen)

F⁻ *mcr*A Δ(*mrr-hsd*RMS-*mcr*BC) Φ80lacΔZM15 Δ*lac*X74 *rec*A1 *end*A1 *ara*D139 Δ (*ara, leu*)7697 *gal*U *gal*K λ⁻ *rps*L *nup*G /pMON14272 / pMON7124

Escherichia coli TOP10 (Invitrogen)

F⁻ *mcr*A Δ(*mrr-hsd*RMS-*mcr*BC) Φ80lacΔZM15 Δ*lac*X74 *rec*A1 araD139Δ(ara-leu) 7697 galU galK rpsL (Str^R) endA1 nupG

Pichia pastoris

KM71H

AOX1::ARG4 arg4

Common reagents and buffers

Ampicillin (Sigma)

Stock at 50 mg/ml in 50% EtOH. Used at 50 μg/ml.

Aprotinin

Stock at 1.7 mg/ml in 0.9% NaCl and 0.9% benzyl alcohol. Used at 1.7 μg/ml. (Sigma-Aldrich)

BSA

Bovine Serum Albumin, 30% Stock solution (Sigma).

BMG medium

100 mM potassium phosphate, pH 6.0, 1.34% YNB. Store at 4°C for no more than two months.

BMGY medium

1% yeast extract, 2% peptone, 100 mM potassium phosphate pH 6.0, 1.34% YNB, 4 x 10^{-5}% biotin, 1% glycerol. Store at 4 °C for no more than two months.

BMM medium

100 mM potassium phosphate, pH 6.0, 1.34% YNB, 4 x 10^{-5}% biotin, 0.5% methanol. Store at 4°C for no more than two months.

BMMY medium

1% yeast extract, 2% peptone, 100 mM potassium phosphate, pH 6.0, 1.34% YNB, 4 x 10^{-5}% biotin, 0.5% methanol. Store at 4°C for no more than two months.

CLAP

1 mg/ml chymostatin, 1 mg/ml leupeptin, 1 mg/ml antipain, 1 mg/ml pepstatin A (Sigma) in DMSO. Used at 1-10 μg/ml.

Coomassie Brilliant Blue stain

0.5% Coomassie Blue (Sigma) in 100% methanol.

Coomassie Blue stain diluent

35% methanol, 14% acetic acid.

Coomassie Blue fast destain

35% methanol, 10% acetic acid.

Coomassie Blue slow destain

10% methanol, 7% acetic acid.

Cytoskeletal Buffer

137 mM NaCl, 5 mM KCl, 1.1 mM $NaHPO_4$, 0.4 mM KH_2PO_4, 2 mM $MgCl_2$, 2 mM EGTA, 5.5 mM Glucose, 5 mM PIPES, pH 6.1.

10X Dulbecco's Phosphate Buffered Saline (PBS)

1.37 M NaCl, 26.8 mM KCl, 14.7 mM KH_2PO_4, 64.6 mM Na_2HPO_4, pH 7.4.

DAPI

4',6-diamidino-2-phenylindole (Sigma), Stock at 1 mg/ml in dH_2O at –20°C. Used at 0.1 µl/ml.

DMSO

Dimethyl sulphoxide (Sigma).

DTT

Stock at 1M dithiothreitol in dH_2O at –20 °C (Fisher).

EDTA

Ethylenediaminetetraacetic acid. 0.5M solution in dH_2O, pH 8.0.

EGTA

Ethylene glyco-bis (β–amino-ethylether)-N,N,N',N'-tetraacetic acid. 0.25 mM in dH_2O, pH 6.8.

10X Ephrussi-Beadle Ringers solution (EBR)

1.3 M NaCl, 47 mM KCl, 19 mM $CaCl_2$, 100 mM HEPES, pH 6.9.

Ethidium Bromide (EtBr)

Stock at 10 mg/ml in dH_2O. Used at 350 ng/ml.

Gentamicin (Sigma)

Stock at 10 mg/ml in dH_2O. Used at 7 μg/ml.

IPTG

Isopropyl β–D-thiogalactopyranoside. 1M solution in dH_2O.

Kanamycin (Sigma)

Stock at 10 mg/ml in dH_2O. Used at 50 μg/ml.

Laemmli Upper Gel (stacking) Buffer

0.5 M Trizma base, pH 6.8 with HCl.

Laemmli Lower Gel (resolving) Buffer

1.5 M Trizma base, pH 8.8 with HCl.

Laemmli Gel Running Buffer

25 mM Trizma base, 192 mM Glycine, 1% SDS

Luria-Bertani Broth (LB)

1% Bacto tryptone, 0.5% Bacto yeast extract, 1%NaCl, pH 7.4.

5X Loading Dye for DNA run on agarose gels

17.5% Ficoll 400, 100 mM EDTA pH 8.0, 2.5% SDS, 0.25% Bromophenol Blue.

20X MOPS SDS Running Buffer

1 M 3-(N-morpholino) propane sulphonic acid, 1 M Tris base, 2% SDS, 20.5 mM EDTA, pH 7.7.

Mowiol Mounting Solution

10% Mowiol (Calbiochem) , 20% Glycerol in PBS

PBSTx

Dulbecco's PBS with 0.1% TritonX-100

PBSTw

Dulbecco's PBS with 0.1% Tween-20.

PFA

16% paraformaldehyde ampules (TAAB).

3X Protein Sample Buffer

6% SDS, 150 mM Tris pH 6.8, 30% glycerol, 0.03% Bromo-phenol Blue, 6 mM EDTA.

Ponceau S

0.2% Ponceau S in 3% TCA

Phenol/$CHCl_3$/IAA

Phenol : Chloroform : Isoamyl Alcohol (25:24:1), 10 mM Tris pH 8.0, 1 mM EDTA.

SDS

Sodium Dodecyl Sulphate. Stock normally at 20% solution in H_2O.

SOB

2% Bacto-tryptone, 0.5% Bacto-yeast extract, 8.6 mM NaCl, 50 mM $MgCl_2$, 2.5 mM KCl, pH 7.0.

SOC

SOB with 20 mM Glucose.

Stripping solution

100mM β–mercaptoethanol, 2% SDS, 62.5 mM Tris, pH 6.7.

1X TAE

40 mM Tris-acetate, 1 mM EDTA pH 8.0.

1X TBE

45 mM Tris-borate, 1 mM EDTA, pH 8.0.

1X TE

10 mM Tris-HCl, 1 mM EDTA, pH 7.6.

Tetracycline (Sigma)

Stock at 5mg/ml in dH_2O. Used at 10 μg/ml.

Towbin Transfer Buffer

25 mM Tris (Sigma), 20% methanol, 250 mM Glycine (Sigma-Aldrich), 0.1% SDS.

1X Tris Buffered Saline (TBS)

137 mM NaCl, 20 mM Tris-HCl, pH 7.6.

X-Gal

5-Bromo-4-Chloro-3-Indolyl a-D-Galactopyranoside (Sigma-Aldrich). Stock at 2%. Used at 100 μg/ml.

YNB

Yeast Nitrogen Base powder with ammonium Sulfate without amino acid, stock at 13.4% in dH_2O. Store at 4°C for less than one year.

YPDA Medium

20 g/L Difco peptone, 10 g/L Yeast extract, dextrose (glucose) to 2%, pH 6.5.

Zeocin (Invitrogen)

Stock at 100 mg/ml in dH_2O. Used at 25 μg/ml.

2.3 Methods

Making Electroporation-Competent Cells

2 ml of appropriate bacterium culture (e.g. DH5α, BL21, XL-1 Blue) was grown with shaking at 37°C in SOB magnesium free medium overnight. 0.5 ml of the culture was then diluted into two 2 litre flasks containing 250 ml SOB each and grown at 37°C to an OD at 600 nm of 0.8. The flasks were then immediately chilled on ice for 15 to 30 minutes. From then on, all subsequent steps were kept cold, and all resuspension were performed gently. Cells were harvested by centrifugation in sterile, chilled bottles for 15 minutes at 2500 rpm in a Beckman JLA10.500 rotor at 4°C. For each 250 ml culture, supernatant was removed as much as possible, and cells were resuspended in 250 ml sterile ice cold 10% Glycerol in distilled water. The ruspended culture was centrifuged again at 2500 rpm for 15 minutes at 4°C, and the supernatant was subsequently removed. Each pellet derived from the original 250 ml SOB was resuspended in 2.25 ml 10% Glycerol and 200 µl aliquots were snap frozen in 500 µl microfuge tubes by placing them in liquid nitrogen. The cells were then stored at –80°C.

Electroporation Transformation into *E. coli*

Aliquot(s) of electroporation competent cells were removed from -80 °C and thawed on ice. Meanwhile, 1.5 ml Eppendorf tube(s) and 0.2 cm electroporation cuvette(s) (Invitrogen) were also placed on ice. In each 1.5 ml tube, 80 µl of competent cells were

mixed with the appropriate amount of DNA. The mixture was added into a cuvette by tapping so that the sample can go to the bottom, and then eletroporated at the following conditions: resistance set at 200 Ohms, capacitance set at 25 μFD and volts set at 2.5 kV on a BioRad eletroporator. After the electroration, 1 ml of SOC medium was immediately added to each cuvette. The mixture were then transferred back to the 1.5 ml tube and incubated at 37°C for 30-60 minutes. Dilution were plated on agar plates containing the appropriate antibiotic.

Plasmid DNA extraction

For small scale extraction of plasmid DNA, 3 ml of *E. coli* culture were grown overnight at 37°C with shaking, 2 ml of which were used for plasmid DNA extraction using the UltraClean™ Plasmid miniprep kit from MoBio or Qiaprep miniprep kit from Qiagen under manufacturer's instructions and the rest were used for making a frozen glycerol stock. Larger scale extractions were performed using Qiagen midiPrep kit (up to 50 ml) or Qiagen MaxiPrep kit (up to 500ml) under manufacturer's instructions.

Restriction digestion of DNA

In general, restriction digests were performed in 0.5 ml Eppendorf tube, using enzymes from New England Biolabs or Promega with the 10X reaction buffer provide with the enzyme. Digests were normally performed in the 37 °C incubator for 2-3 hours (20 hours for some PCR product when only several bp were present adjacent to

restriction enzyme recognized site). If required, the restriction enzyme was then inactivated by placing the tube at 65°C for 20 minutes.

Ligations

All ligations were performed using T4 DNA ligase from Promega or New England Biolabs with the appropriate reaction buffer at 16-18°C for overnight. Whenever possible, an insert : vector molar ratio of 3:1, 1:1 and 1:3 were all used.

Agarose gel electrophoresis

Unless otherwise stated, all agarose gels were made up at 1% of either Seakem LE Agarose (Flowgen) or High Gel Strength Agarose (Melford) containing 0.3 μg/ml ethidium bromide. Then gel was electrophoresed in electrophoresis tanks in 1X TBE or TAE depend on the buffer composition of the gel. Different gel sizes were used according to the number of samples or the degree of separation required and run under different conditions. Gel size: mini (50 ml agarose, run at 100V), midi (100ml agarose, run at 150V) or maxi (300 ml agarose, run at 150V).

Purification of DNA from agarose gels

Electrophoresis was performed in 1.2% low-melt gel (MacroSieve low melting temperature agarose, Flowgen) in TAE containing 0.3 μg/ml ethidium bromide (run in TAE buffer). Desired bands were excised under UV illumination using a glass coverslip

and placed into 1.5 ml Eppendorf tubes. DNA was purified from the agarose gel by using the Perfectprep Gel Cleanup Kit (Eppendorf) or Qiaquick Gel Extraction kit (Qiagen) under manufacturer's instructions.

PCR Amplification of Plasmid DNA

Most PCR reactions were performed by using either *Pfu* (Promega) or Expand High Fidelity DNA polymerase (Roche).

For products smaller than 2 kb, PCR reactions were usually performed using *Pfu* DNA polymerase under the following conditions:

10X *Pfu* DNA polymerase buffer with $MgSO_4$	5 µl
dNTPs (2.5 mM each)	4 µl
primer mix (100 µM each)	2 µl
$MgSO_4$ (25 mM)	0-4 µl
Pfu DNA polymerase (2-3 U/µl)	0.5-1 µl
DNA template (50-200 ng)	Variable
Sterile deionised water	up to 50 µl (final volume)

PCR reactions were performed in a Biometra Personal Cycler or a Biometra Gradient Cycler, according to the following protocol:

Initial Denaturation	95°C	2 minutes
{Denaturation cycle	95 °C	30 seconds

Annealing cycle	55-65°C	30-60 seconds	30-35 cycles
Extension cycle	74 °C	2-5 minutes}	
Final Extension	74 °C	5 minutes	
Hold	4 °C		

For products larger than 2 kb, PCR reactions were usually performed using Expand High Fidelity DNA polymerase under the following conditions:

10X Expand High Fidelity PCR System Buffer 2	5 µl
dNTP (2.5 mM)	4 µl
primer mix (100 µM each)	2 µl
Expand High Fidelity DNA polymerase	1 µl
DNA template (50-200 ng)	variable
$MgSO_4$ (25 mM)	0-4 µl
Sterile deionised water	up to 50 µl

PCR reactions were performed in a Biometra Personal Cycler or a Biometra Gradient Cycler, according to the following protocol:

Initial Denaturation	95 °C	2 minutes	
{Denaturation Cycle	95 °C	30 seconds	
Annealing Cycle	55-65 °C	30-60 seconds	30-35 cycles
Extension Cycle	68 °C	2-5 minutes}	
Final Extension	68 °C	7 minutes	
Hold	4 °C		

DNA purification from PCR reactions

DNA products from PCR reactions were usually purified by using the UltraClean™ PCR Clean-up DNA purification Kit (MoBio laboratory) under manufacturer's instructions.

Sequencing of plasmid DNA

Sequencing reactions were performed using 250-500 ng of template DNA, 3.2 pmol of the appropriate primer, and 4 µl of Big Dye terminator cycle sequencing kit version 3.1 (Perkin Elmer, Applied Biosystem). The mixture was then brought up to 20 µl with dH_2O and the reaction allowed to proceed in a Biometra Personal Cycler or Biometra Gradient Cycler according to the following protocol:

95 °C	5 minutes	
{95 °C	30 seconds	
55 °C	15 seconds	25 cycles
60 °C	4 minutes}	
Hold	15 °C	

The reactions were then transferred to 0.2 ml PCR strip tubes and taken to the ICMB sequencing facility for loading on to an ABI prism sequencer.

RT-PCR of total RNA isolated from whole flies

Total RNA from whole flies was kindly provided by Ellada Savvidou. Reactions were performed using Access RT-PCR system (Promega) under the following conditions:

Nuclease-free water	31.5 μl
AMV/*Tfl* 5 X Reaction buffer	10 μl
DNTP mix (10 mM each)	1 μl
Primer mix (50 mM each)	2 μl
$MgSO_4$ (25 mM)	2 μl
AMV reverse transcriptase (5 U/μl)	1 μl
Tfl DNA Polymerase (5 U/μl)	1 μl
RNA template	1.5 μl

The reactions were performed in a Biometra Personal Cycler or a Biometra Gradient Cycler according to the following protocol:

first strand DNA synthesis:

Reverse transcription	48°C	45 minutes	
AMV RT inactivation	94 °C	2 mintutes	

Second strand synthesis and PCR amplification:

{Denaturation	94 °C	30 seconds	
Annealing	60 °C	1 minute	40 cycles
Extension	68 °C	2 minutes}	
Final extension	68 °C	7 minutes	
Hold	4 °C		

10 μl of each reaction was analysed by 1% agarose gel electrophoresis.

Preparation of Concanavalin A-treated coverslips

12 coverslips (22 x 22 mm/1.5 thick, VWR) were put into a small ceramic cradle in order to best expose surfaces. Coverslips were washed twice in deionised water for 15 minutes each time before being incubated in 0.5 M HCl for 30 minutes. Coverslips were then washed twice again in deionised water for 15 minutes each time before being placed in absolute ethanol for 30 minutes. Excess ethanol was drained off and individual coverslips were dipped in Concanavalin A solution (0.5 mg/ml in dH_2O) for 30 seconds. Finally coverslips were dried on clean blotting paper and sterilised for 1h by UV irradiation prior to use.

Preparation Poly-L-lysine treated slides

Microcope slides (76 x 26 mm/ 1.0 mm thick, Berliner Glass KG) were washed overnight in deionised water containing diluted detergent, Decon (1:10 in deionised water). Then the slides were rinsed with dH_2O several times until no bubbles could be seen, before being washed with 95% ethanol for 3 hours and rinsed with dH_2O again. Next, slides were incubated in 0.1% poly-L-lysine solution (Sigma-Aldrich) for 45 minutes. Finally, slides were rinsed with dH_2O and dried.

Cell Culture

Drosophila S2 cells were maintained in serum free Schenider's Insect Medium (Sigma, S1046) with 10% Insect qualified Fetal Bovine Serum (Gibco). Cells were grown at 27°C in a humidified atmosphere (Hera Cell, Heraeus) and were passed at 1:10 dilution every 5 days.

SF9 cells (derived from the parental *Spodoptera frugiperda* IPLB-Sf-21-AE cells) were maintained in serum free SF-900 II medium (Gibco). Cells were grown at 27°C in a humidified incubator (Hera Cell, Heraeus) and were maintained by passing the culture at 1:10 dilution every 5 days.

High Five cells (derived from the parental *Trichopulsia ni* cell line) were maintained in serum free Express Five SFM medium (Gibco). Cells were grown at 27 °C in a humidified incubator (Hera Cell, Heraeus) and were maintained by passing the culture at 1:20 dilution every 3 days.

HeLa cells were grown in RPMI medium (GibcoBRL) +10% Fetal Bovine Serum (Gibco) under normal conditions (37°C and 5% CO_2) in a humidified incubator (Hera Cell, Heraeus). They were passed at 1:10 every 2 days. In brief, after the medium was aspirated, cells were washed with 5 ml PBS which was in turn aspirated before allowing cells to stand in 0.1% trypsin in PBS for 5 minutes. When the cells were seen rounding up under microscope, cells were detached from the bottom surface by banging on the side of the flask. 10 ml of RPMI+10% FBS was added to the cells before they were diluted into new flasks containing up to 30 ml RPMI + 10% serum.

Preparation of Cultured Cell protein Extracts

Cells (S2, SF9, High Five, HeLa,) were centrifuged at 300g for 5 minutes and washed with PBS with protease inhibitors (1 μg/ml CLAP, 1 μM/ml PMSF, 1.7 μg/ml aprotinin). The volume of PBS was used according to the confluence of cells for easy counting (start from 0.5 ml if large amount was applied, otherwise it is difficult to completely resuspended the cell clumps). Cells were then counted using a hematocytometer before being centrifuged again at 300g for 5 minutes. The pellet was resuspended at a specific concentration (normally 5 $x10^4$ cells/μl for SF9, S2 and High Five cells, 10^4 cells/μl for HeLa cells) in sample buffer (3X Sample buffer 1/3; DTT 5%; aprotinin, CLAP, PMSF 1% each; PBS up to 100%). Finally, cells were lysed by sonication and boiled at 100°C for 5-10 minutes before being stored at –20°C or loaded directly on a polyacrylamide gel for electrophoresis.

Preparation of Larval brain protein extracts

Third instar larval brains were dissected under the microscope in 1X EBR. 10 wild type brains or 30 *IX-14* mutant brains were lysed in 100 μl of EBR lysis buffer (1X EBR + 10 mM EDTA + 10 mM DTT + 1.7 μg/ml aprotinin, 1 mg/ml CLAP and 1 μM/ml PMSF) using portable sonicator. 50 μl of 3X Sample Buffer and 10 μl of DTT were added to the extracts before the extracts were boiled at 100°C for 5 minutes. The extracts were then directly loaded on a polyacrylamide gel or stored at –20°C.

TCA precipitation

In order to concentrate protein samples, 100% trichloroacetic acid (TCA) was applied to a final concentration of 10%, precipitating on ice for at least 30 minutes. Samples were then centrifuged for 15 minutes at 13,000 rpm in a bench centrifuge (Heraeus Instruments) at 4°C. Supernatant was aspirated with a drawn Pasteur pipette, and the pellet was resuspended by sonicating in 1 ml of wash buffer (70% Acetone, 20% Ethanol, 10 mM Tris, PH 7.4, 0.0015% bromophenol blue). The solution was centrifuged at 13,000 rpm for 10 minutes at 4°C. The pellet was washed a second time again by sonicating in 1 ml of above wash buffer and centrifuged again in the same conditions. Finally, the pellet was resuspend by sonicating in the desired volume of 1X SDS-PAGE sample buffer containing DTT. Samples were boiled for 5 minutes before loading on a gel or freezing at -20 °C.

SDS-PAGE of Protein

Two types of gel were used for protein electrophoresis: Hoeffer 'Vertical Slab Gel unit' rigs for large gels (16 cm x 18 cm/1-0.75 mm or 1-1.5 mm thick), or small NuPAGE pre-cast gels (10 cm x 10 cm/1.0 mm or 1.5 mm) (Invitrogen). The Novex pre-cast gels were used according to manufacturer's instructions and electrophoresed in 1X MOPS Running Buffer at 200 volts while the large gel were prepared as follows:

Two glass plates (16 cm x 18 cm) were washed with dH_2O, Decon (diluted 1:5 in dH_2O), dH_2O again, and finally rinsed with 70% ethanol before wiping with a paper towel to dry. Washed glass plates were separted by 2 spacers, one at either end, and then

clamped together with one end sealed with parafilm. The clamped plates were placed on the gel apparatus and the resolving (lower) acrylamide gel was poured in between the glass plates from the top first, followed by the stacking (upper) gel. The following table describe the amounts of each in a varied of final acrylamide percentages:

Resolving (lower) gel:

Recipes for 1-1.5 mm thick gel (Bold text), or 1-0.75 mm thick gel. The lower buffer consists of 1.5 M trizma-base, PH 8.8. Acrylamide refers to a stock of 30% acrylamide: 0.8 Bis-acrylamide (Severn Biotech Ltd). AMPS is a 10% stock of ammonium Persulphate in dH_2O (Sigma).

Gel percentage	7.5%		10%		12.5%	
Lower buffer	**10 ml**	5 ml	**10 ml**	5 ml	**10 ml**	5ml
Acrylamide	**10 ml**	5 ml	**13.3 ml**	6.65 ml	**18.3 ml**	9.17 m
20% SDS	**200 µl**	100 µl	**200 µl**	100 µl	**200 µl**	100 µl
0.5 M EDTA	**80 µl**	40 µl	**80 µl**	40 µl	**80 µl**	40 µl
dH_2O	**19.72 ml**	9.86 m	**16.42 ml**	8.21 ml	**11.39 ml**	5.69 m
10% AMPS	**400 µl**	200 µl	**400 µl**	200 µl	**400 µl**	200 µl
TEMED	**40 µl**	20 µl	**40 µl**	20 µl	**40 µl**	20 µl

After pouring the resolving gel, butanol saturated with 0.25 X lower buffer was layered over the top in order to create a sharp interface between resolving and stacking gels. Resolving gels were allowed to polymerise for 15 to 20 minutes at room temperature.

The butanol layer was then poured off, washed with dH_2O, and the stacking gel poured on top.

Stacking (upper) gel:

All stacking gels were made up in 10 ml containing:

Upper buffer	2.5 ml
Acrylamide	1.33 ml
20% SDS	50 µl
0.5 M EDTA	20 µl
UREA to 8 M	4.8 g
dH_2O	up to 10 ml
10% AMPS	100 µl
TEMED	10 µl

A plastic comb was placed at the top of the stacking gel to form the wells, and the gel was then allowed to polymerise for 15 minutes at room temperature. The polymerised gel slab was then fixed in position in the buffer tank, and 1X Laemmli Gel Running Buffer was poured into the upper and lower chambers. Protein samples were boiled for 5 minutes before they were loaded into the wells using a Hamilton syringe. 30 µl of a molecular weight marker (SeeBlue Plus 2, Invitrogen) were loaded in wells as needed. Gels were electrophoresed at 55 V overnight at room temperature.

Transfer of SDS-PAGE gels onto nitrocellulose membrane

After electrophoresis, SDS-PAGE gels were transferred to Protran nitrocellulose membrane (Schleicher and Schuell) for immunoblotting. Prior to setting up for transfer, 4 L of Towbin transfer buffer was prepared (3200 ml of dH_2O, 800 ml of methanol, 12.1 g of Sigma 7-9 Tris base, 57.7 g Sigma-Aldrich glycine). From the 4 litre Towin Buffer, 1 litre was decanted for soaking the Protran membrane and 15 ml 20% SDS were then added to give a final concentration of 0.1% SDS.

The blot was then set-up within a cassette in blotting tank (BioRad) in the following order:

(**negative pole**)-Sponge-Whatman Blotting paper-gel-nitrocellulose-Whatman Blotting paper-sponge-(**positive pole**). Blotting was performed at 400 mA for 3.5 hours at 4°C. After transfer, the membrane was rinsed with dH_2O and stained with Ponceau-S (0.2% Ponceau-S in 3% trichloroacetic acid) for 5-10 minutes at room temperature with shaking. The membrane was rinsed with dH_2O with shaking and the position of the molecular weight markers were marked unambiguously with a needle. The membrane was stored at 4°C or washed once with PBSTw and used immediately for immunoblotting.

Immunoblotting

After protein extracts were transferred onto nitrocellulose membranes, membranes were blocked in PBSTw with 5% skimmed milk powder (Sainsbury) for 1 hour at room temperature or overnight at 4°C. After washing 3 times for 10 minutes in PBSTw, the

membranes were incubated with primary antibody in PBSTw or PBSTw with 0.5% milk for 1 hour at room temperature or overnight at 4°C. After washing 6 times for 5 minutes each in PBSTw, the membranes were incubated in horseradish peroxidase-linked (HRP) sencondary antibody for 1 hour at room temperature. Finally, membranes were washed 3 times for 10 minutes each again in PBSTw before processing for detection by incubation in 10 ml enhanced chemiluminescence solution (ECL, Amersham Biosciences) for exactly 1 minutes. The nitrocellulose was then exposed to Kodak XAR-5 film for autoradiography. Films were developed using a Kodak SRX-101A developer.

Stripping of probed nitrocellulose membrane

Membranes were first washed twice with PBSTx for 15 minutes each time and then incubated in Stripping Solution for 30 minutes at 65°C. After that, membranes were rinsed twice for 10 minutes each time with PBSTw and then incubated at 4 °C overnight with PBSTw before blocking and probing with another antibody.

Coomassie Brilliant Blue staining of polyacrylamide gels

After protein extracts were resolved by electrophoresis, the gels were stained with Coomassie Brilliant Blue (0.5% in methanol) diluted 1:5 in Coomassie Blue stain diluent solution for 1 hour at room temperature. The gels were then destained with Fast Destain solution for 1 hour at room temperature. Finally the gels were destained further with Slow Destain solution. The gel was then placed between two cellophanes (IDEA scientific company) which were clamped together using a plastic square box making sure

that no bubbles were present. The gel was placed in a fan incubator (BioRad) to dry for three hours.

Silver staining of gels

After protein extracts resolved by electrophoresis, the gel was fixed 2 x 15 minutes in 100 ml 30% EtOH, 10% acetic acid. In order to reduce the background, the gel was washed in 100 ml 30% EtOH with 0.1 g $Na_2S_2O_3$ (0.01% final concentration), and 2.5 ml 4M sodium acetate (0.1 M final concentration, pH 6.8) for 30 minutes. The gel was washed thoroughly with water until the pH was above 5 (3 x 10 minutes wash was usually sufficient) before it was incubated in 100 ml 0.1 g silver nitrate (0.1% final concentration) ($AgNO_3$), 25 µl formaldehyde (0.01% final concentration) (CH_2O) for 30 minutes. The gel was then quickly washed with water to remove loose silver ions before being developed by 2.5g sodium carbonate (Na_2CO_3), 50 µl formaldehyde (0.02% final concentration) (CH_2O) in 100 ml dH_2O until desired intensity. To stop the reaction, 100 ml 1% acetic acid was added to the gel. Gels were washed in water before storage.

Immunofluorescence on *Drosophila* S2 cells

S2 cells were grown on poly-L-lysine treated cover slips. Cells were fixed in 4% paraformaldehyde dilute from 16% in ampoule (TAAB) in Cytoskeletal Buffer plus 0.5% TritonX-100 for 10 minutes at room temperature, then rinsed in 1X PBS plus 0.1% TrionX-100 (PBSTx). Cells were then blocked in PBSTx plus 3% BSA for one hour at room temperature, followed by 3 x 5 minute washes in PBSTx. Primary and secondary

antibody incubation was carried out in PBSTx plus 0.3% BSA for one hour at room temperature, followed by 3 x 5 minute washes in PBSTx. The DNA was counterstained with 0.1 μg/ml DAPI in the second last wash. The coverslips were mounted onto slides with Mowiol (Calbiochem).

Immunofluorescence staining of larval brains

This protocol has been adapted from Bonaccorsi *et al* (2000) and is recommended for analysis of mitotic spindles in *Drosophila* neuroblasts.

Third instar larvae were collected from vials and washed in EBR in a dissecting dish to remove excess food. Individual larvae were transferred to a new well containing EBR and brains were dissected under a dissecting microscope. Dissected brains were placed into a new well containing EBR until ready, but never for more than 10 minutes. Brains were then fixed in 4% paraformadehyde diluted from 16% in ampoule (PFA) in PBS for 30 minutes at room temperature in a dissecting dish. Then the brains were transferred to a new well containing 45% acetic acid (in dH_2O) for 3 minutes, then transferred to a drop of 60% acetic acid (in dH_2O) on a siliconised coverslip and squashed gently onto a poly-L-lysine slide. The slide was flash-frozen in liquid nitrogen and the coverslip was removed with a razor after breathing on the slide to warm it. The slide was placed in a coplin jar with pre-chilled 100% ethanol at –20°C for 10 minutes. The brains were then permeabilised in PBSTx for 10 minutes at room temperature, washed 2 x 5 minutes in PBS, blocked in PBS + 3% BSA for 1 hour at room temperature. After blocking, the slide was washed for 5 minutes in PBSTx and then incubated overnight at 4°C in the primary antibody diluted in PBS+0.3% BSA. The slide was washed 6 times for 5

minutes each in PBSTx and the appropriate secondary antibody diluted in PBS+0.3% BSA was applied for 1-2 hours at room temperature. The slide was then washed 6 x 5 minutes in PBSTx. The brains were also stained with DAPI (0.1 μg/ml) that was included in the second last wash. Slides were finally drained and mounted in Mowiol, allowing 30 minutes for the Mowiol to set before examining by fluorescence microscopy.

Immunostaining for cyclin B in larval brains

This protocol has been adapted from Loupart *et al* (2000) and is recommended for detection of cyclin B.

In brief, brains were dissected without imaginal discs in 1X EBR, swollen hypotonically for 3 minutes in 0.25X EBR, fixed for 5 minutes in PFA/HOAc/TX (4% paraformaldehyde, 10%acetic acid, 0.1% triton X-100, 0.16X EBR), during which time they were flattened onto polylysine-treated slides under siliconized coverslips. The coverslip was flicked off after breathing in liquid nitrogen as described before. After that the slide was immediately washed for 2 minutes in PBS, permeablized 3 x 10 minutes in PBSTx, blocked in PBS+3% BSA for 1 hour at room temperature, washed for 5 minutes in PBSTx. Primary and secondary antibody incubations and washes were performed as described above.

BrdU incorporation in *Drosophila* neuroblast

BrdU was weight out 50mg and added in 500mg in instant *Drosophila* food (Sigma), rehydrated with 1ml dH_2O+1 drop of food colouring, for a final BrdU concentration of 50

mg/ml. Larvae with food were selected after being fed for 1 hour. However, since the mutant larvae are dying, they tend not to eat food, therefore brains were dissected into fresh Schneider's medium (no FBS), before incubation in BrdU solution at 12 μg/ml in Schneider's medium for 2 hours.

To co-stain for lamin and BrdU, lamin detection was performed according to the steps of 'Immunostaining for cyclin B' except that DAPI was omitted. After anti-lamin detection was complete, slides were post-fixed immediately in 4% PFA in PBS for 1 hour at room temperature, washed for 5 minutes in PBSTx and then incubated for 15 minutes in freshly prepared 2N HCl. After 2 x 5 minute washed in PBSTx, slides were incubated with rat anti-BrdU antibody (1:2 dilution, Harlan Sera Lab) in PBS + 0.3% BSA at 4 °C overnight. After 3 x 5 minute washes, the slides were incubated with Alexa 488 goat anti-rat conjugate (1:500 dilution, Molecular Probes) in PBSTx + 0.3% BSA for 1.5 hours at room temperature. Finally slides were washed 6 x 5 minute in PBSTx including counter-stain with 0.1 μg/ml DAPI at the second last wash. Coverslips were mounted onto slides with Mowiol.

Mitotic Arrest by Colchicine and DAPI staining of *Drosophila* neuroblast squashes

Third instar larvae brains were dissected in 1X EBR and incubated in colchicine for 1 hour at 2 mg/ml in Schneider's medium. Brains were transferred to 0.25X EBR for 3 minutes to hypotonically swell the cells, and then fixed in a drop of 45% acetic acid on a siliconised coverslip for 3 minutes. After that brains were squashed onto a poly-Lysine

slide before flicking off the coverslip in liquid nitrogen as described before. Slides were rinsed in PBS and transferred to PBSTx containing 100 ng/ml of DAPI for 5 minutes. Finally, the slides were washed 5 minutes in PBSTx before mounting in 35 µl of Mowiol in glycerol.

Immunofluorescence of HeLa cells

Cells were seeded on round coverslips (13 mm in diameter)in 6-well dishes and grown under normal conditions using RPMI. The next day, coverslips were fixed in fresh 4% PFA in 1X PBS for 3 minutes, the PFA was rinsed off with PBS for 2 minutes, permeabilised in 0.5% Triton X-100 in PBS for 3 minutes, washed 2 x 3 minutes in PBSTx and blocked in 3% BSA in PBS at room temperature for 1 hour. After the coverslips were washed 5 minutes in PBSTx, the primary antibody incubation was performed at the appropriate dilution in PBS + 0.3% BSA at 4°C overnight. Then the coverslips were washed 3 x 5 minutes in PBSTx before the secondary antibody was applied at the appropriate dilution in 0.3% BSA, PBS at 37°C for 1 hour. Finally the coverslips were washed 4 x 5 minutes in PBSTx (including DAPI at 0.1 µg/ml in the second last wash) and the coverslips were mounted on slides in Vectashield (Vector Laboratories) while the edges were sealed with nail varnish.

Drosophila handling

Flies were cultured in bottles or vials contaning "Dundee" maize medium which was prepared by media staff of Wellcome trust Centre for Cell Biology) using 14 litre of

water, 150 g of agar, 1100 g of glucose, 620 g of brewer's yeast, 1000 g maize, 80 g of dried live yeast, 38 g of nipagin (p-hydroxy benzoic acid methyl ester) mixed with 380 ml of absolute alcohol and 45 ml of propionic acid. Files were passed every two week at room temperature or every month at 18 °C as stock.

Immunofluorescence on *Drosophila* Embryos

Flies were fed yeast paste for 2 days before transfer to a collection cage containing grape concentrate agar plate with a dollop of thick yeast paste in the center. The cage was left undisturbed for the desired laying period at room temperature (22°C) before the agar plate was exchanged. Embryos were rinsed with water and transferred using a large paintbrush into a microsieve. The embryos were rinsed with water in the microsieeve to remove yeast paste and then dechorionated in a freshly prepared 50% hypoclorite bleach solution in dH_2O for 4 minutes with gentle agitation. Bleach was removed by rinsing with dH_2O. Embryos were then transferred to a scintillation vial containing 4.5 ml of PBS. 1.25 ml of 37% formaldehyde (BDH) and 5 ml of Heptane were added into the scintillation vial where embryos were floating between two phases of liquid. The vial was shaken at room temperature on a shaker for 20 minutes. The lower formaldehyde phase was removed after shaking without disturbing embryos and replaced with 10 ml of methanol to remove the vitelline membrane. The vial was shaken vigorously and left to stand upright for one minute. The devitellinised embryos, which had sedimented to the bottom, were removed and transferred into a 1.5 ml Eppendorf tube. The embryos were washed 5 times with fresh methanol with mixing to remove any remaining formaldehyde

or heptane. Fixed embryos were stored in methanol at –20°C until required for immunofluorescent.

For immunofluorescence, fixed embryos were rehydrated by performing five minute washes in a series of methanol solutions as follows:

100% methanol

90% methanol/10% PBSTx (1X PBS + 0.05% Triton-X 100)

75% methanol/25% PBSTx

50% methanol/50% PBSTx

25% methanol/75% PBSTx

100% PBSTx

Non specific binding of antibody to embryos were blocked by incubating in 1% BSA in PBS for one hour with rotation. Excess BSA in PBS was removed by rinsing the embryos in PBSTX with rotation 4 times for 15 minutes each. Embryos were then incubated in primary antibody overnight at 4°C (e.g. VASA antibody 1:500 diluted in PBSTx). Embryos were washed four times with PBSTx (15 minutes each) before incubation for 2 hours at room temperature in the desired secondary antibody at a dilution of 1:500 in PBSTx. After incubation, embryos were washed 4 times with PBSTx, 15 minutes each, including 0.1 μg/ml DAPI in the second last wash. Finally embryos were transferred to a glass slide and mounted with Vectashield under a coverslip while the edges were sealed by nail varnish.

Microscopy

All slides were examined with an Olympus Provis microsope, equipped with epifluorescence optics. Images were captured with an Orca II CCD camera (Hamamatsu) and Smart-capture 2 software (Digital Scientific). All images were processed using Adobe Photoshop software.

In vitro proteolysis of lamin by invadolysin

375 ng of lamin in T7-7 vector, DmIX-14 in pOT2 vector, or GFP control vector were added to one 24-μl aliquot of the RTS 500 *Escherichia coli* Circular Template kit (Roche). Each expression aliquot was incubated in a water bath at 30°C for 1 hour. 10 μl of synthesized DmIX-14 was mixed with 1 or 4 μl of lamin Dm_O or GFP before being incubated in a water bath at either 29°C or 37 °C for 15 minutes, 50 minutes or 1 hour. In some cases, the incubation was with $ZnCl_2$ or $ZnSO_4$, or the zinc chelator 1,10-phenanthroline. After the reaction, samples were boiled at 100°C for 5 minutes in SDS-PAGE sample buffer. Lamin was detected after transfer to nitrocelluose and probing with monoclonal antibody using an mAB gernerated to the *Drosophila* NH_2-terminal head region (amino acids 22-28) (Paul Fisher, SUNY Stong Brook).

Purification of DmIX-14 recombinant C-terminal fragment

125 ng of PRSET vector (His tag at N-terminal) containing DmIX-14 C-terminal fragment (amino acid 401-683) was transfected into 80 μl of BL21 cells. Colonies were grew overnight on LB agar plate and selected by ampicillin resistant. BL21 cells

containing this construct were grown to an OD600 of 0.5 before induction with 0.1 mM IPTG for 3 h at 37°C. Cells were harvested by centrifugation at 2000 x g for 30 minutes at 4°C. Pellets were washed once with 10 ml of TEN and once with 5 ml Bugbuster reagent (Novagen) /g cells containing 1 µl Benzonase/ml. Supernatants were incubated for 20 minutes at room temperature with shaking before centrifugation at 16,000 x g of 20 minutes at 4 °C. Pellets were resuspended at the same volume of Bugbuster reagent as used previously with 20 mg/ml lysozyme and incubated for 5 minutes at room temperature. 6 volumes of 1:10 diluted BugBuster reagent were added to the suspension and vortexed for 1 minute. The pellet was centrifuged at 16,000 x g as above and washed with 1/2 the original volume of 1:10 diluted BugBuster for 6 times. Pellets were resuspended in Ni-NTA Binding buffer (50 mM NaH_2PO_4 pH 8.0, 300 mM NaCl, 10 mM imidazole) containing Ni-NTA His-Bind Resin at 4 ml lysate per 1 ml Resin. The mixture were incubated at 4°C for 1 hour before loading onto a Poly-Prep Chromatography columns (BioRad), then washed with 2 x 4 ml Ni-NTA washing buffer (50 mM NaH_2PO_4 pH 8.0, 300 mM NaCl, 20 mM imidazole). Finally, the protein was eluted with 4 x 0.5 ml 0.1 mM MOPS, pH 7.5.

Binding of C-terminal fragment of DmIX-14 to Affigel

0.5 ml of each Bio-Rad affi-gel 10 and 15 beads were washed twice in 10 ml cold dH_2O before centrifugation at 600 x g at 4°C and resuspended in 10 ml cold dH_2O again. Beads were centrifuged and resuspended in 100 mM MOPS pH7.5. 1 ml of purified protein (estimated 50 µg/ml) was added to the beads and incubated with gentle agitation overnight. The next day, the beads were centrifuged and the supernatant decanted.

Beads were resuspended in 1 ml of 1M Ethanolamine, pH 8.0 and agitated for 1 hour at 4°C, before applying onto a Bio-Rad chromatography column. Columns were washed twice with 5 ml TBS and stored at 4°C.

Affinity purification of antisera

Columns were washed with 5 ml TBS; 5 ml Tris-High Salt (20 mM Tris pH7.5, 500 mM NaCl); 5 ml 100 mM Glycine, pH 2.5; 5 ml 50 mM Tris pH 8.8; 5 ml 100 mM Ethanolamine and 2 x 5 ml TBS. 1 ml of crude serum from rabbit R1318 (2^{rd} bleed) was diluted into 4 ml TBS and applied to the gravity fed column. The flow-through was collected and re-applied to the column 3 more times. Columns were washed with 2 x 5 ml TBS and 5 ml Tris-High salt sequentially. The antibody was eluted with 0.5 ml glycine pH 2.5 directly into 5 microfuge tubes containing 42 µl 1M Tris Base (pH 8.8) and 50 µl 5mg/ml BSA.

Preparation of Antigen for Injection

E. coli expressed and purified DmIX-14 C-terminal fragment in Ni-NTA Elution Buffer (50 mM NaH_2PO_4 pH 8.0, 300 mM NaCl, 250 mM imidazole) was subjected to 12.5% SDS-PAGE. The gel was rinsed 3 x 10 minutes with distilled dH_2O before staining with Aqueous Coomassie Blue (0.1% Coomassie Blue in Laemmli running buffer without SDS) for 1 hour. The gel was destained in 1X Laemmli running buffer without SDS until a band was seen. The band was excised and ground to a fine powder

in liquid nitrogen before being sent to Diagnostics Scotland Pentland Science Park for injection into sheep.

Protein Expression using the Baculovirus system

Constructs to be expressed were cloned into the donor vector of the baculovirus system (Invitrogen). 500 ng of recombinant construct were transfected into DH10Bac by electroporation. After the cells recovered by incubating in SOC medium for 45 minutes at 37°C, they were spread out on LB plates contain 50 μg/ml Kanamycin, 7 μg/ml gentamicin, 10 μg/ml tetracycline, 100 μg/ml X-gal, 40 μg/ml IPTG and grew in 37 °C incubator until blue and white selection could be performed (Blue is un-recombined white is recombined). White colonies were selected and inserts were confirmed by single colony PCR. Confirmed colonies were grown in 100 ml LB medium containing 50 μg/ml Kanamycin, 7 μg/ml gentamicin, 10 μg/ml tetracycline for midiprep. Bacmids were extracted using the High Purity Plasmid midiprep system (Marligen Biosciences Inc, Cat no. 11451-028) under manufacturer's instruction. Isolated bacmid was tranfected into SF9 cells using Cellfectin Reagent (Invitrogen) as follows.

SF9 cells were seeded at 10^6 cells/ml in a 6-well plate (1 ml per well) in SF-900 II Medium with L-Glutamine (Gibco) and grown at 27°C for 1 hour. 1 μg of bacmid DNA was diluted in 100 μl of SF-900 II medium, and 6 μl of Cellfectin was diluted in 100 μl of SF-900 II medium. Bacmid was combined with Cellfectin and incubated for 30 minutes at room temperature. Cells were washed with 2ml of SF-900 II medium before the addition of the lipid:DNA in which 0.8 ml of SF-900 II had been added immediately

before. Cells were incubated for 5 hours at 27°C before washing with 2 ml of SF-900 II Medium with 10% FBS. Cells were then incubated at 27°C for 5 days when signs of viral infection (cells became bigger and detached compared to control cells) became apparent.

Cells were harvested at 500 x g using a Biofuge Primo (Heraeus) and 1 ml of virus containing supernatant was used to infect a larger culture of SF9 cells (20 ml at 10^6/ml). When these infections were repeated 3 times, pfu (plaque forming units) were over 10^8 pfu/ml. Virus titre was determined by adding 1ml of serially diluted virus into 1ml of SF9 cells (10^6 cells /ml). After one week, the most diluted viral concentration causing cell lysis was regard as pfu. Cells were collected to purified protein. 1 ml virus with pfu titre greater than 10^8/ml was used to infect 30 ml SF9 cells at a concentration of 10^6 cells/ml. Upon signs of infection (2-3 days at 27°C), 10 ml of cells were harvested by centrifugation at 500 x g. Pellets was resuspended in Lysis Buffer at a concentration of 5 x 10^6 cells/ml, incubated on ice for 30 minutes before centrifugation at 20,000 x g (5417R, Eppendorf). The supernatant was incubated with Ni-NTA beads (extract of 5 x 10^6 cells per 100 µl) for 1 hour at 4°C and the resin mixture was loaded into a Poly-Prep Chromatography Column (BioRad Cat. 731-1550). The flow through was allowed to bind 3 times. The column was washed with Washing Buffer (2 volume of flow through) before elution by Elution Buffer (half volume of flow through). Elutions were collected 4 times. Beads were boiled in 1X SDS-PAGE Sample Buffer (half volume of flow through). All fractions were analysed by Immunoblotting and Coomassie Blue staining.

	Lysis Buffer	**Washing Buffer**	**Elution Buffer**
Condition 1	50 mM Tris-HCl pH8.0, 400 mM NaCl, 0.5% Deoxychola	1 x Lysis buffer. 1 x with washing buff 1: 50 mM Tris-HCL pH 8.0, 400 mM	10 mM Tris-HCl pH 7.5

	acid, 1% NP40, 1 µM/ml PMSF, 1mg /CLAP, 1,7 µg/n aprotinin	NaCl, 0.1% NP40, 1 µM/ml PMSF, 1 mg/ml CLAP, 1.7 µg/ml aprotinin. 1 x with washing buffer 2: 10 mM Tris-HCl pH 7.5, 150 mM NaCl, 0.1 µM/ml PMS	150 mM NaCl, 0.1 µg/n PMSF, 250 mM Imidaz
Condition 2	10 mM Tris-HCl pH 8.0; 300 mM NaCl; 10 mM NaF; 10 mM Na_2HPO_4; 10 mM NaH_2PO_4; 1% Trion X-100; 1 mg/ml CLAP; 1 mg/ml aprotinin; 1.74 mg/ml PMSF	40 mM Tris-HCl pH 8.0; 260 mM NaCl 2% Triton-X 100; 10% glycerol	40 mM Tris-HCl pH 8.0 260 mM Nacl; 2% Trito X 100; 10% Glycerol; 1 mM immidazole
Condition 3	50 mM Na_2HPO_4 pH 8.0; 10 mM immidazole; 300 mM NaCl; 1% Trion-X 100; 1 mM DTT; 10 mM PMSF; 1 mg/m CLAP; 1 mg/ml aprotinin	Washing buffer 1: 50 mM Na_2HPO_4 pH 8.0; 300 mM NaCl; 1 mM DTT; 10 mM immidazole. Washing buffer 2: 50 mM Na_2HPO_4 pH 8.0; 300 mM NaCl; 1 mM DTT; 20 mM immidazole	50 mM Na_2HPO_4 pH 8.0 300 mM NaCl; 1 mM DTT; 200 mM immidazole
Condition 4	50 mM NaH_2PO_4, pH 8.0; 30 mM NaCl; 10 mM immidazo 1% NP40; 1 mg/ml CLAP; 1 mg/ml aprotinin; 1.74 mg/ml PMSF	50 mM NaH_2PO_4, pH 8.0; 300 mM NaC 20 mM immidazole	50m M NaH_2PO_4, pH 8. 300 mM NaCl; 250 mM immidazole
Denature Condition	100 mM NaH_2PO_4, 10 mM Tris-HCl, 8 M Urea; final pH 8.0	100 mM NaH_2PO_4, 10 mM Tris-HCl, 8 Urea; final pH 6.3	Elution buffer 1: 100 m NaH_2PO_4, 10 mM Tris-Hcl, 8 M Urea; final pH 5.9. Elution buffer 2: 1(mM NaH_2PO_4, 10 mM Tris-Hcl, 8 M Urea; fina pH 4.5.

Purification of Recombinant DmIX-14 from SF9 cells

0.5 ml of chelating Sepharose Fast Flow (Amersham) was washed 5 times in 2.5 ml of dH_2O by centrifugation at 500 x g for 5 minutes. Beads were resuspended in 0.25 ml

0.1 M $ZnSO_4$ and incubated for 5 minutes with shaking at room temperature. Beads were then washed 3 times with 2.5 ml dH_2O each before incubation with 0.5 ml SF9 cells in Lysis Buffer described above at a concentration 5 x 10^6 cells/ ml for 30 minutes at room temperature. Beads were washed 3 times with 2.5 ml PBS pH 7.4 before elution with 1 ml Elution Buffer (PBS pH7.4, 50 mM EDTA) passed over the beads 4 times.

Pichia Pastoris Genomic DNA Extraction

Fresh (just after grown in the incubator, had not stored in fridge) single yeast colony was inoculated into 2 ml YPDA and grown overnight at 30°C with shaking. The next day, 1.5 ml of culture was pelleted in an Eppendorf tube by spinning at 13,000 rpm for 1 minute in a bench centrifuge Biofuge 13 (Heraeus Instruments) at room temperature. (All the following spins were done at this speed and temperature.) Each yeast pellet was then resuspended in 200 µl of Lysis Buffer (2% Triton X-100, 1% SDS, 100 mM NaCl, 10 mM Tris, pH 8.0, 1 mM EDTA) with 200 µl of glass beads. Then 200 µl of Phenol/$CHCl_3$/IAA (25 : 24 : 1) was added before vortexing the tube for 5 minutes. The tube was then centrifuged for 5 minutes and the upper phase was transfer into a new tube. 100 µl of Chloroform was added before vortexing the tube for 30 seconds. The tube was then spun for 2 minutes and the upper phase was transferred to a new tube. 2.5 volumes of 100% ethanol was added to precipitate the DNA before the tube was spun for 5 minutes. 300 µl of 70% ethanol was added to wash the DNA and DNA was pelleted again by spinning for 3 minutes. The pellet was dried for 5 minutes at room temperature before being resuspended in 50 µl TE.

Chemical transformation into *Pichia pastoris*

Pichia pastoris strain KM71H was inoculated into 10 ml of YPDA medium and grown overnight at 30°C with shaking. A 100 ml logarithmic growing culture derived from this culture were harvested at an OD600 of 1.0 by 800 x g 5 minutes, washed once in 10 ml water, and once in 1.5 ml 100 mM CH_3COOLi (Lithium acetate) before resuspending in 250 µl 100 mM LiAc. 50 µl of cell suspension was incubated with 10 µl linearised plasmid (1.5 µg), 240 µl 50% PEG_{3350} and water to give a final volume of 360µl . The mixture was incubated at 30°C for 30 minutes before a 15 minute 42°C heat shock. Cells were centrifuged in a microfuge (Picofuge, Stratagen) for 5 seconds. Cells were then resuspended in 200 µl of YPDA medium and grown for 2 hours at 30°C to give enough time for the cells to express antibiotic resistance gene. Then a serial dilution of cells was spread onto YPDA plate with appropriate antibiotic and incubated for 2-3 days at 30°C when large colonies could be observed.

Electroporation Transformation into *Pichia pastoris*

Pichia pastoris cells (100 ml) were grown to an OD600 between 0.25 and 0.5 (between 5 x 10^6/ml and 1x 10^7 cells/ml). They were harvested by spinning at 4000 rpm (800 x g) for 5 minutes at room temperature in a Megafuge 1.0R centrifuge (Heraeus). The pellet was resuspended in 20 ml of ice cold 1.2 M sorbitol and transferred to a 50 ml falcon tube. The cells were harvested by centrifugation as above. The pellet was resuspended in 10 ml ice cold 1.2 M sorbitol and harvested by centrifugation as above.

The resuspension steps were repeated twice. After centrifugation, the pellet was resuspended in 1.2 M sorbitol to give a concentration of 1x 10^9/ml. The cells were divided into 200 µl aliquots and mixed with 50 ng of DNA per aliquot. After mixing with DNA, the cells were immediately electroporated, using settings of 2.25 kilovolts, 200 Ohms and 25 µF. 1 ml of YPDA medium was added after electroporation. Cultures were grown for two hours to allow expression of antibiotic before different dilutions of cells were spread on selective medium plates. Plates were incubated at 30°C for 2-5 days before transformants appeared.

Expression of Recombinant *Pichia pastoris* strains

After the appropriate construct had been transfected into KM71H *Pichia* strain, recombinant colonies was validated by PCR from yeast genomic DNA. Confirmed recombinant colonies or control colonies were inoculated into 100 ml of BMG or BMGY in a 1 litre flask and grown at 30°C in a shaking incubator (250 rpm) until the culture reached an OD_{600} between 2 and 6. Cells were harvested by centrifuging at 1800 x g for 5 minutes at room temperature using a Megafuge 1.0R centrifuge (Heraeus). To induce expression, the cell pellet was resuspended in methanol inducing medium BMM or BMMY in 1/5 of the original culture volume. The culture was then grown at the conditions as above in a 100 ml flask. At time points (0, 12, 24, 48, 72, 96 hours), 1 ml of culture was taken and centrifuged at 10,000 x g to separately save the supernatant and pellet in –80°C. Methanol was added every 24 hours to maintain a final concentration of 0.5% for keeping induction. To test the expression level, the supernatant from each time point was directly loaded on a SDS-PAGE gel or after concentration for Coomassie

staining or immunoblotting. On the other hand, the pellets from each time point were processed as below:

Cell pellets were quickly thawed and placed on ice. 100 μl of Breaking Buffer (50 mM sodium phosphate, pH 7.4, 1 mM EDTA, 5% glycerol, 1 mM PMSF, 1 μg/ml CLAP, 1.7 μg/ml aprotinin) per 1 ml sample was added to resuspend the pellet. The equal volume of acid-washed glass beads (size 0.5 mm) was added. The mixture was then vortexed for 30 seconds, then incubated on ice for 30 seconds (This was repeated 8 times more). The tube was then centrifuged at 13,000 rpm for 10 minutes at 4°C using a bench centrifuge Biofuge 13 (Heraeus). The supernatant was loaded on a SDS-PAGE gel for Coomassie staining or immunoblotting. The debris was loaded on a SDS-PAGE gel after the boiling and sonicating in SDS-PAGE sample buffer.

2.4 Table of Oligonucleotide primers

1. Primers for HsIX-14

Figure 2.4, panel A

Primer Name	Primer Sequence
yubinhsIX-14seq1	5'-AAGGCAAATCATGTGGTCAAGAG-3'
yubinhsIX-14seq2	5'-CCAGACCAAGAAGGCATCTC-3'
yubinhsIX-14seq3	5'-GGAGAGATTATGGGATGTTCG-3'
yubinhsIX-14seq4	5'-CAGCGCAGCTCAGATTGTAG-3'
yubinhsIX-14seq5	5'-CTATGGCGCTGAAAAGTATG-3'

2. Primers for DmIX-14

Figure 2.4, panel B

Primer name	Primer Sequence
DmIX-14Geneseq1	5'-TTTTTGGCGTGGGCTGAGATTGG-3'
DmIX-14Geneseq2	5'-GGCATCTGCTCTTGGCTCCTCGTT-3'
DmIX-14Geneseq3	5'-CCGATGCGCACTTGGATGTATGTC-3'
DmIX-14Geneseq3.5	5'-ATTCTTTAGGGACGATGATG-3'
DmIX-14Geneseq4	5'-ACACAGTCGCCGGTCTTCTCG-3'
DmIX-14Geneseq4.5	5'-AAGGACGGCGAGGAGGGGTTCT-3'

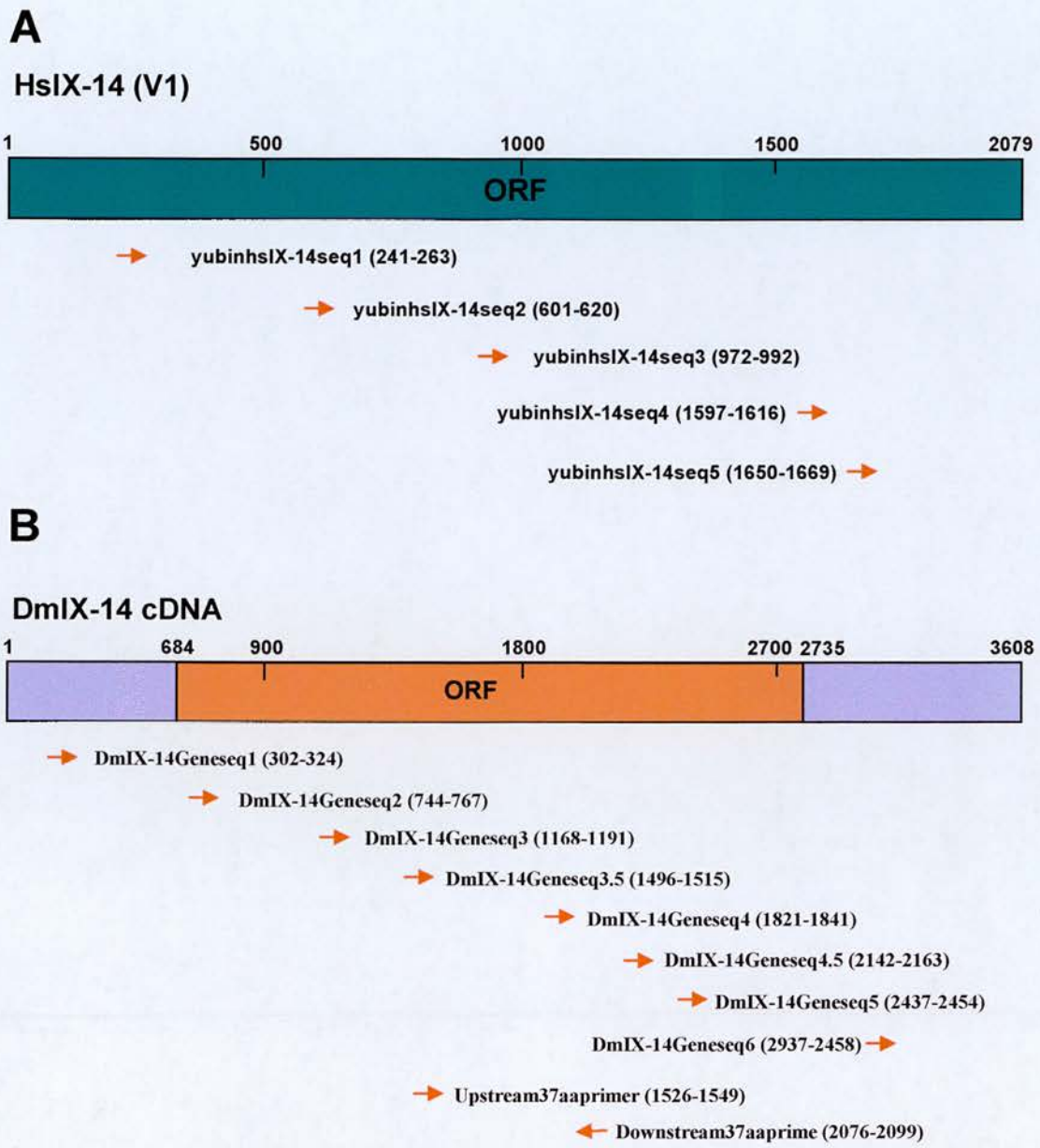

Figure 2.4A: Primer placement in human and *Drosophila* IX-14.

A: The primers for HsIX-14 and their relevant placements to HsIX-14 ORF. B: The primers for DmIX-14 and primers around 37 amino acid insertion and their relevant placements to DmIX-14 cDNA. The orange block shows the ORF of DmIX-14. All the arrows show the direction of the primers and the number shows the positions of the primers.

DmIX-14Geneseq5	5'-ACATCCTGGTGGGCAACT-3'
DmIX-14Geneseq6	5'-CTTTGCCATTTAATAGTCTTTG-3'

3. Primers around 37 amino acid insertion to perform RT-PCR

Figure 2.4A, Panel B

Primer Name	Primer Sequence
Upstream37aaprimer	5'-AACGCCCCGAAAATTAGACACTGG3'
Downstream37aaprime	5'-CTCAAACTCATGGCGGATAAGATT-

4. Primers to construct Donor vectors containing DmIX-14 fragments for Baculovirus system expression

Primer Name	Primer sequence
DmIX-14c-terminal ta	5'-GCAGATCTCTAATGATGATGATGATGATGACTGAATCCCCATCGCAG-3'
IX-14ORFSpeIupper	5'-CACTAGTCATGGCCAAAACGCCCCCG-3'
IX-14ORFSpeIupper2	5'-AACTAGTAATGGCCAAAACGCCCCCG-3'

IX-14ORFXballower	5'-GCTCTAGATTTGTGCGAAGTGGATACGA-3'
IX-14ORFXballower	5'-AATCTAGACGGTAAATATCCGAGGACACACT-3'
Dm-IX-14SpeI-N(30	5'-CACTAGTCGGTAACATGGCCAAATTC-3'
Dm-IX-14SpeI-N(30)	5'-CACTAGTATGCATCACCATCACCATCACGGTAACAT GGCCAAATTC-3'
Not-1N30DmIX-14OR	5'-ATAAGAATGCGGCCGCCCGGTAACATGGCCAAATTC TGGCA-3'
DmIX-14ORFXhoIC6	5'-CCCTCGAGCTATTTCTCACTGCCCGCTCCACAGGC 3'
DmIX-14ORFXbaIC6	5'-GCTCTAGACTATTTCTCACTGCCCGCTCCACAGGC 3'

5. Primers for baculovirus system

Primer name	Primer sequecne
PFastBacTMHTAseq	5'-AGTGGTTCGCATCCTCGGTTTTCT-3'
M13 Forward	5'-CGTTGTAAAACGACGGCCAGT-3'
M13 Reverse	5'-TTTCACACAGGAAACAGCTATCAC-3'

6. Primers to construct *Pichia* expression vector containing DmIX-14 fragments.

Primer name	Primer sequence
PichiaPsec16upper	5'-ACCCAGACACTCGACAAACC-3'
PichiaPsec16lower	5'-GCCGGTAAGTTGTACCTCCA-3'
PichiaPkar2upper	5'-CACTTGGGTGGTGAGGACTT-3'
PichiaPkar2lower	5'-TCTTGACACCAGCGTCTTTG-3'

Chapter 3: Characterisation of the Invadolysin phenotype

3.1 Mitotic arrest reveals a chromosome structure defect in *IX-14* mutant neuroblasts.

Colchicine is a well-known microtubule-depolymerizing drug that inhibits the assembly of the spindle, and consequently activates the mitotic spindle checkpoint that arrests cell division at metaphase (Rieder and Palazzo 1992). There is no report claim that colchicines have direct effect on chromosome condensation or chromosome structure.

I first tested the effect of colchicine by examining the microtubules of wild type cells with and without colchicine treatment. As shown in Figure 3.1A, microtubules in the colchicine treated cells were depolymerized compared to the control microtubules. Comparing the chromosomes of wild type neuroblasts (with and without colchicine treatment), to mutant neuroblasts (with and without colchicine treatment), it is evident that mitotic arrest gives the wild type chromosomes the chance to hypercondense (Figure 3.1B). But it is different from the appearance that the *IX-14* mutant gives, since although the chromosomes of the *IX-14* mutant are also hypercondensed in length, chromosomes appear 'loosely' condensed at the edge of hypercondensed mitotic chromosomes (Figure 3.1C). Moreover, colchicine can not make the mutant chromosomes condense further, in other words, it can not tighten the 'loosely' condensed chromosomes. This implies *IX-14*

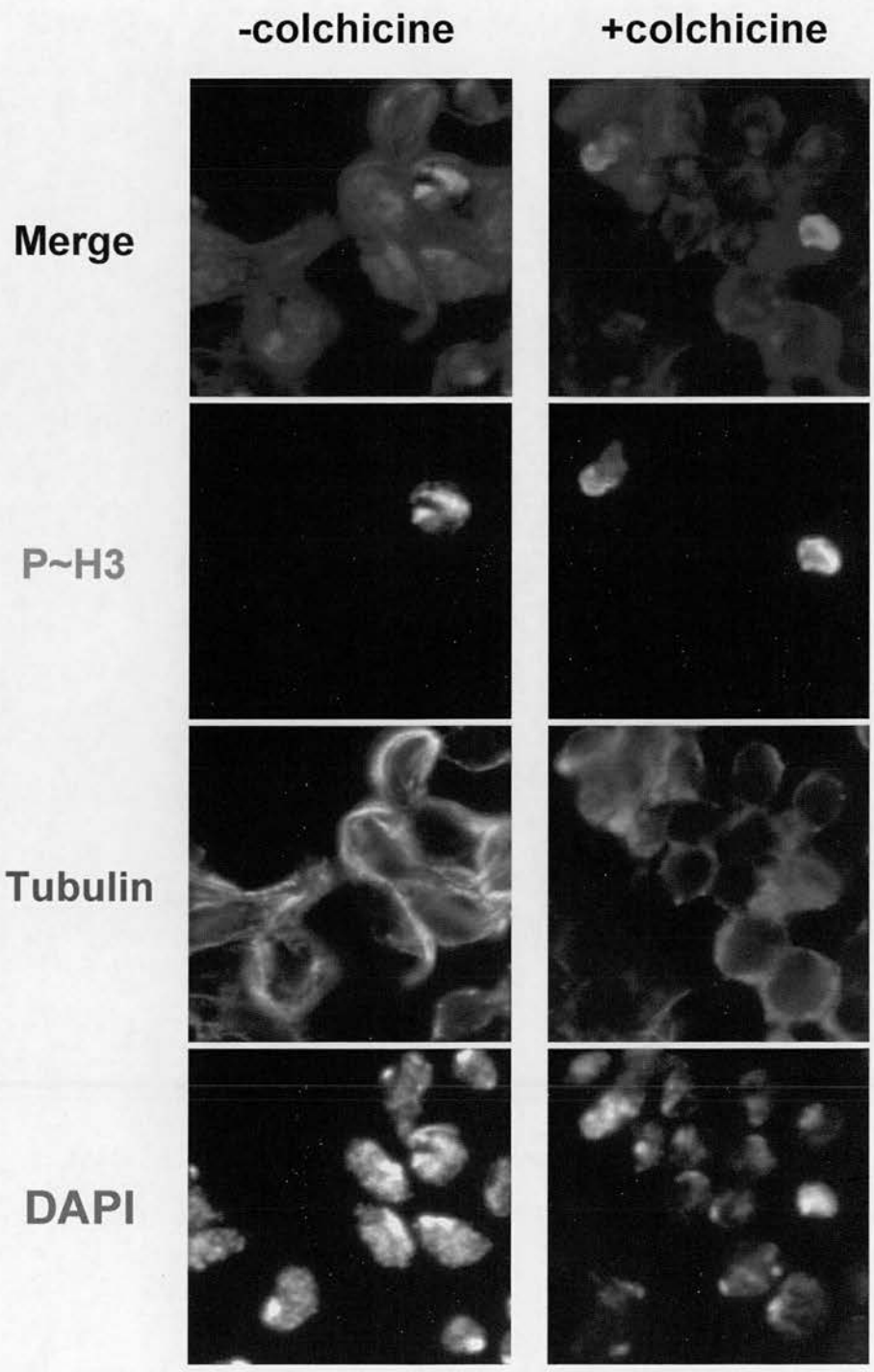

Figure 3.1A: Colchicine depolymerises Microtubules.

Comparison of the microtubules of wild type neuroblasts treated with and without colchicine. Green is tubulin, red is P~H3 and blue is DAPI. The microtubules obviously depolymerized (no individual filament could be seen) in the cells treated with colchicine (right Panel) compared to the control cells (left Panel).

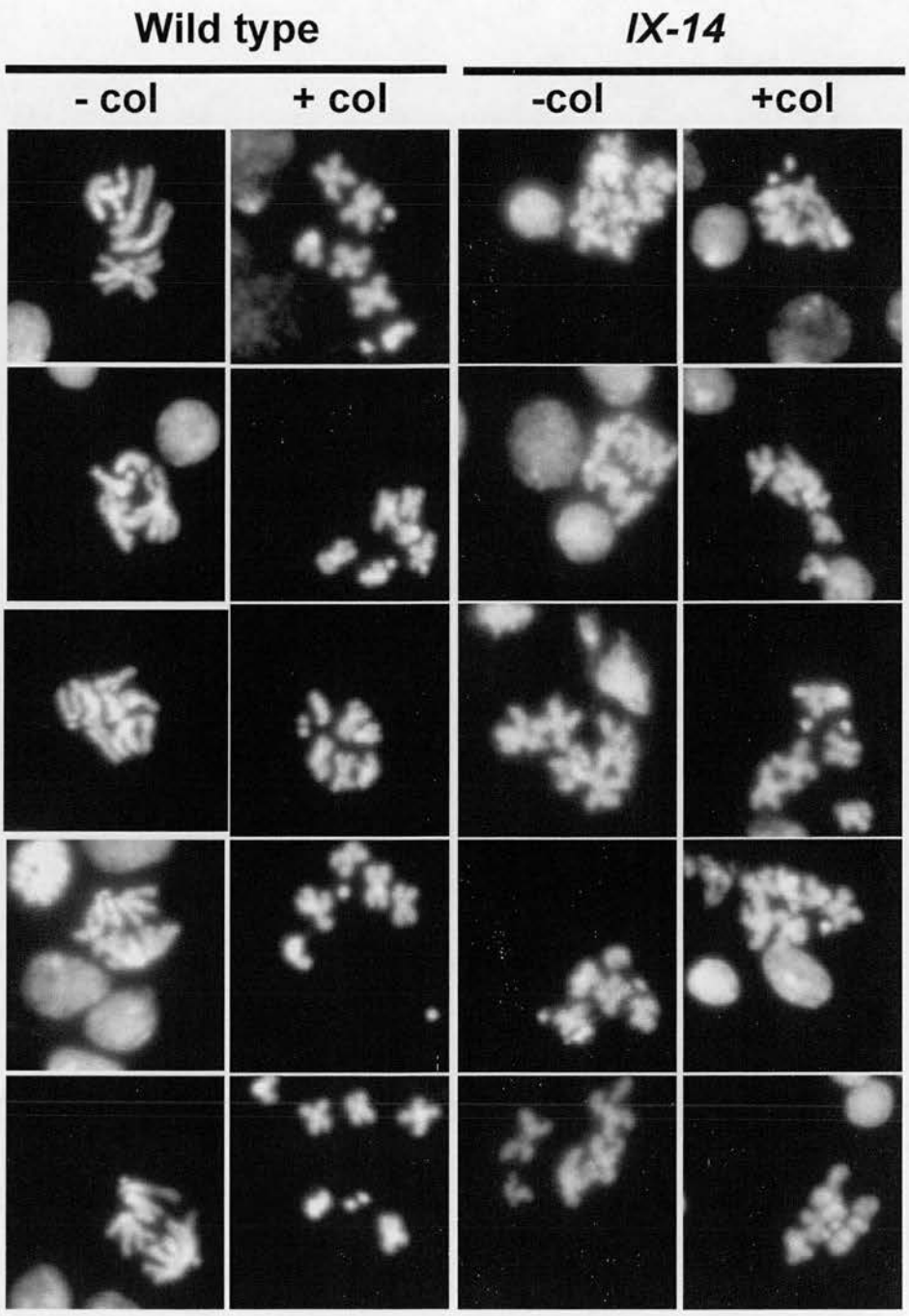

Figure 3.1B: Comparison of wild type and *IX-14* mutant neuroblasts with and without colchicine treatment.

Colchicine gives wild type cells a hyper-condensation phenotype (compare -col and +col columns) and can not condense the mutant further (compare -col and +col columns). The phenotype given by colchicine is different from that given by the *IX-14* mutant, since there is loosely condensed chromatin surrounding the hypercondensed chromosomes in the *IX-14* mutant, but not in wild type cells (compare wild type +col column and mutant -col columns).

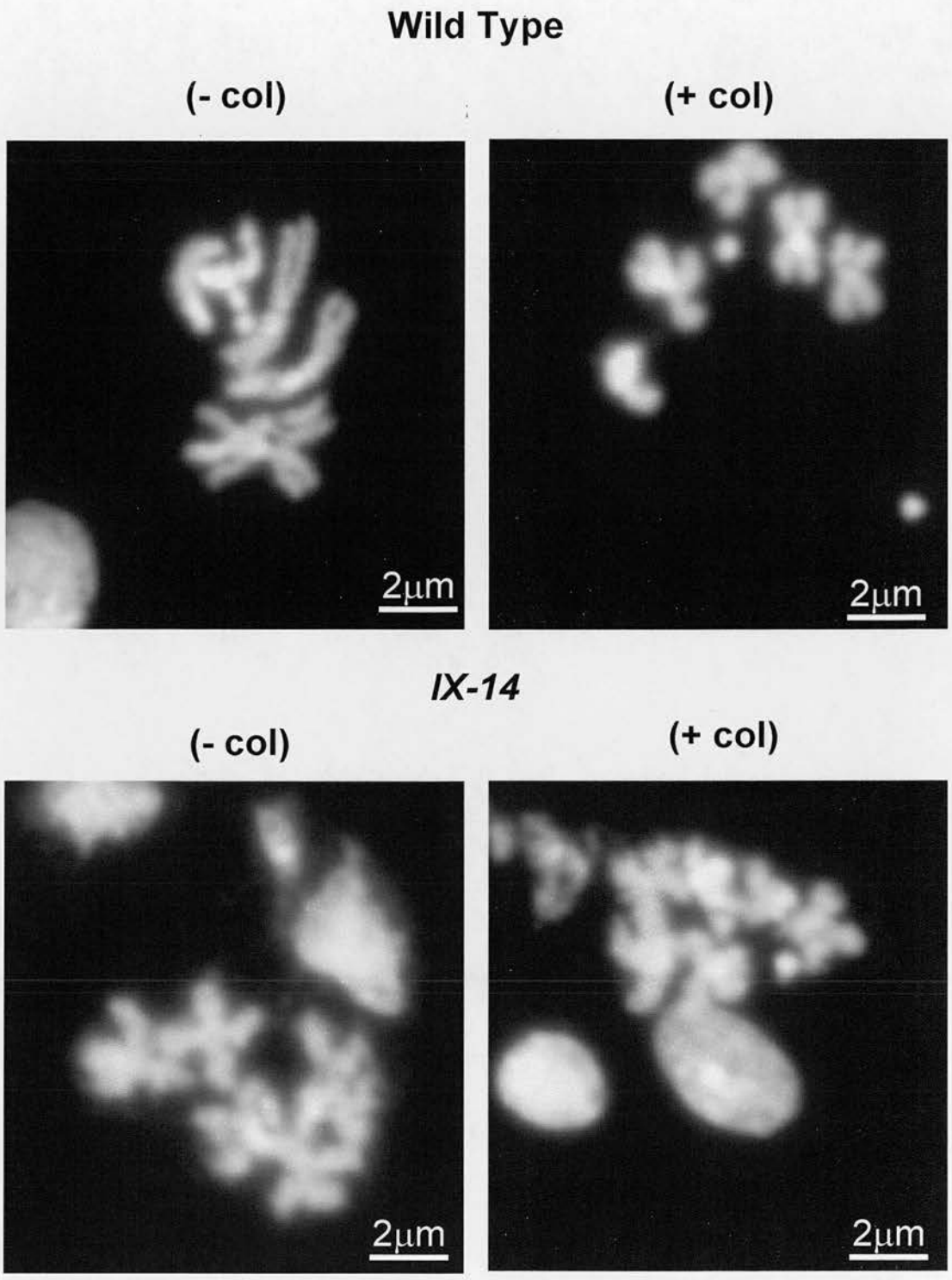

Figure 3.1C: Enlarged view of loosely condensed chromatin.

These are enlarged images of wild type and mutant with or without colchicine treatment to highlight the loosely condensed chromatin present in mitotic mutant cells.

mutants have an intrinsic chromosome structure defect that can not be rescued by simply spending more time in mitosis.

Mitotic arrest was confirmed in the mutant by determining the percentage in each of the five stages (late G2, prophase, prometaphase/metaphase, anaphase and telophase) included in P~H3 positive cells in wild type and mutant neuroblasts. Since no anaphase or telophase figures were found in the mutant neuroblasts, and the percentage of metaphase figures in the mutant is higher than in wild type, we suggest a mitotic arrest in the mutant (Figure 3.1D).

3.2 Lamin Dm0, otefin and lamin A/C increase in *IX-14* mutant neuroblasts.

The nuclear envelope is composed of nuclear membranes, nuclear pore complex, and the nuclear lamina. The nuclear membranes are divided into three morphologically distinct but interconnected domains: outer nuclear membrane, inner nuclear membrane and nuclear pore membranes. Pore membranes connect the inner and outer nuclear membranes at numerous points and are associated with nuclear pore complex (Worman and Courvalin 2005). The nuclear lamina was first described as a fibrous structure underlying the inner nuclear membrane in vertebrate cells, taking observed by electron microscopy (Fawcett 1966). Interphase lamina is associated with nuclear pore complexes and three major bands had been isolated from the pore complex-lamina fraction which are components of the lamina (Dwyer and Blobel 1976). These components were further confirmed by raising antibodies against them and observing their localizations (Gerace,

Percentage of P~H3 positive cells in indicated phases

	G1	S	G2	Mitosis
Wild type	45.1%	39%	13.4%	2.5%
mutant	77.3%	11.5%	5.4%	5.8%

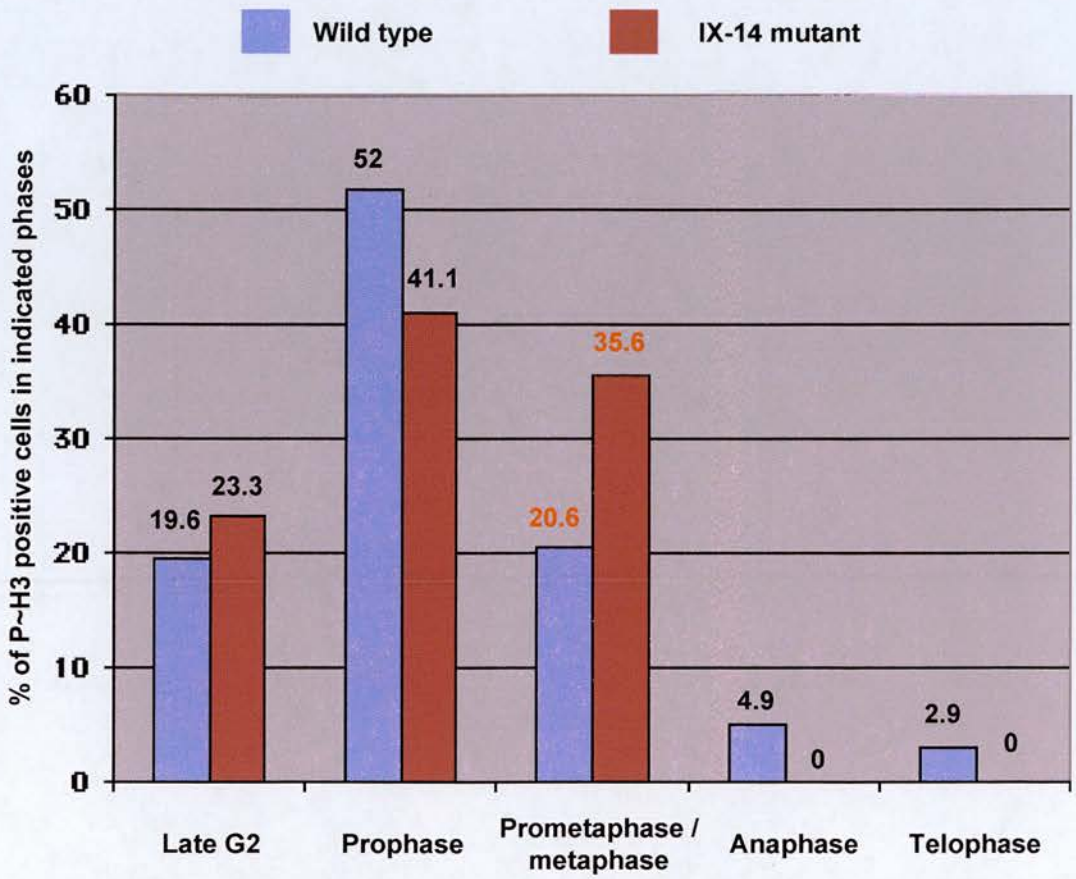

Figure 3.1D: Quantitation of different stages in cell cycle in wild type and *IX-14* mutant neuroblasts.

IX-14 mutant cells are arrested in metaphase since a higher percentage of prometaphase/metaphase cells appeared in the *IX-14* mutant and no anaphase or telophase were observed.

Blum et al. 1978) and named lamin A, lamin B and lamin C (Gerace and Blobel 1980). The nuclear lamina undergoes reversible depolymerization during cell division, a process that is believed to result from reversible enzymatic phosphorylation (Gerace and Blobel 1980). A decade later, accompanying papers were published to describe specific mitotic phosphorylation sites that are associated with lamina disassembly. Cdc2 kinase was reported to phosphorylate lamin B at its N-terminus which result in its depolymerization during mitosis (Peter, Nakagawa et al. 1990). Lamin C was shown to have phosphorylation sites in its N-terminal and C-terminal, which are conserved in different organisms. S6 kinase II phosphorylates lamin C at Ser-404 (Ward and Kirschner 1990). Mutation of two conserved phosphorylation sites (Ser-22 and Ser 392) in lamin A blocks the disassembly of lamina in an overwhelming majority of mitotic cells (Heald and McKeon 1990). Lamin proteins were shown to belong to the intermediated filament family by both morphological (Aebi, Cohn et al. 1986) and biochemical evidence (Goldman, Maul et al. 1986). The complete nucleotide sequence of the coding region of the A and C lamins shows striking homology with the entire family of cytoplasmic intermediate filament protein (McKeon, Kirschner et al. 1986) which further verifies this hypothesis. Lamins contain head and tail domains of variable structure and conserved alpha-helical central rod domain and polymerise to form filaments approximately 10 nm in diameter, like other cytoplasmic intermediate filaments (Herrmann and Aebi 2004). Lamins have orthologs in several eukaryotic species, but not in yeast. In human, there are three genes encode nuclear lamins which is *LMNA (Lin and Worman 1993)* , *LMNB1* (Lin and Worman 1995) and *LMB2* (Biamonti, Giacca et al. 1992). Lamin A and C are raised by alternative splicing of mRNA encoded by *LMNA* while lamin B1 and lamin B2

are encoded by *LMNB1* and *LMNB2* individually. Except for lamin C, lamins contain CAAX boxes in which A is an aliphatic-hydrophobic residue and X is generally S, M, C, A, or Q. Lamin B post-translational modification includes farnesylation of the cysteine residue in CAAX box, removal of the AAX tripeptide and subsequent methylation of the now carboxyl-terminal cysteine (Farnsworth, Wolda et al. 1989). Lamin A maturation also has the three sequential post-translational modifications as lamin B, but differ in that the C-terminus (the farnesylated, methylated cysteine) of the prelamin A molecule is removed from the mature protein (Sinensky, Fentle et al. 1994) (Weber, Plessmann et al. 1989). This molecular difference between mature lamins A and B might account for the observation that all cells express lamin B, while lamin A expression to be reserved to cells of differentiated tissues (Lehner, Stick et al. 1987) (Stewart and Burke 1987). Two lamin genes appear in *Drosophila*: one encodes a B-type lamin, termed Lamin Dm0 and the other encodes an A-type lamin, termed lamin C (Gruenbaum, Landesman et al. 1988) (Bossie and Sanders 1993).

Brian McHugh discovered a novel phenotype of *IX-14* mutants, that being an increase in lamin Dm0 levels in some mitotic cells (McHugh, Krause et al. 2004). This may be because lamin Dm0 is a substrate of IX-14. In the null mutant of *IX-14*, where there is no detectable IX-14 metalloprotease activity, lamin Dm0 protein accumulates. Figure 3.2A shows the co-staining of lamin Dm0 and P~H3 in wild type and $IX\text{-}14^{4Y7}$ neuroblasts. Compared to interphase cells, lamin Dm0 disperses in mitotic cells in wild type but increases in some mitotic cells in mutant neuroblasts.

Extracts were prepared from brains dissected from 3rd instar larvae of wild type and *IX-14* mutants. Two wild type brains or 6 mutant brains (since the mutant brains are

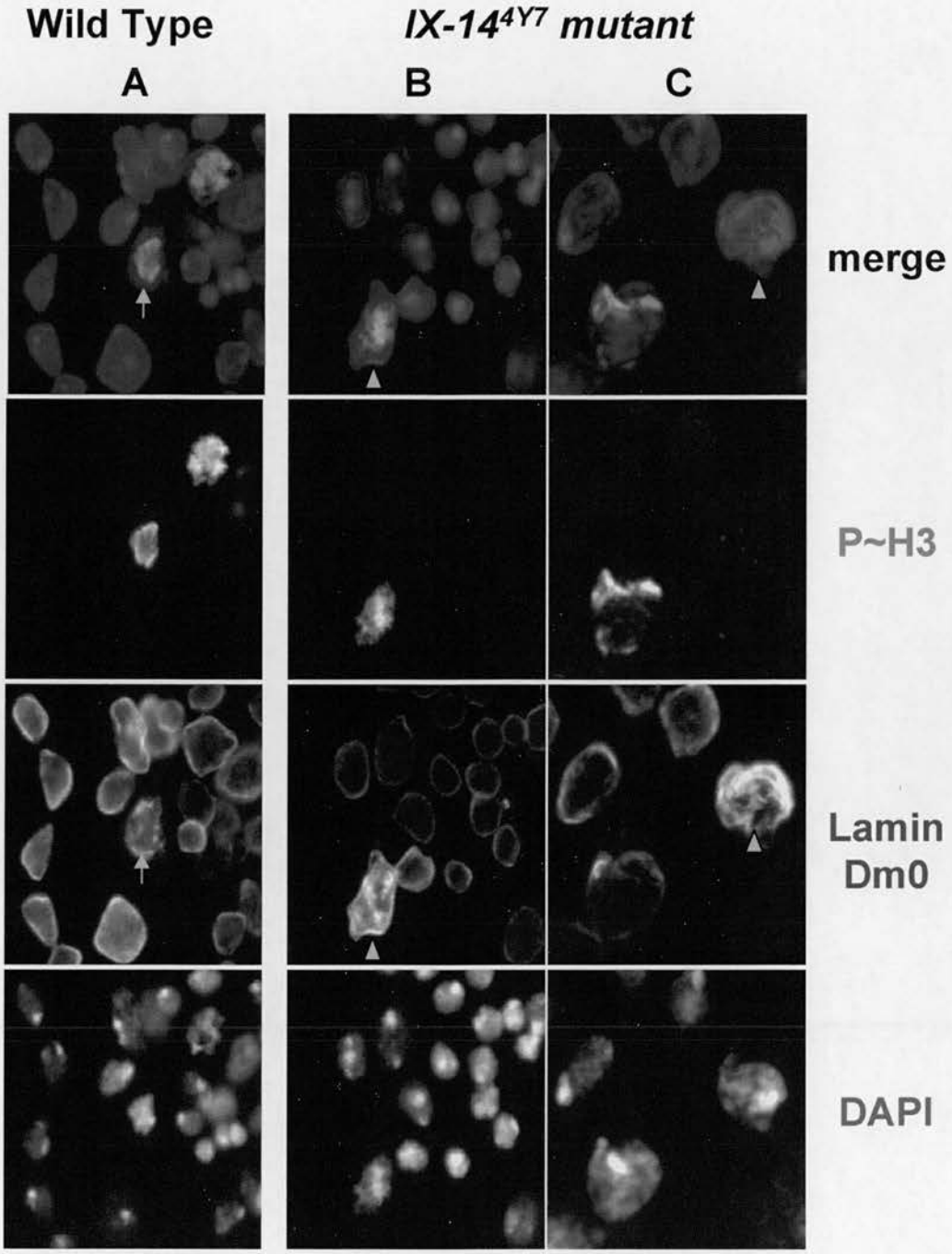

Figure 3.2A: Co-stain lamin Dm0 with P~H3 on neuroblasts.

Analysis of the level of lamin Dm0 in mitosis by co-staining lamin Dm0 with P~H3. While lamin Dm0 seems to disperse (yellow arrow) in mitosis in wild type (A column), it increases dramatically (yellow arrowhead) in *IX-14* mutant mitotic cells (B column). The lamin Dm0 increase was also found in some mutant cells which are P~H3 negative, indicating interphase cell (C column). DNA (DAPI) is in blue, P~H3 is in red and lamin Dm0 is in green.

much smaller than wild type brains) were loaded per lane for SDS-PAGE analysis. The gel was transferred to nitrocellulose membrane and probed for Lamin Dm0 antibody. Lamin Dm0 was found to be increased in the mutant brain extracts compared to wild type. Tubulin was used as a loading control (Figure 3.2B, Panel A and B). Figure 3.2C shows the densitometric analysi of lamin using Image J. Sample loading difference was compensate by comparing the Integrated Density of wild type lamin band divided by tubulin band with Integrated Density of mutant lamin band divided by tubulin band. It shows that lamin increase in *invadolysin* mutant 1.88, 1.6 and 2.22 times than in wild type in three individual experiments.

To rule out the possibility that the lamin Dm0 increase was due simply to a mitotic arrest, wild type brains were incubated in Schneider's medium with colchicine at 2 mg/ml for 2 hours before preparing protein extract. Control brains were incubated in Schneider's medium for 2 hours with no colchicine. Then proteins in the control and colchicine-treated brain extracts were resolved by SDS-PAGE and protein was transferred to nitrocellulose. Lamin Dm0 was detected by immunoblotting. As shown in Figure 3.2B (Panel C), lamin Dm0 did not increase in colchicine-treated wild type brain extracts compared to control brain extracts. Some brains, both -col and +col, were prepared for immunofluorescence with DAPI staining to examine the mitotic arrest. The mitotic index in control neuroblasts was 1% compare to 3.2% in colchicine-treated brains. Therefore the lamin Dm0 increase was due to the *IX-14* mutation, not solely mitotic arrest.

I was interested to see whether other nuclear envelope proteins might increase in *IX-14* mutant neuroblasts. I decided to examine otefin and lamin A/C in wild type and

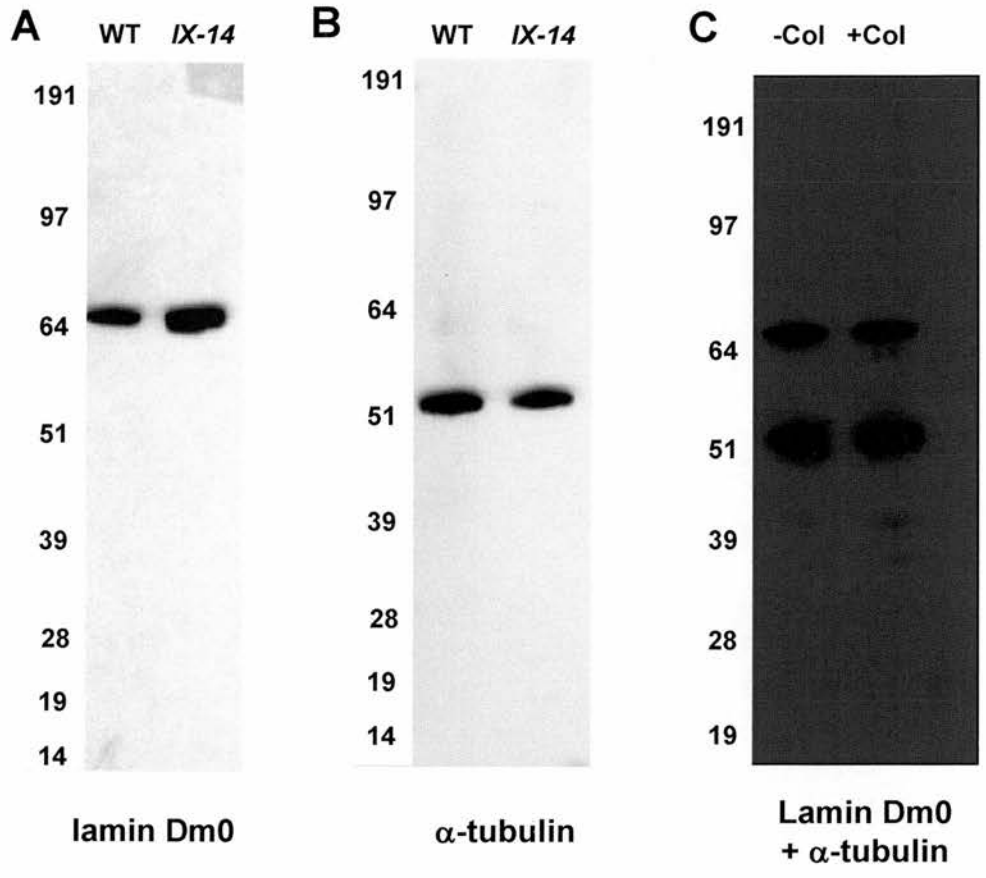

Figure 3.2B: Immunoblotting shows lamin Dm0 increases in *IX-14* neuroblasts and it is not due solely to mitotic arrest.

A: Immunoblotting for lamin Dm0 on wild type and mutant brain extracts. An expected 71 kDa (size of lamin Dm0) band can be seen in both the wild type and the mutant. However, the band in the wild type is obviously weaker than in the mutant. B: Using α-tubulin as a loading control for A. C: Lamin Dm0 does not increase in wild type *Drosophila* neuroblasts treated with colchicine. In colchicine treated brains (+col), lamin Dm0 signal is the same density to control cells. α-tubulin was used as a loading control.

A

	1	2	3
lamin-wt	1087320	837165	19635
lamin-mut	1604460	1444830	58905
tubulin-wt	1365270	1198245	1495830
tubulin-mut	1078905	1292340	2016795
lamin mut/wt	1.4756	1.7285	3
tubulin mut/wt	0.7902	1.0785	1.3483
mut(lamin/tubulin)	1.4871	1.118	0.0292
wt(lamin/tubulin)	0.7964	0.6987	0.0131
mut(lamin/tubulin)/ wt(lamin/tubulin)	1.8672	1.6002	2.225

	1	2
otefin-wt	79815	2040
otefin-mut	622455	13005
tubulin-wt	1635825	51765
tubulin-mut	1336710	57375
otefin mut/wt	7.7987	6.375
tubulin mut/wt	0.7882	1.1084
mut(otefin/tubulin)	0.4656	0.2267
wt(otefin/tubulin)	0.0471	0.0394
mut(otefin/tubulin)/ wt(otefin/tubulin)	9.8853	5.7538

B

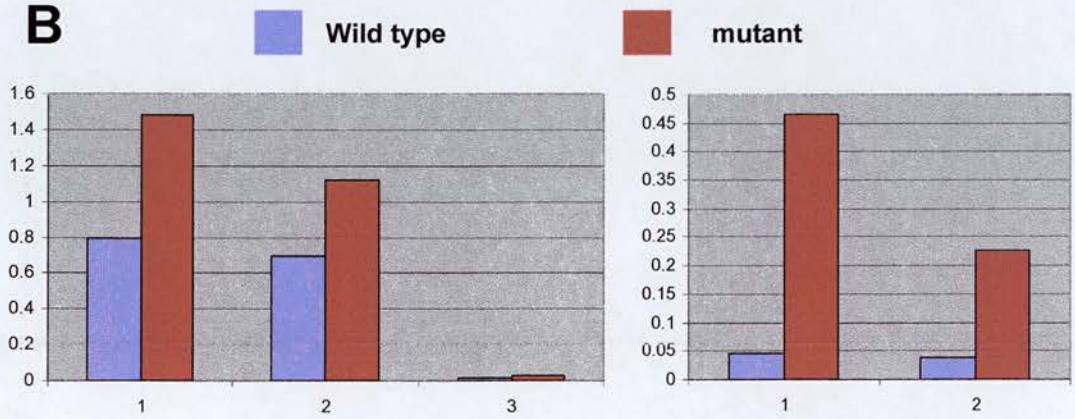

Figure 3.2C: Densitometric analysi of lamin and otefin increase.

Panal A shows the Integrated Density (the sum of the values of the pixels in the selected band) of tubulin, lamin or otefin band (both wild type and mutant) from immunoblotting film. The analysis was done using Image J and a threshold has been set for the calculated pixels to segment the image into features of interested and background. Lamin increase was analysed in 3 individual experiment and otefin increase was analysed in 2 individual experiments. Panel B left shows the graph of Integrated Density of lamin/tubulin in wild type and mutant. Panel B right shows the graph of Integrated Density otefin/tubulin of wild type and mutant.

mutant neuroblasts. Otefin is a nuclear envelope protein localized to the periphery of the nucleus (Harel, Zlotkin et al. 1989), and co-localizes with lamin Dm0 *in situ*. It is present in all somatic cells during *Drosophila* development. It plays an essential role in *Drosophila* nuclear envelope assembly and is phosphorylated by cdc2 kinase at serine 36 (Ashery-Padan, Ulitzur et al. 1997). Otefin was shown to interact with lamin Dm0 in a two hybrid screen (Goldberg, Lu et al. 1998). Figure 3.2D shows that otefin, like lamin Dm0, disperses during mitosis in wild type, whereas some *IX-14* mutant mitotic cells show an increase in otefin.

To discern whether the otefin increase happens in the same cells as the observed Dm0 increase, co-staining for otefin and lamin Dm0 was performed in wild type and mutant neuroblasts. As shown in Figure 3.2E, otefin and lamin Dm0 significantly accumulate in the same mutant cells. Immuoblotting of neuroblasts shows an otefin increase in *IX-14* mutant compared to wild type neuroblasts (Figure 3.2F). Figure 3.2C shows the densitometric analysi using the same method as analysis lamin increase. From 2 indivitual experiments, it shows otefin level increase 9.88 and 5.75 times in *invadolysin* mutant than in wild type.

In addition to the B-type lamin, lamin Dm0, *Drosophila* also has an A-type (lamin C). I was interested to see whether it also was elevated in level in *IX-14* mutant neuroblasts. Figure 3.2F showed the immunoblot of lamin A/C antibody on wild type and mutant neuroblasts. Lamin A/C increased in the mutant in the same manner as Lamin Dm0 and otefin.

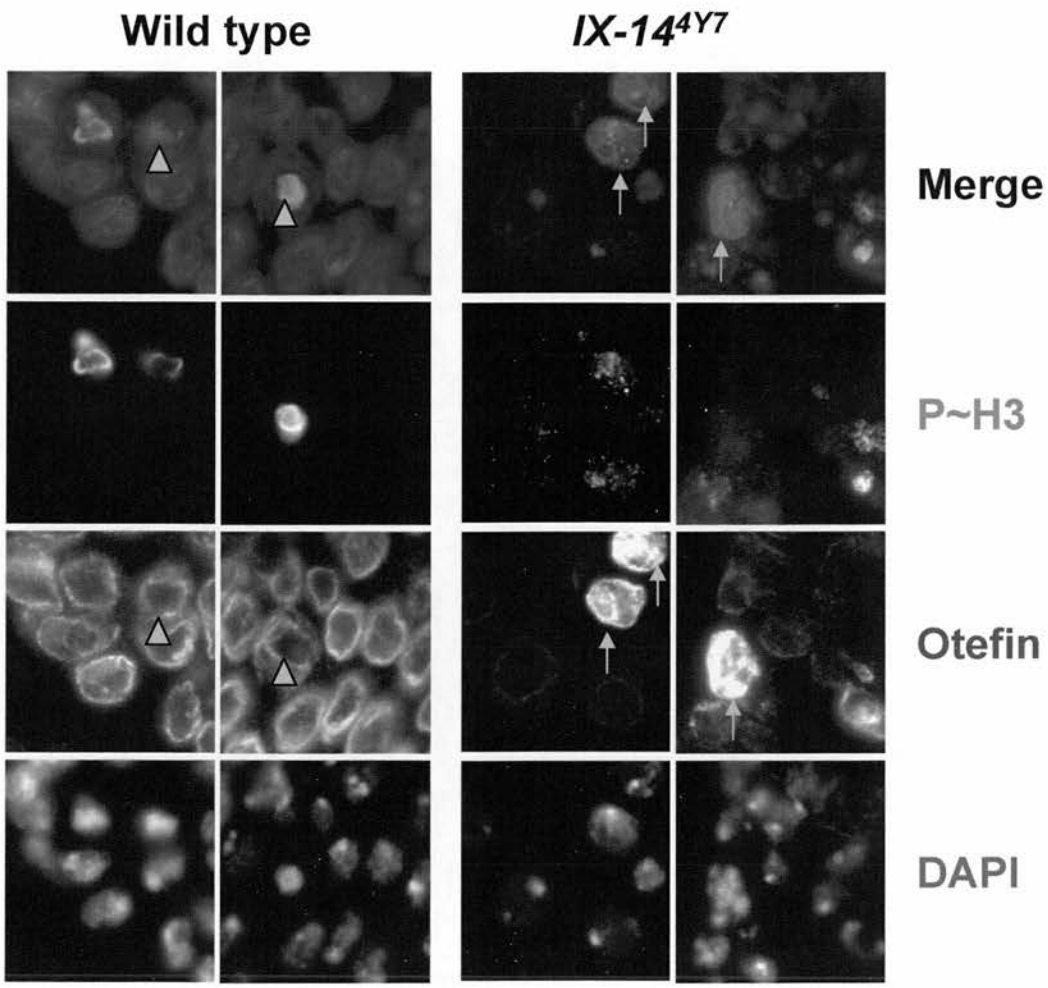

Figure 3.2D: Otefin increases in IX-14 mutant neuroblasts.

Co-staining of otefin and P~H3 in wild type and mutant neuroblasts. Otefin disperses like lamin Dm0 in mitosis in wild type cells (arrowhead). Otefin also increases abnormally in some mutant cells (arrow).

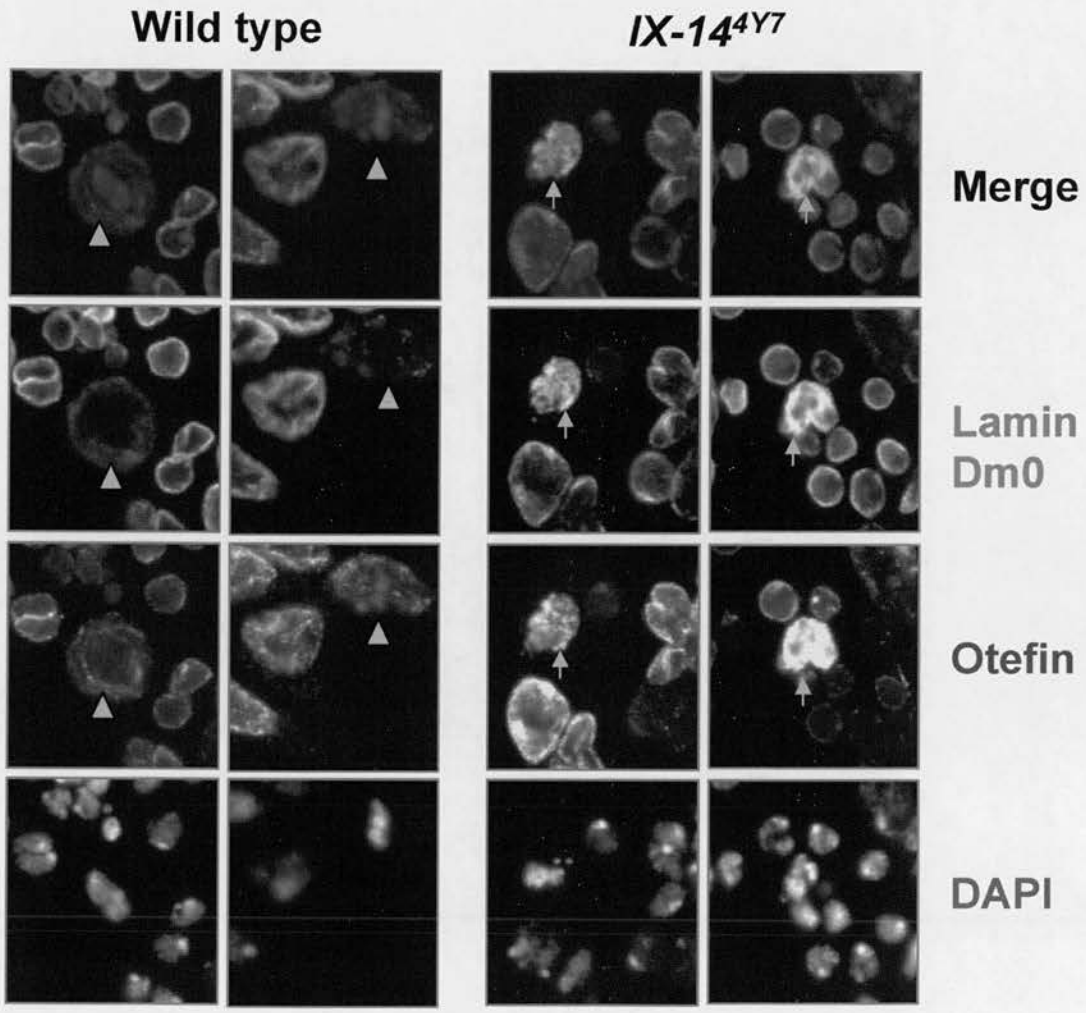

Figure 3.2E: Otefin increases in the same cells that lamin Dm0 increases in.

Co-staining of lamin Dm0 and otefin. When lamin Dm0 disperses in a mitotic wild type cell, otefin disperses as well (arrowheads). When lamin Dm0 increases in a mutant cell, otefin increases as well (arrows).

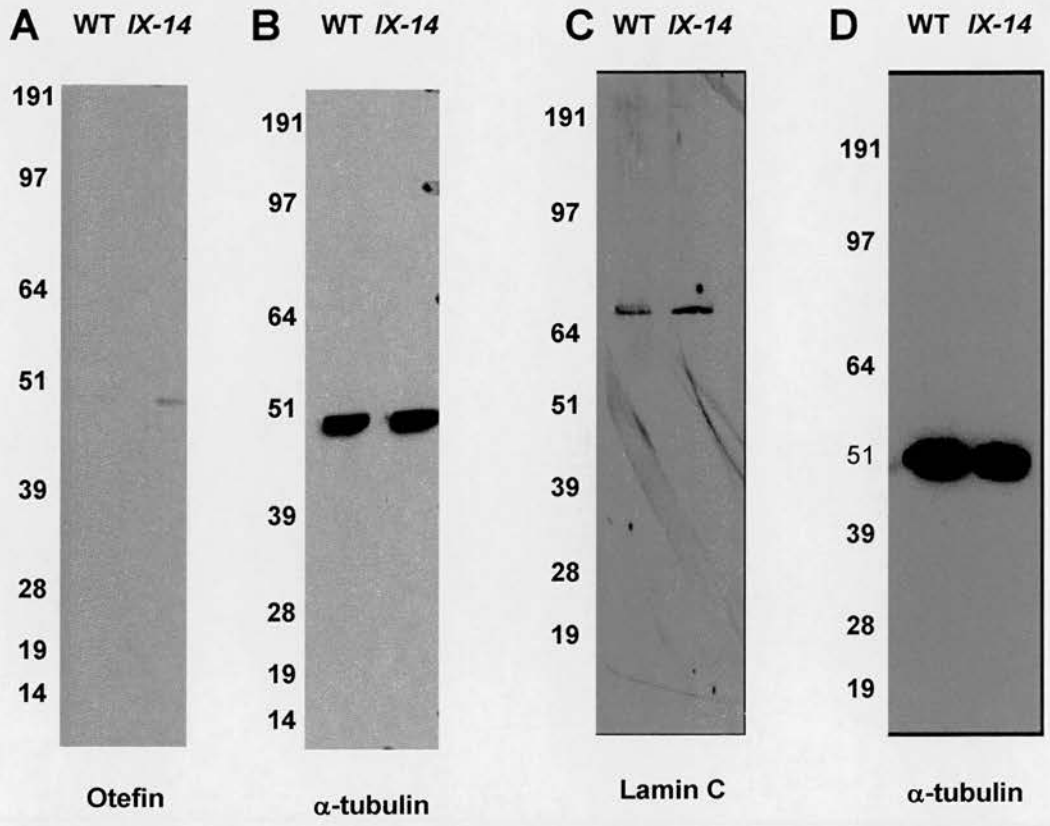

Figure 3.2F: Otefin and lamin C accumulate in *IX-14* mutant neuroblast.

A: Immunoblotting for otefin on wild type and mutant brain extracts. An expected 46 kDa band (size of otefin) was seen in *IX-14* mutant. In the same way as for lamin Dm0, the band in the wild type is much weaker (hardly see anything) than in the mutant. B: Using α-tubulin as a loading control for A, indicating sample are equally loaded. Two wild type brains or 6 mutant brains were loaded in each lane. C: Wild type and *IX-14* mutant neuroblasts were probed for antibody against lamin C. Lamin C increased in mutant brains compare to wild type. D: The α-tubulin loading control for lamin C probed in panel C.

3.3 Lamin increase is not cell cycle dependent.

I found that lamin Dm0 was increased in some mutant cells that are P~H3 negative, which indicates they are not in G2 or mitosis (Figure 3.2A). Compared with the 5.8 % of P~H3 positive cells in the whole population of IX-14 mutant neuroblasts (Figure 3.3A), in neuroblasts showing lamin Dm0 increase, 37.9% of them were P~H3 positive while 62.1% of them were P~H3 negative (Figure 3.3B). This resemble a significant accumulation of lamin in mitosis

It is logical to ask when might the lamin Dm0 increase happens? To answer this question, I co-stained wild type and *IX-14* mutant neuroblasts for lamin Dm0 and incorporated BrdU or cyclin B. BrdU is a thymidine analogue incorporated into DNA during replication that can be detected with an antibody, used it as an S-phase indicator. Cyclin B is synthesized in S/G2 phase and destroyed following the completion of chromosome attachment to the spindle. Since I can distinguish cells in G2 from those in mitosis using DAPI staining, I used Cyclin B as a G2 and early mitosis indicator. What I found was that 7.8% of wild type cells were BrdU positive after 2 hour BrdU incorporation, while only 2.3% of mutant cells were BrdU positive (Figure 3.3A). The lower percentage of BrdU incorporation indicates a cell cycle delay (other than S phase) in terms of pulse versus postion. But, replication defect could not be claimed in the *IX-14* mutant neuroblasts since it is possible that less cell enter into S phase due to the cell cycle delay. Lamin has been reported involved in DNA replication but at which stage of replication lamin play a role remains controversial. Ellis has reported lamin filament assembly is required for the formation but not for the maintenece of replication center (Ellis, Jenkins et al. 1997). On the other hand Spann and Goldman argue that the factors

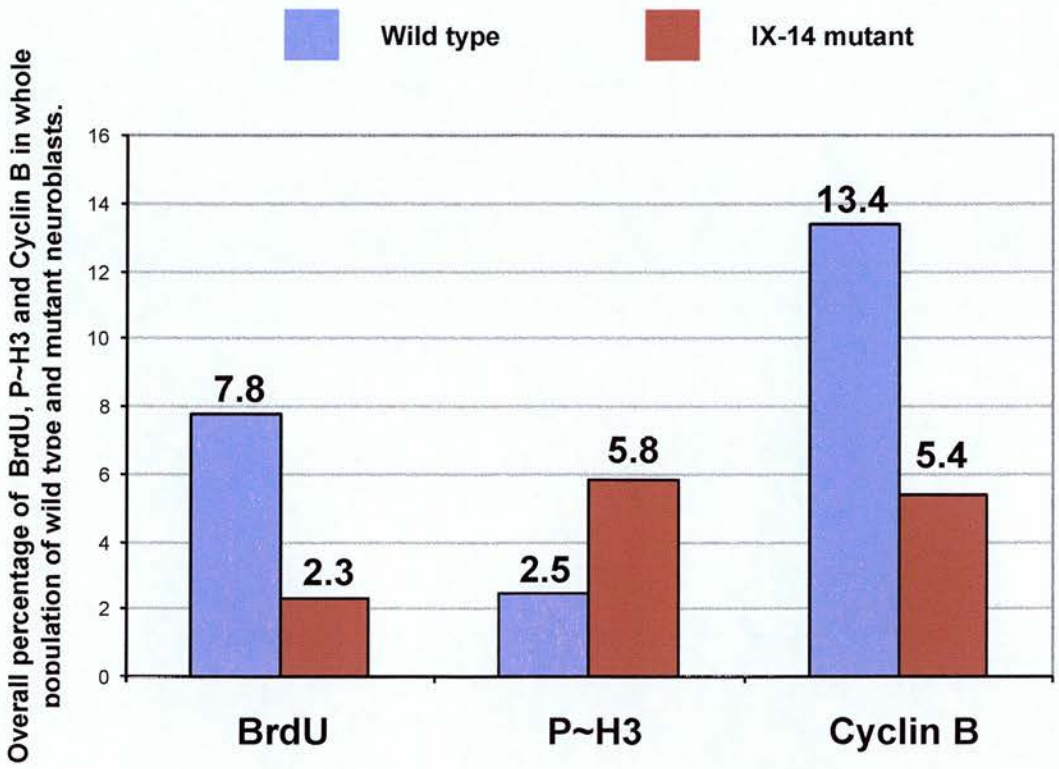

Figure 3.3A: Overall percentage of BrdU, P~H3 and Cyclin B in total population of wild type and mutant neuroblasts.

In the total population of wild type and *IX-14* mutant neuroblasts, a higher percentage of mutant cells (5.8% out of 1112) were in mitosis than in wild type (2.5% out of 627). A lower percentage of mutant cells (2.3% out of 1430) were in S phase than in wild type (7.8% out 2365). Mutant cells has less Cyclin B staining (5.4% out of 759) than wild type (13.4% out of 538).

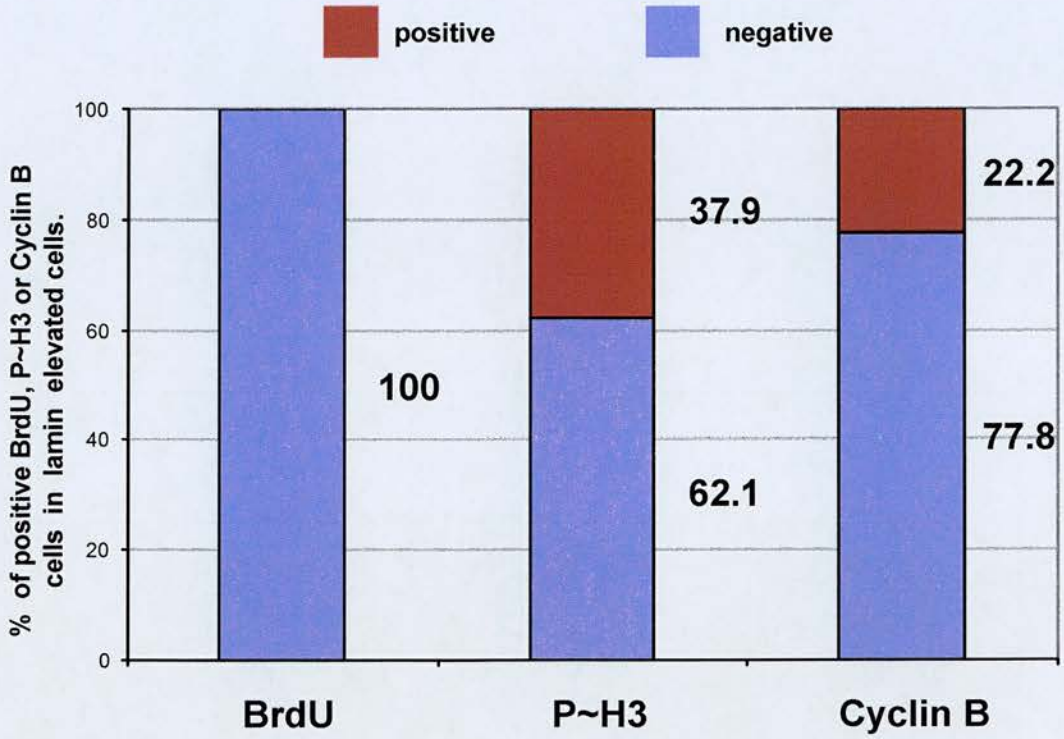

Figure 3.3B: When does the increase in lamin Dm0 occur.

Lamin Dm0 was co-stained with cell cycle markers such as P-H3, BrdU or Cyclin B on *IX-14* mutant neuroblasts to elucidate when the lamin Dm0 increase occurred. Out of all the cells sharing elevated levels of lamin Dm0 in *IX-14* mutant, 37.9% are P-H3 positive, 0% are BrdU positive, 22.2% are cyclin B positive.

necessary for initiation phase of DNA replication such as DNA polymerase and ORC was not affect when lamin organization was disrupted but factor necessary for DNA elongation like PCNA and RFC were affected instead (Spann, Moir et al. 1997). Figure 3.3C-D showed the BrdU and lamin Dm0 co-staining in wild type (3.2C) and mutant (3.2D) neuroblasts. And of all 33 BrdU-positive cells in the mutant, none of them had elevated lamin Dm0, and 2 lamin Dm0 elevated cells were BrdU-negative. Figure 3.2D shows images of lamin Dm0 and Cyclin B co-staining. Eighteen lamin Dm0 elevated cells were found, 4 of which were cyclin B-positive (22.2%) (Figure 3.3E). *IX-14* mutant neuroblasts have less Cyclin-B signal compare to wild type (Figure 3.3A and Brian McHugh, personal communication). So, the lamin Dm0 increase seems to take place after replication. Cyclin B negative cells with lamin accumulation could be in early G2, if not in G1 nor S phase.

3.4 Summary.

The first part of this chapter has reported the mitotic chromosome structure defect of *IX-14* mutants, the appearance differs from colchicine treated mitotic arrest in wild type cells. A periphery of loosely or poorly condensed chromatin is surrounding the hypercondensed chromosome in *IX-14* mutant. In the following part of this chapter, three nuclear envelope protein (lamin Dm0, otefin and lamin A/C) were seen to be elevated in level by both immunoblotting and immunofluorescence. Lamin Dm0 was further characterized by its increasing time. However, lamin increase does not seem to correlate with a particular stage in the cell cycle. Thus it is worthy to do histology to address which type of cell in *Drosophila* larvar brain has lamin increasing. The *Drosophila*

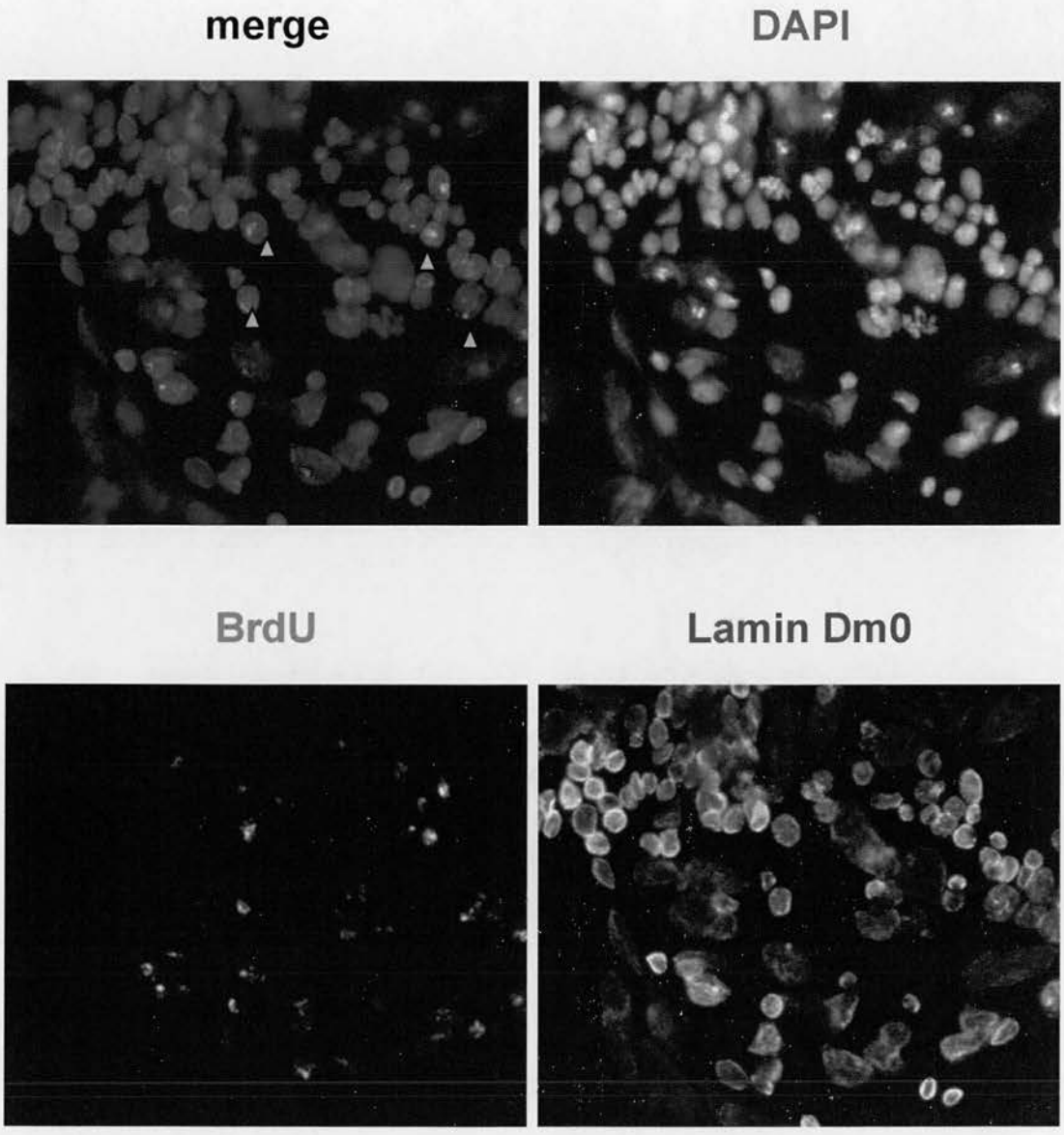

Figure 3.3C: Co-staining of BrdU with lamin Dm0 on wild type neuroblasts.

The arrow head indicates cells which are BrdU positive. DNA is in blue, BrdU is in red and lamin Dm0 is in green. I found 184 out of 2365 cells (7.8%) were BrdU positive after a 2 hours incubation in BrdU.

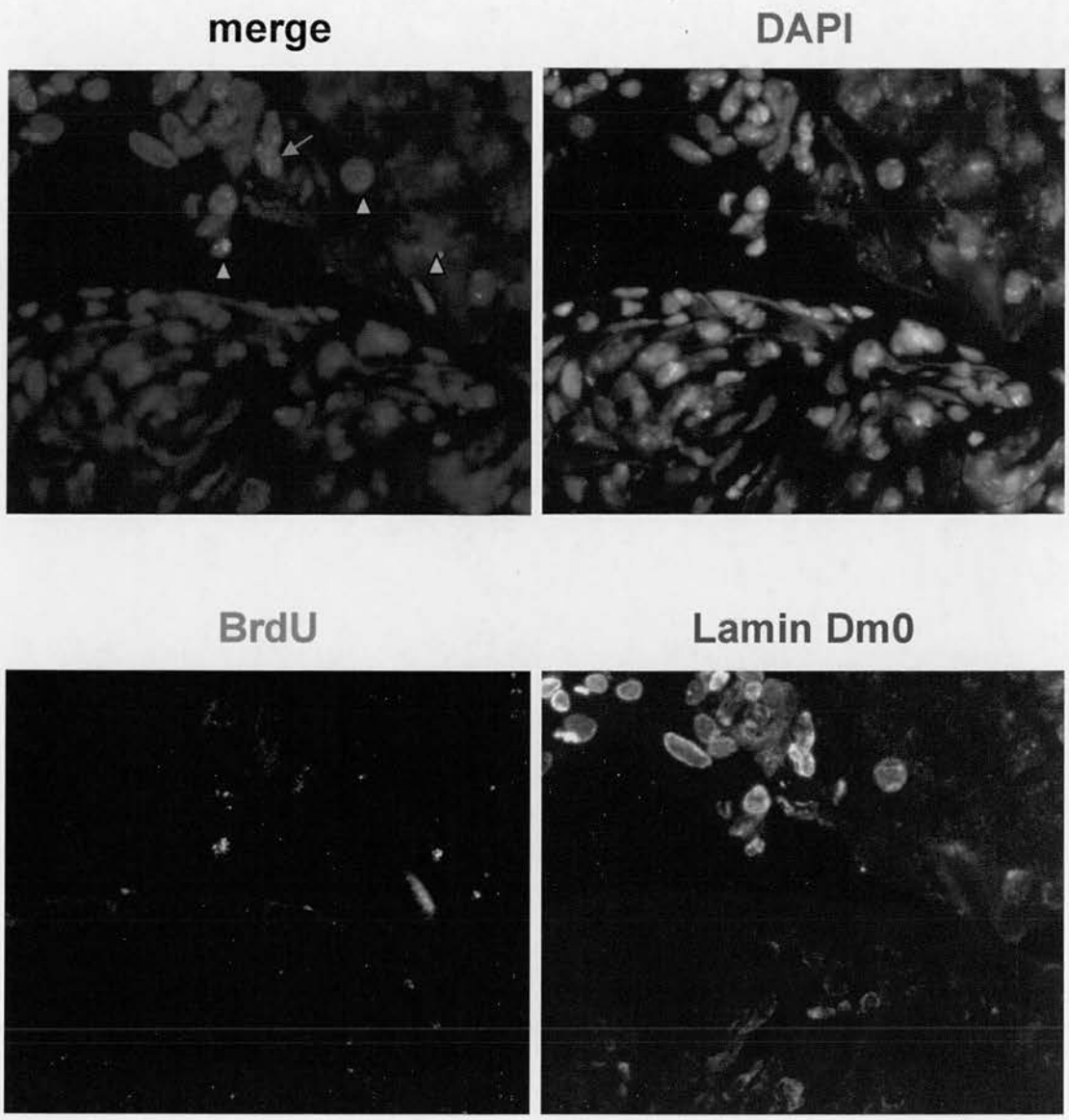

Figure 3.3D: Co-staining of BrdU and lamin Dm0 in *IX-14^{4Y7}* neuroblasts.

The arrow indicates cell which has increased lamin Dm0 staining and are BrdU negative while the arrowhead indicate cells positive for BrdU (have the normal level of lamin Dm0). I found 33 out of 1430 cells (2.3%) which had normal level of lamin Dm0 were BrdU positive. In this experiment, I only found two cells which had elevated lamin Dm0 levels, both of which were BrdU negative.

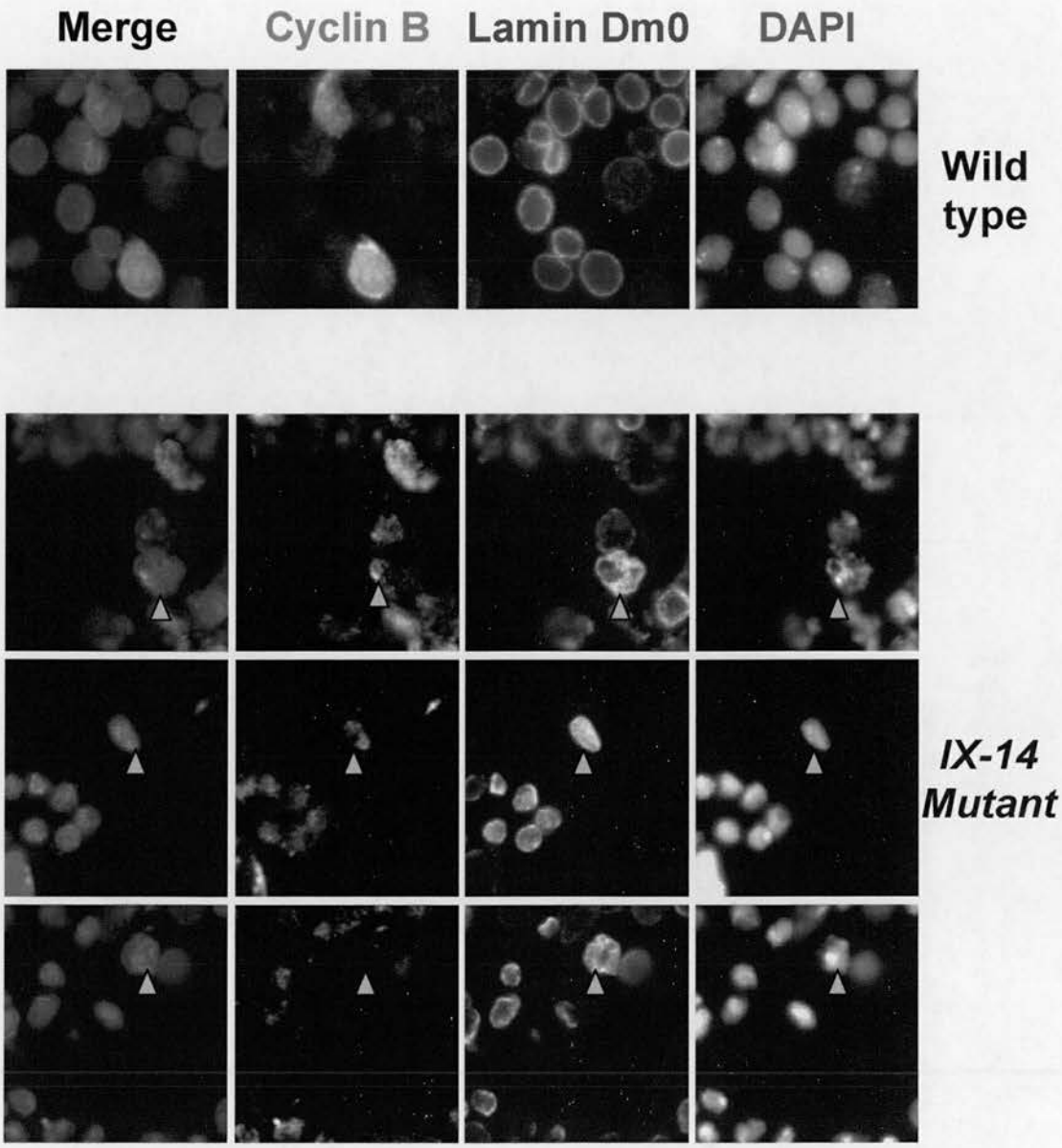

Figure 3.3E: Co-staining for Cyclin B with lamin Dm0 in wild type and mutant neuroblasts.

The arrowhead indicates lamin Dm0 elevated cells in the mutant. In the *IX-14* mutant images, the top panel shows lamin Dm0 increase cell in early mitosis indicated by the positive cyclin B signal and already condensed chromosome. The middle panel shows Lamin Dm0 increase cell in early G2 indicated by the positive cyclin B signal and interphase chromosome. The bottom panel shows lamin Dm0 increase cell in phase other than early G2 and mitosis indicated by the negative cyclin B signal. 22.2% (4/18) of lamin Dm0 increased cells were cyclin B positive. The percentage of cyclin B positive cells in the overall mutant neuroblasts was 5.4% (29 of 539).

larvar brain comprises cellular cortex that surrounds a central neuropile. The glials sheaths envelope the cortex surface that include surface glial, cortex glial and neuropile glial. The central neuropile is formed by two structural elements: long axon tracts and terminal axon tracts (Younossi-Hartenstein, Salvaterra et al. 2003). It would be interested to know whether lamin increase was limit to any of those histological cells.

However, there are limitations of using immunofuluorescence for studies of lamin level. 32 lamin proteins were in cross-section of lamin intermediate filament that assembly together under nuclear envelope. Not all epitopes are exposed to antibody. Lamin increase could be observed without actual increased in lamin level when 1) an increase of percentage of phosphorylated lamin (for example by CDK1-cyclinB or by protein kinase C) resulted in disaseembling of lamin from filaments which in turn exposing more epitopes to the antibody. 2) a lamin partner protein (such as LBR) is degraded that also result in increasing lamin epitope accessibility. The second possibility is less likely since the lamin staining was also more diffuse, which would be more consistent with the first possibility. Thus the immunoblot data is the only clear data to support lamin increase in this chapter.

Cyclin B was used to distinguish cell in G2 phase, interestingly I found its level is decrease in IX-14 mutant.

Chapter 4: Germ Cell Migration defect

4.1 Vasa staining of *IX-14* heterozygous embryos to exam germ cells.

IX-14 has a cytoplasmic localization pattern indicated by antibody staining as ring-like structures in HeLa cells. In migrating macrophages stained with the IX-14 antibody, the majority of the protein was observed at the leading edge of migrating macrophages. This indicates that IX-14 might have a role in cell migration in addition to its role in mitosis. In order to verify this hypothesis, migrating cells in developing *Drosophila* embryos was examined. The best candidate migrating cells in *Drosophila* embryos are the pole cells, the precursor cells of the gonads. Furthermore, gonads were previously not observed in third instar larvae of $IX\text{-}14^{1}/IX\text{-}14^{1}$ and $IX\text{-}14^{4Y7}/IX\text{-}14^{4Y7}$ which may indicate a defect in germ cell migration. Pole cells, the progenitors of the germ line, form at the posterior end of *Drosophila* embryo from a region of specialized cytoplasm rich in ribonucleoprotein particles termed polar granules (Mahowald 1968). The posterior polar plasm, germinal plasm, is essential for pole cell formation since transferring this particular kind of cytoplasm to a new region of the embryo results in an induction of cells functioning as primordial germ cells in these regions (Illmensee, Mahowald et al. 1974). The Vasa protein is localized to the posterior pole of the *Drosophila* embryo and is a component of the polar granules. The sequence of the Vasa protein suggests that it may

be an RNA binding helicase involved in the function of the posterior determinant system. Vasa protein is present in *Drosophila* germ cells throughout development (Hay, Ackerman et al. 1988a) (Hay, Jan et al. 1988b), thus have been widely used in many animals as germ cell markers (Matova and Cooley 2001). Absence of Vasa during embryogenesis leads to abdominal defects and the failure to form pole cells (Schupbach and Wieschaus 1986). A rabbit polyclonal antibody has been raised against amino acid 16-433 of the Vasa protein (Lasko and Ashburner 1990).

Drosophila embryo development could be divided into 16 stages according to their morphology (Roberts, Grigliatti et al. 1986) (Hartenstein 1993). Canton S (wild type), *IX-14*^{4Y7}*/TM6B* flies were collected overnight to obtain all stages of embryonic development. Figure 4.1A-4.1E shows wild type and *IX-14* mutant embryos from stage 1 to stage 14 stained with DAPI and the Vasa antibody. All the timings mentioned below are the approximate time of growth taken to reach each stage at room temperature (22°C). In stage one (0-15 min), the embryo has just been freshly laid and the cytoplasm of the embryo is homogeneous. In stage two (15 min to 1 h and 20 min), more nuclei were visible by DAPI staining with the early rounds of syncytial divisions occur. A cap of clear cytoplasm becomes visible at the posterior pole. In stage three (1 h 20 min to 1 h 30 min), more nuclei are present from further divisions, and the nuclei migrate to the cortex of the embryo. Then the pole cells stand out from the surface of the posterior pole of the embryo. In stage four (1 h 30 min to 2 h 30 min), syncytial division is continuous and the cortical cytoplasm become thicker and distinct from the underlying yolk. In stage five (2 h 30 min to 3 h 15 min), the syncytial rounds of division finish. The nuclei elongate and cell membranes move down between adjacent nuclei to start cellularization of the

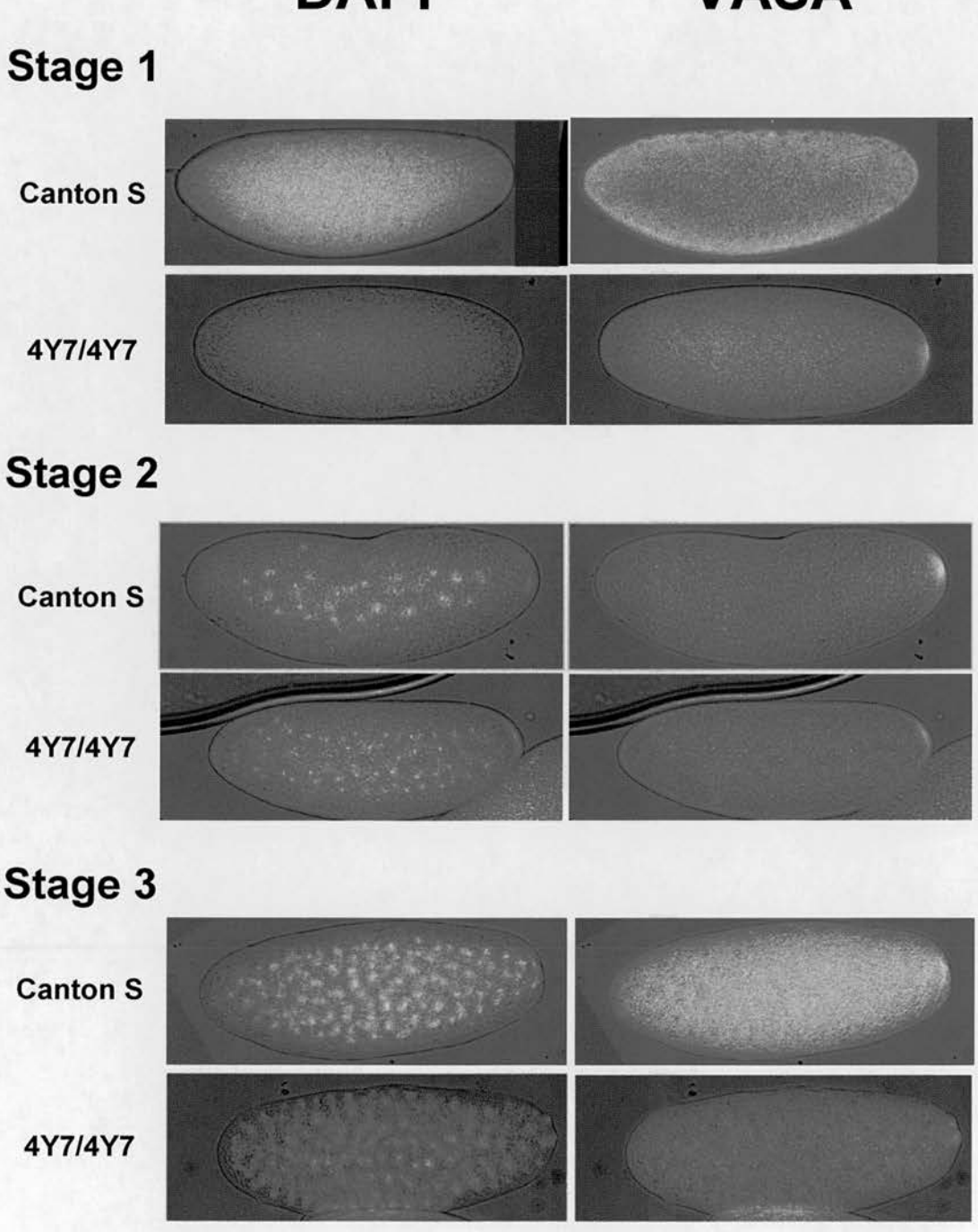

Figure 4.1A: Image of wild type and IX-14 homozygous mutant embryos (Stage 1 to Stage 3)

Wild type and *IX-14* mutant embryos from stage 1- stage 3 stained with DAPI and VASA. Germ cells labelled by VASA are initially formed during stage 3 at the posterior pole of the embryo.

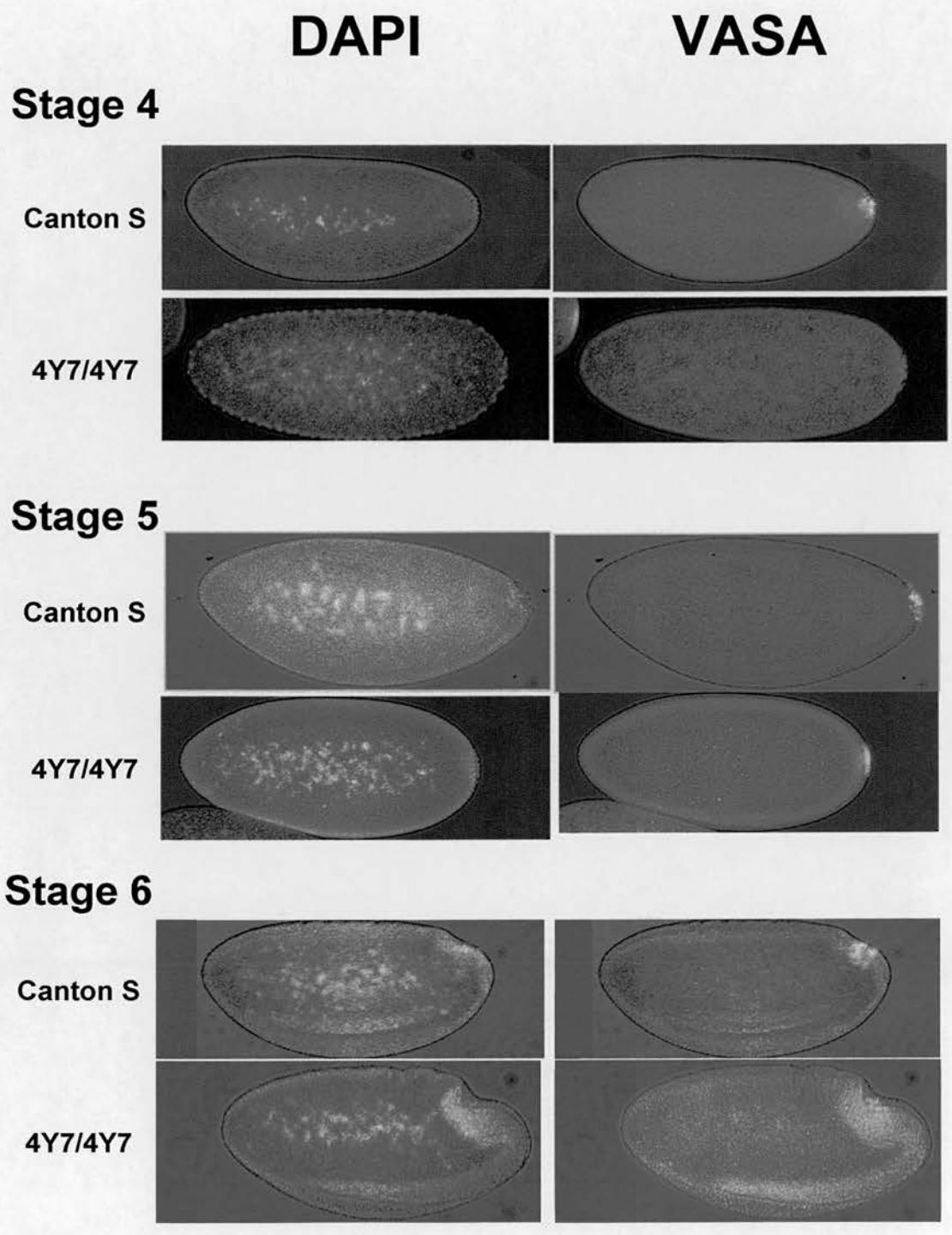

Figure 4.1B: Image of wild type and IX-14 homozygous mutant embryos (Stage 4 to Stage 6)

Wild type and *IX-14* mutant embryos from stage 4- stage 6 stained with DAPI and VASA. Germ cells labelled by VASA forming an obvious cluster of 34-37 cells by stage 5. From stage 6, germ cells move with the midgut invagination.

embryo. In stage six (3 h 15 min to 3 h 35 min), gastrulation begins as soon as the cells on the ventral side of the embryo complete cellularization. A ventral furrow forms as a longitudinal cleft along the ventral midline of embryo. Pole cells migrate dorsally at this stage. In stage seven (3 h 35 min to 3 h 45 min), the posterior midgut is parallel to the long axis of the embryo and the pole cells are migrated to the dorsal side of the embryo. In stage eight (3 h 45 min to 4 h 30 min), the posterior midgut invagination is still at the posterior dorsal region of the embryo, carrying poles cells into the lumen of the midgut. In stage nine (4h 30 min to 5 h 10 min), the gut opening has reached the head region about two-thirds of the embryo length. Pole cells were still stayed in the lumen of the posterior midgut rudiment. In stage ten (5 h 10 min to 6 h 50 min), foregut invagination occurs, and invagination moves posteriorly. Pole cells are still associated with the posterior midgut invagination. In stage 11 (6 h 50 min to 9 h), the defined segments of the developing embryo are visible, the anterior midgut has flattened and grown along the ventral germ band. The posterior midgut moves along the dorsal side of the germ band. Pole cells begin to pass through the posterior midgut and become located between the dorsal surface of the posterior midgut rudiment and the mesoderm. In stage 12 (9 h to 10 h 30 min), the germ band contracts, and the posterior gut opening moves posteriorly. The pole cells begin to form clusters on either side of the embryo. This cluster is in close to a set of mesoderm cells that will later give rise to the gonad sheath. In stage 13 (10 h 30 min to 11 h 30 min), the germ band is completely retracted. Three Thoracic (T) segments and nine Abdominal (A) segments can be observed easily. The pole cells form as two elongated clusters on either side of the embryo. In stage 14 (11 h 30 min to 13 h), head

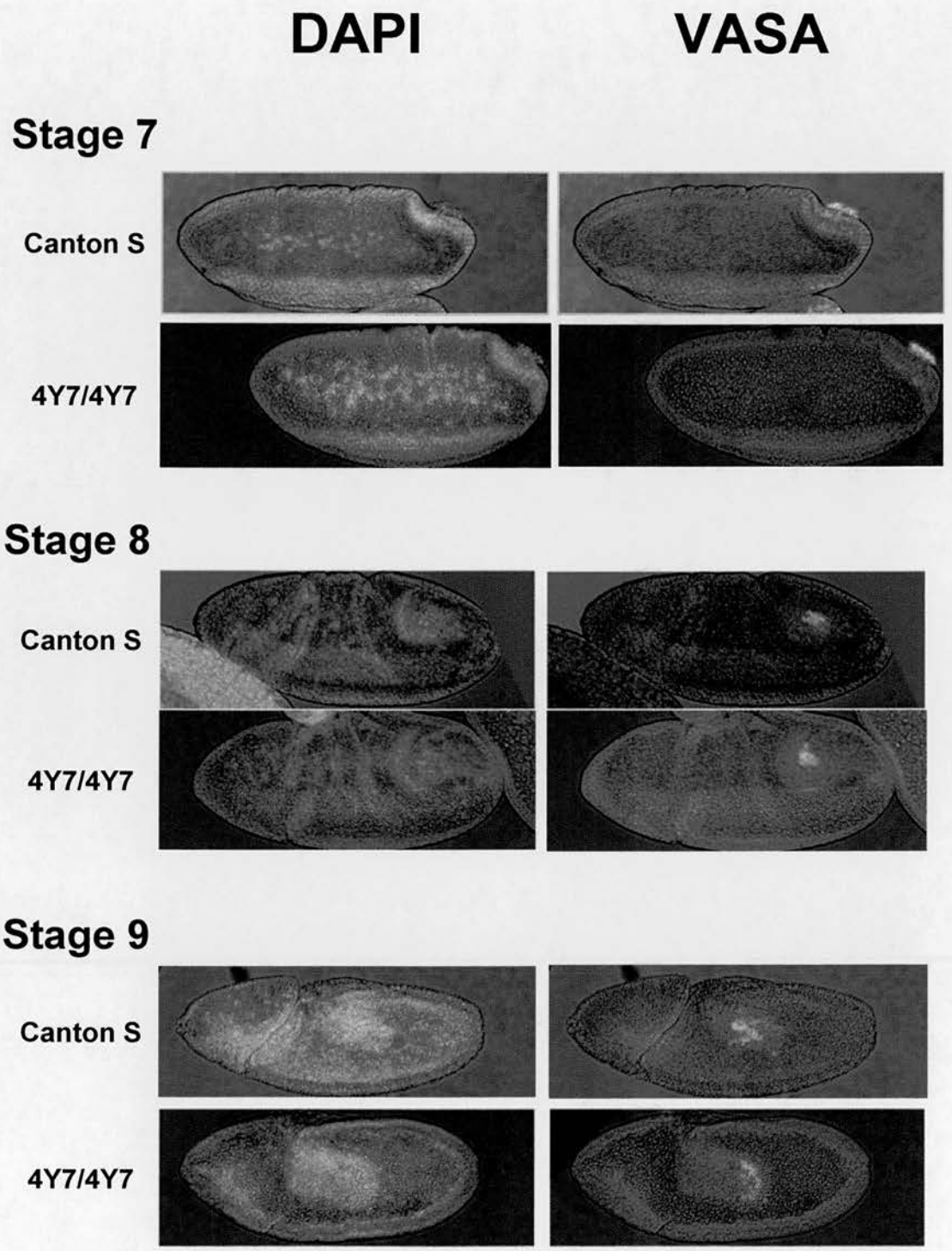

Figure 4.1C: Image of wild type and IX-14 homozygous mutant embryos (Stage 7 to Stage 9)

Wild type and *IX-14* mutant embryos from stage 7- stage 9 stained with DAPI and VASA. Germ cells labelled with VASA antibody migrate into the lumen of the posterior midgut rudiment at stages 8 and 9.

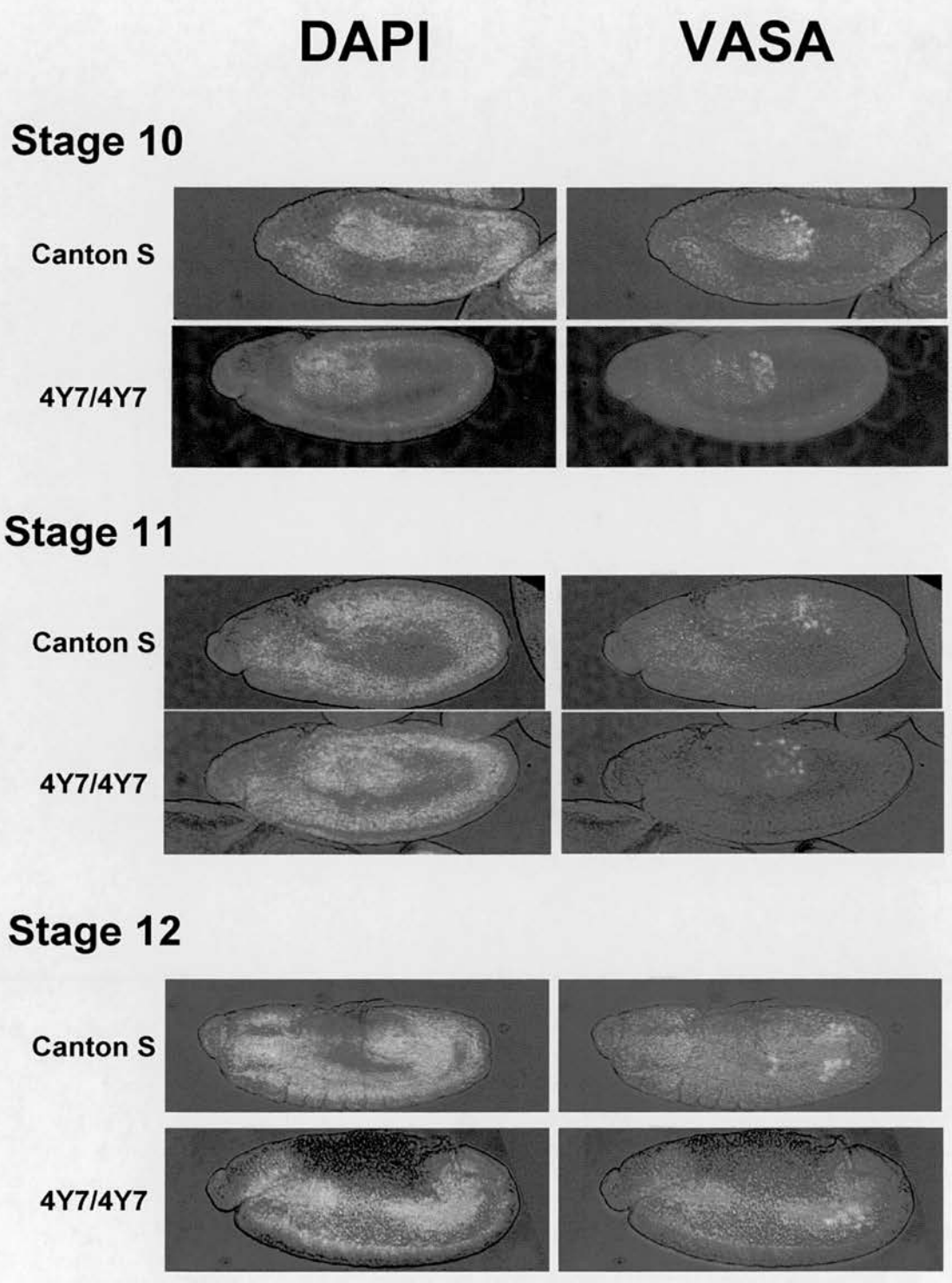

Figure 4.1D: Image of wild type and IX-14 homozygous mutant embryos (Stage 9 to Stage 12)

Wild type and *IX-14* mutant embryos from stage 10- stage 12 stained with DAPI and VASA. In stage 10, germ cells begin to migrate out of the midgut rudiment while in stage 11 they migrate dorsally. At stage 12 and, the pole cells begin to cluster on either side of the embryo.

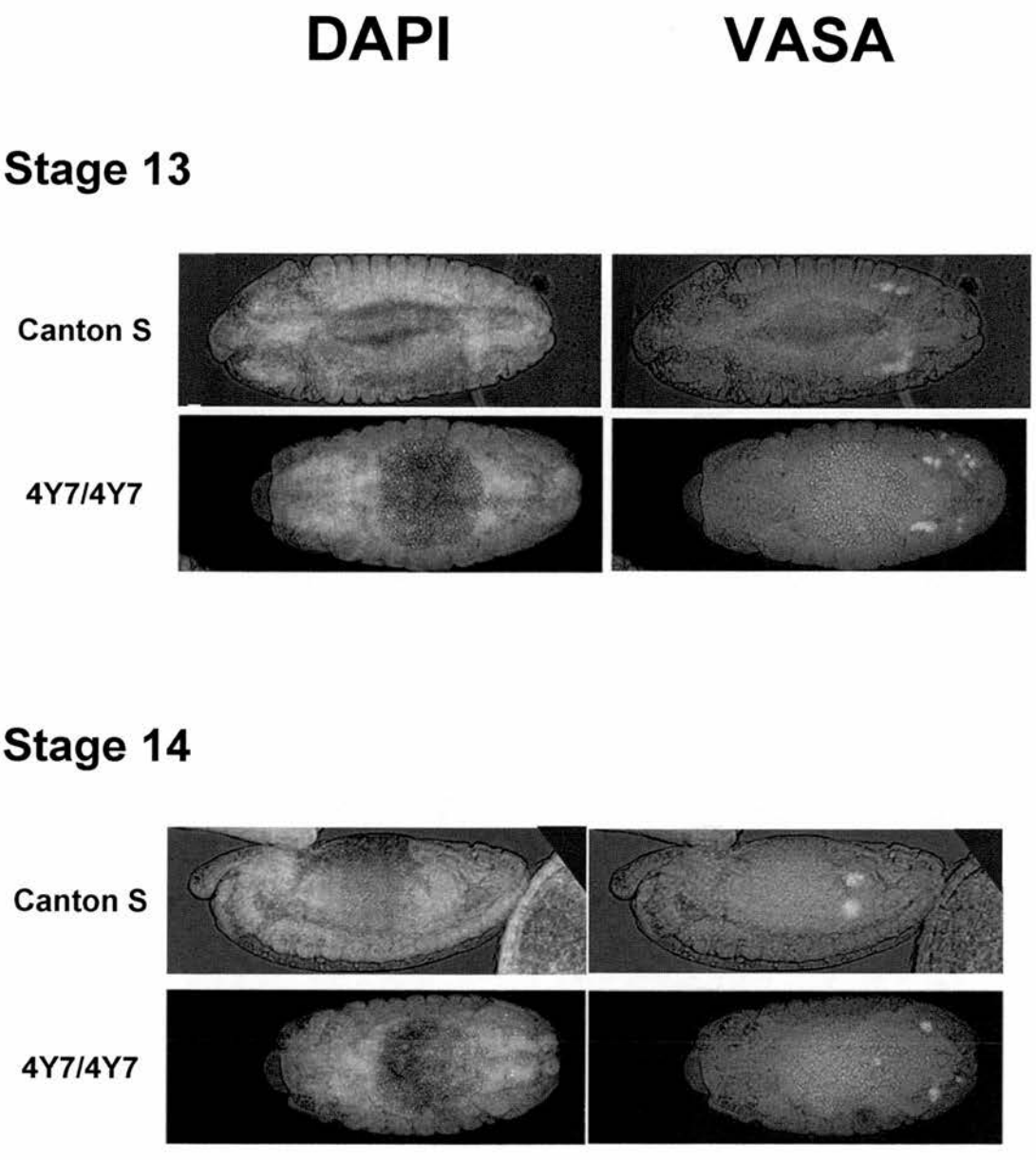

Figure 4.1E: Image of wild type and IX-14 homozygous mutant embryos (Stage 13 to Stage 14)

Wild type and *IX-14* mutant embryos from stage 13- stage 14 stained with DAPI and VASA. At stage stage 13, the pole cells form an elongated cluster on either side of the embryo. Finally germ cells and surrounding mesodermal sheath cells form the gonads at stage 14.

involution can be observed and the pole cells and surrounding mesodermal sheath cells form the gonads.

Embryos laid by *IX-14^{4Y7}/TM6B* heterozygotes will be a mixture of the following genotypes: *IX-14^{4Y7}/IX-14^{4Y7}* (3rd instar lethal) , *IX-14^{4Y7}/TM6B* (viable), *TM6B/TM6B* (embryonic lethal). These embryos were still normal compared to wild type until some embryos show defects in pole cells migration at stage 12-13, the time when the pole cells had passed through the midgut rudiment and on their way to assemble as clusters on each side of the embryos. IX-14 mutant embryos could form very small gonads finally (Figure 4.1A-4.1E).

In order to obtain an enriched population of the developmental stage when the *IX-14/TM6B* embryos show a defect, the embryos of wild type and *IX-14^{4Y7}/TM6B* heterozygous flies were collected at room temperature for 3 hours. The adult files were removed and embryos were then aged for 9-12 hours. Thus allowed more specific characterisation of the defect at stage 12-13. As shown in Figure 4.1F, all the stage 12-13 wild type embryos (242 in total) form clusters of pole cells on each side of the embryos. On the other hand, 7 out of 139 (5%) embryos laid by *IX-14^{1}/TM6B* heterozygous flies and 7 out of 80 (8.75%) embryos laid by *IX-14^{4Y7}/TM6B* heterozygous flies fail to form the cluster of pole cells. Poles cells were diffusely spread in the embryo without forming any characteristic clusters. This is an indication that homozygous *IX-14* mutant embryos may have a pole cell migration defect. To rule out the possibility that the defect is due to a mutation on the balancer chromosome TM6B, embryos from *Poly/TM6B* were collected under the same conditions as above and stained with Vasa antibody and DAPI. As

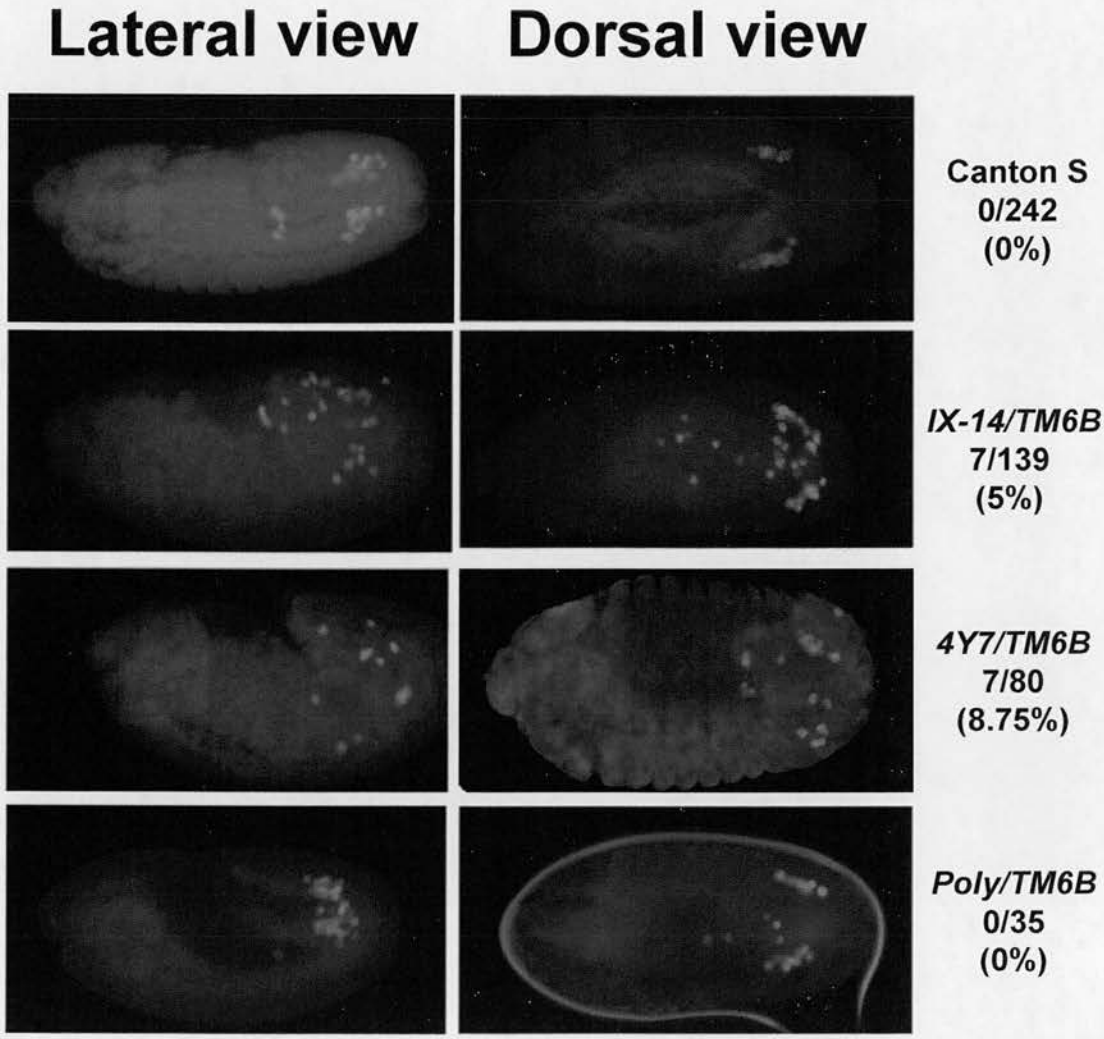

Figure 4.1F: Migration defect of embryos of two heterozygous *IX-14* alleles.

Images shown are lateral or dorsal views of stage 12-13 embryos. In wild type, germ cells form two clusters on either side of the embryo. In the original *IX-14* heterozygous allele and the P element *IX-14* heterozygous allele, there is a noticeably higher percentage of embryos with abnormal germ cell migration. These cells do not form two clusters as observed in wild type. As a control, another mutant over TM6B balancer *Poly/TM6B* does not have this germ cell migration defect which indicates that the defect is specific to the *IX-14* mutation.

expected, the pole cells in all the 35 *Poly/TM6B* embryos migrate efficiently to form the two clusters.

4.2 Migration defect of homozygous *IX-14* embryos.

To specifically select homozygous *IX-14* mutant embryos, *IX-14^{4Y7}/TM6B* was crossed to *D/TM3p [KrGFP]* (D stand for Dichaete) to establish a *IX-14^{4Y7}/ TM3p [KrGFP]* line. *IX-14^{4Y7}/ IX-14^{4Y7}* homozygous mutant embryos can be selected by absence of a GFP signal using a fluorescence stereo microscope.

Crosses were performed at room temperature. In order to rebalance IX-14 lines with a fluorescent balancer chromosome, virgin female *IX-14* allele flies collected as soon as possible after eclosion were mated with male TM3,KrGFP balance flies as follows:

♀ *IX-14^{1}*/TM6B X *D*/TM3,Kr-GFP ♂

↓

IX-14^{1}/TM3,Kr-GFP *IX-14^{1}/D* TM6B/TM3-KrGFP *D*/TM6B

Virgin female and male of IX-14^{1}/TM3,Kr-GFP were selected using dominant banlancer markers to establish lines

♀ *IX-14^{1}*/TM3,Kr-GFP X *IX-14^{1}*/TM3, Kr-GFP ♂

IX-14^{4Y7}/TM3,Kr-GFP was created following the same scheme. Homozygous *IX-14^{1}/IX-14^{1}* and *IX-14^{4Y7}/IX-14^{4Y7}* embryos were isolated based on a lack of GFP signal and hence absence of balancer. Homozygous embryos collected, fixed and stained with Vasa antibody and DAPI after. No migration defects were observed in the 24 GFP

positive embryos (*IX-14^{4Y7}/ TM3p [KrGFP]* and *TM3p [KrGFP] / TM3p [KrGFP]*) while 6 out of 23 (26%) GFP negative embryos (*IX-14^{4Y7}/IX-14^{4Y7}*) showed pole cell migration defects (Figure 4.2 A). Figure 4.2 B is the dorsal view of embryos showing the defect from a developmental perspective view. Compared to wild type, homozygous mutant embryos are still normal at stage 10-11 when germ cells are passing through the midgut, but germ cells failing to migrate and form clusters at either side of the embryo are observed in stage 13.

4.3 Examination of the somatic cells of the gonad.

In *Drosophila* gonadal development, the mesodermal origin SGP cells (somatic gonadal precursor cells) begin to associate with germ cells when the germ cells are passing through the midgut and mesoderm until they together form the gonad (Brookman, Toosy et al. 1992) (Boyle and DiNardo 1995). In order to rule out that the gonad forming defect was due to the SGP cells instead of the germ cells themselves, SGP cells were observed labelling by EYA antibody. In *Drosophila*, EYA is encoded by the *Drosophila* eyes *absent* gene which is required to promote the differentiation or survival of eye progenitor cells anterior to the morphogenetic furrow. Moreover, EYA biologically synergizes ectopic eye formation in conjunction with eyeless (Bonini, Bui et al. 1997). In addition to its role in eye development, EYA plays a role in the formation of the gonad in the developing embryos. An additional allele of *eyes absent*, *clift*, is an embryonic lethal mutation with defects in head development. (Boyle, Bonini et al. 1997). Two versions of EYA cDNAs are present in *Drosophila* which differ at the N-termini (~450 bp in type I cDNA and ~300 bp in type II cDNA) but the about 2800 bp of their C-termini are shared.

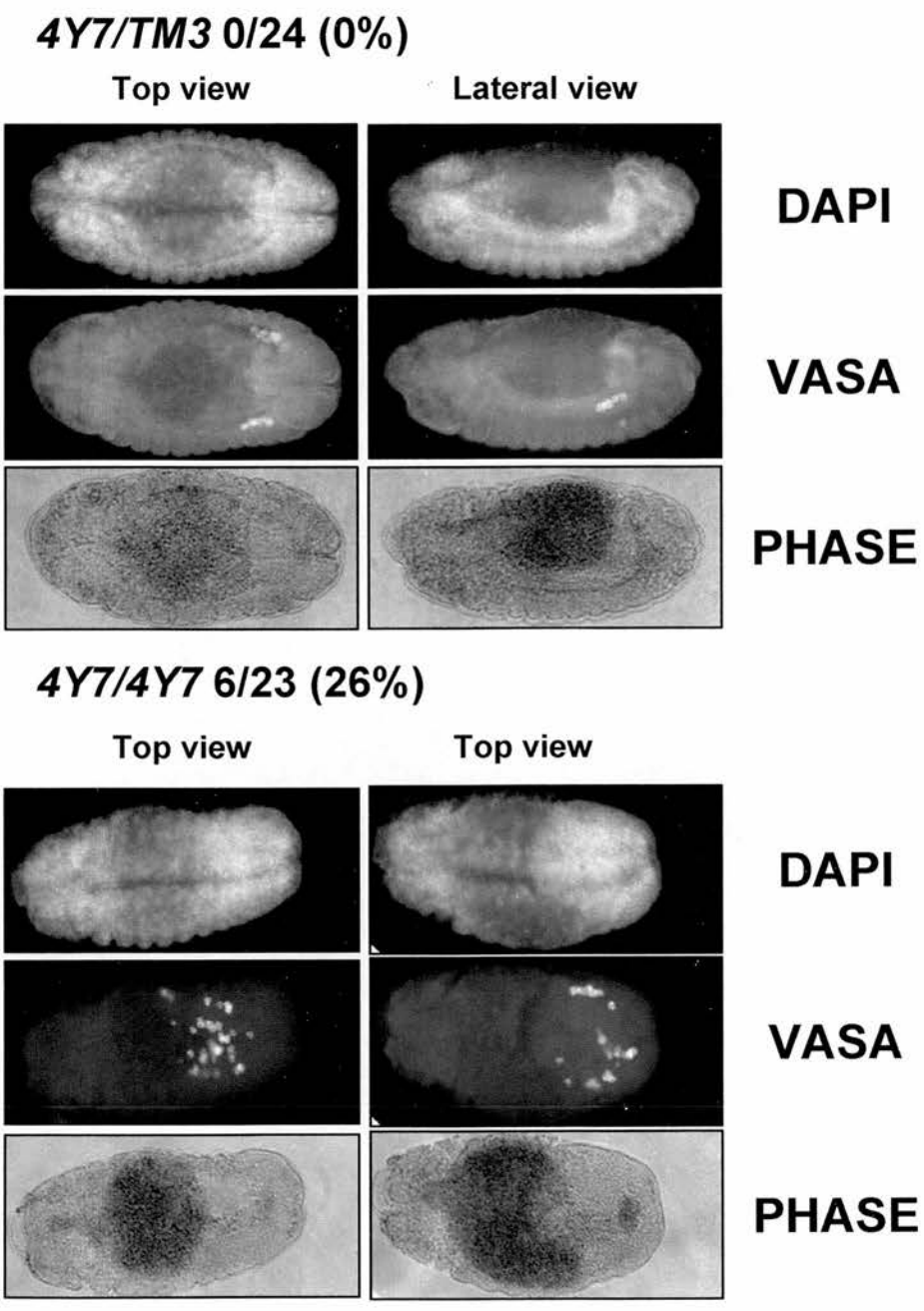

Figure 4.2A: Migration defect of *4Y7/4Y7* embryos.

IX-14 mutant files were crossed to a GFP balancer line to allow selection of homozygous embryos. Germ cell migration was normal in all stage 12-13 heterozygotes, however, a higher percentage (26%) of selected homozygous mutants displayed germ cell migration defects.

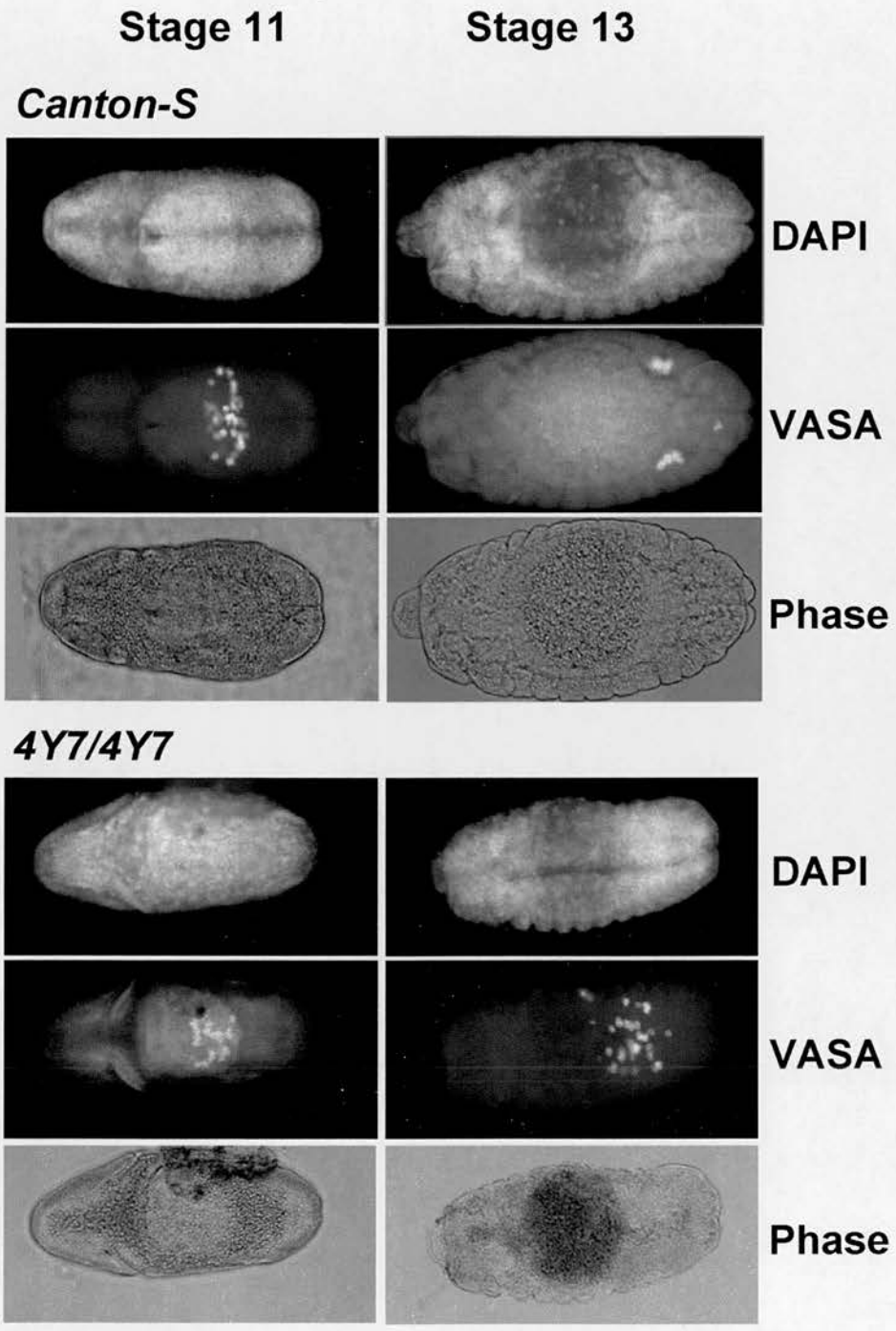

Figure 4.2B: Migration defect of *4Y7/4Y7* embryos in stage 11 and stage 13.

Embryos are viewed from the top and stained for DNA, VASA and shown in conjunction with the phase image. In wild type embryos, germ cells were observed passing through the midgut in stage 11. By stage 13, they have formed two clusters on either side of the embryo. In the selected homozygous *IX-14 mutant*, the germ cells show no defect in migrating out of the midgut in stage 11, but they fail to form distinct clusters on either side of the embryo by stage 13.

The EYA antibody is a mouse polyclonal anitserum raised against the carboxy-terminal 551 amno acids of the cDNA that is common to both type I and type II cDNAs (Bonini, Leiserson et al. 1993).

The images shown in figure 4.3A are embryos double stained with EYA and Vasa. Wild type embryos form gonads on both lateral sides by stage 14, and the tight association between somatic cells and germ cells inside the gonad can be observed under high magnification. Conversely, *IX-14*^{4Y7}/ *IX-14*^{4Y7} homozygous mutant embryos fail to form proper gonads by the same stage. Embryos viewed at higher magnification show that the SGP cells still form a sheath around the gonads, but there are no germ cells associated with them. This is consistent the previous observation that showed SGP cells can cluster into a gonad normally in the absence of germ cells (Brookman, Toosy et al. 1992).

4.4 Summury.

Consistent with a role for IX-14 in migration in human macrophages, its *Drosophila* homologue plays a role in migration as well. This was verified by examining migrating germ cells in *Drosophila* embryos. Some *IX-14* homozygous mutant embryos fail to form clusters on both sides of the embryos in stage 12-13, instead germ cells lose their way and become dispersed in embryos. This migration defect had not been observed in wild type embryos nor in embryos from other mutations over TM6B, such as *Poly/TM6M.* The reason not all homozygous embryos exhibit germ cell migration defect could because that I categorise some gonad of the homozygous mutant with lagging germ cells (Figure 4.1, stage 13 *4Y7/4Y7)* as normal since it does happen in wild type. Our

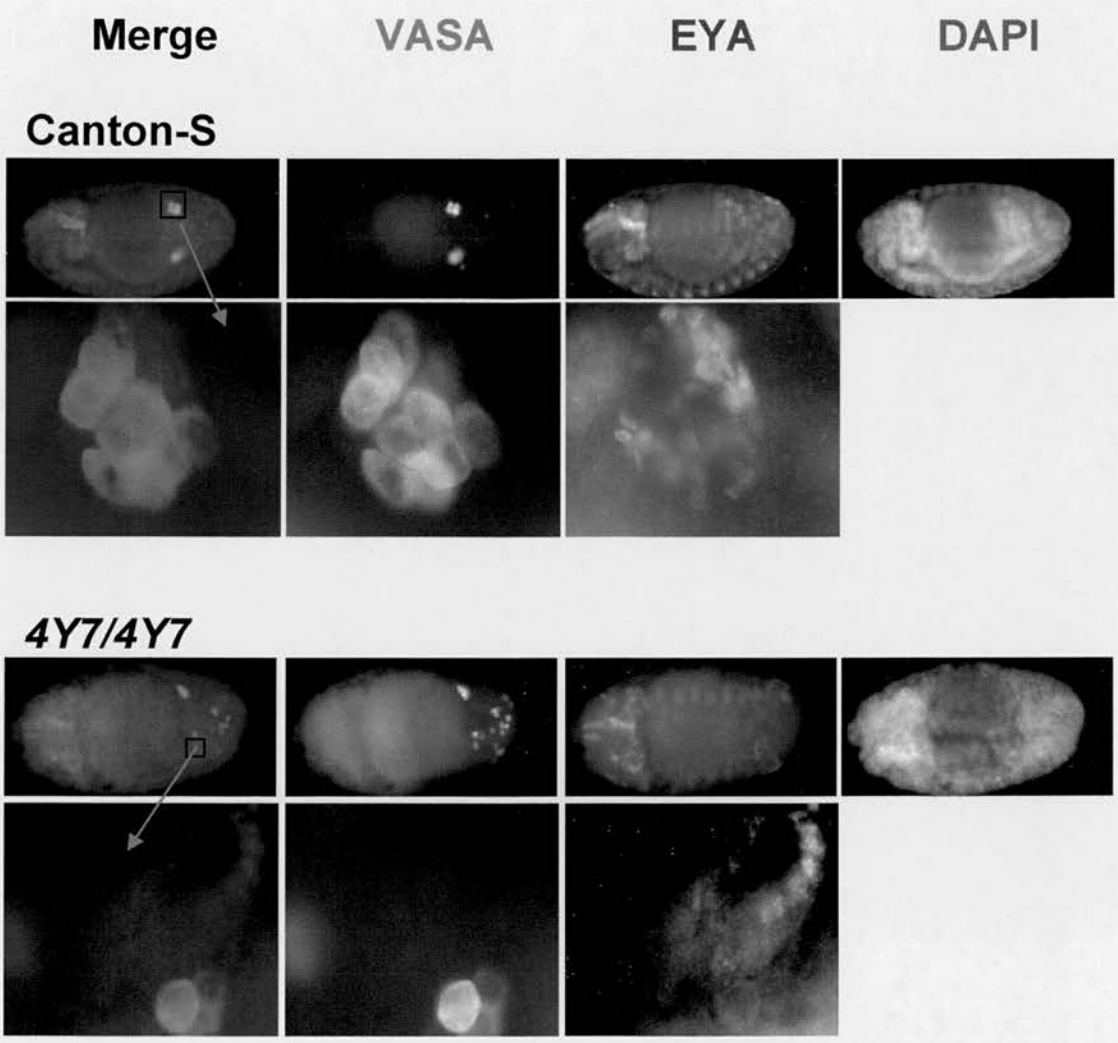

Figure 4.3A: Gonad defect in *4Y7/4Y7* was not due to somatic cells in gonad.

Dorsal view of stage 14 embryos stained for DNA, VASA and EYA. The top panel shows a wild type embryo which formed gonads on both sides. Higher magnification image shows the germ cells labelled by VASA antibody were tightly associated with the surrounding somatic cells labelled by EYA antibody. The bottom panel shows a *IX-14* mutant embryo with germ cell migration defects and with no gonads on either side. Higher magnification image shows that the surrounding somatic cells are still able to form a sheath around the gonads but there was no germ cells associated with the structure.

coordinator, Dr Ivan Clerk, has made a movie confirmed this germ cell migration defect. In his movie, there are some lagging germ cells appear in wild type gonad, but it finally assemble into the gonad. This is different from the homozygous mutant while the lagging germ cells could never assemble into the gonad. The possibility that gonads fail to form because of abnormality in somatic cells around the gonad has been eliminated since the somatic cells can still form the gonad sheaths even without germ cells associated with them. Mutants of *Abdominal A*, *Abdominal B* and *clift* affect somatic gonadal precursor cells formation from mesoderm and affect germ cells migration (Boyle and DiNardo 1995; Boyle, Bonini et al. 1997). The possibility that germ cells failing to migrate to gonad is due to the interaction defect between somatic cells is less likely. E-cadherin is presenct in both somatic cells and germ cells and is essential for proper germ cell-soma interaction during gonad morphogenesis. *E-cadherin* mutant shows different germ cell migration defect from *invadolysin* mutant since the germ cells still migrate to the gonad but do not associate with somatic cells in *E-cadherin mutant* while germ cells were completely lost in *invadolysin* mutant (Jenkins, McCaffery et al. 2003). Although germ cells travel a long way, they finally fail to migrate to the right place during the last stages of migration. Invadolysin could passively affect germ cell migration by affecting germ cells response to the migration signal during stage 12/13. Mutants such as *tre1* (trapped in endoderm), *wunen* and *wunen 2* were all defined as mutantion affecting germ cell migration while the germ cells migrate a long way but fail to target to the right place (Santos and Lehmann 2004). Therefore, we can conclude that IX-14 have a migration role in *Drosophila* in addition to its mitotic role. Being a good model for visualizing cell migration *in vivo*, *C. elegans* bear the advantage of limited morphological variability and

a translucent body. There is no experimental report that the *C. elegans* homologue of invadolysin, Y43F4A.1a, is involved in cell migration. Thus, this is the first time invadolysin homologous protein was reported involved in cell migration.

Chapter 5: Protease analysis

5.1 DmIX-14 cleaves Lamin Dm0 *in vitro*.

Several nuclear envelope proteins including lamin Dm0, lamin A/C and otefin were increased in the neuroblasts of 3rd instar larval extracts of *IX-14* homozygous animals as seen by immunoblotting and immunofluorescence. Since the IX-14 gene encodes a protease, these experiments suggest that lamin Dm0 or other nuclear envelope proteins might be substrates of DmIX-14. Previous work demonstrated the protease activity of DmIX-14 using an zymogram gel in protease assay (McHugh, Krause et al. 2004). Brain extracts from *DmIX-14* mutant flies were unable to cleave the substrate casein in this system. Therefore, an *in vitro* protease assay was developed to test this hypothesis that lamin Dm0 might be a substrate of DmIX-14.

The RTS 500 *E.coli* Circular Template *in vitro* transcription and translation kit (Roche) (Circular template kit) was used to express proteins. Reactions were set up with the following cloned gene vectors: DmIX-14 in pOT2 vector, lamin Dm0 in T7-7 vector, GFP in pIVEX vector or C-terminal HsIX-14 (amino acid: 331-665) in pRSET (containing the his-tag). The transcription and translation extracts were then incubated at 30°C for one hour to express the proteins. An aliquot with no added vector was incubated at the same condition as a control. *In vitro* expressed GFP, lamin Dm0 and C-terminal DmIX-14 proteins were eletrophoresed on 4%-12% gradient protein gels and transferred to nitrocelluose membranes. The membranes were then incubate with the appropriate GFP, lamin Dm0 or His antibodies. All proteins (lamin Dm0, DmIX-14 and GFP) were

expressed at the predicted size (Figure 5.1A). These protein bands were not observed in control no vector lanes.

Protease analysis was performed when DmIX-14 and lamin Dm0 were mixed *in vitro* and incubated under the following different conditions. DmIX-14 (10 μl) and lamin Dm0 (5 μl) expressed *in vitro* were incubated together at 29°C for 15 minutes. In some cases, the incubation included $ZnCl_2$, $ZnSO_4$ or the zinc chelator 1,10-phenanthroline (OPA). After the incubation, sample were boiled at 100°C for 5 minutes in SDS-PAGE sample buffer. Samples were loaded on a 12% protein gel to better separate smaller molecular weight proteins. Then the gels were transferred to nitrocelluose membranes which were blotted with monoclonal antibody against the N-terminal region of lamin Dm0 (Figure 5.1B). Although high background was present in this blot, no band of the expected size for lamin Dm0 (lane 2) was observed in the DmIX-14 lane only (lane 1) which indicates specificity of the anti-lamin antibody. Adding DmIX-14 to lamin Dm0 only (lane 3) did not induce change in lamin Dm0. However, protease activity was appear when $ZnCl_2$ was added to a final concentration of 1 mM (lane 4) or 10 mM (lane 5), or $ZnSO_4$ was added to a final concentration of 1 mM (lane 6) or 10 mM (lane 7). OPA is a general chelator iron of zinc and other divalent cations. It was previously reported to inhibit the cleavage of synthetic peptide substrates of gp63, the paralogue of IX-14, at millimolar concentrations (Bouvier, Schneider et al. 1990). OPA was added with $ZnCl_2$ or $ZnSO_4$ to determine if it could inhibit the activity of DmIX-14. As expected, lamin Dm0 cleavage by DmIX-14 was inhibited by the addition of OPA to a final concentration of 1 mM, indicated by the strong signal of lamin Dm0 observed in lane 8. In attempt to enhance the cleavage of

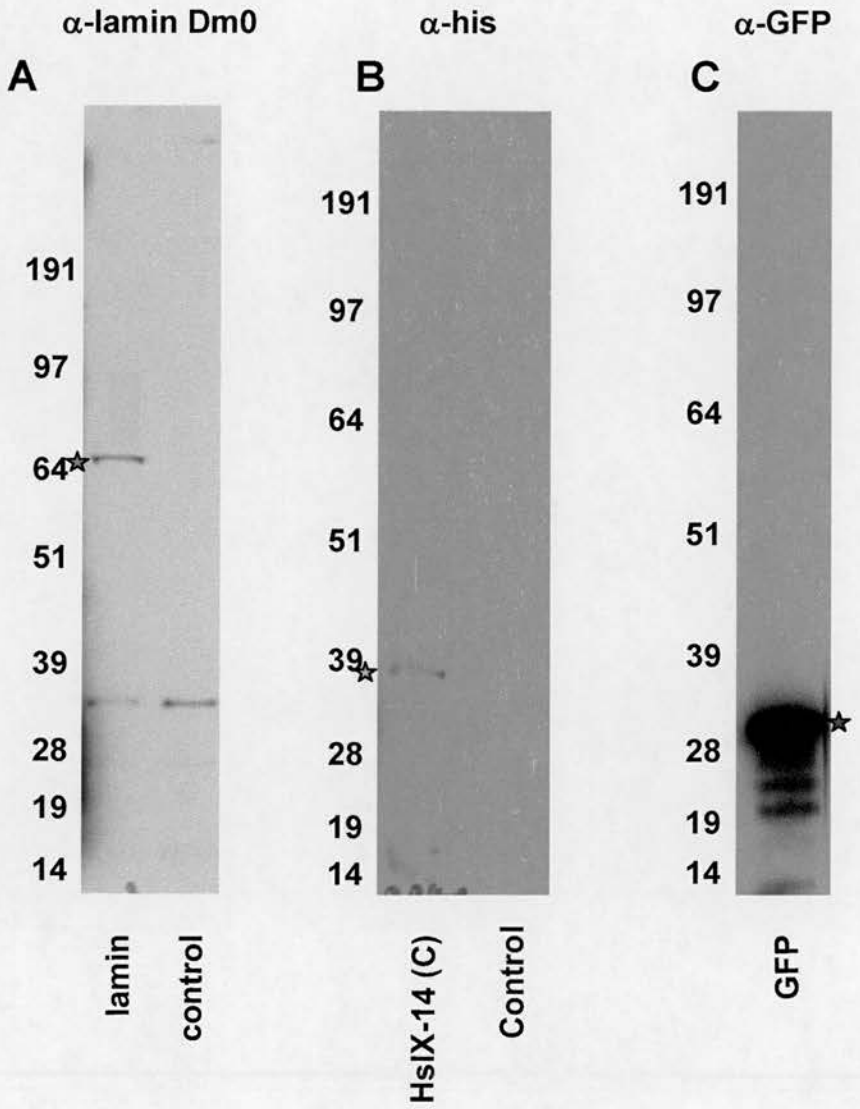

Figure 5.1A: Lamin, C-terminal HsIX-14 and GFP was able to be expressed by Circular kit.

In vitro transcript kit was used to express proteins. Reactions were set up with the following cloned gene vectors: DmIX-14 in pOT2 vector, lamin Dm0 in T7-7 vector, GFP in pIVEX vector or C-terminal HsIX-14 (amino acid: 331-665) in pRSET (contain his-tag) in each aliquot. An aliquot with no added vector was incubated at the same condition as a control. A: The membrane was probed with a monoclonal antibody against the N-terminal 22-28 amino acid of lamin Dm0. The red asterisk shows the *in vitro* expressed lamin Dm0 band which does not appear in the control. B: The membrane was probed with anti-his antibody. The yellow asterisk shows the expressed his tagged C-terminal HsIX-14 band which did not appear in the control. C: The membrane was probed by an anti GFP antibody. Expressed GFP was detected about 30 kDa (blue asterisk).

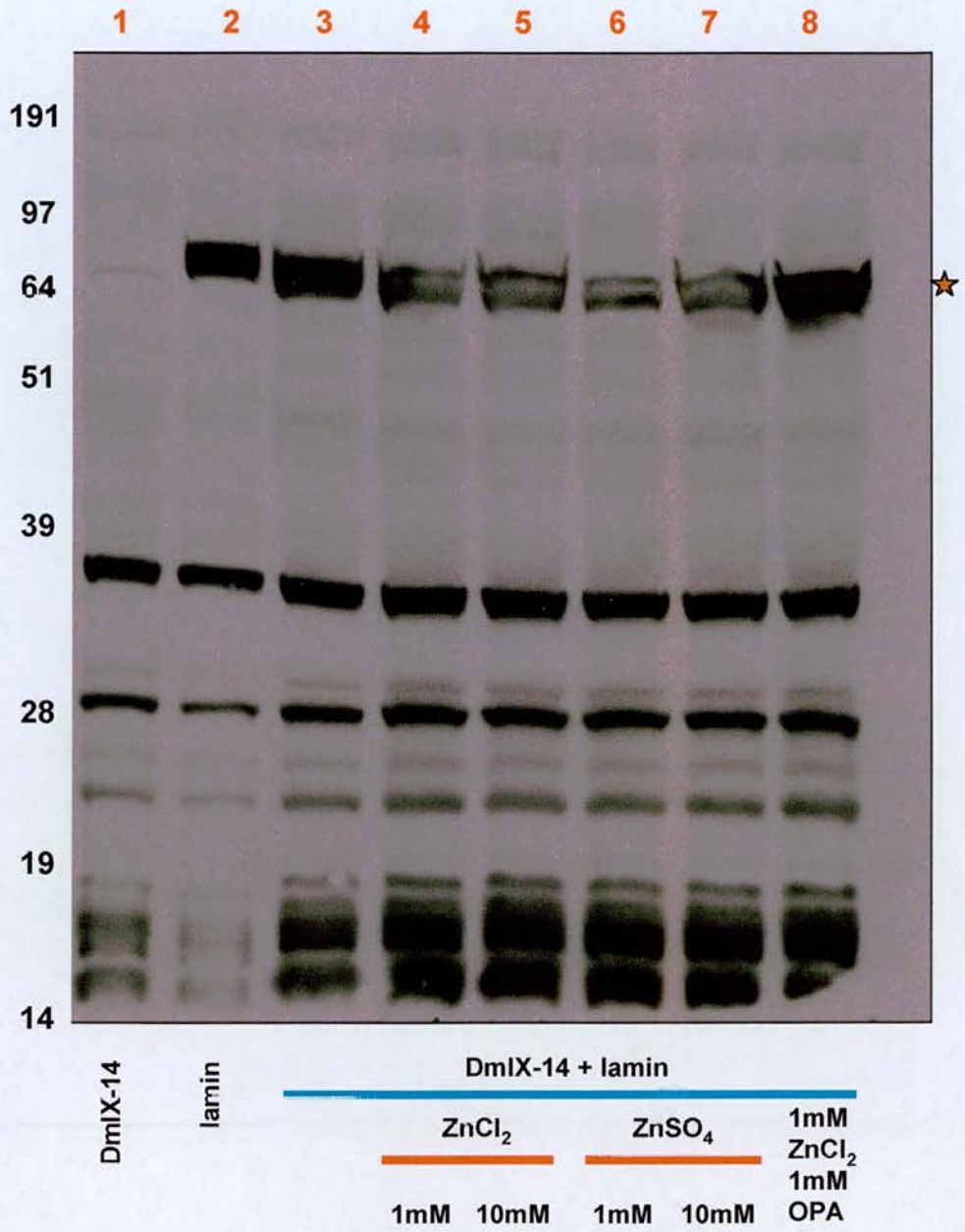

Figure 5.1B: DmIX-14 expressed by Circular kit cleave lamin.

In vitro expressed lamin Dm0 (5 µl) and DmIX-14 (10 µl) were incubated together at 29°C for 15 minutes. The gel was blotted with a monoclonal antibody against the N-terminal 22-28 amino acid of lamin Dm0. The predicted band size of lamin Dm0 (red asterisk) was absent in lane 1. No obvious cleavage of lamin Dm0 was observed when it was mixed with DmIX-14 (lane 3). Both $ZnCl_2$ and $ZnSO_4$ at final concentration of 1 mM and 10 mM increased DmIX-14 cleavage of lamin Dm0 (lane 4-7). When the zinc chelator orthophenanthroline (OPA) was added (lane 8) the cleavage was inhibited to levels seen in lanes 2 and 3.

lamin Dm0 by DmIX-14, a higher incubation temperature and a longer incubation time were applied. Similar to the previous experiment, *in vitro* expressed lamin Dm0 (5 μl) and *in vitro* expressed DmIX-14 (10 μl) were removed from a freshly translated aliquot and incubated together. Instead of 29°C for 15 minutes, they were incubated at 37°C for 50 minutes. The membrane was blotted with antibody against the N-terminal region of lamin Dm0. Under these conditions, lamin Dm0 cleavage by DmIX-14 was apparent even in the absence of $ZnCl_2$ (Figure 5.1C, Panel A, lane 3). Adding $ZnCl_2$ to a final concentration of 1 mM (lane4), or 10 mM (lane 5) or $ZnSO_4$ to a final concentration of 10 mM (lane 6) showed almost completely cleavage of lamin Dm0 by DmIX-14. The cleavage of lamin Dm0 was inhibited when OPA (1 mM final concentration) was incubated with $ZnCl_2$, DmIX-14 and lamin Dm0 (lane 7). The cleavage of GFP by DmIX-14 was used as a control. GFP was not cleaved by DmIX-14 when they were incubated at 37°C for 50 minutes without $ZnCl_2$ and with $ZnCl_2$.

Due to high background of the N-terminal (amino acid: 22-28) antibody of lamin Dm0, a monoclonal antibody against the C-terminal (amino acid: 548-620) lamin Dm0 was used. Although 37°C enhanced cleavage of lamin Dm0, it is not a physiologically relevant condition for *Drosophila*. Therefore, 3 μl of *in vitro* expressed lamin Dm0 and 10 μl of *in vitro* expressed DmIX-14 were removed immediately from their respective *in vitro* expressed aliquots and incubated together at 29°C for 1 hour. As shown in Figure 5.1D, DmIX-14 alone can not cleave lamin Dm0 without the addition of $ZnCl_2$. Lamin Dm0 cleavages were apparent when $ZnSO_4$ were added at different final concentrations to reactions containing DmIX-14 and lamin Dm0 (lane 4, 6 and 8). Cleavage was inhibited when OPA was added to a final concentration of 1 mM (lane 5,7 and 9).

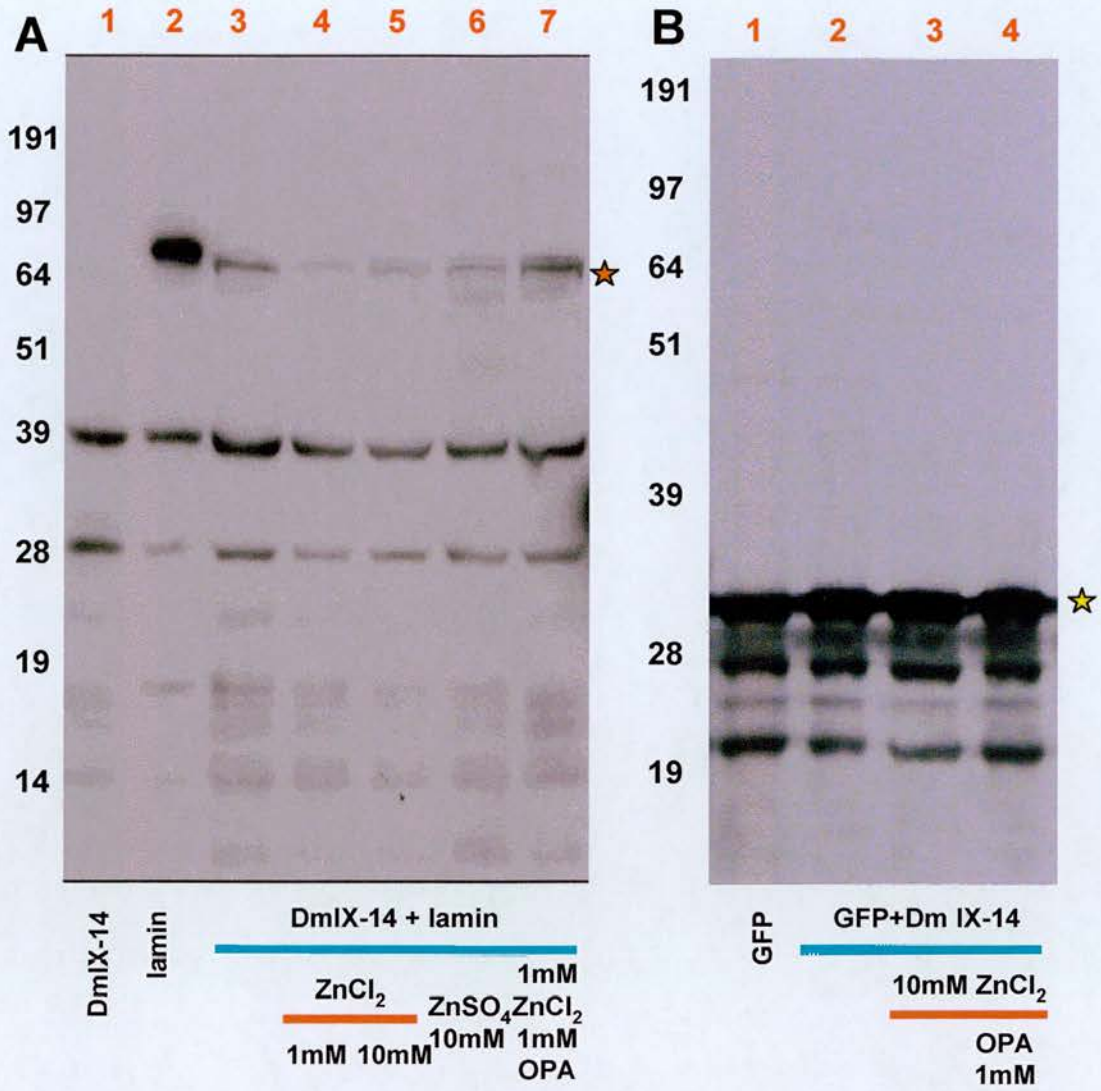

Figure 5.1C: DmIX-14 expressed by Circular kit cleave lamin but not GFP.

A: *In vitro* expressed lamin Dm0 (5 µl) and DmIX-14 (10 µl) were incubated together at 37°C for 50 minutes. The gel was blotted with a monoclonal antibody against the N-terminal 22-28 amino acid of lamin Dm0. The predicted band size of lamin Dm0 (red asterisk) was absent in lane 1. Cleavage of lamin Dm0 was obvious under this condition in the absence of $ZnCl_2$. Adding $ZnCl_2$ to a final concentration of 1 mM, or $ZnCl_2$ or $ZnSO_4$ to a final concentration of 10 mM with DmIX-14 almost completely cleaved lamin Dm0. The cleavage of lamin Dm0 was inhibited to about the same extent as without $ZnCl_2$ when OPA was incubated $ZnCl_2$. B: GFP (yellow asterisk) was not degraded when it was incubated with DmIX-14 at 37°C for 50 minutes without $ZnCl_2$ (lane 2) and with $ZnCl_2$ (lane 3).

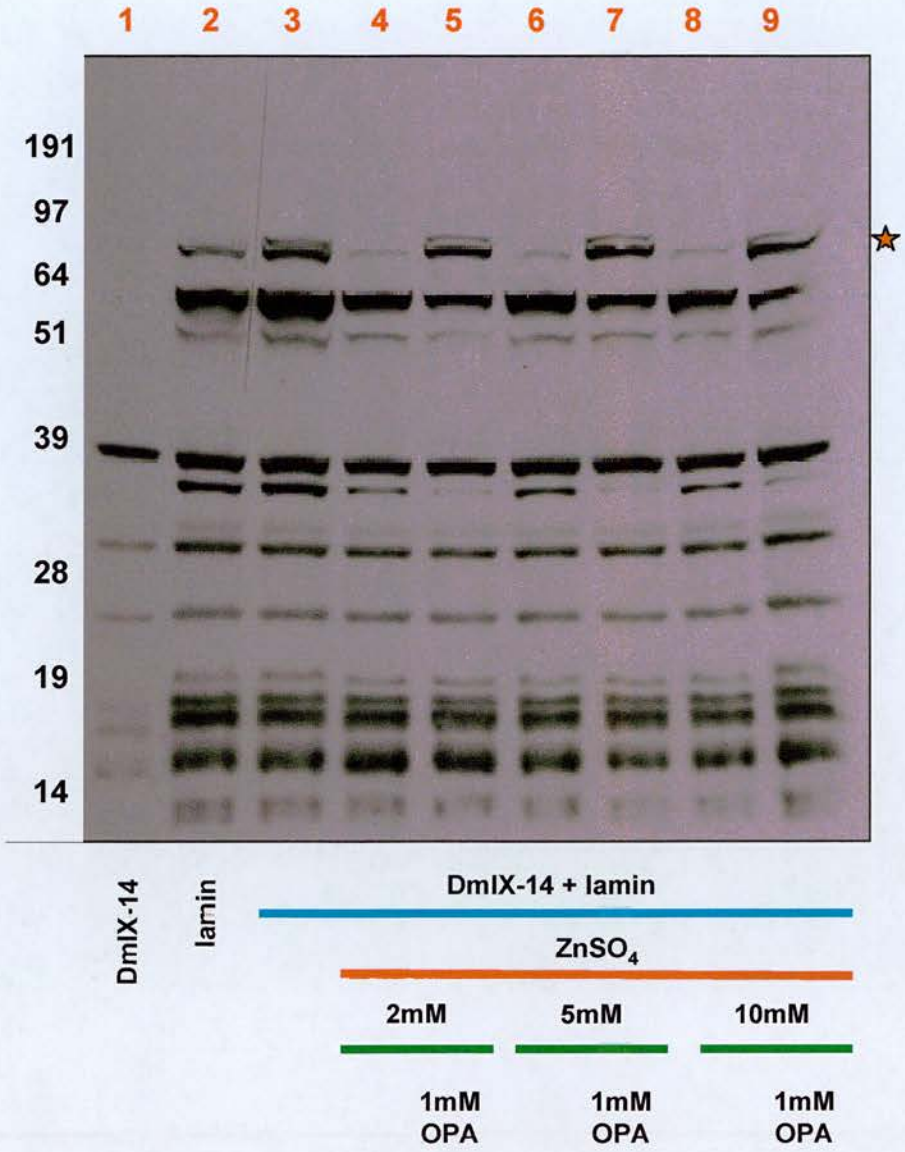

Figure 5.1D: Detect lamin cleavage by antibody against N-terminal lamin.

In vitro expressed lamin Dm0 (3μl) and DmIX-14 (10μl) were incubated together at 29°C for 1 hour. The gel was blotted with a monoclonal antibody against the C-terminal 548-620 amino acid of lamin Dm0. The predicted size band of lamin Dm0 (red asterisk) was absent in lane 1. Cleavage of lamin Dm0 by DmIX-14 was not obvious under this conditions in the absence of $ZnSO_4$. Adding $ZnSO_4$ to a final concentration of 2mM, 5mM and 10mM together with DmIX-14 can result in cleavage of lamin Dm0 and the cleavage was inhibited when OPA was added together with $ZnSO_4$.

An alternative polyclonal antibody raised against full length lamin Dm0 was used to blot the same membrane. This antibody has reduced the background without altering the ability to detect lamin Dm0 (Figure 5.1E).

Lamin Dm0 could not be cleaved by $ZnSO_4$ alone (Figure 5.1F, lane 3) or with an aliquot of the *in vitro* expression kit containing no vector in the presence and absence of $ZnSO_4$ (lane 4-lane8).

The paralogue of DmIX-14, gp63 cleaves a potential substrate MARCKS (Myristoylated alanine-rich C kinase substrate) related protein (MRP) in its effector domain (ED), Ser^{92} Phe^{93} Lys^{94}. (Corradin, Ransijn et al. 1999). MARCKS and MRP are both belongs to the MARCKS family and play roles in brain development and regulation of membrane-cytoskletal interactions. MARCKS and MRP have different localization and share the almost identical ED which exhibit membrane binding, Ca^{2+}-calmodulin and actin binding activity. These bindings could be reversed by PKC-dependent phosphorylation in ED (Arbuzova, Schmitz et al. 2002). This cleavage sequence, Ser Phe Lys, was found in ED of both MARCKS and MRP, also in lamin Dm0. If cleaved at that site, lamin Dm0 would be divided into two fragments with the resultant sizes of 25 kDa and 46 kDa. No obvious homology was observed between MRP, MARCKS and its Drosophila homologue (DAKAP200) and any of the accumulated proteins (lamin Dm0, lamin C and otefin) in *Drosophila* except the common cleavage site between lamin Dm0 and MRP.

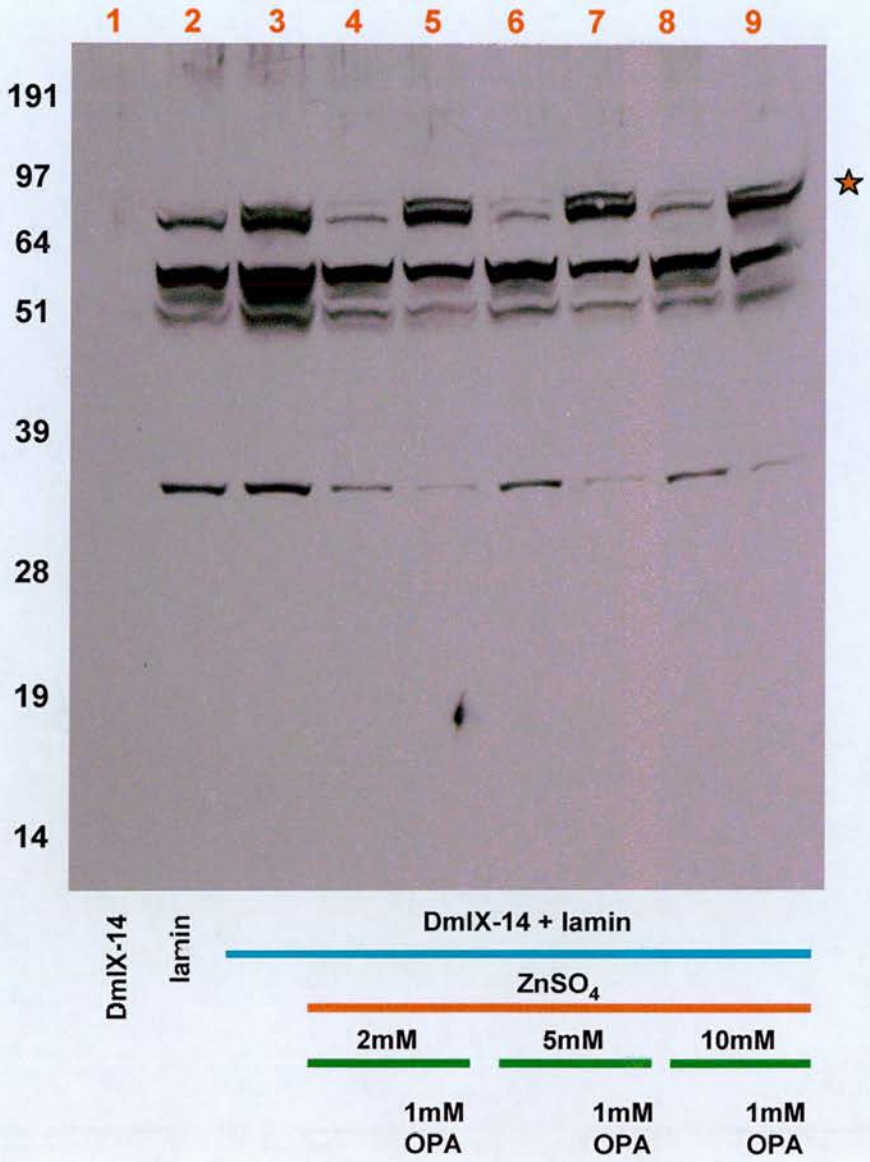

Figure 5.1E: Detect lamin cleavage by antibody against C-terminal lamin.

The gel in Figure 5.1D was stripped and probed with the polyclonal lamin Dm0 antibody. Lamin Dm0 cleavage by DmIX-14 in the presence of $ZnSO_4$ can still be observed (red asterisk) while the background was reduced.

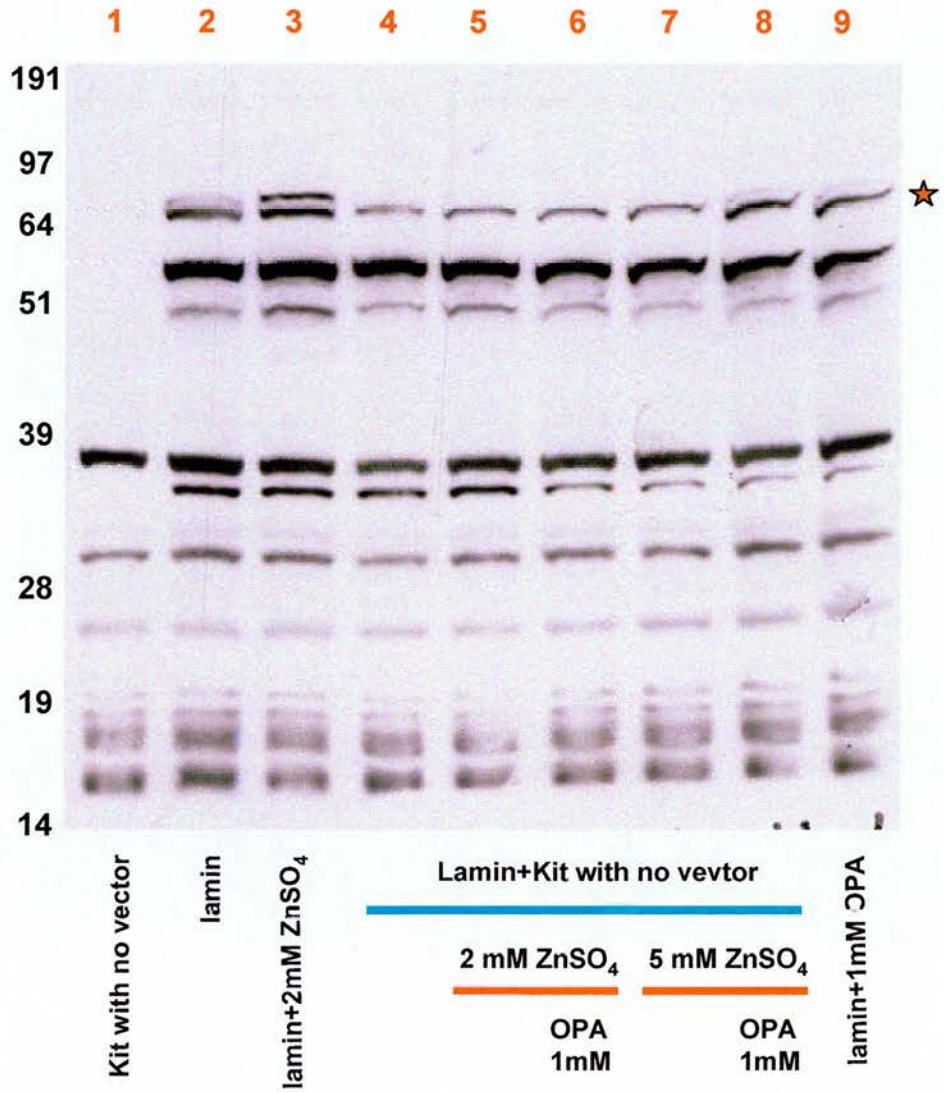

Figure 5.1F: Circular kits lysate with no vector could not cleave lamin.

In vitro expressed lamin Dm0 (3µl) and *in vitro* expression kit containing no vector (10µl) were incubated together at 29°C for 1 hour. The gel was blotted with a monoclonal antibody against the C-terminal 548-620 amino acid of lamin Dm0. The predicted size band of lamin Dm0 (red asterisk) was absent in lane 1. Cleavage of lamin Dm0 was not observed under this conditions in the presence or absence of $ZnSO_4$ (lane 4-8). Lamin could not be cleaved by $ZnSO_4$ (lane 3) or OPA itself (lane 9).

5.2 Use of radio-labelled lamin Dm0 to identify cleavage products.

In order to identify the cleavage products of lamin Dm0, lamin Dm0 was synthesised by TNT® T7 Coupled Reticulocyte Lysate System (Promega) (Reticulocyte kit) in the presence of ^{35}S. Full length DmIX-14 (77 kDa, 12 methionines) and lamin Dm0 (71 kDa, 7 methionines) were radio-labelled during synthesis using this system. Radio-labelled luciferase was used as a positive control of the efficiency of this system (Figure 5.2A lane 1). The band of radio-labelled DmIX-14 migrated at a size very close to the band of radio-labelled lamin Dm0 (Figure 5.2A lane 3&4). This generated a potentially confusing signal when the two were used together. To overcome this problem, DmIX-14 without a radioactive label was synthesized using the RTS 500 ProteoMaster *E. coli* HY Kit from Roche (ProMaster kit) since the "Circular template kit" was no length available from Roche. The expression was performed by adding DmIX-14 in pOT2 vector (1 µl) in a 50 µl aliquot of the kit and incubated at 30°C for 2 hours. A cleavage band of lamin Dm0 was observed above 51 kDa when DmIX-14 was added (lane 5). This band become more obvious when 1mM $ZnCl_2$ was added together with DmIX-14 and was less apparent when 9mM OPA was added (Figure 5.2A, lane 6 & 7).

Figure 5.2B demonstrated that DmIX-14 synthesised by ProteoMaster kit could not cleave GFP, an nonspecific substrate, in the presence or absence of $ZnCl_2$ under the same condition as used in Figure 5.2A. Radio-labelled luciferase was used as a positive control for this radioactive label system (lane 1) while non-radioactively labelled DmIX-14 synthesised by RTS 500 ProteoMaster *E.coli* HY Kit served as a negative control for this

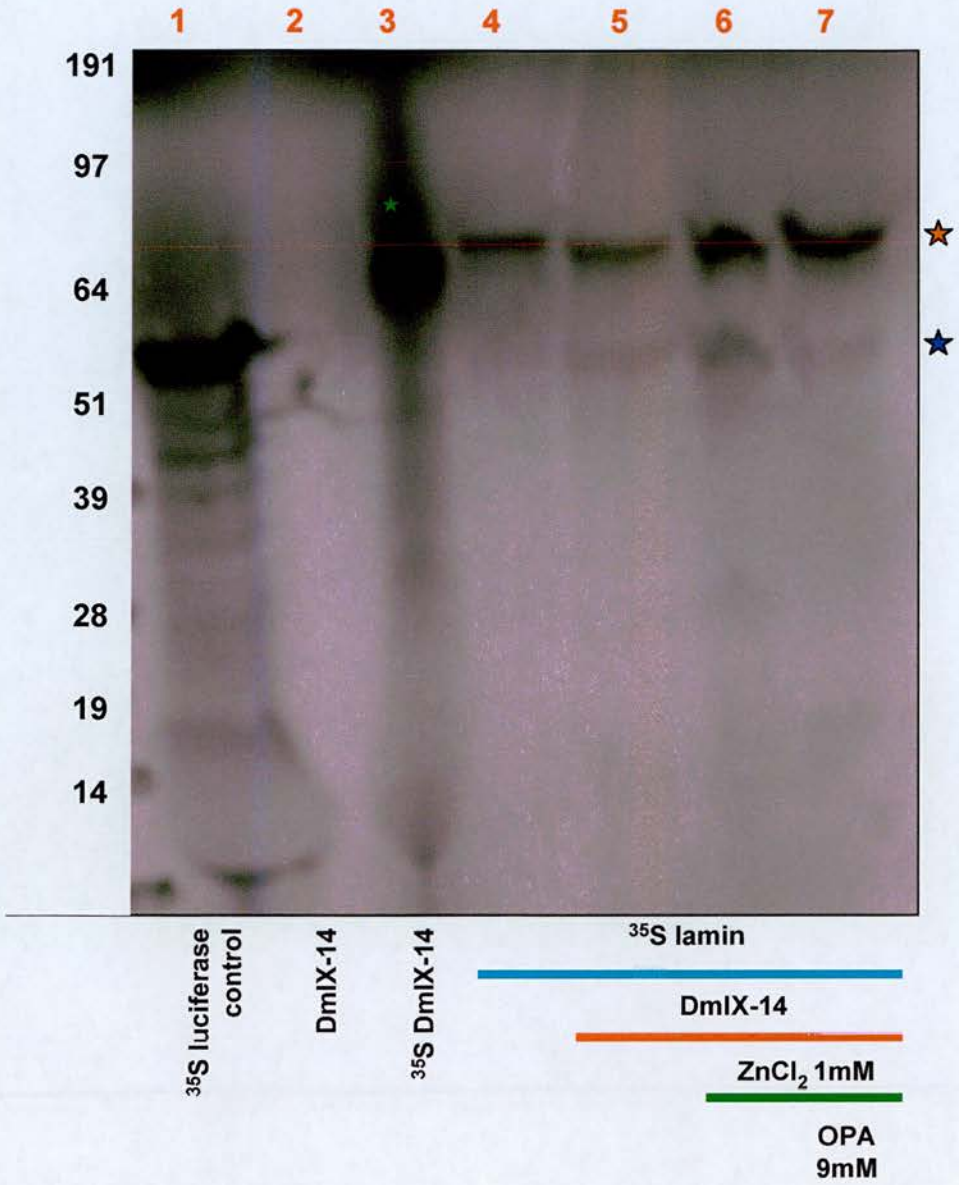

Figure 5.2A: Lamin cleavage band was observed when lamin was expressed by reticulocyte kit and IX-14 was expressed by Proteomaster kit.

Luciferase in pUC (1 μg), DmIX-14 in pOT2 (1 μg) and lamin Dm0 in T7-7 (1 μg) were added to an aliquot of reticulocyte lysate kit to synthesise S^{35}-methionine-labelled protein. Lane 1 contains radio-labelled luciferase. Non radio-labelled DmIX-14 (lane 2) was synthesised by ProteoMaster kit and shows no signal. Green asterisk indicates the signal of radioactive DmIX-14 while red asterisk shows the signal of radioactive lamin Dm0. A potential cleavage band of lamin Dm0 (blue asterisk) appeared when 10 μl of non-radioactive DmIX-14 was incubated with 4 μl of radioactive lamin Dm0 at 29°C for 1 hour. This band became more obvious when $ZnCl_2$ was added to a final concentration of 1 mM. The cleavage signal was disappeared when OPA was added with $ZnCl_2$.

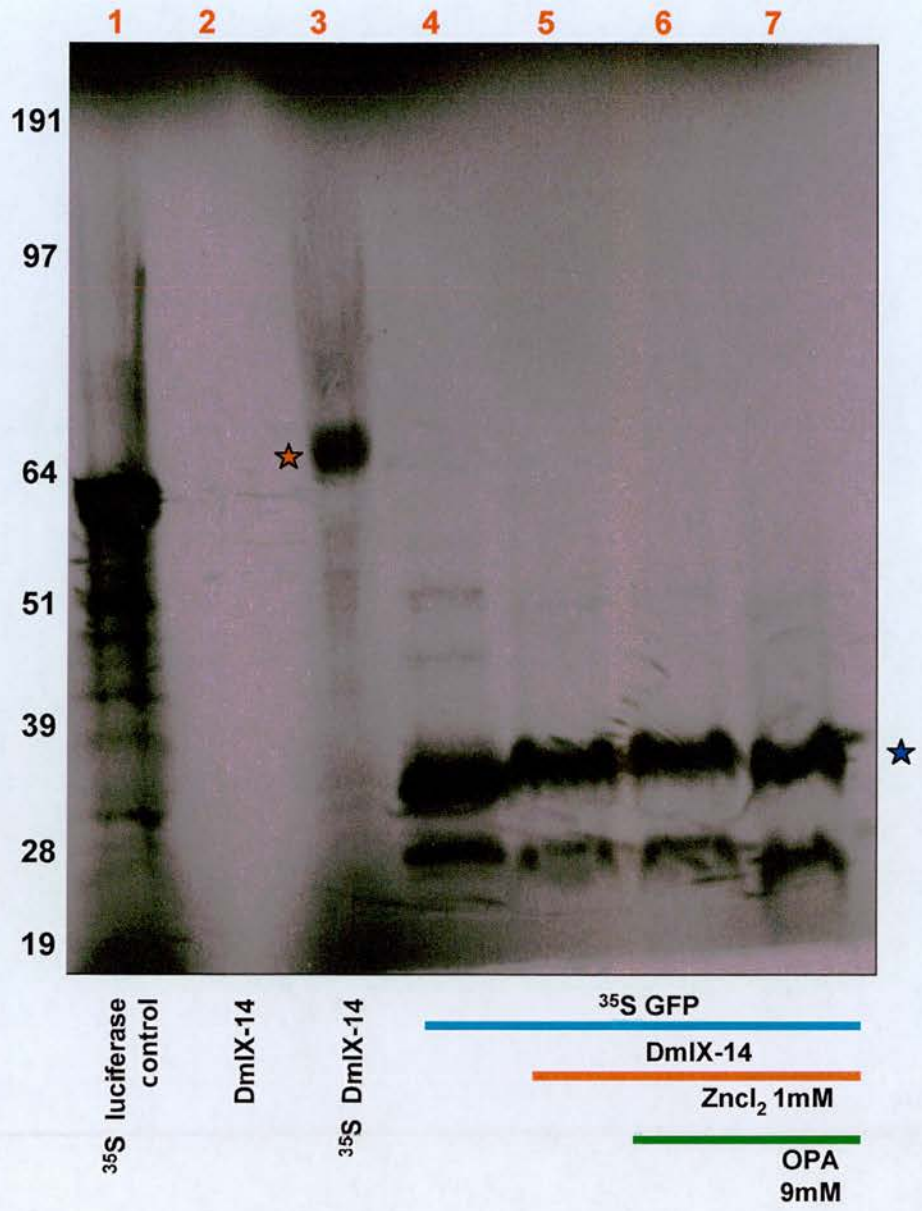

Figure 5.2B: DmIX-14 expressed by reticulocyte kit was not able to cleave GFP.

Luciferase in pUC (1 μg), DmIX-14 in pOT2 (1 μg) and GFP in pIVEX (1 μg) were added to an aliquot of reticulocyte lysate kit to synthesise-S^{35}-methionine labelled protein. Lane 1 contains the radio-labelled luciferase. Non radio-labelled DmIX-14 was synthesised by ProteoMaster kit and shows no signal (lane 2). Red asterisk indicates the signal of radioactive DmIX-14 while blue asterisk shows the signal of radioactive GFP. While 10 μl of non radio-labelled DmIX-14 was incubated with 4 μl of radioactive GFP at 29°C for 1 hour, no GFP degradation band can be observed in the presence or absence of $ZnCl_2$.

radioactive label system (lane 2). Another control was performed by mixing radio-labelled lamin Dm0 with non-radio-labelled GFP synthesised by ProteoMaster. Lamin Dm0 was cleaved when incubated in the presence or absence of zinc at 29°C for 1 hour with freshly expressed GFP from ProteoMaster Kit (Figure 5.2C). This result was puzzling. To get to the bottom of this problem, 10 µl ProteoMaster kit was added to express protein without the addition of vector. This was added to 4 µl radio-labelled lamin Dm0 and incubated at 29°C for 1 hour. Lamin Dm0 cleavage was still observed (lane 9) which meant the cleavage was due to the mixture of extracts from the two kits (ProteoMaster kit and reticulocyte kit). The possibility that lamin Dm0 was cleaved by each kit alone was ruled out because lamin Dm0 expressed by each kit was not cleaved by adding the mock expressed exact from the same kit (Figure 5.1F and Figure 5.2D). It appeared that mixture of the two kits activated some endogenous protein which cleaved lamin Dm0. The original cleavage of lamin Dm0 must due to IX-14 itself.

DmIX-14 was then synthesised by reticulocyte kit with no ^{35}S methionine and incubated with ^{35}S-labelled lamin Dm0 expressed from the same kit. No cleavage of lamin Dm0 was observed (Figure 5.2D). When DmIX-14 and lamin Dm0 were both expressed by ProteoMaster kit, no lamin Dm0 cleavage was observed in the presence or absence of $ZnCl_2$ when incubated at 29°C for 1 hour (Figure 5.2E). Higher $ZnCl_2$ concentrations were also tried, but no lamin Dm0 cleavage was observed (Figure 5.2F).

Expressway HTP Cell-Free *E. coli* expression kit from Invitrogen (HTP kit) was used to express DmIX-14 and lamin Dm0. DmIX-14 in pOT2 (0.5 µg) and lamin Dm0 in T7-7 (0.5 µg) were added to a 25 µl aliquot of *E.coli* lysate from Invitrogen and incubated at 23°C for 2 hours with shaking (300 rpm). Expressed lamin Dm0 and DmIX-

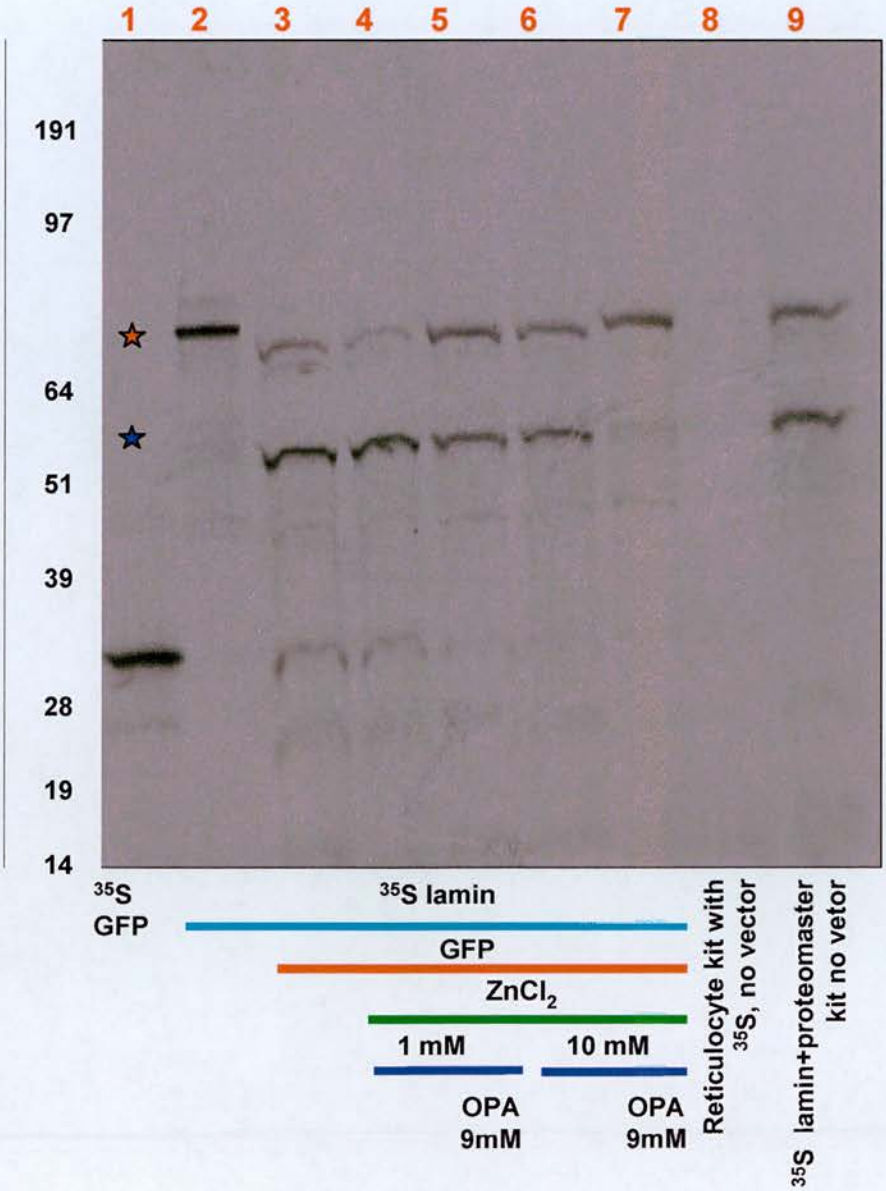

Figure 5.2C: Mixture of reticulocyte kit and Proteomaster kit cleaves lamin.

DmIX-14 in pOT2 (1 μg) and GFP in pIVEX (1 μg) were added to an aliquot of reticulocyte lysate kit to synthesise ^{35}S-methionine-labelled protein. Lane 1 shows radio-labelled GFP. Red asterisk shows the signal of radioactive lamin Dm0 (lane 2) while the blue asterisk shows the cleavage bands. This cleavage band was observed even when mock expressed protein from ProteoMaster kit (underwent the expression without the addition of vector) was added to radioactive lamin Dm0 (lane 9). Expression from the reticulocyte lysate kit without the addition of vector shows no expressed protein in the exposure (lane 8).

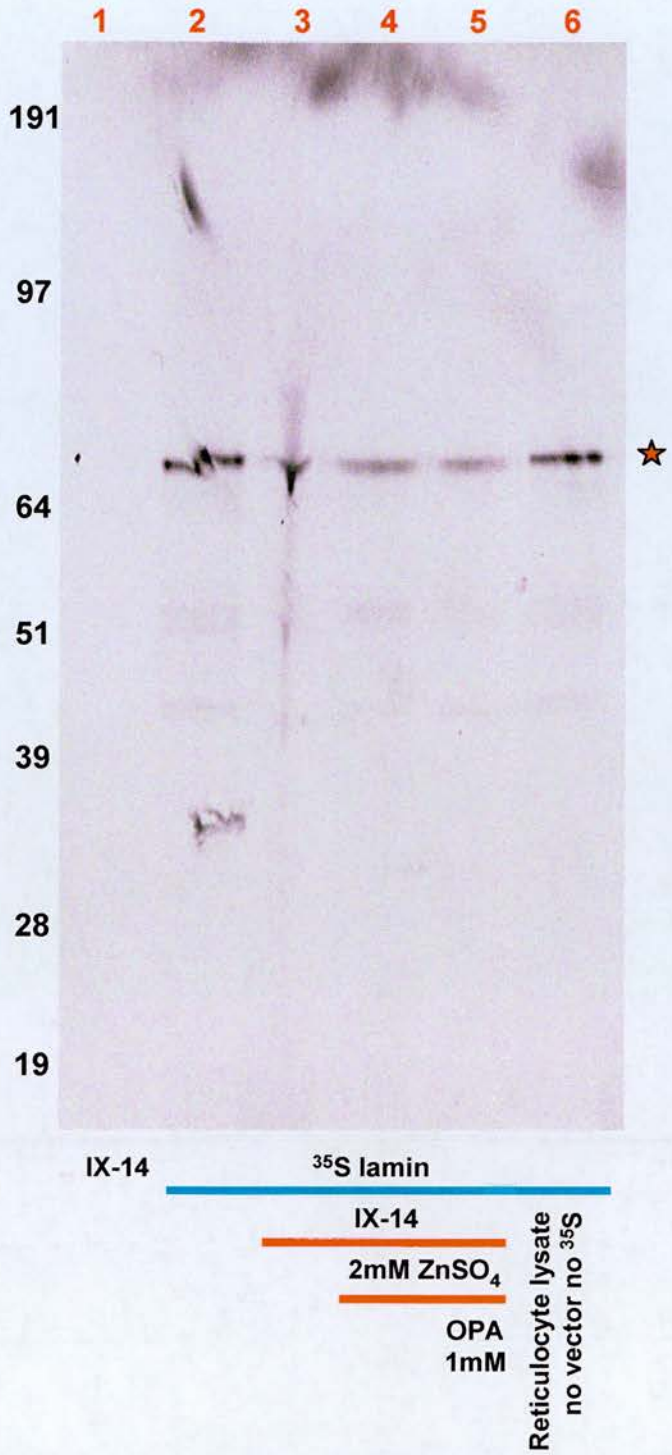

Figure 5.2D: DmIX-14 expressed by reticulocyte kit was not active.

Lamin Dm0 was synthesised by reticulocyte kit and radioactive labelled by ^{35}S. IX-14 was synthesised by reticulocyte kit too but with no radioactive label which give no signal on this exposure (lane 1). 10 µl of DmIX-14 was incubated with 4 µl of lamin Dm0 at 29°C for 1 hour. Lamin Dm0 (red asterisk) was not cleaved by IX-14 in the presence and absence of $ZnSO_4$ (lane 3-5) nor by reticulocyte lysate with no vector (lane 6).

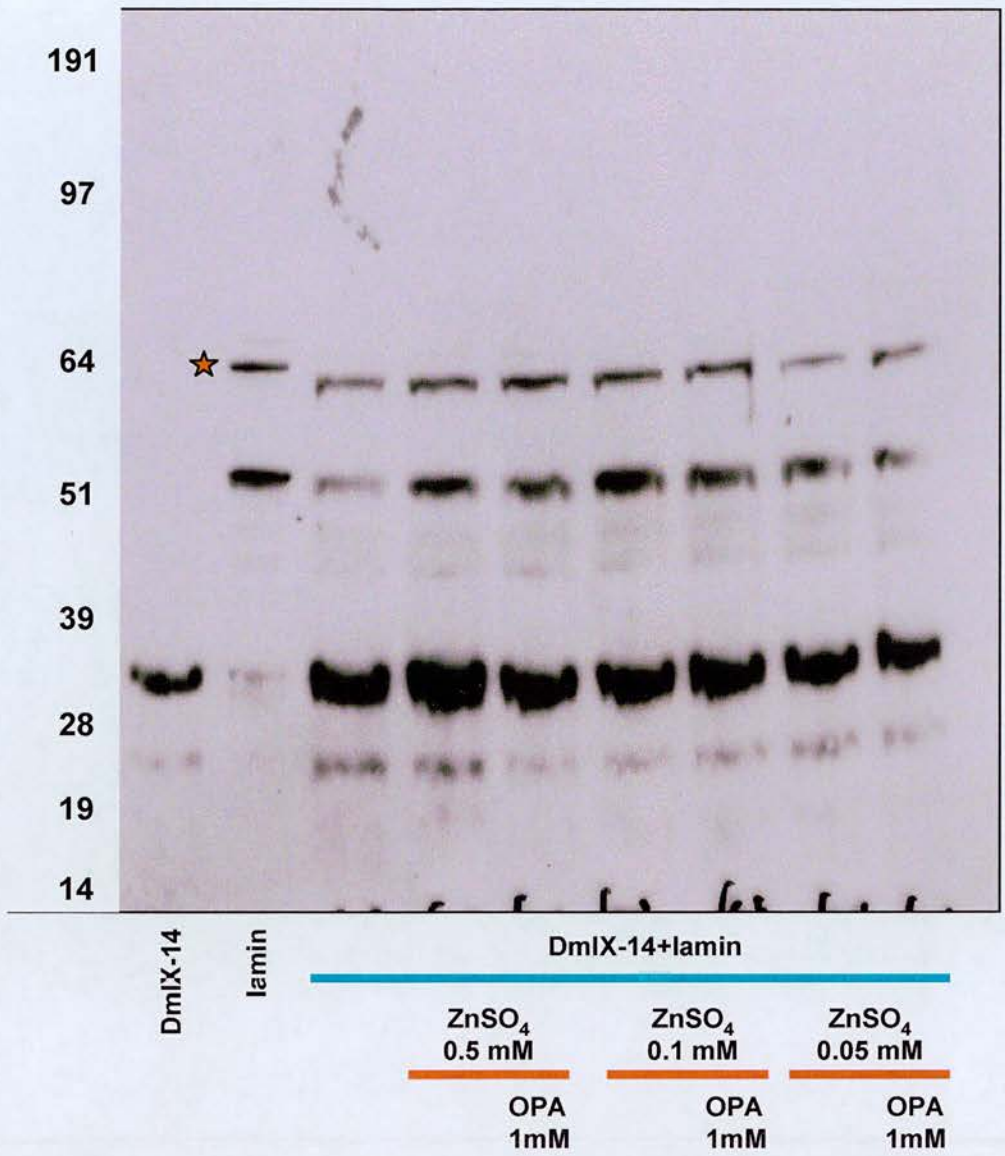

Figure 5.2E: DmIX-14 expressed by Proteomaster kit was not active.

DmIX-14 in pOT2 (1 μg) and lamin Dm0 in T7-7 (1 μg) were added to an aliquot of ProteoMaster kit. The gel was blotted with an monoclonal antibody against the N-terminal 22-28 amino acid of lamin Dm0. No lamin Dm0 cleavage (red asterisk) was observed when 4 μl of DmIX-14 was incubated with 5 μl of 1:5 diluted lamin Dm0 at 29 °C for 1 hour in the presence or absence of $ZnSO_4$.

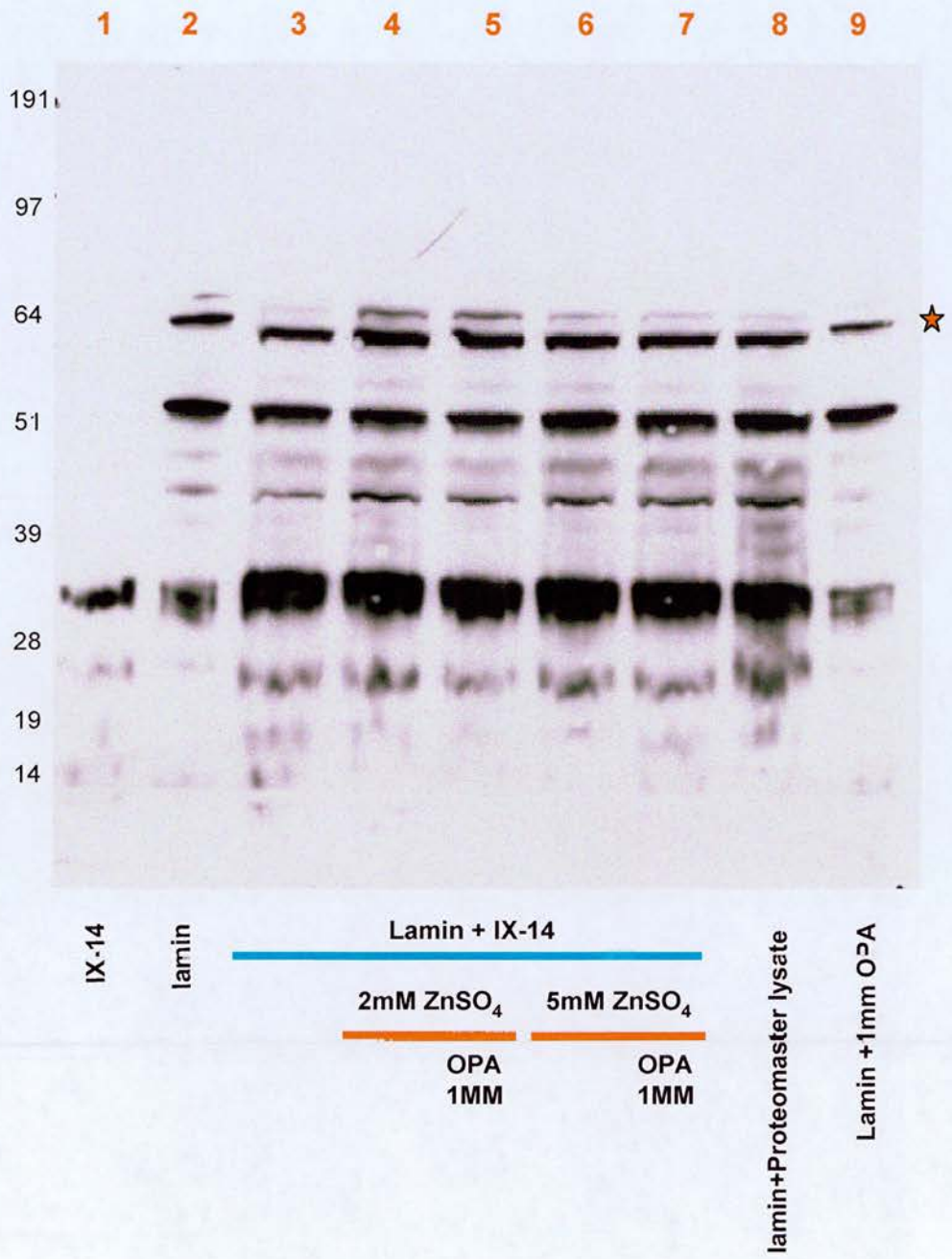

Figure 5.2F: DmIX-14 expressed by Proteomaster kit was not active.

DmIX-14 in pOT2 (1 μg) and lamin Dm0 in T7-7 (1 μg) were added to an aliquot of ProteoMaster kit. The gel was blotted with an monoclonal antibody against the N-terminal 22-28 amino acid of lamin Dm0. No lamin Dm0 cleavage (red asterisk) was observed when 4 μl of DmIX-14 was incubated with 5 μl of 1:5 diluted lamin Dm0 at 29 °C for 1 hour in the presence or absence of $ZnSO_4$.

14 were mixed and incubated at 29°C for 1 hour. Lamin Dm0 was not cleaved by DmIX-14 in the presence or absence of $ZnCl_2$ (Figure 5.2G).

5.3 Summary

DmIX-14 expressed by Circular template kit can cleave lamin Dm0 *in vitro* in the presence of $ZnCl_2$ or $ZnSO_4$, this cleavage can be inhibited by the chelator, OPA. Lamin Dm0 was almost completely cleaved when incubated with DmIX-14 at 37°C in the presence of $ZnCl_2$. DmIX-14 cleaved lamin Dm0 under these conditions even in the absence of $ZnCl_2$. However, since the cleavage bands were not observed, there are possibilities that lamin cleavage (not detected by lamin antibody) was due to reasons other than invadolysin directly cleavage. 1) Invadolysin could induce lamin precipitation then reduce the possibility lamin epitopes being recognized by antibody. 2) Invadolysin could cleave chaperon protein which keep lamin soluble. This would result in lamin precipitation indirectly. 3) Invadolysin cleaved and activated a baterial enzyme in the *E. coli* lysate which cleaved lamin subsequently. 4) Invasolysin absorbs the protease inhibitors of the *in vitro* expression system and in turn lamin was degraded by protease. 5) Epitopes recognised by lamin antibody was cleaved off into small fragment and run out of the gel. The other potential problem of this analysis is that OPA was reported to cause protein cross-linking in the presence of Cu, in turn change the structure of active and inactive state of protein (Hamdan, Ward et al. 2002). It is still possible that the protease inhibition activity of OPA was not due to its chelating property, but was due to its crosslinking activity in the presence of copper in the *E.coli* lysate instead. Invadolysin DmIX-14 expressed by reticulocyte kit, ProteoMaster Kit and HTP kit failed to cleave

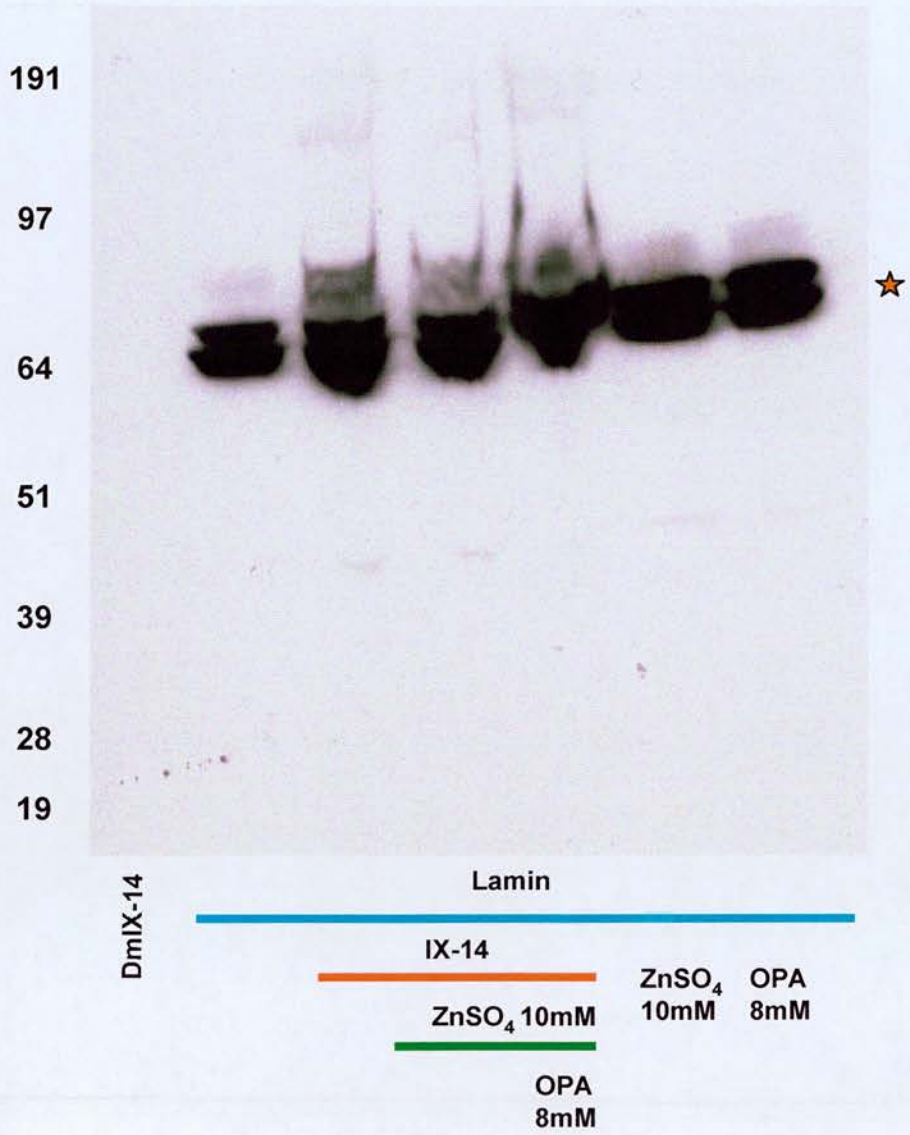

Figure 5.2G: DmIX-14 expressed by HTP kit was not active.

DmIX-14 in pOT2 (0.5 μg) and lamin Dm0 in T7-7 (0.5 μg) were added to an aliquot of HTP kit and incubated at 23°C for 2 hours with shaking (300 rpm). The membrane was blotted with monoclonal antibody against N-terminal 22-28 amino acid of lamin Dm0. No lamin Dm0 cleavage (red asterisk) was observed when 6 μl of DmIX-14 was incubated with 2 μl of lamin Dm0 at 29 °C for 1 hour in the presence or absence of $ZnSO_4$.

lamin Dm0 in the presence or absence of $ZnCl_2$. One possible explanation is that protein expression.in the "Circular template kit" may have been significantly slower than the other three kits. This could provide DmIX-14 enough time to finish all the required proper folding. Another possibility is that the Circular template kit contained factors that activated DmIX-14 or possibly induced the self-cleavage and activation of DmIX-14. I predict these factors are not present in the other 3 kits. Actually, the paralogue of DmIX-14, GP63, needs to undergo an auto-processing event (cysteine switch) for activation. This removes Cys48 from the pro-region, releasing blockage by abolishing protease inhibitory coordination between Cys48 and active-site zinc (Figure 1.3C). Full protease activity was exhibited after activation with $HgCl_2$ (Macdonald, Morrison et al. 1995).

Condition used for protease essay

Kit used	Conditions	Cleavage
Circular kit for lamin Dm0 and DmIX-	29°C for 15 minutes lamin Dm0: DmIX-14 (5:10	Depend on $ZnCl_2$, inhibited by OPA
Circular kit for lamin Dm0 and DmIX-	37°C for 50 minutes lamin Dm0: DmIX-14 (5:10	Depend on $ZnCl_2$, Inhibit by OPA
Circular kit for lamin Dm0 and DmIX-	29°C for 1 hour lamin Dm0: DmIX-14 (3: 10	Depend on $ZnCl_2$, Inhibit by OPA
Proteomaster kit for DmIX-14 Reticulocyte kit for ^{35}S lamin Dm0	29°C for 1 hour lamin Dm0: DmIX-14 (4: 10	Artificial cleavage
Reticulocyt kit for DmIX-14 Reticulocyte kit for ^{35}S lamin Dm0	29°C for 1 hour lamin Dm0: DmIX-14 (4: 10	No cleavage
Proteomaster kit for DmIX-14 Proteomaster kit for lamin Dm0	29°C for 1 hour lamin Dm0: DmIX-14 (1:4)	No cleavage
HTP kit for DmIX-14 HTP kit for lamin Dm0	29°C for 1 hour lamin Dm0: DmIX-14 (2:6)	No cleavage

Chapter 6: *In Vitro* Expression of DmIX-14

6.1 Expression of DmIX-14 using the Baculovirus system.

Further characterization of DmIX-14 protease activity would require large amounts of active DmIX-14. The available *in vitro* transcription and translation systems mentioned in Chapter 5 did not give reliable protease activity, were expensive, and on very small scale. *E. coli* expression was not further explored as it lack post-translation modifications and Brian McHugh had previously that it failed to express full-length DmIX-14 (perhaps due to toxicity).

We therefore decided to use Bac–to-Bac baculovirus expression system from Invitrogen to express DmIX-14. This system can express high levels of protein, typically larger proteins than other systems and is suitable for expression of proteins cytotoxic on other systems. It also can support eukaryotic post translational modifications. Figure 6.1A shows a schematic of the Bac-to-Bac baculovirus system (Invitrogen). The DmIX-14 ORF was cloned into a donor vector, pFastBacHT A which contains a miniTn7 transposons to recombine the inserted gene with a bacmid and a his-tag fused to the inserted protein at the N-terminus. This construct was then transformed into *E.coli* DH10Bac, which contains a baculovirus shuttle vector (bacmid) with a mini attTn7 target site and a helper plasmid. After transforming the construct, transposition occurs between the min-Tn7 element on the pFastBacHT A vector and the min-attTn7 target site on the bacmid to generate a recombinant bacmid in the presence of transposition proteins

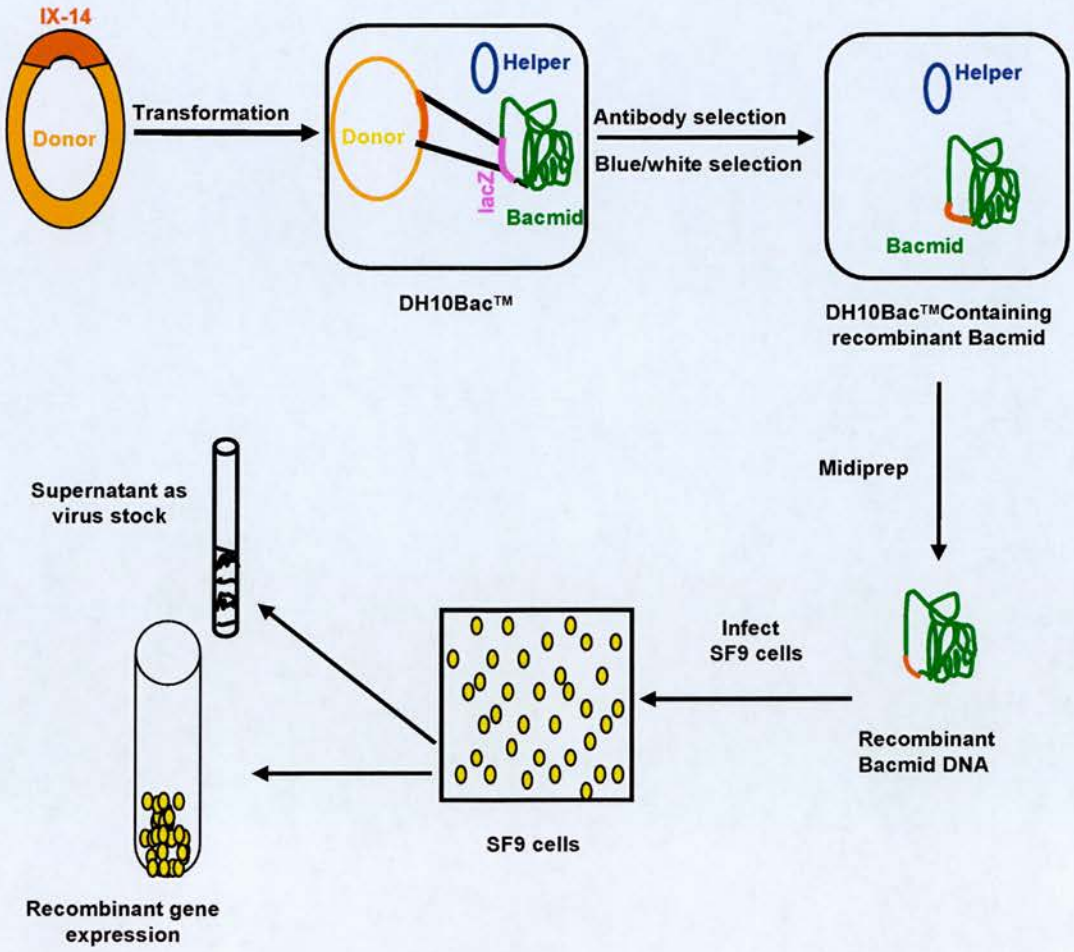

Figure 6.1A: Schematic of the Bac-to-Bac baculovirus system.

DmIX-14 ORF was cloned into pFastBacHTA vector which has a his-tag fused to the inserted protein on the N-terminus. The construct was then transformed into DH10Bac where DmIX-14 recombined with bacmid and was selected by antibody and blue/white colour. Recombinant bacmid was isolated by midiprep and used to infect SF9 insect cells. After infection, SF9 cells were centrifuged to collect expressed protein while supernatant was stored as virus stock.

supplied by the helper plasmid. The recombination was selected by kanamycin (carried by the bacmid), tetracycline (carried by the helper vector) and gentamicin (inside the mini Tn7 transposon in pFastBacHT A). Recombination disrupts expression of the flanking lacZ gene, allowing identification of recombinant by blue and white selection (recombinant colonies are white, non-recombinant colonies are blue). A pair of M13 primers flanking the mini attTn7 on the shuttle vector can be used to verify the recombination by PCR (Figure 6.1B, panel A). Several white colonies (cell with recombined bacmid) were picked to perform colony PCR and compared to nonrecombinant bacmid. All the PCR products from white colonies gave a band of the expected size, approximately 4500 bp (2430 bp from vector + 2052 bp for DmIX-14 ORF). One of these colonies was selected and grown to isolate bacmid by midiprep (Figure 6.1B, panel B-red arrow). SF9 cells (derived from the parental *Spodoptera frugiperda* ovary cell line) were infected with this recombinant bacmid. Cells were collected and centrifuged when signs of infection were observed (cells became bigger, stopped dividing and detached from the bottom of the flask) (Figure 6.1B, panel C). Figure 6.1C shows the purification of DmIX-14. An aliquot of cells in media was saved as T (total). The rest of the culture was centrifuged, saving the virus-containing supernatant as S1 (supernatant 1) and cell pellet was lysed in lysis buffer as P1 (Pellet 1). The lysate was centrifuged and the supernatant was saved as S2 (supernatant 2, this should contain any soluble DmIX-14). The pellet was resuspended in 1X SDS-PAGE sample buffer as P2 (pellet 2). S2 was incubated with Ni-NTA agarose beads and the beads were washed with washing buffer (w1-w3). DmIX-14 was eluted from the beads

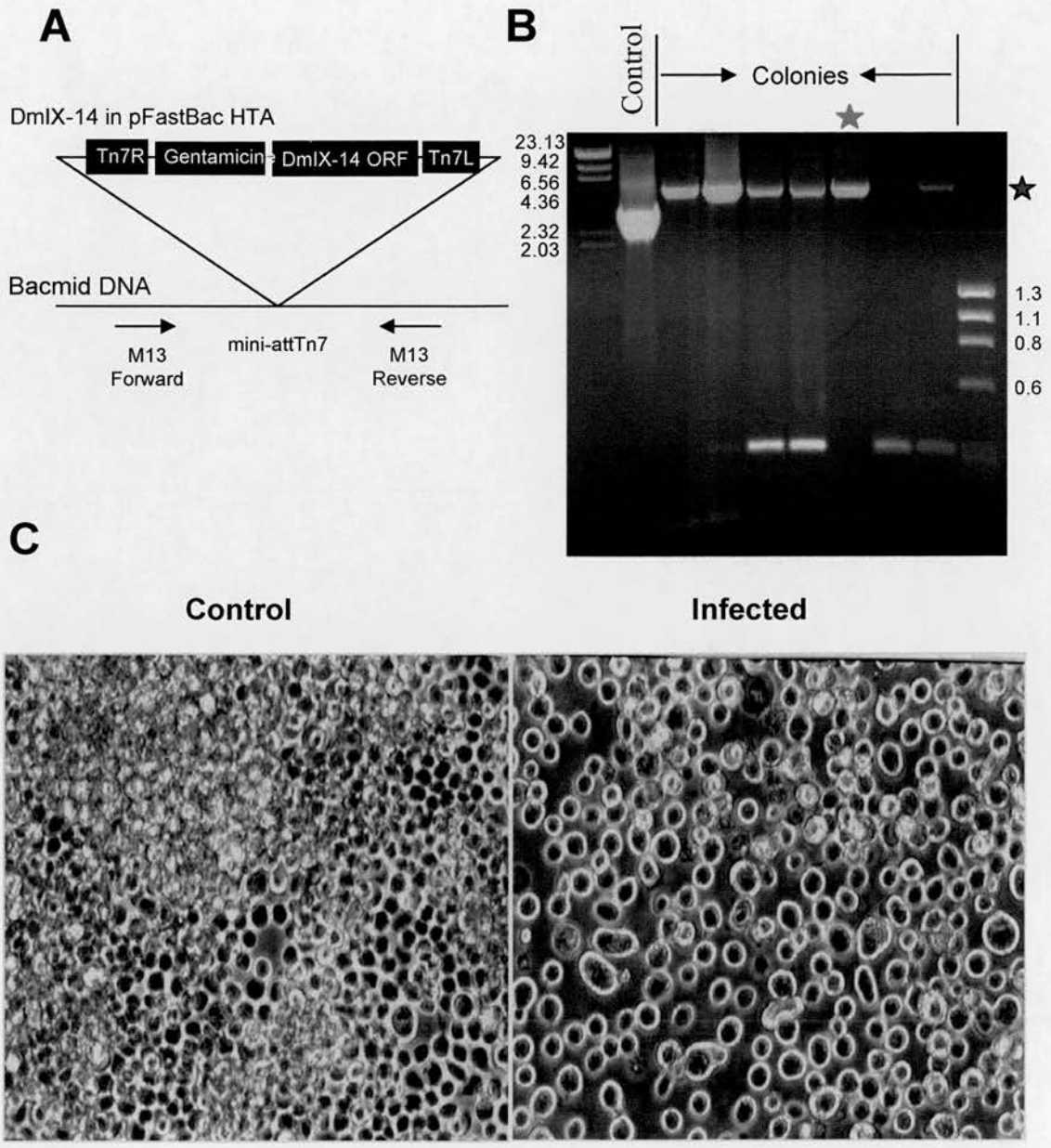

Figure 6.1B: Bacmid recombination and infection.

A: DmIX-14 ORF cloned in pFastBacHT A vector that could recombine with bacmid by the mini-attTn7 Transposon. M13 forward and reverse sequences were beside the mini-attTn7 sequence. B: Using M13 primer pairs to verify recombination. Nonrecombinant bacmid served as a positive control. After transformation, white colonies were used as a PCR template. All PCR reactions show the expected size band for DmIX-14 (blue asterisk). The red asterisk indicates the colony picked for expression. C: Demonstration of the difference between noninfected and infected SF9 cells with baculovirus. Cells stop dividing, increase in size and detach from the flask.

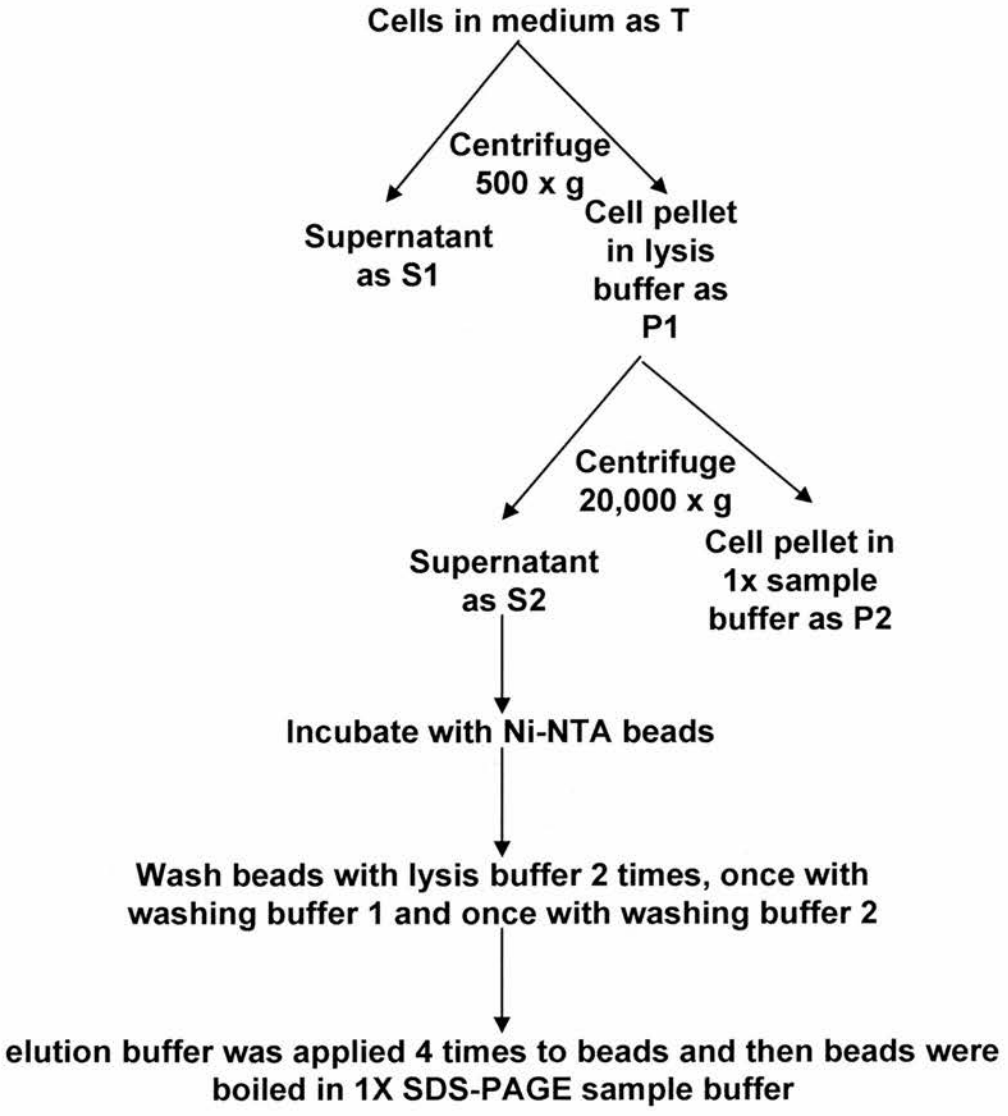

Figure 6.1C: Steps of fractionation and purification

After infection, cells in an aliquot of medium were collected and saved as Total (T). Then, cells were centrifuged and resuspended in lysis buffer as P1, the supernatant containing virus was saved as S1. Resuspended P1 was centrifuged again and the supernatant was collected as S2. S2 should contain the soluble protein. The pellet was resuspended in 1X sample buffer and saved as P2. S2 was incubated with Ni-NTA agarose beads. The beads were washed with lysis buffer and subsequent washing buffers. Elution buffer was applied to the beads before beads were boiled in 1X SDS-PAGE sample buffer.

with elution buffer as (e1-e3) The beads were boiled in 1X SDS-PAGE sample buffer prior to loading on gel.

Figure 6.1D shows the characterisation of DmIX-14 antibody which would be used for expression detection. R747 gives several bands near the predict size on S2 extracts. On immunofluorescence, R747 2nd bleed staining was limit to cytoplasm of S2 cells. Since the anbibody is not purified, the immunoflurorescence data is meaningless. This R747 bleed was used to immunoblot on SF9 cells for the expressed protein detection. Under condition 1 (see material and methods), a band near expected size for DmIX-14 appeared in all the fractions of T, S1, P1, S2, P2 indicating that some DmIX-14 was secreted into the medium and finally the pellet was not totally solubilized (Figure 6.1E). To help in initial characterization, I used constructs of his-Borealin as a control and the band for DmIX-14 was not observed in Borealin infection. DmIX-14 did not appear to bind to the Ni-NTA beads, as seen by the same amount of the DmIX-14 band in the input and flow through from the beads. In addition, no bands appeared in any of the wash or elution fractions, or the final sample buffer eluate. TCA precipitation was used to concentrate the original elution and bead fractions to rule out the possibility that protein was not observed due to its low concentration. These precipitations allowed all of the remaining sample to be run in one lane each. No band was detected in the elution and boiled beads fraction (Figure 6.1F). Other conditions such as using different concentration of salt or different detergent or adding reducing reagent have been tried to help solubilization (see material and method, condition 2-4). However, I found no DmIX-14 binding to the Ni-NTA beads in any of these conditions. Denaturing conditions were also used in order to disrupt any folding which might inhibit solubiliation

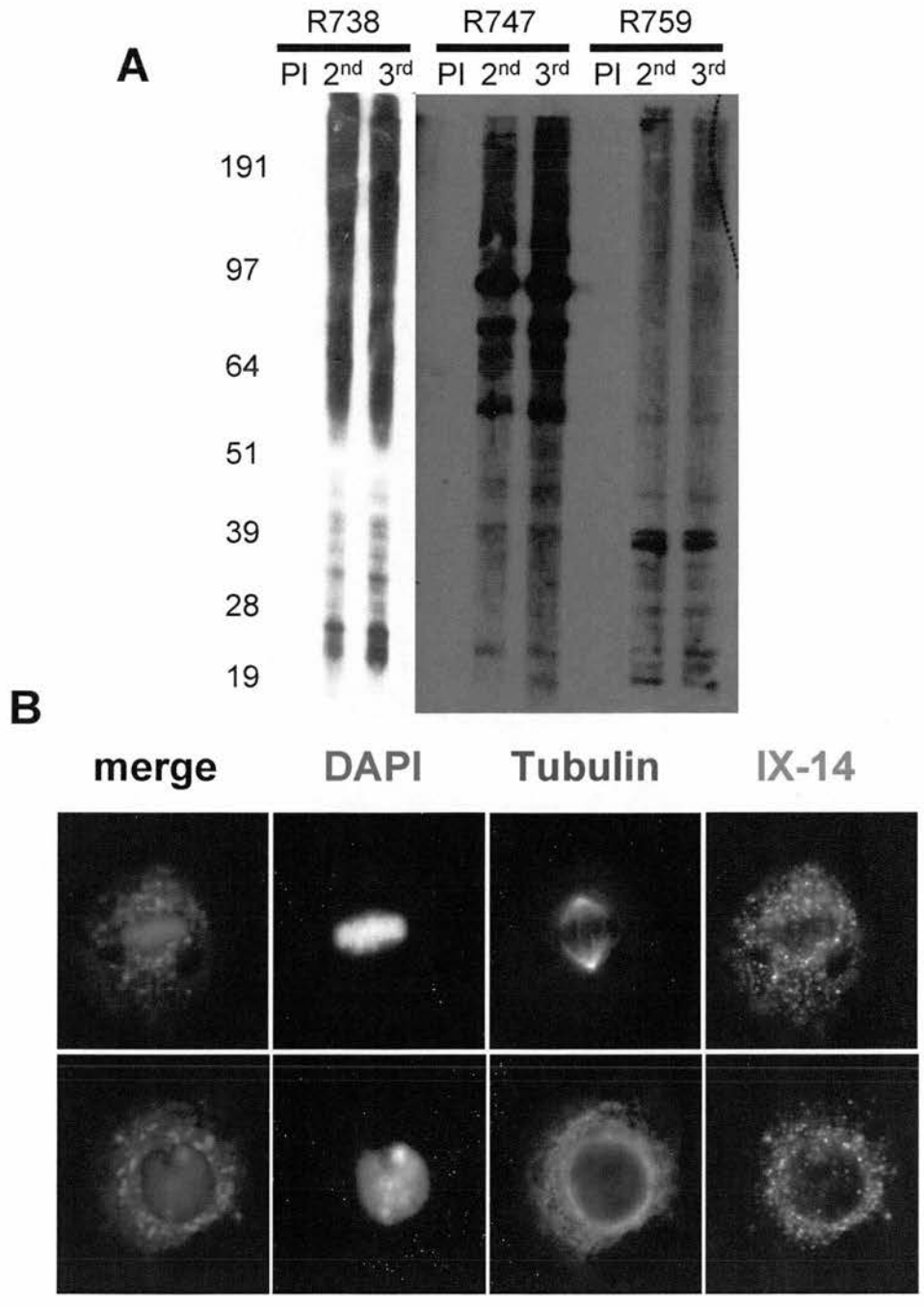

Figure 6.1D: Characterise the DmIX-14 antibody used for expression detection.

A: The immunoblotting of three DmIX-14 antibody (R738, R747, R759), using the pre-immune bleed (PI), immune second bleed (2^{nd}) and immune third bleed (3^{rd}) on S2 cells extract (all in 1:1000 dilution of the serum). Only R747 give bands in immune serum relatively close to predict size (77kDa). R738 antibody was shown in a much less exposure time than R747 and R759. B: Using R747 2^{nd} to immunostain on S2 cells. In both mitosis and interphase, the protein is limit to the cytoplasm. But since the antibody is not affinity purified, it is meaningless.

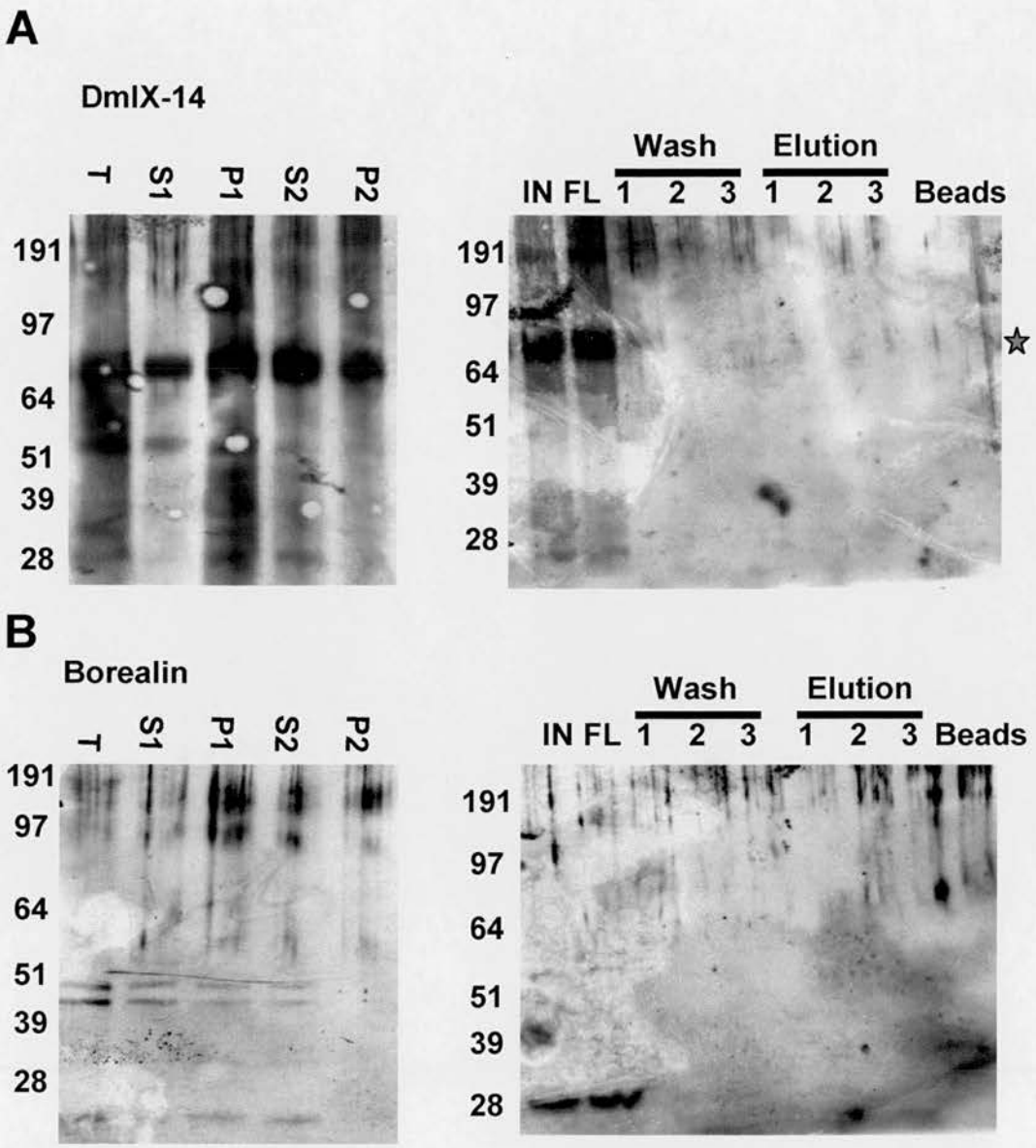

Figure 6.1E: Expression of N-terminally his-tagged DmIX-14.

A: All the membranes were blotted with polyclonal antibody to DmIX-14 (R747). Fractions T, S1, P1, S2, P2 were loaded into each lane of 2 x 10^4 infected cells, while fractions IN, FL, w1-w3, e1-e3, beads were loaded at 10 more concentrated of infected cells into each lane. DmIX-14 was expressed in all the fractions of T, S1, P1, S2, P2. DmIX-14 was unable to bind Ni-NTA beads indicated by the same signal intensity between input (IN) and flow through (FL) and the absence of a signal at the elutions (e1-e3) and beads (red asterisk). B: As expected, no DmIX-14 signal was detected in any of the Borealin infection fractions.

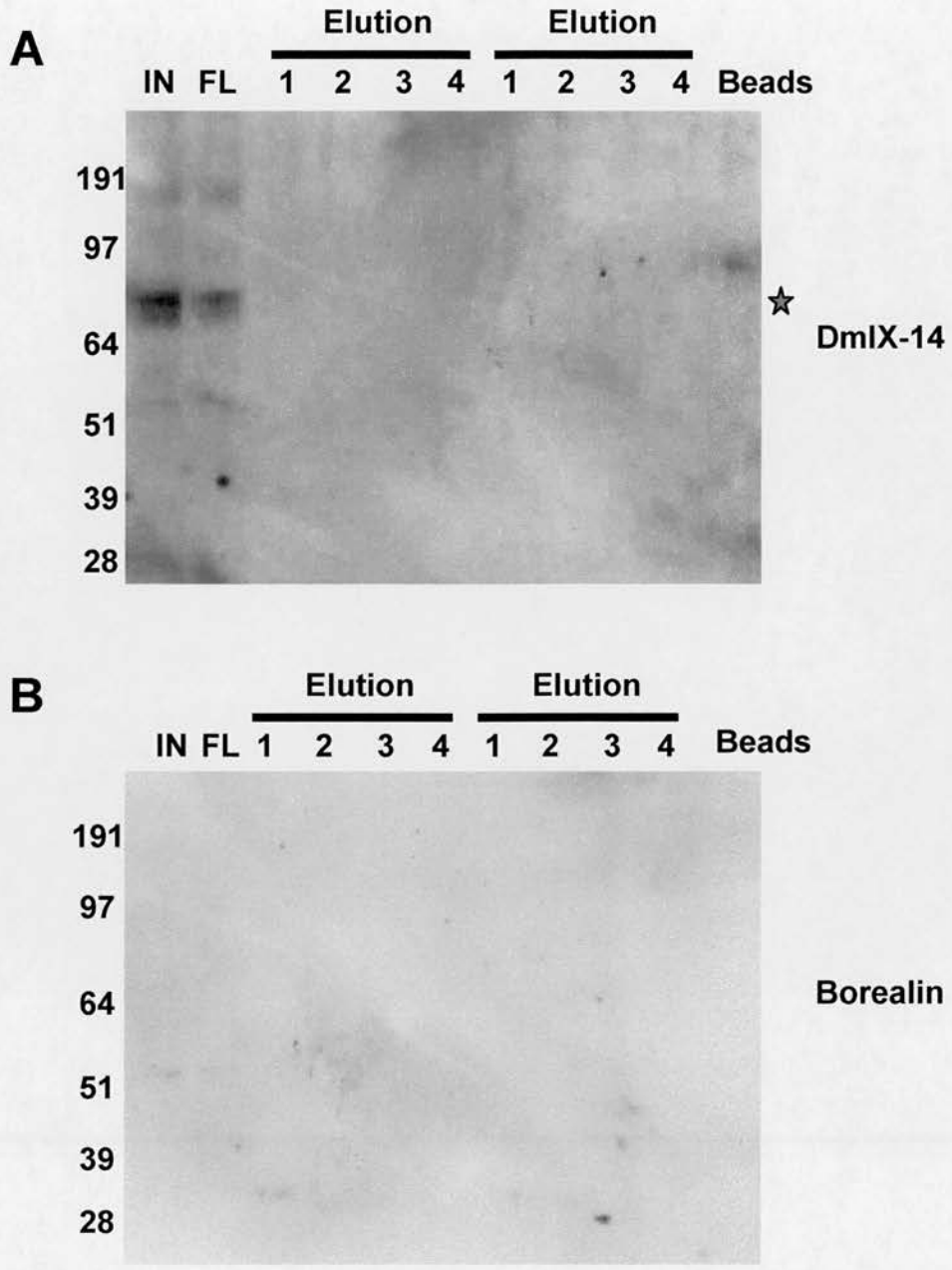

Figure 6.1F: Concentrated fraction of N-terminally his-tagged DmIX-14.

All the membranes were blotted with polyclonal antibody to DmIX-14 (R747). A: Fractions IN, FL were loaded at 2 x 10^5 each lane while fractions w1-w4, e1-e4 and beads were loaded ate 1.35 x 10^7 per lane. DmIX-14 was still unable to bind Ni-NTA beads indicated by the same signal intensity between input (IN) and flow through (FL) and the absence of a signal at the elutions (e1-e4) and beads (red asterisk). B: As expected, no DmIX-14 signal was detected in any of the Borealin infection fractions.

(see material and method). As shown in Figure 6.1G, DmIX-14 did not bind Ni-NTA beads. These results suggest that the his-tag has been lost from DmIX-14. Actually, when antibody to his-tag was used to immunoblot infected cells (fraction T), there was a loss of the N-terminal his-tag from DmIX-14 (Figure 6.1H). No his-tag signal was observed in the cells infected by DmIX-14 recombinant bacmid during the specific time course. A band of the expected size for his-borealin was observed in cells infected by Borealin recombinant bacmid. This indicated that the his-tag on DmIX-14 was cleaved in the baculovirus system.

An alternative vector (pFastBac1) was used to engineered a his-tag on the C-terminus of DmIX-14. Unlike pFastBacHT A which contains a his-tag at N-terminus, pFastBac1 does not have any additional tag fused to the inserted protein. DmIX-14 expression and purification procedures were followed as described earlier (see material and method, condition 1). Similar to previous results, C-terminally his-tagged DmIX-14 also failed to bind to Ni-NTA beads suggesting that the his-tag was lost from this tagged fusion as well (Figure 6.1I). Analysing the sequence of DmIX-14 has identified a signal sequence near the N-terminus and a GPI anchor site near the C-terminus. Both of them might be processed during protein production. This may explain why the his-tag appears to be lost during protein expression. SF9 cells infected by bacmid recombined with Borealin underwent the same expression and purification steps as a positive control. Borealin was not secreted into the medium (S1) but appeared in other fractions, T, P1, S2, P2 (Figure 6.1J). N-terminally his-tagged Borealin bound Ni-NTA beads, as indicated by a difference between input and flow through (although the samples are over loaded, the

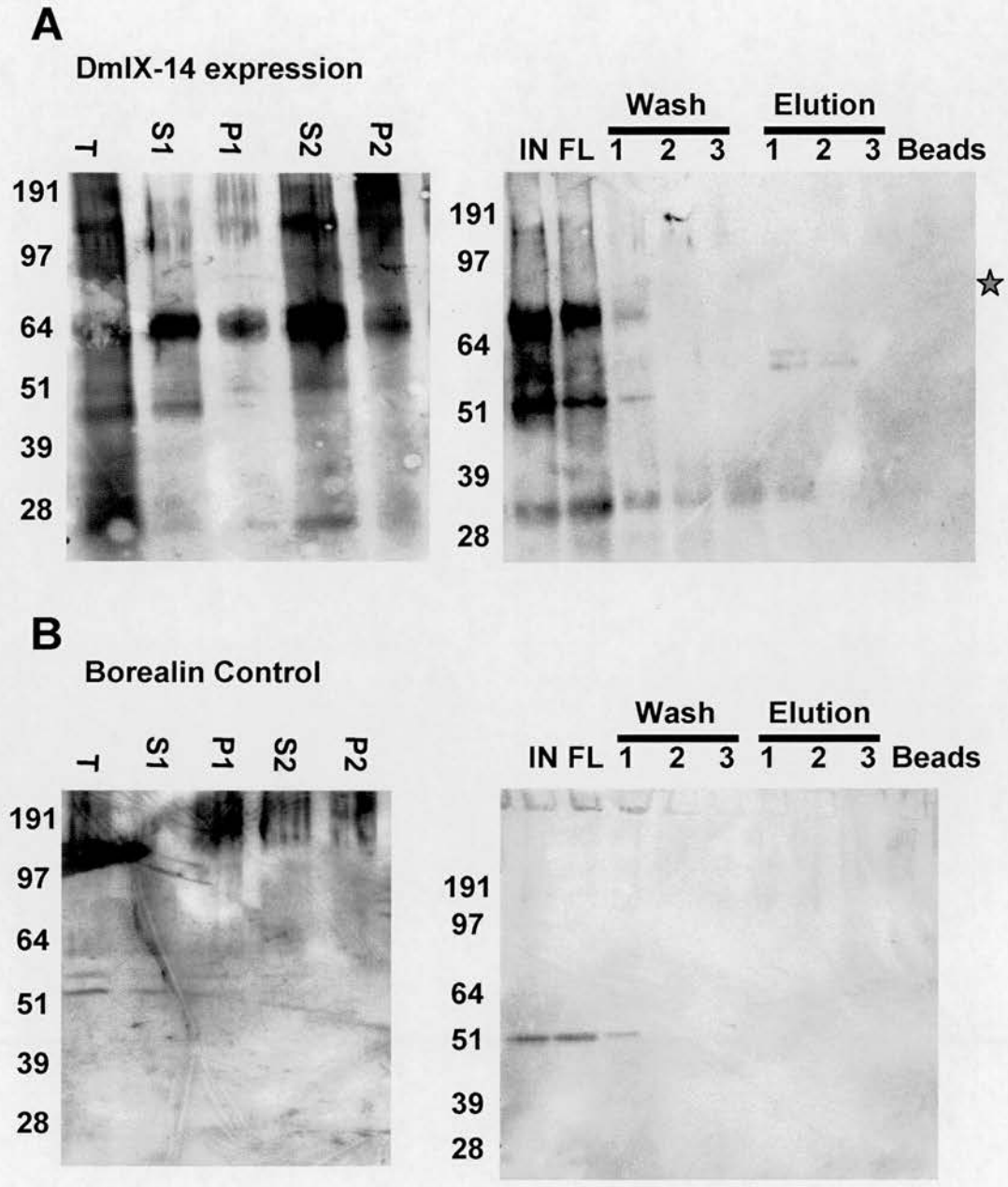

Figure 6.1G: DmIX-14 expression and purification under denaturing conditions.

A: All the membranes were immunoblotted with polyclonal antibody to DmIX-14 (R747). Fractions T, S1, P1, S2, P2 were loaded into each lane of 2 x 10^4 infected cells, while fractions IN, FL, w1-w3, e1-e3, beads were loaded at 10 more concentrated of infected cells into each lane. DmIX-14 was observed in all the fractions of T, S1, P1, S2, P2. DmIX-14 was unable to bind Ni-NTA beads under denaturing conditions (red asterisk). B: As expected, no DmIX-14 signal was detected in any of the fractions from Borealin infection.

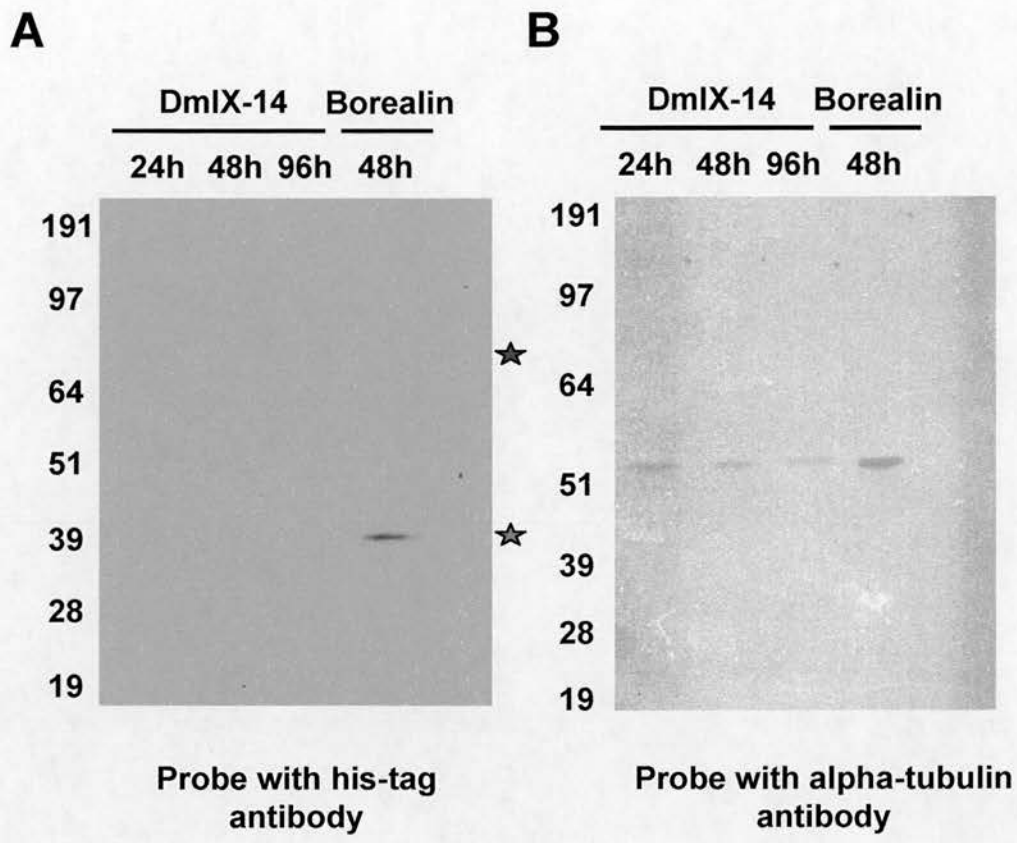

Figure 6.1H: The N-terminal his-tag was lost from DmIX-14.

A: SF9 cells infected by his-tag DmIX-14 were immunoblotted with his antibody during infection time course. Each fraction was loaded into each lane of 2 x 10^4 infected cells. The predict DmIX-14 size signal was not observed (blue asterisk). SF9 cells infected with his-tag Borealin were used as a positive control and the predicted size signal (red asterisk) was observed. B: loading control for A indicated by alpha-tubulin immunoblotting.

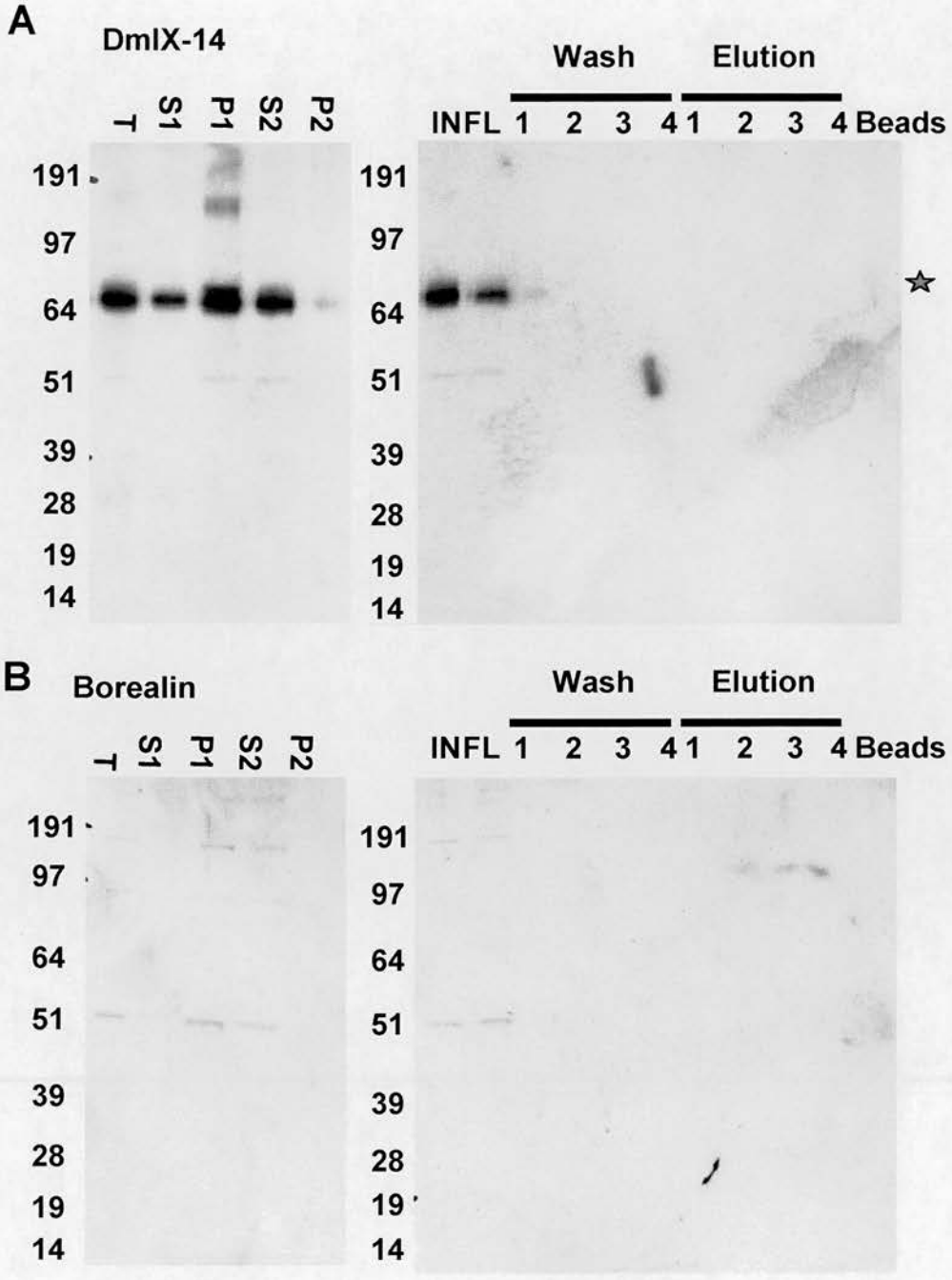

Figure 6.1I: C-terminally his-tagged DmIX-14.

A: All the membranes were immunoblotted with polyclonal antibody to DmIX-14 (R747). Fractions T, S1, P1, S2, P2 were loaded into each lane of 2 x 10^4 infected cells, while fractions IN, FL, w1-w4, e1-4, beads were loaded at 10 more concentrated of infected cells into each lane. DmIX-14 appeared in all the fractions of T, S1, P1, S2, P2. DmIX-14 was unable to bind Ni-NTA beads with its C-terminal his-tag (red asterisk). DmIX-14 signal was not detected in any of the fractions from Borealin infection.

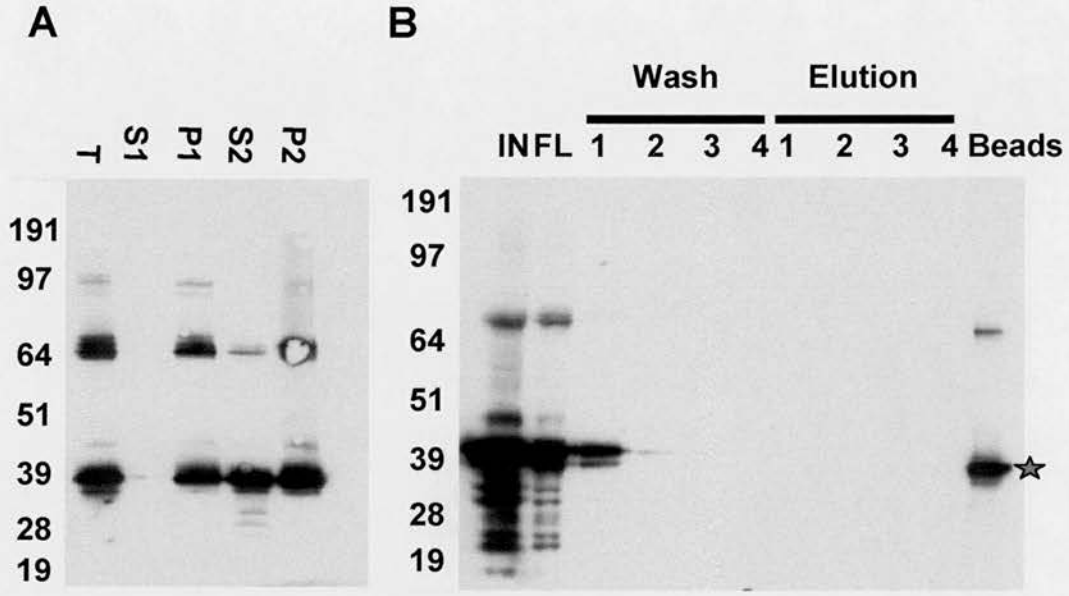

Figure 6.1J: Borealin expression and purification

All the membranes were blotted with anti-Borealin antibody. Fractions T, S1, P1, S2, P2 were loaded into each lane of 2 x 10^4 infected cells, while fractions IN, FL, w1-w4, e1-4, beads were loaded at 10 more concentrated of infected cells into each lane. A: Borealin (about 40 kDa) was expressed in the T, P1, S2, P2. Fractions. However, it was not secreted into the medium that contained the virus (S1). B: Some Borealin bound Ni-NTA beads through its N-terminal his-tag. However his-tagged Borealin could not be eluted from the beads using elution buffer and the protein remains on the beads (red asterisk).

difference was very obvious) but could not be eluted off from the beads indicated by the absence of DmIX-14 band in elution fraction and presence of protein in boiled beads.

The bound borealin demonstrated that the procedure of protein expression and purification did not affect protein binding to the beads. I believe that DmIX-14 did not bind to the beads because its his-tag was lost in the baculovirus system. His-tagged borealin could not be eluted off from the beads might due to their high affinity.

Unfortunately, DmIX-14 could not be purified using his-tags at the N and C-termini in the baculovirus system. Instead, I attempted to use metal sepharose to purify this protein, hoping to take of advantage DmIX-14 being a metalloprotein. After the binding of metal sepharose to $ZnSO_4$, the S2 Baculovirus fraction was incubated with this $ZnSO_4$: sepharose complex. DmIX-14 should bind to the sepharose beads through the interaction at the HEXXH metalloprotease motif. The beads were washed with PBS and DmIX-14 was eluted from the beads by EDTA, a metal chelator that competes with DmIX-14 for $ZnSO_4$. DmIX-14 bound the sepharose beads and could be eluted off by EDTA, although some protein remained on the beads (Figure 6.1K). Sepharose incubated with dH_2O instead of $ZnSO_4$ was used as a negative control. DmIX-14 could not bind to plain sepharose beads as expected in the absence of zinc ion.

In order to check whether the expressed DmIX-14 from baculovirus has activity, protease assays were performed. The elution fraction (e1) (500 µl) was concentrated using a Biomax-5 column (Millipore) and washed several times with PBS to attempt to separate DmIX-14 from EDTA (which could potentially inhibit protease activity of DmIX-14). The e1 fraction was concentrated to 50 µl from an original amount of 3×10^6 infected SF9 cells. Concentrated DmIX-14 (10 µl) was incubated with 4 µl of *in vitro*

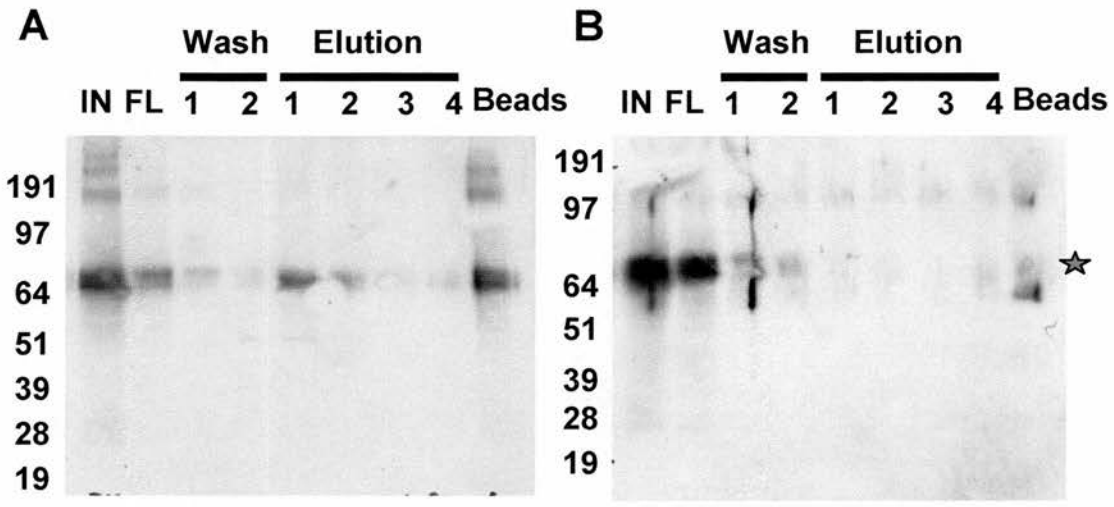

Figure 6.1K: DmIX-14 purification by metal sepharose

All membranes were blotted with polyclonal antibody to DmIX-14 (R747). Fractions were loaded in each lane at 2 x 10^5 of infected cells. A: DmIX-14 (red asterisk) bound the zinc ion : sepharose complex and was not washed off by PBS, but was eluted off by EDTA. B: little DmIX-14 binds to plain sepharose that was not incubated with zinc beforehand.

lamin Dm_O expressed from ProteoMaster kit as described in chapter 5. Lamin Dm0 was completely cleaved by DmIX-14 in the presence or absence of $ZnSO_4$. OPA completely blocked lamin Dm_O cleavage by DmIX-14 e1. However, e1 fraction from Borealin control also cleave lamin Dm_O but not completely. A little lamin Dm_O was left undegraded under the same condition (Figure 6.1L). The e1 fraction from uninfected SF9 cell could also degrade lamin Dm_O to a lesser extent under the same conditions (Figure 6.1L). This could be due to the presence of other metalloproteases co-purified from SF9 cells by the metal sepharose beads. These metalloprotease may also cleave lamin Dm_O. The lamin Dm_O cleavage difference between uninfected SF9 cells and borealin recombinant bacmid infected SF9 cells might be due to some protease that are over expressed during infection. The lamin Dm_O cleavage difference between borealin recombinant bacmid infected SF9 cells and DmIX-14 recombinant infected SF9 cells might be due to activity of DmIX-14.

In summary, both N and C–termini his-tags fusion was lost in baculovirus system during of after protein production. Metal sepharose could not purify DmIX-14 specifically. There are a lot of other metalloprotease was purified as well, some of which could cleave lamin Dm0.

6.2 Expression of *DmIX-14* using Pichia pastoris.

Since the his tags of DmIX-14 keep losing in baculovirus system and it takes months for the whole procedure from cloning to purification, *Pichia pastoris* was used as an alternative system to express DmIX-14. Yeast expression systems bears the advantage of easy genetic manipulation, rapid growth like prokaryotic organisms, available subcellular

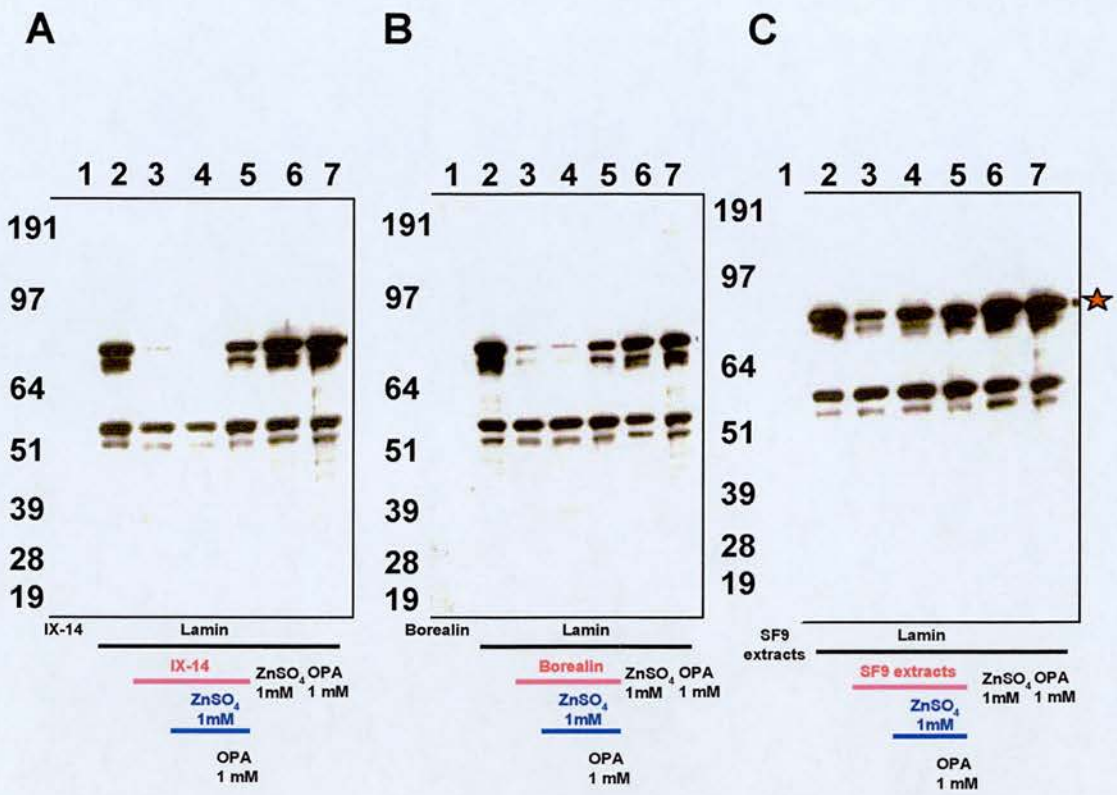

Figure 6.1L: Protease activity of elution fractions.

All the membranes were blotted with polyclonal antibody against full length lamin Dm0 (lamin Dm0 signal was indicated by red asterisk). Elution one (e1) fraction from Zn^{++} : sepharose beads was incubated with lamin Dm0 expressed from ProteoMaster kit described in Chapter 5. A: lamin Dm0 cleavage using the e1 fraction from DmIX-14 infection. DmIX-14 elution fraction alone does not show any signal by this antibody (lane 1). Lamin Dm0 was almost completely cleaved when it was mixed with e1 from DmIX-14 infection in the presence (lane 4) or absence (lane 3) of $ZnSO^4$. Addition of OPA inhibited lamin Dm0 cleavage (lane 5). Panel B: lamin Dm0 cleavage was also observed when the e1 from Borealin infection was assayed. Panel C: lamin Dm0 cleavage was observed when e1 from control SF9 cell extracts with no infection was assayed although the cleavage was in a far less extend.

machinery for potentially post-translational protein modifications of eukaryotic cells. *Pichia pastoris* is a methylotrophic yeast, which use methanol as its sole carbon source.

The first step of utilization of methanol is the oxidation of methanol to formaldehyde using oxygen by the enzyme alcohol oxidase (Invitrogen). There are two genes coding for alcohol oxidase in *Pichia pastoris*, AOX1 and AOX2. These genes share 97% homology in their coding sequence but no homology outside the protein coding sequences. AOX1 accounts for the majority of alcohol oxidase activity in the cell while AOX2 metabolizes methanol slower than AOX1. The difference sequence located 5' of the protein coding region of the genes might account for this activity difference. This slow growth allows isolation of Mut^S (Methanol utilisation Slow) strains such as KM71H, which has a mutated form of AOX1 gene (substitute 0.6 kb of *AOX1* from the 5'-most site by a 3.0-kb gragment containing the *S. cerevisiae ARG4* gene) (Cregg, Madden et al. 1989) (Koutz, Davis et al. 1989).

I cloned the DmIX-14 ORF into the pPICZalpha A vector. This vector fused a protein alpha-factor sequence at the N-terminus of DmIX-14 and c-myc and his-tags at the C-terminus. After being linearised, recombinant plasmid was transformed into the KM71H stain where it integrates within the *Pichia* genome. Transformed yeast were plated on zeocin selective YEPD plates. Recombination of the yeast genome was confirmed by PCR, using the isolated yeast genome as template. As Figure 6.2A shows, one of the yeast colonies was verified by PCR to have the right construct. This colony was selected together with a colony from KM71H yeast transformed with the pPICZalpha A vector (excluding the insertion) and a colony from KM71H yeast that was not transformed. All colonies were grown in BMG medium. When the OD600 reached 2.5,

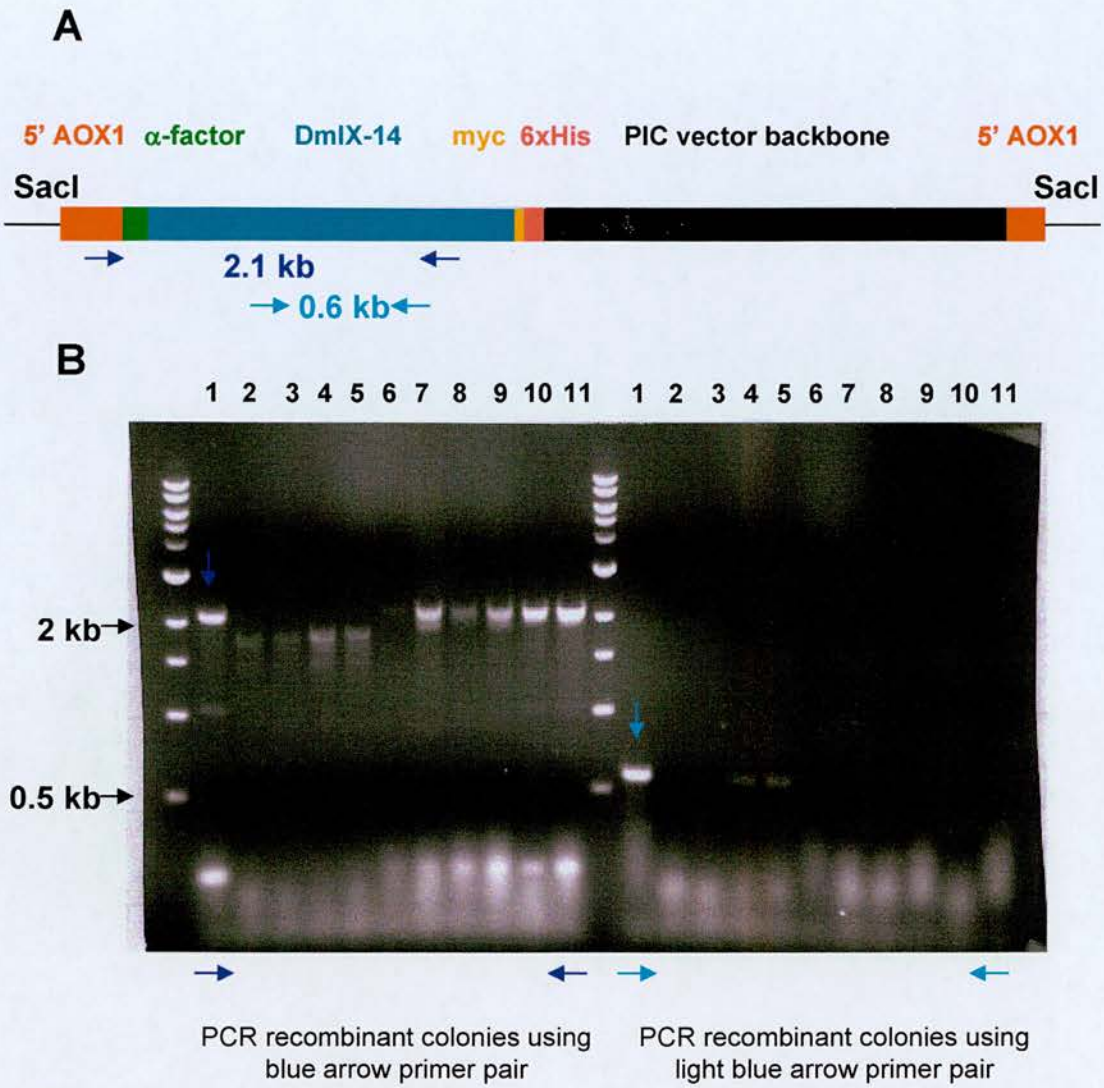

Figure 6.2A: Verification that DmIX-14 recombined into the *Pichia* genome.

A: Schematic graph of linear *DmIX-14* ORF in pPICZalpha A used to be transformed into the KM71H stain. B: PCR confirmation of recombined construct into the *Pichia* genome. Eleven colonies were picked for PCR analysis using the pairs of primers indicated in panel A. Only one (lane 1) had the appropriately sized band for both PCR reactions. This clone was used for protein purification.

the cultures were induced by the addition of methanol (BMM medium, 1/10 of the original volume). Aliquots of sample cultures (1 ml) were removed for analysis at the time points: 0h, 9h, 12h. Figure 6.2B is a schematic of the fractionation and solubilization of expressed DmIX-14. In brief, sample cultures were centrifuged, the supernatant was saved as S1 (supernatant 1) and the pellet was resuspended in breaking buffer (see material and method) as P1 (pellet 1). Resuspended P1 was vortexed on ice with glass beads in a centrifuge tube, followed by centrifugation. The new supernatant was saved as S2 while the pellet (P2) was resuspended with 1X SDS-PAGE sample buffer and boiled. Although alpha-factor is fused to the N-terminus of DmIX-14, and should be processed to allow protein secretion into the medium, no DmIX-14 was detected in the medium, S1 (Figure 6.2C Panel A). DmIX-14 was induced by methanol at the time points 9h and 12h in yeast by the vector containing the DmIX-14 insert, but not the vector only (Figure 6.2C, arrow). However, DmIX-14 was not solublized in the supernatant fractions under these conditions. DmIX-14 was observed in the P1 (panel B) and P2 (panel D) blots, but not in S1 (panel A) and S2 (panel C).

Alternative approaches are now being explored in the laboratory to identify the best lysis conditions to allow protein purification. These include using several different lysis buffers and mechanical lysis methods such as grinding cells with glass beads in a larger volume container (perhaps appropriate cell lysis was not achieved with glass beads in the centrifuge tube) or grinding cells in liquid nitrogen or lyse cells using French Press. Under these new conditions, other lab members have been able to partially solubilize DmIX-14. However, this solubilization process is still being optimised.

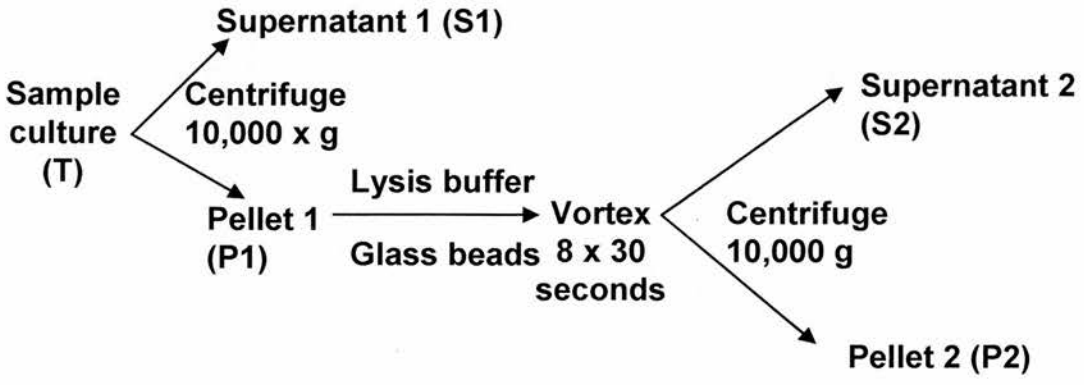

Figure 6.2B: Schematic graph of the fractionation and solubilization of expressed DmIX-14.

The recombinant colony was grown in BMG medium and induced by changing the medium to BMM medium. Aliquots were removed from the BMM medium at different time points (0, 9, 12 hrs). Cultures were centrifuged and the initial supernatant was saved as S1 and pellet as P1. P1 was resuspended in lysis buffer and vortexed after glass beads were added. Another centrifugation was performed to separate soluble protein in the second supernatant (S2). P2 was resuspended in 1X sample buffer.

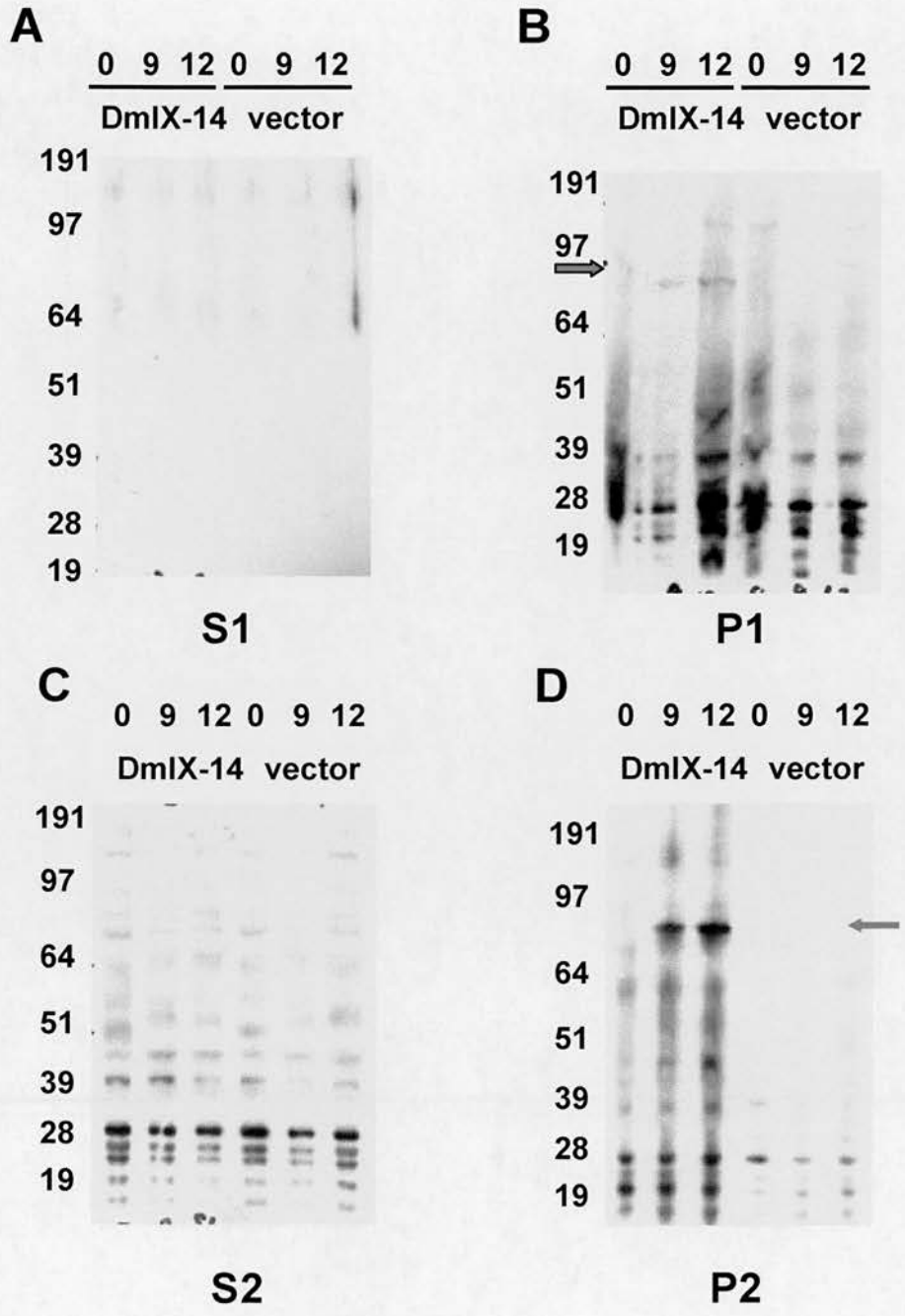

Figure 6.2C: DmIX-14 was not solublized from the pellet fractions.

All blots were probed with the anti-myc antibody. A: No band of expected size of DmIX-14 was observed in S1. B: A band of the expected size for DmIX-14 appeared in *Pichia* after 9 and 12 hrs inductions (arrow). This band was not observed in *Pichia* cells transformed with vector only. C: The DmIX-14 band did not appear in the S2 fraction of DmIX-14 or vector. D: The induced DmIX-14 band appeared in the P2 fraction and not in the vector control.

Chapter 7: Discussion

During the three years research on IX-14/Invadolysin, I get the conclusion that three nuclear envelope proteins were accumulated in *IX-14* mutant; IX-14 could cleave lamin Dm0 *in vitro*; there is a germ cell migration defect in *IX-14* mutant; His-tags at N and C terminal of *Drosophila* IX-14 were cleaved in baculovirus system. These results suggest that lamin Dm0, lamin A/C, otefin was potential substrates of *Drosophila* IX-14; IX-14 is involved in cell migration in *Drosophila*; *Drosophila* IX-14 might went through translation and post-translation modification to cleave off its signal sequence near N-terminus and GPI replacement signal near C-terminus.

7.1 Role of Invadolysin.

Invadolysin is a metalloprotease which links the cell cycle with cell migration. The *Drosophila Invadolysin* mutants have defects in spindle formation, centrosome separation, cell cycle progression, chromosome structure and condensation, abnormal accumulation of nuclear envelope proteins, and germ cell migration.

It is possible that the spindle defects may be due to an upstream defect of some other cell cycle defect and not due to abnormal centrosome separation. This assumption is based on the observation that almost normal-looking bipolar spindles were observed in the background of *asterless*, a mutant which abolishes centrosome formation, in *Drosophila* neuroblasts and ganglion mother cells (Bonaccorsi, Giansanti et al. 2000). In addition, the checkpoint protein BubR1 remains on chromosome and maybe important

for cell cycle arrest in metaphase. A metaphase arrest was also confirmed by the higher percentage of P-H3 positive cells in this mutant compared to wild type and a complete absence of anaphase and telophase cells in the *Invadolysin* mutant. It is not surprising to see the chromosome passenger protein INCENP did not display the dynamic localisation pattern but instead was only limited to the centromeres since there is no anaphase cells. Whether this change affects other passenger proteins like Survivin (which is a member of the inhibitor of apoptosis protein (IAP) family) and in turn may be responsible for the high apoptosis rate observed in *Invadolysin* mutants would be an interesting hypothesis to test. Currently, there is no evidence for a direct role for Invadolysin in centrosome separation or spindle assembly. However, Invadolysin might affect centrosome separation through its substrates.

Mask (multiple ankyrin repeats single KH domain) and tankyrase, which are structural constituents of the cytoskeleton, were identified as potential interactors of Invadolysin in a genome-wide two-hybrid screen (Giot, Bader et al. 2003). They both contain ankyrin repeats which bind actin. Actin has been shown to participate in centrosome separation during the G2/M transition and works in synergy with the microtubules to accelerate centrosome separation during mitosis (Uzbekov, Kireyev et al. 2002). Spindle formation can occur independently of the centrosomes as described above, but it could still be affected by actin. Actin has been reported to regulate spindle orientation (Hwang, Kusch et al. 2003). This may suggest a different pathway that involves actin regulation of centrosome separation and spindle formation.

Invadolysin mutants also have unusually hypercondensed chromosomes with loose edges in metaphase which suggests a chromosome structure or condensation defect. This

could be due partly to the cell cycle arrest at metaphase which would allow more time for chromosome condensation. Alternatively, Invadolysin could have a direct role on components such as topoisomerase II or condensin, or be a result of disruption of a novel pathway in which proteolysis plays a role in chromosome condensation. However, loosely condensed chromatin was found around the periphery of hypercondensed chromosomes in this mutant which may argue a structural role for this protein in chromosome condensation. Invadolysin might affect chromosome scaffold binding to SARs of DNA. This may make the edge of the chromosomes fuzzy even though the overall level of condensation was increased. This loosely condensed chromatin could not be condensed normally by colchicine treatment which delays cells in metaphase. This indicated again the loosely condensed chromatin was due to a distinct pathway separate from overall chromosome condensation. Invadolysin also appears to have a role in chromosome architecture during interphase because mutations exhibit poorly structured polytene chromosomes in salivary gland and have compromised heterochromatin, as assayed by position effect variegation.

The other phenotype of the *Invadolysin* mutant is the accumulation of several nuclear envelope proteins (lamin Dm0, lamin A/C and otefin) in neuroblasts. This funding suggests that Invadolysin or one of its downstream targets normally promotes the turnover of these nuclear envelope proteins. In fact, cleavage may be due to Invadolysin itself, as the *Drosophila* Invadolysin can cleave *Drosophila* lamin Dm0 in vitro in a zinc-dependent manner. Lamina dynamics in mitosis are regulated by reversible phosphorylation of CdK1:cyclin B and are reused at nuclear envelope reformation during telophase (Gant and Wilson 1997). Cyclin B was used as a marker to distinguish G2

cells, interestingly I have observed low levels of cyclin B in the *Invadolysin* mutant. Whether a low level of cyclin B in *Drosophila Invadolysin* mutants act upstream the lamin accumulation directly or indirectly remains unclear. This is because lamin accumulation is not cell cycle dependent (while the CdK1:cyclin B remains at low level consistently throughout interphase). The low level of cyclin B could due to the fact that invadolysin could alter the activity of a phosphatase. Cdc25 phosphatase was well know to regulate cyclin B/Cdk1 acticity (Strausfeld, Labbe et al. 1991). Recently, it was reported that cyclin B translation was suppressed by protein phosphatase 1 (PP1) until break down of nuclear envelope, when a potent translational activator (most like the PP1 inhibitor) was delivered to the cytoplasm (Lapasset, Pradet-Balade et al. 2005). Invadolysin does play a role to prevent nuclear envelope broke down during mitosis, it might prevent releasing the PP1 inhibitor and keep suppressing cyclin B translation. GP63, the *Leishmania* protease, can cleave its potential substrate MRP between the consensus cleavage site in its effector domain, Ser^{92} / Phe^{93} Lys^{94}. Intriguingly, this cleavage sequence was also found in lamin Dm0. If utilized, the resultant cleavage products should be 25 and 46 kDa. However no cleavage bands of this size could be detected by immunoblotting in the protease assay with lamin antibodies. Radioactive labelled lamin was needed to identify the cleavage band. Investigation of lamin or otefin sequence showed that ser / phe lys was not present in either lamin A/C or otefin. This cleavage site was not present in *Drosophila* lamin A/C or otefin. Whether Invadolysin cleaves lamin Dm0 at the same cleavage site as GP63 cleaves MRP remains unknown. If Invadolysin uses the same cleavage site as gp63, lamin A/C and otefin accumulation must be a downstream event of lamin Dm0 cleavage as they could not be cleaved themselves.

No obvious homology was observed between MRP and any of the accumulated proteins (lamin Dm0, lamin A/C and otefin) in *Drosophila*, except the common cleavage site between lamin Dm0 and MRP. However, although the mechanism and timing of the Invadolysin-dependent nuclear envelope turnover has yet to be determined, the phenomenon is important because it reveals previously unsuspected complexity of nuclear envelope dynamics during the cell cycle. Significantly, lamin is reported to be involved in a wide range of diseases known collectively as "laminopathies". These include striated-muscular dystrophy, partial lipodystrophy, peripheral neuropathy and premature aging syndromes eg. progeria (Worman and Courvalin 2005). Further research on Invadolysin may shed light on the intricate molecular mechanism of lamin turnover, and may in turn lead to information into these diseases.

Beside Invadolysin, there must be other proteases which can cleave lamin as indicated by cleavage of lamin in the un-transformed SF9 cell extracts in baculovirus expression system. Whether those as yet unidentified proteases interact with Invadolysin might be an interesting question to be answered. How the nuclear envelope protein defects coordinate with the chromosome condensation and architecture defects is an interesting issue. One possibility is that Invadolysin might regulate interactions between chromatin and the nuclear envelope that are important for gene expression and/or mitotic chromosome condensation.

Although a nuclear pool of Invadolysin is detectable in human cells, the protein is also localized to the cytoplasm, where it is concentrated in unusual ring-like structures in human cells. These structures are observed during interphase in a number of transformed human cultured cells, but become dispersed during mitosis, when the protein adopts a

more diffuse distribution. These ring-like structures resemble invadopodia, cytoplasmic structures that have been proposed to have an important role in cell migration and cancer metastasis. Like invadopodia, the ring-like structures containing Invadolysin are localized to the lower third of the cell close to the substratum. This finding led us to test the migration role of Invadolysin in both human and *Drosophila* cells. When migrating human macrophages were labelled with the Invadolysin antibody, the Invadolysin protein was strikingly localized to leading edge of the cells. In *Drosophila* mutants, I observed a germ cell migration defect in embyros. These results suggested strongly that Invadolysin is involved in cell migration. Ching-Wen Chang, a Ph.D. student in the Heck laboratory has performed wound healing experiments to further analyse a role for Invadolysin in cell migration. When HeLa cells were "wounded" by a pipette tip, Invadolysin localize to the wound edge within 3 hours. GP63, the ortholog of Invadolysin has been shown to enhance migration of *Leishmania* through the extracellular matrix (ECM) (McGwire, Chang et al. 2003). This activity might be due to the fact that GP63 can degrade ECM components. Invadolysin might affect cell migration by degrading the ECM to clear a pathway for cells, hence the localisation at the leading edge or invadopodia. It is reported that cell migration is driven by the protrusive activity at the leading edge of the cell, where continuous remodelling of actin and adhesive contacts are required (de Curtis 2001). The potential interactors of Invadolysin, mask and tankyrase, which possess actin binding activity, may present a possible explanation for the migratory role of Invadolysin. It is also possible that Invadolysin is involved in cell migration by regulating some signaling proteins such as cell surface receptors. Actually, it was report that EGF

(epidermal growth factor) and EGF receptor signalling are necessary for invadopodia formation (Yamaguchi, Lorenz et al. 2005).

Intriguingly, dynamin 2, which is also found in invadopodia, has been shown to play a role in centrosome cohesion (Thompson, Cao et al. 2004). This connection ties in well with our results linking migration with mitosis.

7.2 Why Invadolysin has diverse functions.

Invadolysin has been shown to play diverse roles in the cell cycle and cell migration. How these different roles are coordinated by Invadolysin raises a very interesting question. Invadolysin might perform its diverse role through its interactors. As mention above, mask and tankyrase, which were found as interactors of Invadolysin in a genome-wide two hybrid screen, might affect cell migration through their actin binding activity. A Ph.D. student in the Heck laboratory, Shubha G. Rao, has found a genetic interactor for Invadolysin, *non-stop*. Non-stop is a ubiquitin-specific protease that is involved in glial cell migration and affects the target layer selection in the visual system of *Drosophila* (Poeck, Fischer et al. 2001). S. Rao has also shown that the *non-stop* mutant has hypercondensed chromosomes in metaphase neuroblasts cells similar to those observed in the *Invadolysin* mutant. In addition, both *Invadolysin* and *non-stop* mutants show accumulation of ubiquitinated proteins in larval extracts. When S. Rao compared the immunoblotting pattern of ubiquitinated proteins and histone H2B in larval extracts, she observed similar patterns. This may indicate that the ubiquitinated proteins might in fact be ubiquitinated histone H2B. The yeast homologue of *non-stop*, ubp8 (ubiquitin specific protease 8), exhibits the ability to deubiquitylate histone H2B and regulate transcriptional

activity (Henry, Wyce et al. 2003). Whether ubiquitinated histone H2B is associated with the defects in chromosome condensation has not yet been clearly determined. Invadolysin might be involved in protein degradation pathways directly or through interaction with non-stop, which may in turn regulate many other cell cycle or cell migration events.

The other way in which Invadolysin may carry out roles in such diverse functions is through the presence of different variants. In human, there are current four variants. Four variants were described in Chapter 1. They differ in with or without a 37 amino acid insertion and with or without a N-terminal signal sequence as described previously. The variants that bears N-terminal signal sequences would be targeted to the ER and GPI anchored on the cell membrane, thus might be involved in cell migration. The other variants that lack the N-terminal signal sequences would not be targeted to ER and thus likely not GPI anchored on the cell membrane, and possibly involved in the cell cycle. In *Drosophila*, only one variant has been found to date (include N-terminal signal sequence, GPI–anchored and the 37 amino acid insertion), but the existence of alternative splice forms of Invadolysin in flies is still possible. Identification of such forms would help us to understand more about the diverse functions of Invadolysin.

7.3 How to activate Invadolysin.

In order to further characterise the *in vitro* activity of DmInvadolysin, it is necessary to express the protein in a large scale. However this has proved to be very difficult. Perhaps this is because the protease requires a "cysteine switch" to be activated. The presence of signal sequence near the N-terminus and the GPI anchor signal near the C-

terminus also make its difficult to tag and purify this protein as they would be potentially cleaved during translation and post-translational modification. Tagging the protein in the middle may run the risk of altering the tertiary structure and thus altering the protein's function. It is possible that the cleavage observed with the first *ivTnT* kit, (Circular template kit), was due to its slower expression allowing the protease enough time to fold properly or to perform auto-cleavage, or to be activated by other proteases. An alternative method utilising *Pichia* (allowing slow induction by methanol) was also initiated to express the protein. However, whether *Pichia* expression could result in a large enough quantity of active protein remains unknown.

7.4 Future Direction.

Invadolysin is an interesting and dynamic protein involved in a wide range of activities from cell cycle to cell migration. The potential for this protein to be involved in many fundamentally crucial pathways is enormous, and warrants a great deal more investigation.

Large quantity expression of active Invadolysin would provide a platform for many other aspects of research on Invadolysin. Tagging the protein at a site where surface insertions occur (based on comparison with the GP63 sequence) would be a potential way to try to purify Invadolysin. Treating the inactive Invadolysin *ivTnT* expressed from Reticulocyte kit, ProteoMaster Kit and HTP kit with $HgCl_2$ might make GP63 active by abolishing the protease inhibitory coordination between Cysteine and the active-site zinc. This might activate Invadolysin based on the hypothesis that homologues would use the same mechanism to be activated.

Finding alternative splice forms and substrates of Invadolysin would be an important way to understand the link between this protein and its activities. RT-PCR on different tissues or cell lines from both human and *Drosophila* could be performed to examine the tissue or cell specific distribution of alternatively spliced forms of Invadolysin. Although genome-wide two-hybrid screen has been performed in *Drosophila*, a more specific two-hybrid screen performed in the laboratory may be able to identify more relevant or stronger interactors. Other biochemical methods such as immuno-precipitation or multiple tag pull downs could be performed to "fish out" further interactors of Invadolysin. A genetic screen using a deficiency library that covers about 50 percent of the whole *Drosophila* genome has been performed to identify genetic interactors of Invadolyisin. With the availability of more deficiency lines, a whole genome-wide genetic screen could be performed for Invadolysin. Further characterization of some of already identified interactors of Invadolysin such as lamin Dm0, nonstop and mask should also be performed.

IX-14 mutant was originally characterised as a mutation affecting imaginal disc formation and chromosome condensation, but it was found involving in a much wider range of biological process than original findings such as cell cycle and cell migration. In turn, IX-14/Invadolysin was implicated in some important medical roles, for example, cancer metastasis and laminopathies. Further characterisation of Invadolysin would shed light on understanding of cancer and laminopathies and finally make them more treatable. Among the 27 interactor of invadolysin, three has been found to connect with human disease in their human homologues in OMIM. Henna (CG7399) is a phenylalanine hydroxylase whose human homologue is connected to Huntington's disease (HD) that

results from genetically programmed degeneration of neurons in certain areas of the brain. CG12789 poses scavenger receptor activity, its human homologue is connected to Carotid Intimal-Medial Thickness. CG6508 have cathepsin D activity, its human homologue is connected to Huntington Disease, Ceroid Lipofuscinosis (CL) (a metabolic disease which affects the nerve cells of the body), and Alzheimer disease (AD) (neurodegenerative disease). Explore interactor of invadolysin and their interaction will give more information about these diseases.

References:

Aebi, U., J. Cohn, et al. (1986). "The nuclear lamina is a meshwork of intermediate-type filaments." Nature. **323**: 560-564.

Arbuzova, A., A. A. Schmitz, et al. (2002). "Cross-talk unfolded: MARCKS proteins." Biochem J. **362**: 1-12.

Ashery-Padan, R., N. Ulitzur, et al. (1997). "Localization and posttranslational modifications of otefin, a protein required for vesicle attachment to chromatin, during *Drosophila melanogaster* development." Mol Cell Biol. **17**: 4114-4123.

Baldassarre, M., A. Pompeo, et al. (2003). "Dynamin participates in focal extracellular matrix degradation by invasive cells." Mol Biol Cell. **14**: 1074-1084.

Beynon, R. and J. S. Bond (2001). Proteolytic enzymes. Oxford, Oxford Univeristy Press.

Biamonti, G., M. Giacca, et al. (1992). "The gene for a novel human lamin maps at a highly transcribed locus of chromosome 19 which replicates at the onset of S-phase." Mol Cell Biol. **12**: 3499-3506.

Bonaccorsi, S., M. G. Giansanti, et al. (2000). "Spindle assembly in *Drosophila* neuroblasts and ganglion mother cells." Nat Cell Biol. **2**(1): 54-56.

Bonini, N. M., Q. T. Bui, et al. (1997). "The *Drosophila* eyes absent gene directs ectopic eye formation in a pathway conserved between flies and vertebrates." Development. **124**: 4819-4826.

Bonini, N. M., W. M. Leiserson, et al. (1993). "The eyes absent gene: Genetic control of cell survival and differentiation in the developing *Drosophila* eye." Cell. **72**: 379-395.

Bossie, C. A. and M. M. Sanders (1993). "A cDNA from *Drosophila melanogaster* encodes a lamin C-like intermediate filament protein." J cell Sci. **104**: 1263-1272.

Bouvier, J., P. Schneider, et al. (1990). "Peptide substrate specificity of membrane-bound metalloprotease of *Leishmania*." Biochemistry. **29**: 10113-10119.

Boyle, M., N. Bonini, et al. (1997). "Expression and function of clift in the development of somatic gonadal precursors within the *Drosophila* mesoderm." Development. **124**: 971-982.

Boyle, M. and S. DiNardo (1995). "Specification, migration and assembly of the somatic cells of *Drosophila* gonad." Development. **121**: 1815-1825.

Brinckerhoff, C. E. and L. M. Matrisian (2002). "Matrix metalloproteinases: a tail of a frog that became a prince." Nat Rev Mol Cell Biol. **3**: 207-214.

Brookman, J. J., A. T. Toosy, et al. (1992). "The 412 retrotransposon and the development of gonadal mesoderm in *Drosophila*." Development. **116**: 1185-1192.

Corradin, S., A. Ransijn, et al. (1999). "MARCKS-related Protein (MRP) is a substrate for the *Leishmania* major surface protease Leishmanolysin (gp63)." J Biol Chem. **274**: 25411.

Cregg, J. M., K. R. Madden, et al. (1989). "Functional characterization of the two alcohol oxidase genes from the yeast, *Pichia pastoris*." Mol Cell Biol. **9**: 1316-1323.

de Curtis, I. (2001). "Cell migration: GAPs between membrane traffic and the cytoskeleton." EMBO Rep. **2**: 277-281.

Dwyer, N. and G. Blobel (1976). "A modified procedure for the isolation of a pore complex-lamina fraction from rat liver nuclei." J Cell Biol. **70**: 581-591.

Ellis, D. J., H. Jenkins, et al. (1997). "GST-lamin fusion proteins act as dominant negative mutants in Xenopus egg extract and reveal the function of the lamina in DNA replication." J cell Sci **110**: 2507-2518.

Farnsworth, C. C., S. L. Wolda, et al. (1989). "Human lamin B contains a farnesylated cysteine residue." J Biol Chem. **264**: 20422-20429.

Fawcett, D. W. (1966). "On the occurrence of a fibrous lamina on the inner aspect of the nuclear envelope in certain cells of vertebrates." Am J Anat. **119**(1): 129-145.

Gant, T. M. and K. L. Wilson (1997). "Nuclear assembly." Annu Rev Cell Dev Biol. **13**: 669-695.

Gatti, M. and B. S. Baker (1989). "Genes controlling essential cell-cycle functions in *Drosophila melanogaster*." Genes & Dev. **3**(4): 438-453.

Gerace, L. and G. Blobel (1980). "The nuclear envelope lamina is reversibly depolymerized during mitosis." Cell. **19**: 277-287.

Gerace, L., A. Blum, et al. (1978). "Immunocytochemical localization of the major polypeptides of the nuclear pore complex-lamina fraction. Interphase and mitotic distribution." J Cell Biol. **79**(2): 546-566.

Gimona, M. and R. Buccione (2006). "Adhesions that mediate invasion." Int J Biochem Cell Biol. **38**(11): 1875-1892.

Giot, L., J. S. Bader, et al. (2003). "A protein interaction map of *Drosophila melanogaster*." Science. **302**: 1727-1736.

Goldberg, M., H. Lu, et al. (1998). "Interactions among *Drosophila* nuclear envelope proteins lamin, otefin, and YA." Mol Cell Biol. **18**: 4315-4323.

Goldman, A. E., G. Maul, et al. (1986). "Keratin-like proteins that coisolate with intermediate filaments of BHK-21 cells are nuclear lamins." Proc Natl Acad Sci U S A. **83**: 3839-3843.

Gross, J. and C. M. Lapiere (1962). "Collagenolytic activity in amphibian tissues: a tissue culture assay." Proc Natl Acad Sci U S A. **48**: 1014-1022.

Gruenbaum, Y., Y. Landesman, et al. (1988). "*Drosophila* nuclear lamin precursor Dm0 is translated from either of two developmentally regulated mRNA species apparently encoded by a single gene." J Cell Biol. **106**: 585-596.

Hamdan, F. F., S. D. Ward, et al. (2002). "Use of an in situ disulfide cross-linking strategy to map proximities between amino acid residues in transmembrane domains I and VII of the M3 muscarinic acetylcholine receptor." Biochemistry. **41**: 7647-7658.

Handsley, M. M. and D. R. Edwards (2005). "Metalloproteinases and their inhibitors in tumor angiogenesis." Int J Cancer. **115**: 849-860.

Harel, A., E. Zlotkin, et al. (1989). "Persistence of major nuclear envelope antigens in an envelope-like structure during mitosis in *Drosophila melanogaster* embryos." J cell Sci. **94**: 463-470.

Hartenstein, V. (1993). Atlas of *Drosophila* Development. New York, Cold Spring Harbor Laboratory Press.

Hay, B., L. Ackerman, et al. (1988a). "Identification of a component of *Drosophila* polar granules." Development. **103**: 625-640.

Hay, B., L. H. Jan, et al. (1988b). "A protein component of *Drosophila* polar granules is encoded by vasa and has extensive sequence similarity to ATP-dependent helicase." Cell. **55**: 577-587.

Heald, R. and F. McKeon (1990). "Mutations of phosphorylation sites in lamin A that prevent nuclear lamina disassembly in mitosis." Cell. **61**: 579-589.

Heck, M. M. (1997). "Condensins, cohesins, and chromosome architecture: how to make and break a mitotic chromosome." Cell. **91**: 5-8.

Henry, K. W., A. Wyce, et al. (2003). "Transcriptional activation via sequential histone H2B ubiquitylation and deubiquitylation, mediated by SAGA-associated Ubp8." Genes & Dev. **17**: 2648-2663.

Herrmann, H. and U. Aebi (2004). "Intermediate filaments: molecular structure, assembly mechanism, and integration into functionally distinct intracellular Scaffolds." Annu Rev Biochem. **73**: 749-789.

Hoyt, M. A., L. Totis, et al. (1991). "S. cerevisiae genes required for cell cycle arrest in response to loss of microtubule function." Cell. **66**: 507-517.

Hwang, E., J. Kusch, et al. (2003). "Spindle orientation in Saccharomyces cerevisiae depends on the transport of microtubule ends along polarized actin cables." J Cell Biol. **161**: 483-488.

Illmensee, K., A. P. Mahowald, et al. (1974). "Transplantation of posterior polar plasm in *Drosophila*. Induction of germ cells at the anterior pole of the egg." Proc Natl Acad Sci U S A. **71**: 1016-1020.

Jenkins, A. B., J. M. McCaffery, et al. (2003). "Drosophila E-cadherin is essential for proper germ cell-soma interaction during gonad morphogenesis." Development. **130**: 4417-4426.

Kink, J. A. and K. P. Chang (1988). "N-glycosylation as a biochemical basis for virulence in Leishmania mexicana amazonensis." Mol Biochem Parasitol. **27**: 181-190.

Koutz, P. J., G. R. Davis, et al. (1989). "Structural comparision of the *Pichia pastoris* alcohol oxidase genes." Yeast. **5**: 167-177.

Lapasset, L., B. Pradet-Balade, et al. (2005). "Nuclear envelope breakdown may deliver an inhibitor of protein phosphatase 1 which triggers cyclin B translation in starfish oocytes." Dev Biol. **285**: 200-210.

Lasko, P. and M. Ashburner (1990). "Posterior localization of vasa correlates with, but is not sufficient for , pole cell development." Genes Dev. **4**: 905-921.

Lehner, C. F., R. Stick, et al. (1987). "Differential expression of nuclear lamin proteins during chicken development." J Cell Biol. **105**: 577-587.

Lin, F. and H. J. Worman (1993). "Structural organization of the human gene encoding nuclear lamin A and nuclear lamin C." J Biol Chem. **268**: 16321-16326.

Lin, F. and H. J. Worman (1995). "Structural organization of the human gene (LMNB1) encoding nuclear lamin B1." Genomics. **27**: 230-236.

Llano, E., G. Adam, et al. (2002). "Structural and enzymatic characterization of Drosophila Dm2-MMP, a membrane-bound matrix metalloproteinase with tissue-specific expression." J Biol Chem. **277**: 23321-23329.

Llano, E., A. M. Pendas, et al. (2000). "Dm1-MMP, a matrix metalloproteinase from Drosophila with a potential role in extracellular matrix remodeling during neural development." J Biol Chem. **275**: 35978-35985.

Macdonald, M. H., C. J. Morrison, et al. (1995). "Analysis of the active site and activation mechanism of the *Leishmania* surface metalloproteinase GP63." Biochim Biophys Acta. **1253**: 199-207.

Mahowald, A. P. (1968). "Polar granules of *Drosophila*. II. Ultrastructural changes during early embryogenesis." J Exp Zool. **167**: 237-262.

Matova, N. and L. Cooley (2001). "Comparative aspects of animal oogenesis." Dev Biol. **231**: 291-320.

McCawley, L. J. and L. M. Matrisian (2001). "Matrix metalloproteinases: they're not just for matrix anymore!" Curr Opin Cell Biol. **13**: 534-540.

McGwire, B. S., K. P. Chang, et al. (2003). "Migration through the extracellular matrix by the parasitic protozoan Leishmania is enhanced by surface metalloprotease gp63." Infect Immun. **71**: 1008-1010.

McHugh, B., S. A. Krause, et al. (2004). "Invadolysin: a novel, conserved metalloprotease links mitotic structural rearrangements with cell migration." J Cell Biol. **167**(4): 673-686.

McKeon, F. D., M. W. Kirschner, et al. (1986). "Homologies in both primary and secondary structure between nuclear envelope and intermediate filament proteins." Nature. **319**: 463-468.

Murray, H. W., J. D. Berman, et al. (2005). "Advances in leishmaniasis." Lancet. **366**: 1561-1577.

Page-McCaw, A., J. Serano, et al. (2003). "Drosophila matrix metalloproteinases are required for tissue remodeling, but not embryonic development." Dev Cell. **4**: 95-106.

Pendas, A. M., Z. Zhou, et al. (2002). "Defective prelamin A processing and muscular and adipocyte alterations in Zmpste24 metalloproteinase-deficient mice." Nat Genet. **31**(1): 94-99.

Pender, S. L. and T. T. MacDonald (2004). "Matrix metalloproteinases and the gut - new roles for old enzymes." Curr Opin Pharmacol. **4**: 546-550.

Peter, M., J. Nakagawa, et al. (1990). "*In vitro* disassembly of the nuclear lamina and M phase-specific phosphorylation of lamins by cdc2 kinase." Cell. **61**: 591-602.

Poeck, B., S. Fischer, et al. (2001). "Glial cells mediate target layer selection of retinal axons in the developing visual system of Drosophila." Neuron. **29**: 99-113.

Pollard, T. D. and W. C. Earnshaw (2002). Cell biology. Philadelphia,Pennsylvania, Elsevier Science.

Ramsden, J. J. (2000). "MARCKS: a case of molecular exaptation?" Int J Biochem Cell Biol. **32**: 475-479.

Rieder, C. L. and R. E. Palazzo (1992). "Colcemid and the mitotic cycle." J cell Sci. **102**(pt 3): 387-392.

Roberts, D. B., T. Grigliatti, et al. (1986). *Drosophila* a practical approach. Oxford, IRL Press Limited.

Russell, D. G. and H. Wilhelm (1986). "The involvement of the major surface glycoprotein (gp63) of Leishmania promastigotes in attachment to macrophages." J Immunol. **136**: 2613-2620.

Santos, A. C. and R. Lehmann (2004). "Germ cell specification and migration in Drosophila and beyond." curr Biol. **14**: 578-589.

Schlagenhauf, E., R. Etges, et al. (1995). "Crystallization and preliminary X-ray diffraction studies of leishmanolysin, the major surface metalloproteinase from Leishmania major." Proteins. **22**: 58-66.

Schlagenhauf, E., R. Etges, et al. (1998). "The crystal structure of the Leishmania major surface proteinase leishmanolysin (gp63)." Structure. **6**: 1035-1046.

Schupbach, T. and E. Wieschaus (1986). "Germline autonomy of maternal-effect mutations altering the embryonic body pattern of *Drosophila.*" Dev Biol. **113**(2): 443-448.

Shearn, A., T. Rice, et al. (1971). "Imaginal disc abnormalities in lethal mutants of *Drosophila.*" Proc Natl Acad Sci U S A. **68**(10): 2594-2598.

Sinensky, M., K. Fentle, et al. (1994). "The processing pathway of prelamin A." J cell Sci. **107**: 61-67.

Spann, T. P., R. D. Moir, et al. (1997). "Disruption of nuclear lamin organization alters the distribution of replication factors and inhibits DNA synthesis." J Cell Biol. **136**: 1201-1212.

Stewart, C. and B. Burke (1987). "Teratocarcinoma stem cells and early mouse embryos contain only a single major lamin polypeptide closely resembling lamin B." Cell. **51**: 383-392.

Stocker, W. and W. Bode (1995). "Structural features of a superfamily of zinc-endopeptidases: the metzincins." Curr Opin Struct Biol. **5**: 383-390.

Strausfeld, U., J. C. Labbe, et al. (1991). "Dephosphorylation and activation of a p34cdc2/cyclin B complex in vitro by human CDC25 protein." Nature. **351**: 242-245.

Sundaram, M., H. W. Cook, et al. (2004). "The MARCKS family of phospholipid binding proteins: regulation of phospholipase D and other cellular components." Biochem Cell Biol. **82**: 191-200.

Thompson, H. M., H. Cao, et al. (2004). "Dynamin 2 binds gamma-tubulin and participates in centrosome cohesion." Nat Cell Biol. **6**: 335-342.

Uzbekov, R., I. Kireyev, et al. (2002). "Centrosome separation: respective role of microtubules and actin filaments." Biol Cell. **94**: 275-288.

Ward, G. E. and M. W. Kirschner (1990). "Identification of cell cycle-regulated phosphorylation sites on nuclear lamin C." Cell. **61**(561-577).

Wasserman, Z. R. (2005). "Making a new turn in matrix metalloprotease inhibition." Chem Biol. **12**: 143-144.

Weber, K., U. Plessmann, et al. (1989). "Maturation of nuclear lamin A involves a specific carboxy-terminal trimming, which removes the polyisoprenylation site from the precursor; implications for the structure of the nuclear lamina." FEBS Lett. **257**: 411-414.

Wilson, K. L. and M. S. Zastrow (2001). "Lamins and disease: insights into nuclear infrastructure." Cell. **104**(5): 647-650.

Worman, H. J. and J. C. Courvalin (2005). "Nuclear envelope, nuclear lamina, and inherited disease." Int Rev Cytol. **246**: 231-279.

Yamaguchi, H., M. Lorenz, et al. (2005). "Molecular mechanisms of invadopodium formation: the role of the N-WASP-Arp2/3 complex pathway and cofilin." J Cell Biol. **168**: 441-452.

Yao, C., J. E. Donelson, et al. (2003). "The major surface protease (MSP or GP63) of Leishmania sp. Biosynthesis, regulation of expression, and function." Mol Biochem Parasitol. **132**: 1-16.

Younossi-Hartenstein, A., P. M. Salvaterra, et al. (2003). "Early development of the Drosophila brain: IV. Larval neuropile compartments defined by glial septa." J Comp Neurol. **455**(4): 435-450.

Proposal to test whether *Drosophila* Invadolysin (DmINV) binds to, and can cleave Lamin Dm0

Submitted as a condition for the completion of Ph.D. thesis

Bin Yu

(Supervised by Dr Margarete Heck)

Experimental Outline

- All proteins would be expressed in *E. coli*, and purified by use of affinity tags.

- Protein Interaction would be tested by GST-pull down.

  JIL-1 (aa 1065-1187) would be used as a positive control.
  GFP would be used as a negative control.

- Lamin Dm0 Cleavage would be tested by *in vitro* protease assay.

  DCP-1 would be used as a positive control.
  GFP would be used as a negative control.
  The mutated "catalytic-dead" form of DmINV [E258A] would be used as another negative control.

Introduction of Different Affinity Tags

Affinity tag	Sequence	Bound by	Elution conditions
Poly His	HHHHHH	Ni-NTA	Imidazole 20-250mM or low pH (5.0)
FLAG	DYKDDDDK	Anti-Flag monoclonal antibody	Low pH
HA tag	YPYDVPDYA	Anti-HA antibody	Low pH
C-myc tag	EQKLISEEDL	Anti-c-myc monoclonal antibody	Low pH
S tag	DETAAAKFERQHMDS	S-fragment of RNaseA	Very low pH
Strep-tag II	WSHPQFEK	Strep-Tactin	2.5 mM desthiobiotin
SBP tag	38 residues	Streptavidin	2 mM Biotin
GST tag	211 residues	Glutathione	5-10 mM reduced Glutathione

Cloning of Constructs for Expression

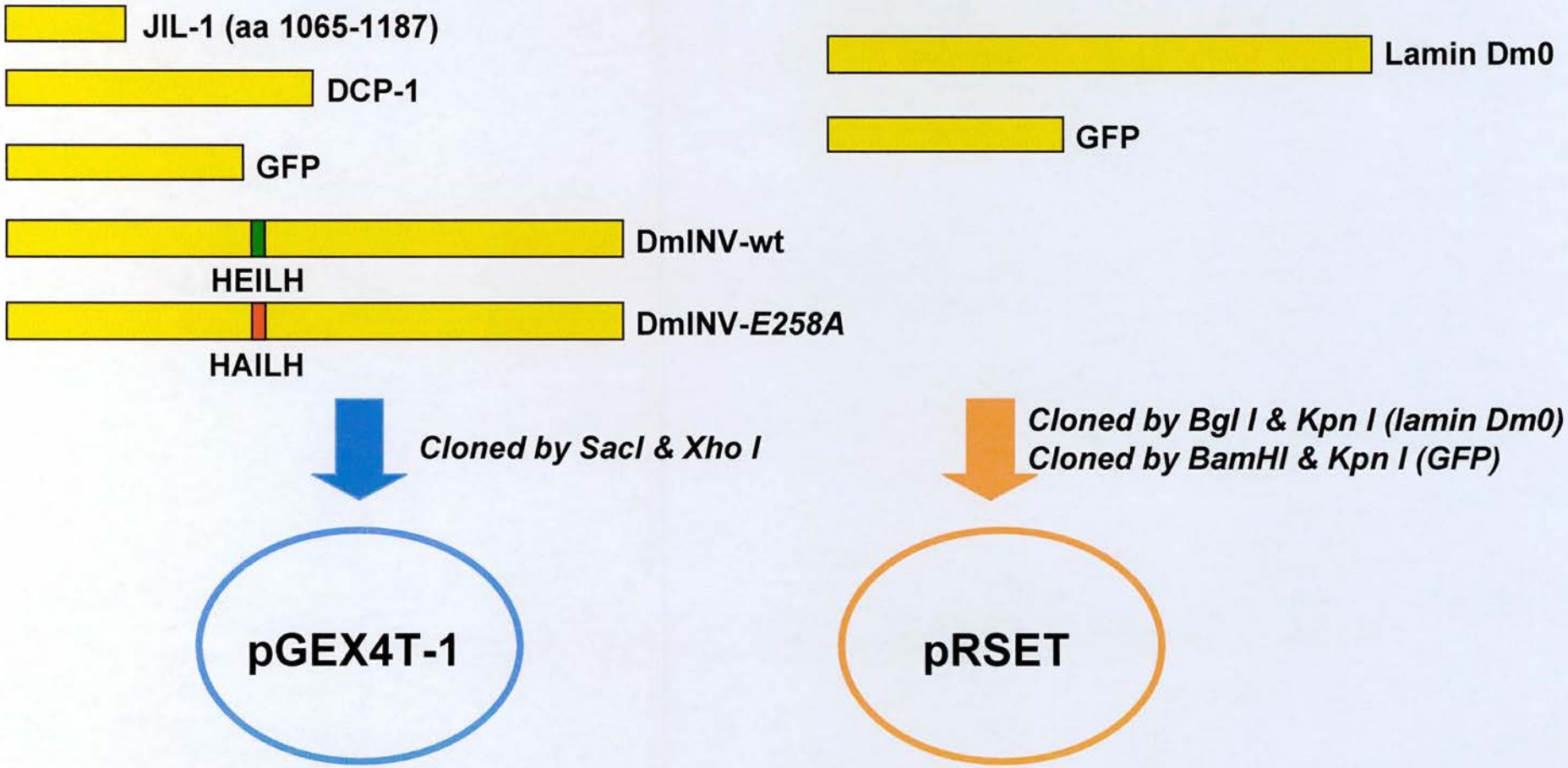

Expression of Recombinant Proteins

pGEX4T:
- JIL1
- DCP-1
- GFP
- DmINV
- DmINV-E258A

pRSET:
- lamin Dm0
- GFP

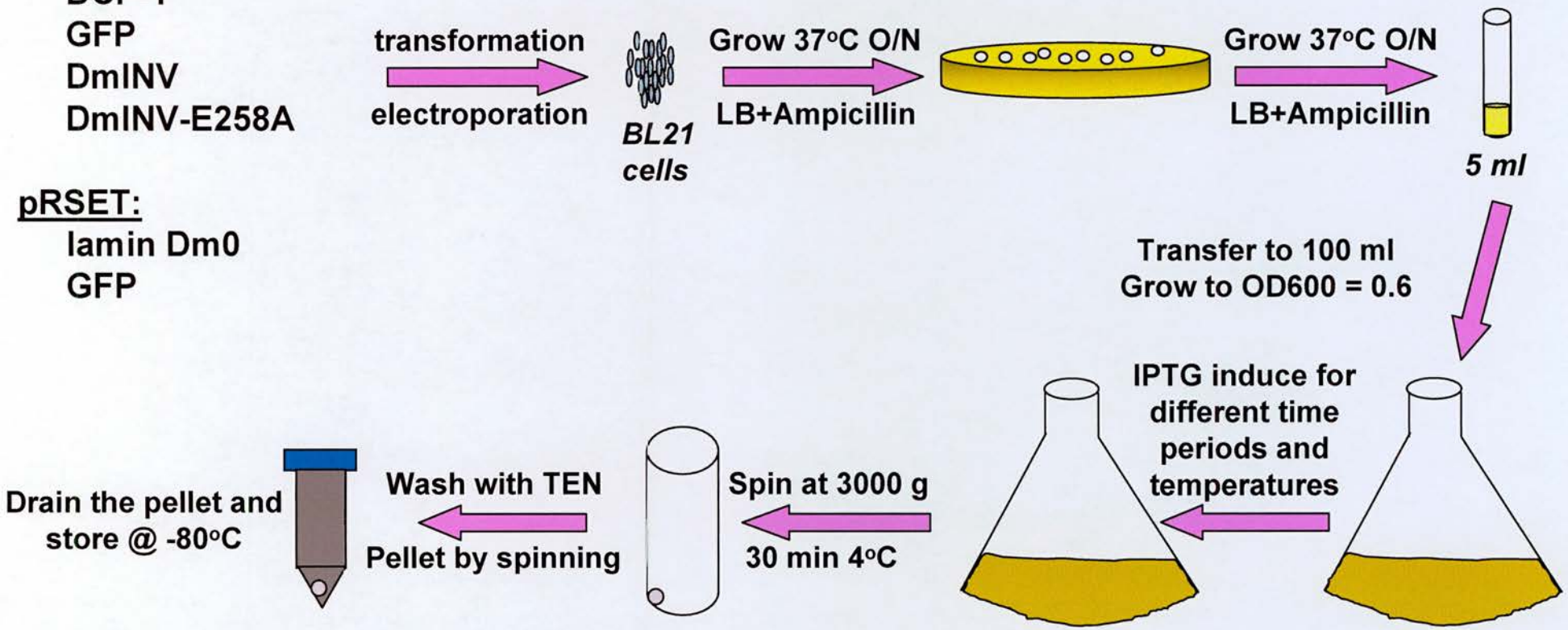

Protein Extraction

Thaw from -80°C

Weigh the pellet

Add Bugbuster lysis buffer
Add Benzonase endonuclease
Incubate for 20 min @ RT

Spin @ 16,000 g

20 min 4°C

Supernatant saved as
Fraction S

Pellet was resuspended in Bugbuster and lysozyme @ RT for 5 min

Wash the pellet with Bugbuster for 6 times and follow by spinning @ 16,000 g (4°C) for 15 min each time.

Resuspend the pellet in binding buffer (50 mM NaH_2PO_4 pH 8.0, 300 mM NaCl)
Pellet saved as
Fraction P

Protein Purification

GST-tagged JIL-1, DCP-1, GFP, DmINV and DmINV E258A:

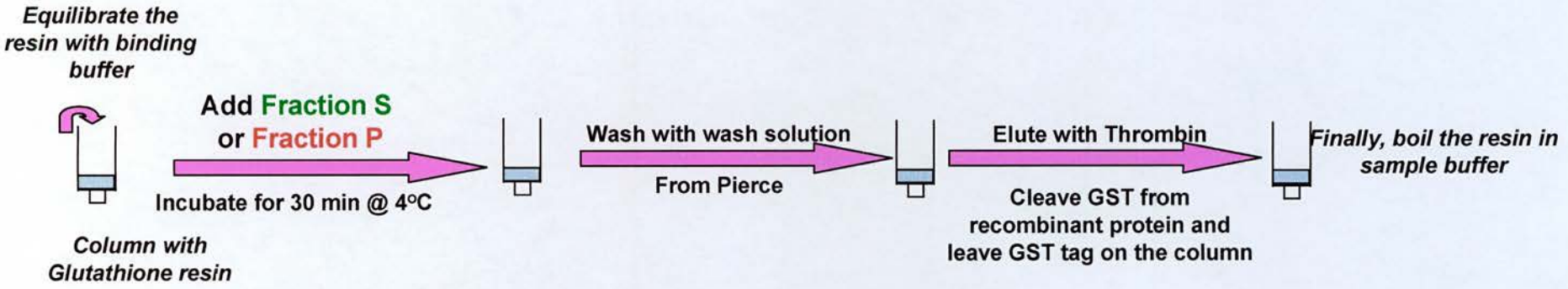

His-tagged lamin Dm0 and GFP:

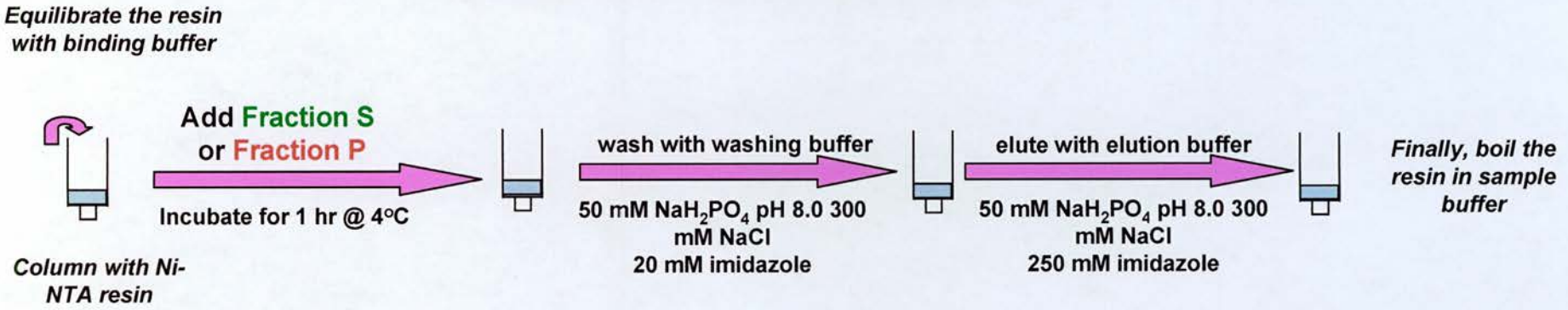

Detection of Protein Expression and Purification

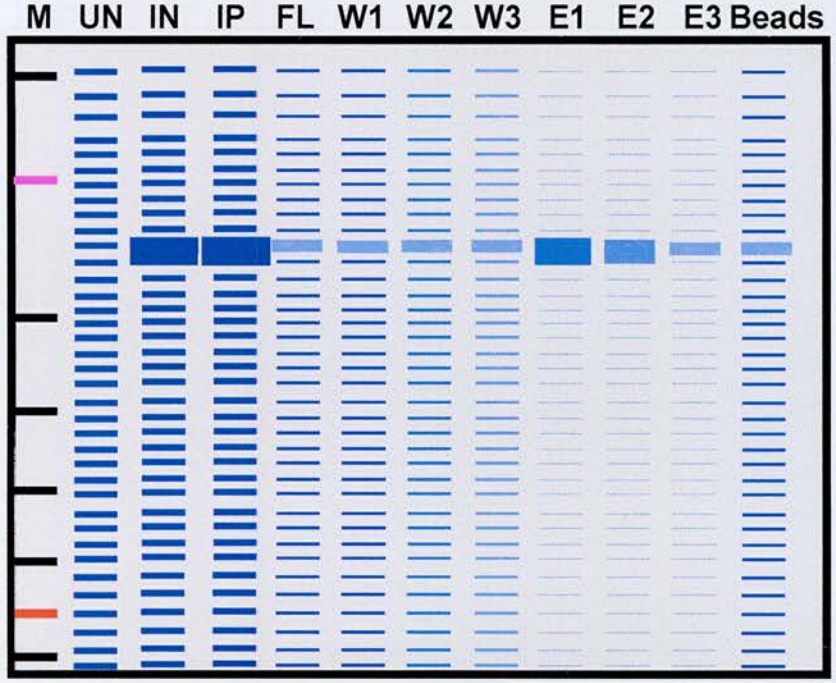

visualised by Coomassie Brilliant Blue staining

M: marker; UN: uninduced; IN: induced; IP: Input; FL: flow through; W: wash; E: elution

To Test for an Interaction Between DmINV and Lamin Dm0

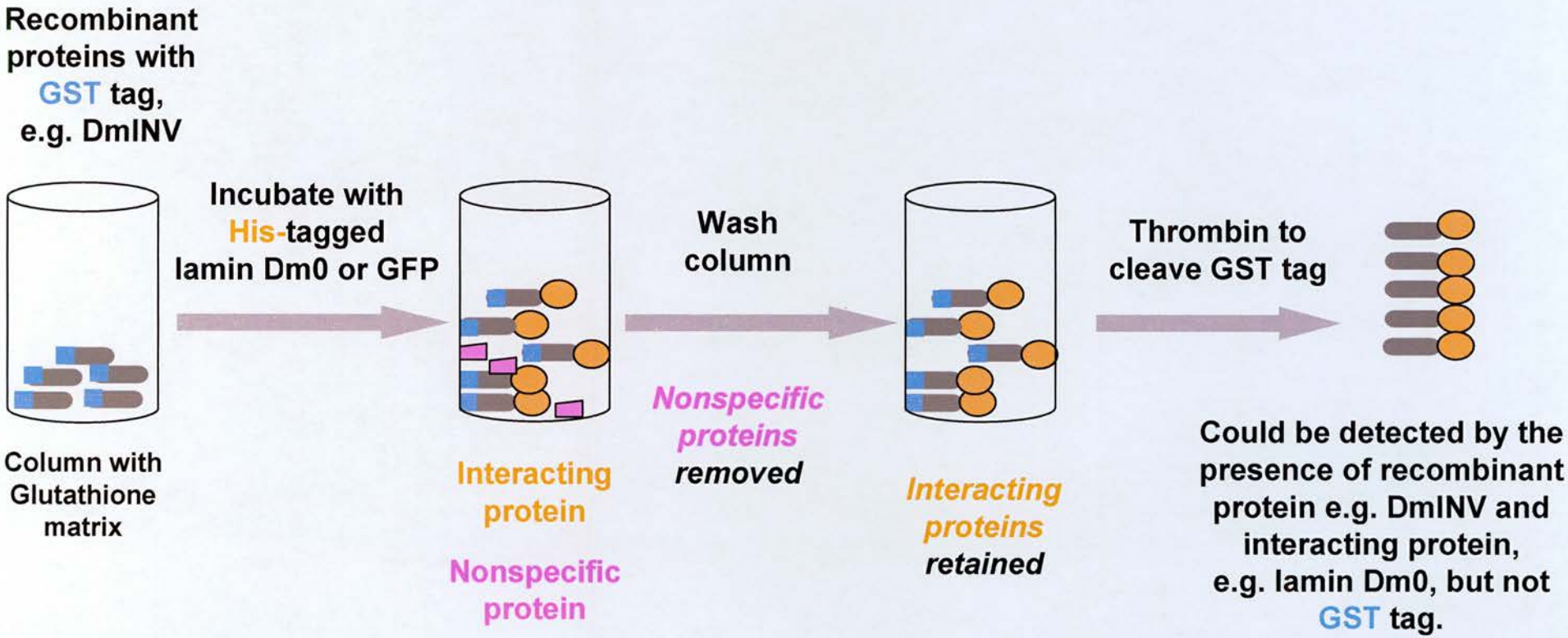

Test for Cleavage of Lamin Dm0 by DmINV

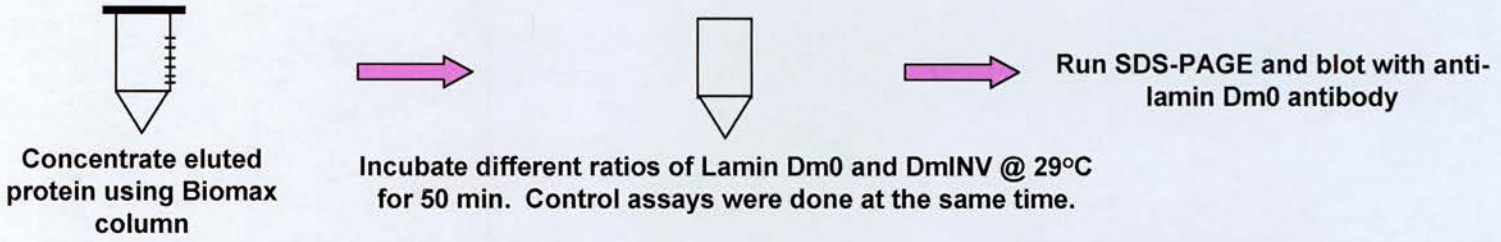

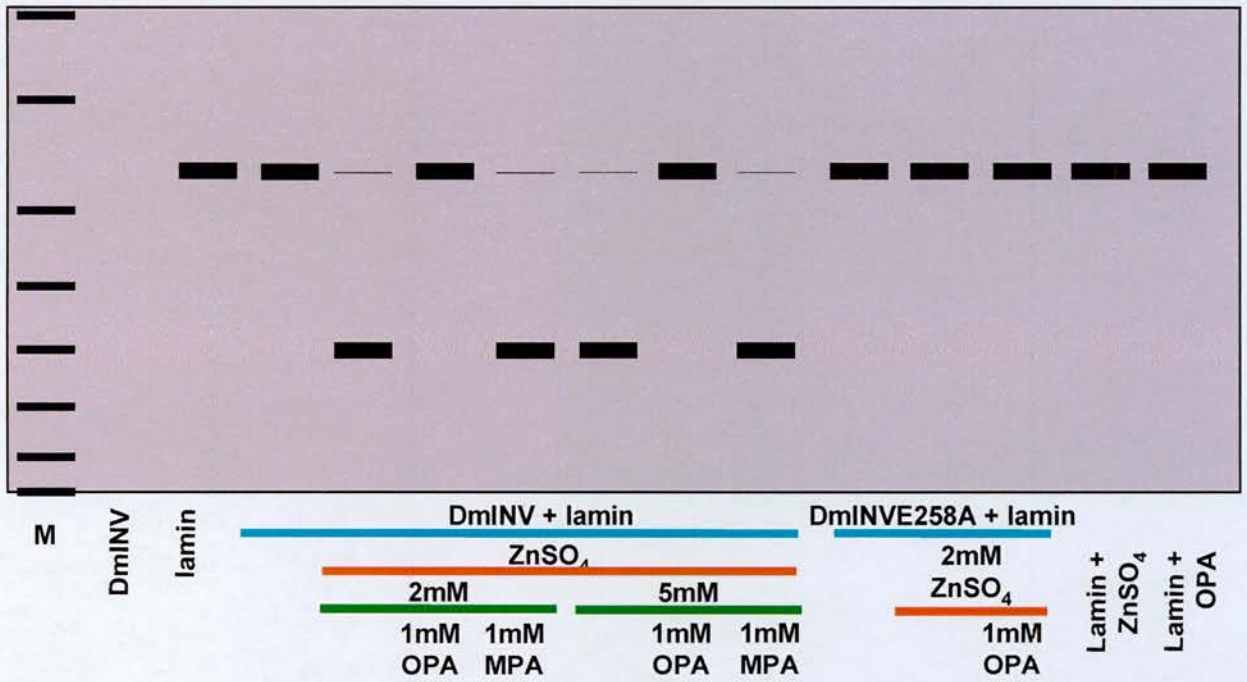

Predicted results: *Protein expression*

Expressed protein	Size of induced protein	Size of purified protein
His-lamin Dm0	74 kDa	74 kDa
His-GFP	31 kDa	31 kDa
GST-DmINV	102 kDa	76 kDa (without tag)
GST-DmINVE258A	102 kDa	76 kDa (without tag)
GST-GFP	54 kDa	28 kDa (without tag)
GST-JIL-1 (aa 1065-1187)	42 kDa	16 kDa (without tag)
GST-DCP-1	62 kDa	36 kDa (without tag)

Predicted results:
Interaction / Cleavage assay

Assay	Interaction?	Cleavage?
DmINV / lamin Dm0	Yes	Yes
DmINV-E258 / lamin Dm0	Yes	No
GFP / lamin Dm0	No	No
DCP-1 / lamin Dm0	Yes	Yes
JIL-1 / lamin Dm0	Yes	Not known
DmINV / GFP	No	No

Discussion I: expression and interaction

Observed result	*Explanation*
Recombinant proteins not induced.	Recombinant proteins have been toxic to bacteria or the induction conditions need to be optimized.
Recombinant proteins not purified.	Affinity tags have been lost during the expression or purification step.
Lamin Dm0 does not interact with JIL-1 in the GST pull down assay.	This system give false negative result.
Lamin Dm0 interact with GFP in the GST pull down assay.	Lamin Dm0 interact with GFP; the assay system could give false positive result.
DmINV interact with GFP in the GST pull down assay.	DmINV interact with GFP; the assay system could give false positive result.
DmINV does not interact with lamin Dm0 in the GST pull down assay.	Lamin Dm0 did not interact with DmINV; Lamin Dm0 / DmINV interaction required the presence of other protein(s); Lamin Dm0 or DmINV did not fold properly or did not obtain necessary post-translational modification in *E.coli*.

Discussion II: cleavage

Observed result	*Explanation*
Lamin was cleaved and cleavage band (s) were observed with the N-terminal antibody, but not the C-terminal antibody.	DmlNV cleaves lamin Dm0 just upstream or inside the C-terminal antibody recognition site.
Lamin was cleaved and cleavage band (s) was seen using C-terminal antibody but not N-terminal antibody.	DmlNV cleaves lamin Dm0 just downstream or inside the N-terminal antibody recognition site.
Lamin was cleaved and cleavage band (s) was not seen using C-terminal antibody nor N-terminal antibody.	DmlNV cleaves lamin Dm0 at both sites that near or inside N-terminal antibody recognition site and C-terminal antibody recognition site.
Lamin was cleaved and cleavage band (s) were seen using both C-terminal antibody and N-terminal antibody.	DmlNV cleaves lamin Dm0 somewhere near the the middle, so that both N-terminal cleaved and C-terminal cleaved fragments are big enough to be detected by immunoblotting.

Discussion III: controls

Observed result	*Explanation*
Lamin was not cleaved by DmINV.	Full length DmINV expressed in bacteria is not active (perhaps improperly folded, or inadequately modified); DmINV could not cleave lamin Dm0 directly.
Lamin was not cleaved by DCP-1.	The system gives false negative result since positive control does not work.
Lamin was cleaved by GFP.	The system gives false positive result.
GFP was cleaved by DmINV.	The system gives false positive result. DmINV cleaves GFP.
Lamin was cleaved by DmINV E258A.	The HEILH catalytic motif is not responsible for lamin Dm0 cleavage.

Acknowledgements

Supervisor: Margarete Heck

Current members of Heck lab:

Sharron Vass
Neville Cobbe
Kate Marshall
Shubha Gururaja Rao
Ching-Wen Chang
Edward Duca

Past members of Heck lab:

Brian McHugh
Ellada Savvidou
Marie-Louise Loupart
Brvce Nelson

wellcome trust

CSE Studentship

Invadolysin: a novel, conserved metalloprotease links mitotic structural rearrangements with cell migration

Brian McHugh,[1] Sue A. Krause,[1] Bin Yu,[1] Anne-Marie Deans,[1] Sarah Heasman,[2] Paul McLaughlin,[1] and Margarete M.S. Heck[1]

[1]Wellcome Trust Centre for Cell Biology, University of Edinburgh, Edinburgh EH9 3JR, Scotland, UK
[2]Medical Research Council Centre for Inflammation Research, University of Edinburgh, Edinburgh EH8 9AG, Scotland, UK

The cell cycle is widely known to be regulated by networks of phosphorylation and ubiquitin-directed proteolysis. Here, we describe IX-14/invadolysin, a novel metalloprotease present only in metazoa, whose activity appears to be essential for mitotic progression. Mitotic neuroblasts of *Drosophila melanogaster IX-14* mutant larvae exhibit increased levels of nuclear envelope proteins, monopolar and asymmetric spindles, and chromosomes that appear hypercondensed in length with a surrounding halo of loosely condensed chromatin. Zymography reveals that a protease activity, present in wild-type larval brains, is missing from homozygous tissue, and we show that IX-14/invadolysin cleaves lamin in vitro. The IX-14/invadolysin protein is predominantly found in cytoplasmic structures resembling invadopodia in fly and human cells, but is dramatically relocalized to the leading edge of migrating cells. Strikingly, we find that the directed migration of germ cells is affected in *Drosophila IX-14* mutant embryos. Thus, invadolysin identifies a new family of conserved metalloproteases whose activity appears to be essential for the coordination of mitotic progression, but which also plays an unexpected role in cell migration.

Introduction

Recent years have witnessed remarkable strides in our understanding of the control of cell cycle progression. It is now clear that cell cycle progression is driven by the successive activation and inactivation of the Cdks, and that abrupt transitions are often enforced by the cleavage of key targets by the proteasome after their ubiquitination by various E3 ubiquitin ligases (for review see Murray, 2004). Cdk phosphorylation of key components regulates the entry of cells into S phase and choreographs the subsequent firing of replication origins. Entry into mitosis is also determined by Cdks, and Cdk phosphorylation of the nuclear lamins drives the cycle of nuclear envelope disassembly and reassembly that is characteristic of mitosis in metazoa. The exit from mitosis is triggered not only by proteolysis of mitotic cyclins but also of securin leading to the activation of separase, a CD clan protease that cleaves the rad21/Scc1 non-structural maintenance of chromosomes cohesin subunit, thereby triggering the separation of sister chromatids.

One aspect of mitosis about which we still know relatively little is the process of mitotic chromosome formation. The compaction of chromatin into mitotic chromosomes is essential to avoid sister chromatid entanglement and cleavage of chromatin at cytokinesis. Recent breakthroughs, such as the discovery of the structural maintenance of chromosomes–containing condensin complex, at first appeared to provide the key, but recent analyses of condensin mutations and RNAi depletions have revealed that mitotic chromosomes form even in the absence of condensin subunits (Bhat et al., 1996; Steffensen et al., 2001; Coelho et al., 2003; Hudson et al., 2003). Further evidence suggests that correct mitotic chromosome condensation is linked to replication timing and checkpoint control (Loupart et al., 2000; Krause et al., 2001; Pflumm and Botchan, 2001). Thus, the search for factors that give the mitotic chromosome its characteristic form and integrity is still very much on.

The online version of this article includes supplemental material.

Correspondence to M.M.S. Heck: margarete.heck@ed.ac.uk

B. McHugh's present address is Medical Research Council Centre for Inflammation Research, University of Edinburgh, Edinburgh EH8 9XD, UK.

S.A. Krause's present address is University of Glasgow, Institute of Biological and Life Sciences, Glasgow G11 6NU, UK.

A.-M. Deans's present address is Institute of Immunology and Infection Research, University of Edinburgh, Edinburgh EH9 3JT, UK.

Abbreviations used in this paper: MMP, matrix metalloproteases; S2, Schneider 2.

The Journal of Cell Biology, Vol. 167, No. 4, November 22, 2004 673–686
http://www.jcb.org/cgi/doi/10.1083/jcb.200405155

Supplemental Material can be found at:
http://www.jcb.org/cgi/content/full/jcb.200405155/DC1

This work began as part or our ongoing characterization of *Drosophila melanogaster* mutations that are defective in mitotic chromosome condensation. Mitotic events are particularly amenable to study in *Drosophila* as many mutations affecting mitosis are lethal only at the late larval stages due to the maternal store of proteins in the embryo and the fact that larvae do not require mitotic activity for growth and development. This allows the use of mitotically active tissues such as larval brains and imaginal discs for studying proliferation in wild-type and mutant states (Gatti and Baker, 1989; Theurkauf and Heck, 1999). As a result, *Drosophila* has proven useful both for the characterization of known cell cycle regulators (O'Farrell et al., 1989; Edgar and Lehner, 1996; Fogarty et al., 1997; Sibon et al., 1997; Jager et al., 2001) and for the identification of novel factors, such as the polo and aurora kinases that have subsequently proven to be important for cell cycle regulation in diverse organisms (Sunkel and Glover, 1988; Llamazares et al., 1991; Glover et al., 1995).

We examined the *l(3)IX-14* mutation because of its dramatic effects on mitotic chromosome formation, distinct from other mitotic mutations. Our detailed analyses have revealed the gene to be important for other aspects of mitosis, including spindle assembly and nuclear envelope dynamics. Furthermore, the identification of the gene and characterization of its higher eukaryotic counterparts led to several surprises. The *IX-14* gene encodes a metalloprotease that is concentrated in cytoplasmic structures resembling invadopodia. Invasive tumor cells have the ability to elaborate invadopodia that facilitate extracellular matrix degradation, thus aiding metastasis (Bowden et al., 2001; Buccione et al., 2004). The IX-14 protein is structurally related to leishmanolysin, a major surface protease from *Leishmania* protozoa, which is thought to have a significant role in the pathogenesis of leishmaniasis (Yao et al., 2003). As a result of the subcellular localization and the sequence homology, we have termed the protein product of the IX-14 gene "invadolysin." We have discovered that invadolysin is highly concentrated at the leading edge of migrating macrophages. Consistent with a role in cell migration, we observe that the active migration of primordial germ cells is affected in mutant fly embryos. Thus, IX-14/invadolysin, a member of a new class of metalloproteases, links mitosis with cell migration.

Results

Chromosome structure is disrupted in the *IX-14* mutation

l(3)IX-14^{1} is a late larval lethal mutation on the right arm of the third chromosome, generated in an ICR-170 chemical mutagenesis screen for imaginal disc mutations (Shearn et al., 1971). Preliminary analysis reported that the mutation was characterized by metaphase arrest and hypercondensed mitotic chromosomes (Gatti and Baker, 1989). We generated a transposon insertion allele of the gene, *l(3)IX-14*^{4Y7}, by local hopping of a nearby P-element insertion. Here, we report a detailed phenotypic analysis of both alleles, investigating not only chromosome morphology but also other aspects of cell division.

Whole mount preparations of *IX-14* third instar larval brains and imaginal discs showed that mutant tissues had proliferation defects resulting in much-reduced brain size and missing imaginal discs (unpublished data). Fig. 1 shows typical DAPI-stained mitotic figures observed in wild-type (Fig. 1 A) and in *IX-14* mutant (Fig. 1 C) neuroblasts. The *IX-14* neuroblasts show the length-wise hypercondensation of mitotic chromosomes initially observed after orcein staining, but additionally demonstrate that the mutant chromosomes appear loosely condensed with a ragged periphery. This phenotype differs from the extreme hypercondensation in other mutations that produce a mitotic arrest phenotype (Heck et al., 1993) or treatment of wild-type cells with microtubule poisons such as colchicine (Fig. 1 B). Allowing more time in mitosis with colchicine does not rescue the lateral condensation defect in *IX-14* mutant neuroblasts (Fig. 1 D), thus we believe the phenotype represents a specific condensation defect rather than "conventional" hypercondensation in response to mitotic delay.

The *IX-14* mutation affects interphase polytene chromosomes as well as mitotic chromosomes. Polytene chromosomes from salivary glands of wild-type third instar larvae are distinctively banded along the chromosome arms, and the centromeres of the endo-reduplicated chromosomes are clustered at the chromocenter (Fig. 1 E). This characteristic banding pattern is abolished in *IX-14* mutant polytenes and the chromosome arms appear twisted and frayed (Fig. 1 F). In many nuclei it is difficult to identify an obvious chromocenter. Additionally, mutant polytenes were approximately half the size seen in wild type. This reduction in size may be due to under-replication, as BrdU incorporation is clearly reduced in *IX-14* mutant neuroblasts, though the structural defects are not merely explicable by reduced replication.

To further investigate an effect of the *IX-14* mutation on interphase chromatin structure suggested by the polytene phenotype, we addressed whether or not this mutation might act as a modifier in a position effect variegation assay. We examined the effect of one copy of each *IX-14* allele on expression of the *white* gene in a *white mottled 4* (w^{m4}) background. In w^{m4}, inversion of much of the X chromosome places the *white* gene (expression of which is responsible for normal red eye color) adjacent to heterochromatin, thereby reducing its expression. Mutations that enhance variegation, E(var)s, further reduce expression of the *white* gene (whiter eyes) potentially by increasing the "spreading" of heterochromatin. Suppressors of variegation, Su(var)s, result in greater expression of the *white* gene (redder eyes) by decreasing the heterochromatic environment of the reporter gene. Fig. 1 G shows a pronounced increase in the redness of flies' eyes with one copy of each *IX-14* allele in a w^{m4} background, indicating that *IX-14* alleles are acting as Su(var)s and "opening" heterochromatin. By inference, one role of wild-type IX-14 may be to promote chromatin compaction or heterochromatin formation, which is consistent with the observed mitotic defects. Therefore, we conclude that IX-14 is required for chromosome architecture during both mitosis and interphase.

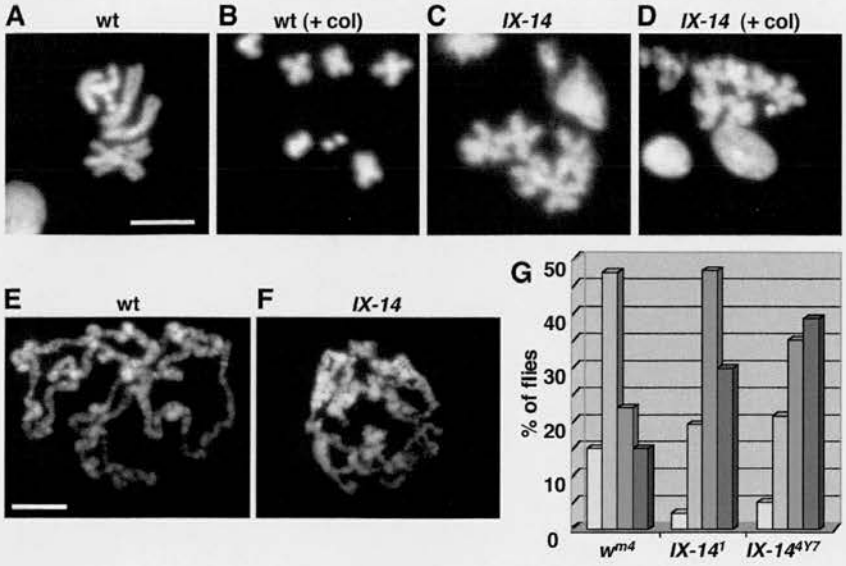

Figure 1. **Chromosome defects in *l(3)IX-14*.** (A–D) Mitotic chromosome spreads from wild-type (wt) and homozygous *l(3)IX-14* mutant (*IX-14*) third instar larval brains. "+ col" denotes images from the representative genotype after treatment with colchicine for 90 min. Note that even with colchicine treatment, the *IX-14* chromosomes are unable to condense as tightly as the wild-type chromosomes. Bar, 5 μm. (E and F) Polytene chromosome spreads from wild-type and *IX-14* homozygous mutant third instar larval salivary glands. Banding and a chromocenter are not as obvious in the mutant chromosomes. Bar, 10 μm. (G) Position effect variegation assay using "white" as a reporter gene (w^{m4}). Flies were sorted into categories based on redness of the adult eyes (white bars, 0–25% redness; yellow bars, 26–50% redness; orange bars, 51–75% redness; red bars, 76–100% redness). The distribution of eye color is shown for the original w^{m4} stock as well as for w^{m4} stocks containing one copy of each of the two mutant *l(3)IX-14* alleles. The majority of w^{m4};*l(3)IX-14* (both alleles) flies grouped toward the red end of the spectrum, implying that the mutant alleles act as suppressors of variegation (enhancing expression of the reporter gene) and, conversely, that the wild-type gene product acts to compact chromatin.

Spindle and centrosomal abnormalities are common in *IX-14* mutants

The over-shortened mitotic chromosomes suggested that *IX-14* mutants may experience a metaphase delay possibly caused by aberrant spindles. Neuroblasts of *IX-14* mutants indeed exhibited abnormal spindle morphology (Fig. 2, B–D and F), and in fact only 2% of mitotic cells had a normal bipolar spindle. Spindle abnormalities included monopolar spindles (37%; Fig. 2 B, inset 1), disorganized spindles (34%; Fig. 2 B, insets 2 and 3), and mitotic figures where the spindle appeared bipolar, but asymmetric (27%, Fig. 2 C, inset 4). Mutant spindles also appeared to have thicker bundles of microtubules, compared with the finer fibers observed in wild type (Fig. 2 A). Almost no anaphase figures were observed in DAPI-stained neuroblasts from *IX-14* mutant larvae, which is consistent with a metaphase delay or arrest.

Nearly 70% of mitotic figures in *IX-14* neuroblasts appeared to have only one focus of centrosomal staining, as judged by CP190 localization (Fig. 2, B–D and F). Cells with monopolar spindles always had a single centrosome, whereas 75% of the asymmetric bipolar spindles also had only one CP190 "spot" (Fig. 2 G). This single centrosome phenotype was also verified with another mitotic centrosomal marker, centrosomin (unpublished data). In many cases, centrosomes appeared to have a dumbbell shape (Fig. 2 F, arrow), suggesting that centrosomes had duplicated but not separated. Although CP190 normally has a nuclear localization during interphase (binding to specific loci on polytenes), the protein dissociates from chromosomes in mitosis (Whitfield et al., 1995). Mitotic chromosomes from *IX-14* homozygous cells curiously appeared to have higher levels of CP190 than wild-type chromosomes (Fig. 2 F).

The aberrant spindles in the *IX-14* mutation afford an explanation for the length-wise hypercondensation of chromosomes, as spindle defects would be expected to arrest cells in mitosis. However, the loose compaction and ragged edges of the chromosomes cannot be accounted for by spindle abnormalities as this is not observed when cells are arrested in mitosis in response to microtubule poisons or other spindle defects (Heck et al., 1993). Thus, IX-14 has essential roles both in chromosome and spindle architecture in *Drosophila* cells.

IX-14 mutant mitotic cells accumulate abnormally high levels of nuclear envelope proteins

As higher eukaryotic cells enter mitosis, chromosome condensation and spindle assembly are accompanied by the disassembly of the nuclear envelope. Surprisingly, the majority of *IX-14* mitotic cells showed dramatically increased levels of lamin Dm0 (a B-type lamin), compared with wild-type mitotic cells (Fig. 3, A and B). Strikingly, the level of another *Drosophila* nuclear envelope protein, otefin, also appeared elevated in *IX-14* mitotic cells (Fig. 3, C and D). When double immunofluorescence was performed, we observed a simultaneous increase of lamin and otefin in the same cells (unpublished data). We believe this elevation occurs before mitosis as late G2 cells (those positive for mitosis-specific phosphorylation of Serine 10 on histone H3) also exhibited increased lamin and otefin fluorescence.

The increase in immunofluorescence corresponds to an actual increase in protein level. Immunoblotting for lamin Dm0 and otefin very clearly showed that these proteins accumulated to unusually high levels in *IX-14* larval brains (compare with the α-tubulin loading control in Fig. 3 [E and F]). We additionally detected an increase in the level of *Drosophila* lamin C (unpublished data). We only detected increase of full-length forms by immunoblotting, with no evidence for accumulation of alternative forms. Merely arresting wild-type cells in mitosis with colchicine did not elevate lamin levels (unpublished data).

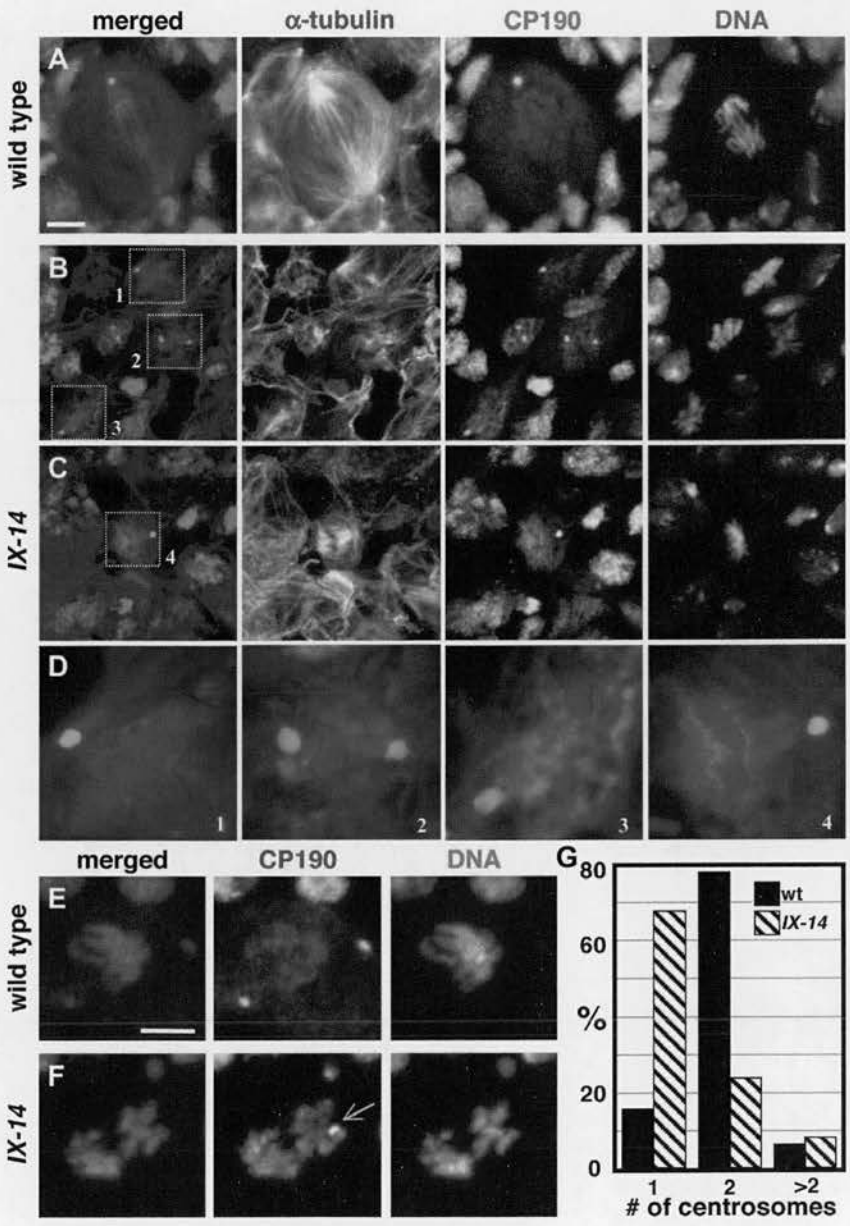

Figure 2. **Centrosome and spindle phenotypes of *l(3)IX-14*.** (A) Wild-type larval neuroblasts stained for α-tubulin (green), CP190 (red), and DAPI (blue). Wild-type metaphase figures contain normal bipolar spindles with two centrosomes. (B–D) *IX-14* larval neuroblasts labeled as in A show extreme spindle abnormalities. Boxed mitotic figures in *IX 14* mutant panels are enlarged in D to highlight mutant phenotypes of monopolar (1), disorganized (2 and 3), and asymmetric (4) spindles. Bar, 5 μm. (E) Wild-type larval neuroblasts stained for CP190 (green) and DAPI (red), showing duplicated and separated centrosomes at metaphase. (F) *IX-14* larval neuroblast stained as in E, showing chromosome condensation and centrosome separation defects (arrow) in mitosis. Additionally, CP190 appears to persist on *IX-14* mutant chromosomes longer than in wild-type cells. Bar, 5 μm. (G) Quantitation of centrosome number in the wild-type and *IX-14* mitotic cells. Nearly 70% of mitotic figures in the *IX-14* mutation appeared to have only one focus of centrosomal staining.

We conclude that the *IX-14* mutation appears to affect multiple aspects of structural rearrangement as cells enter mitosis.

The *IX-14* gene encodes a novel metalloprotease

We mapped the original *IX-14* allele to the 85E10-F16 region by crossing to deficiency lines with known breakpoints. We then generated a P-element insertion allele by local hopping a nearby P-element, *l(3)04017*. The P-element allele allowed cloning of adjacent genomic DNA by inverse PCR; hybridization of this fragment to a *Drosophila* P1 array refined our mapping to 85F14-15. A candidate *IX-14* gene was cloned by identifying a 3.6-kb full-length *Drosophila* adult head library EST whose sequence overlapped with the ~700-bp genomic fragment flanking the P-element. The gene was composed of nine exons, with the first exon separated from the remaining eight by a large (~8.6 kb) intron (Fig. 4 A, asterisk). This gene has been designated CG3953 in the *Drosophila* genome annotation database.

We mapped the P-element insertion site to 40 bp upstream of the start of transcription of the *IX-14* gene. Precise excision of this P-element was shown to revert the mutant phenotype and restore viability. The insertion appeared to disrupt the *IX-14* promoter, resulting in a strong hypomorphic or null mutation. To determine whether or not expression of this gene was affected in *IX-14* alleles, Northern blot analysis was performed on total RNA from third instar larvae. This showed that the predicted 3.6-kb mRNA was indeed missing in larval extracts prepared from both *IX-14* alleles (Fig. 4 B).

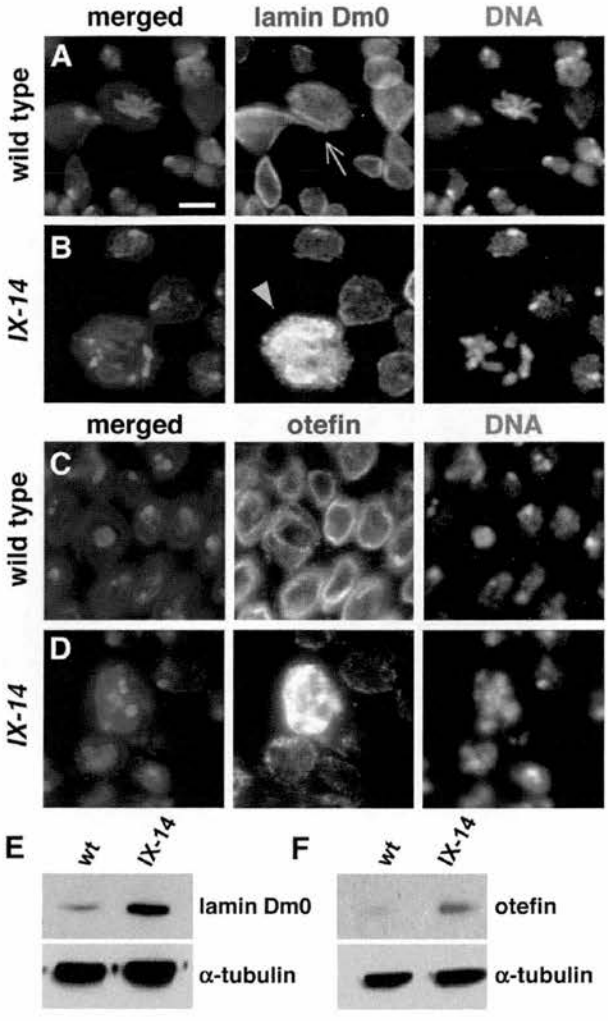

Figure 3. **Abnormal levels of nuclear envelope proteins in *l(3)IX-14* mutant cells.** Larval brains from wild-type and *IX-14* homozygous mutant animals were processed for lamin and otefin detection. (A) Wild-type mitotic cells (arrow) show homogeneous lamin staining as the nuclear lamina becomes dispersed during mitosis. (B) In contrast, both *IX-14* alleles have greatly increased lamin staining during mitosis (arrowhead). Bar, 5 μm. (C) Wild-type neuroblasts show distinct nuclear envelope staining similar to lamin. (D) Both *IX-14* alleles also show greatly increased otefin staining during mitosis. Protein extracts from wild-type and *IX-14* larval brains were probed for Dm0 lamin (E) and otefin (F). α-tubulin (bottom) served as a loading control, and confirmed that the samples were similarly loaded. The levels of both lamin and otefin detectable by immunoblotting was significantly greater in the mutant tissues than in wild-type brains.

The 2,052 nucleotide ORF in the *IX-14* cDNA encodes a 683 amino acid protein (predicted M_r = 71 kD) with homology to proteins in the M8 class of zinc-metalloproteases focused on the characteristic "HEXXHXXG[X]$_N$H" catalytic motif. The founding member of this family is the leishmanolysin cell surface protein (also called GP63) from the pathogen *Leishmania major*. In vitro mutagenesis of leishmanolysin has determined that the glutamic acid and three histidine residues are essential for protease activity (McMaster et al., 1994; Macdonald et al., 1995; McGwire and Chang, 1996). We have been able to identify orthologues in all higher eukaryotes examined, but conspicuously not in bacteria or yeasts, suggesting that the IX-14 gene product may only be required in metazoa.

The worm, human, mouse, and fly orthologues are shown in the alignment of Fig. 4 C, but other more divergent orthologues (e.g., *Arabidopsis thaliana* and *Dictyostelium discoideum*) are not included. Although the most obvious homology with leishmanolysin is centered on the conserved zinc-metalloprotease motif (Fig. 4 C, boxes) and immediate surrounding regions, the NH_2- and COOH-terminal regions are considerably more divergent. A potential signal sequence is present near the NH_2 terminus of all orthologues, although whether or not this sequence acts to target the protein is currently unknown. Intriguingly, there are at least nine blocks (Fig. 4 C, numbered double-headed arrows) shared among the worm, human, mouse, and fly orthologues that are absent from the leishmanolysin sequence. Despite this finding, the positions of 14 cysteines are remarkably conserved between leishmanolysin and the higher eukaryotic proteins (Fig. 4 C, asterisks). This result suggests strongly that the "core" of the IX-14 protease should resemble that of leishmanolysin (Schlagenhauf et al., 1998), and furthermore predicts that the indicated "insertions" should lie at the surface of this structure. Indeed, the sites of these insertions all map to the surface of the leishmanolysin structure (Fig. 4 D, black numbered spheres; the internal zinc ion essential for catalysis is represented by a magenta sphere). Therefore, we conclude that IX-14 is a member of a subgroup of the leishmanolysin protease group.

RNAi depletion of IX-14 in cultured cells phenocopies neuroblast defects

As further evidence that the gene we identified is responsible for the defects observed in *IX-14* larval tissues, we performed dsRNA-mediated interference of *IX-14* in *Drosophila* Schneider 2 (S2) cells. The abnormal spindle phenotypes seen in the mutant alleles, typically monopolar or disorganized, were phenocopied in roughly 25% of the *IX-14* RNAi mitotic cells (Fig. 5 A). In addition, mitotic figures from RNAi cultures were frequently observed to have single centrosomes or what appeared to be two closely apposed centrosomes (Fig. 5 B). Although control S2 cells have a low level of aneuploidy and occasional abnormal numbers of centrosomes, neither the aberrant spindles nor unseparated centrosomes were observed in control cells (Fig. 5, −dsRNA panels). Therefore, we are confident that loss of the IX-14 protein is responsible for the observed cellular phenotypes.

IX-14 cleaves lamin in vitro

To examine whether or not IX-14 has protease activity, suggested by its homology to the catalytic motif of leishmanolysin, we performed two complementary approaches. In the first, protein extracts prepared from wild-type and *IX-14* mutant larval brains were examined for protease activity (Fig. 6 A). Protease activity was assayed in zymogram gels containing casein as substrate. Whole larvae harbor a high level of protease activity at numerous molecular masses when assessed by zymography (unpublished data). Therefore, we prepared protein extracts

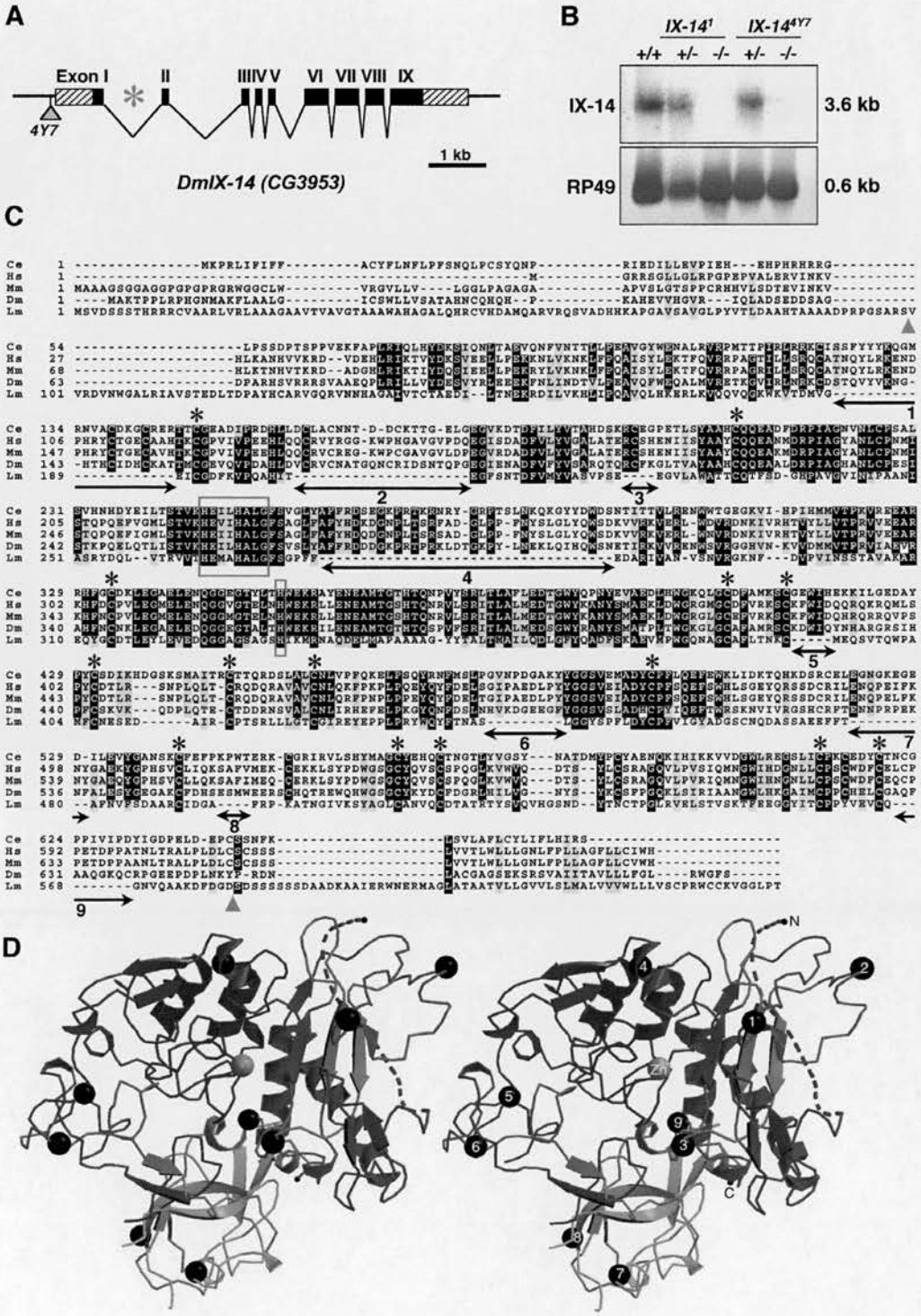

Figure 4. **Molecular characterization of *l(3)IX-14*.** (A) Map of the DmIX-14 gene (CG3953), with exons depicted as black boxes and 5′ and 3′ UTRs as hatched boxes. The position of the P element insertion in *l(3)IX-14*^{4Y7} is 40 bp upstream of the transcription start site (gray triangle). The first intron (8.6 kb, asterisk) is not shown to scale in this figure. (B) Northern blot of wild type and *IX-14* heterozygous (+/−) and homozygous (−/−) total larval RNA probed with IX-14 full-length cDNA. The same blot probed for ribosomal protein RP49 mRNA is shown as a control. The IX-14 mRNA is undetectable in RNA obtained from homozygous *IX-14* alleles. (C) T-COFFEE alignment showing homology between *Drosophila melanogaster* IX-14, metazoan orthologues, and Leishmanolysin, with the conserved HEXXHXXG (and third required H) zinc-metalloprotease motif boxed. Sequences shown are as follows: Ce, *Caenorhabditis elegans* (CAB16471); Hs, *Homo sapiens* (CAC42882); Mm, *Mus musculus* (NP 766411); Dm, *Drosophila melanogaster* (NP 652072); Lm, *Leishmania major* (AF039721). Although the homology between leishmanolysin and the other proteins appears to be largely limited to regions surrounding the metalloprotease motif, the placement of 14 cysteines (asterisks) is strikingly conserved. Nine regions shared among the higher eukaryotic ortho-

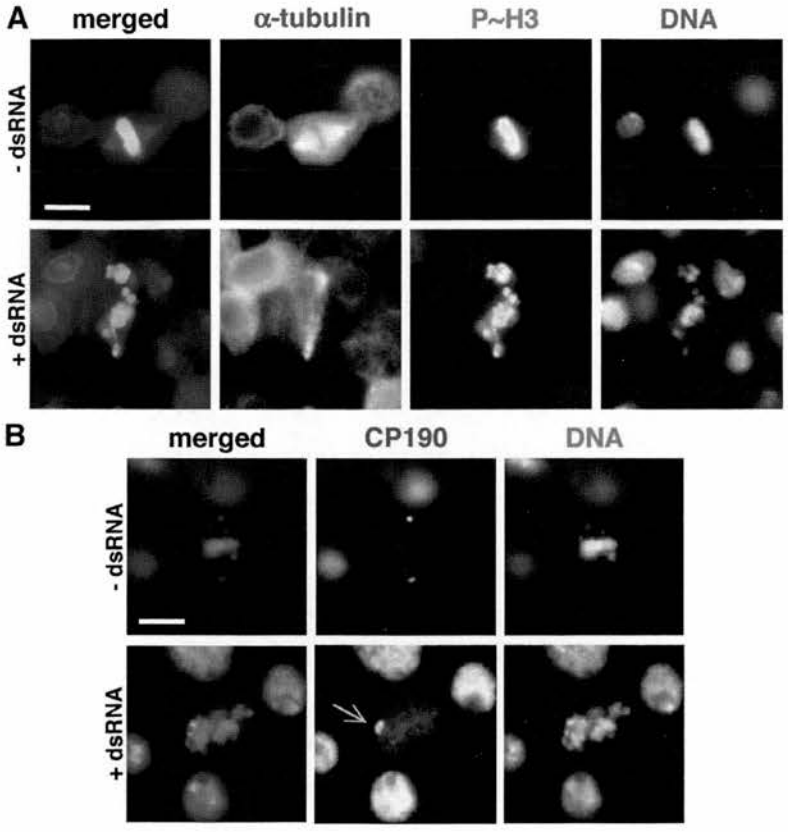

Figure 5. **dsRNA-mediated interference of IX-14 in *Drosophila* S2 cells phenocopies the mutation.** (A) Spindles of S2 cells: control (top) and 72 h after dsRNA treatment (bottom). Cells are stained for α-tubulin (green), P~H3 (red), and DAPI (blue). The normal bipolar spindle in the control S2 cell is to be contrasted with the disorganized spindle shown in the treated cell. This is similar to that observed in *IX-14* homozygous mutant alleles. Bar, 5 μm. (B) Centrosomes of S2 cells: control (top) and 72 h after dsRNA treatment (bottom). Cells are stained for CP190 (green) and DAPI (red). The treated cells show the centrosome separation defect (arrow) similar to that observed in *l(3)IX-14* homozygous mutant alleles. Bar, 5 μm.

from larval brains only, as the phenotypes were clearly apparent in this proliferating tissue. Wild-type brain lysates had two visible bands of protease activity, migrating at ~120 and 135 kD (Fig. 6 A, asterisks). Remarkably, these two bands of activity were almost completely absent in *IX-14* brains, indicating that mutant extracts were indeed missing proteolytic activity. A separate stained gel documents that wild-type and mutant lanes were equivalently loaded (Fig. 6 B). As these zymogram gels are nondenaturing, the molecular mass of the observed activity is not necessarily related to predicted molecular mass, but may suggest that IX-14 migrates as a multimer or part of a complex. The lack of protease activity in mutant brains further suggests that the IX-14 gene product is responsible not only for the mutant phenotypes but also for the protease activity observed under these conditions (either directly or potentially through the activation of other proteases).

The increase in nuclear envelope proteins observed by immunofluorescence and immunoblotting in mutant brains suggested that lamin (or otefin) might be a substrate of the IX-14 metalloprotease. As shown in Fig. 6 C, in vitro synthesized Dm0 lamin is cleaved by in vitro synthesized IX-14. Furthermore, the cleavage of lamin can be inhibited by the inclusion of ortho-phenanthroline, a chelator of zinc (Fig. 6 C, asterisks). Although full-length lamin was detected by immunoblotting in this experiment (Fig. 6 C, arrowhead), we failed to detect any cleavage products (they may not be recognized by the antibody used). Thus, IX-14 is a novel essential protease capable of cleaving at least one component of the nuclear envelope.

IX-14 localizes to distinct structures in the cytoplasm of *Drosophila* and human cells

Several approaches were used to determine the subcellular localization of the IX-14 protein. *Drosophila* S2 cells transiently transfected with expression plasmids tagging either the NH_2 or COOH terminus with EGFP showed cytoplasmic localization, whereas vector alone localized to both the nucleus and cytoplasm (Fig. 7 A). The human genome contains a single *IX-14* gene, which we have shown by preliminary siRNA analysis to be essential for viability (unpublished data). Due to the limit of resolution with the relatively small and generally nonadherent S2 cells, we turned to examining IX-14 localization in human cells. A COOH-terminal EGFP fusion construct of HsIX-14 in HeLa cells was also localized

logues (absent from leishmanolysin) are indicated by double-headed arrows. The gray triangles delimit the region of the leishmanolysin protein that is shown in D. (D) Stereo pair of the three-dimensional structure of leishmanolysin is shown (PDB accession code is 1LML). The black numbered spheres represent the higher eukaryotic "insertions" (relative to leishmanolysin), which all map to the surface of the leishmanolysin structure. The internal magenta sphere represents the zinc ion required for catalysis.

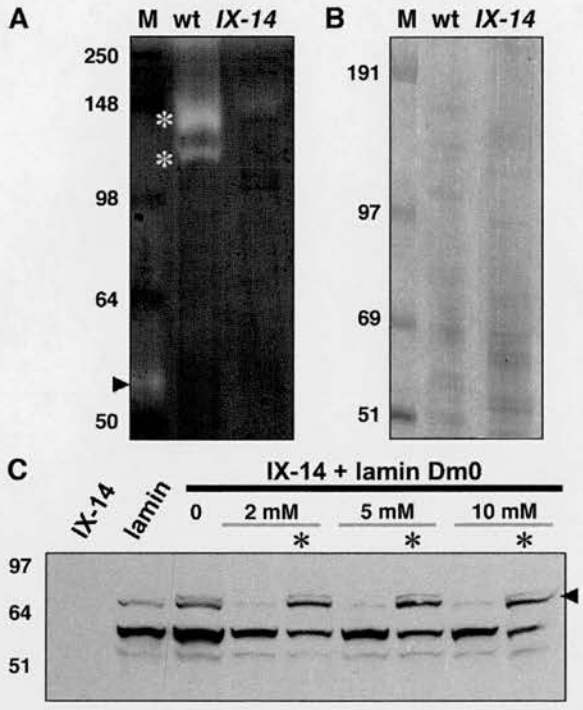

Figure 6. **The IX-14 protein exhibits protease activity.** (A) Colloidal Coomassie blue–stained nondenaturing casein zymogram gel showing one brain equivalent of wild type (+/+) versus three brain equivalents of homozygous (*IX-14*) third instar larval brain extract. A doublet of protease activity is observed in wild-type extracts (asterisks), but is greatly depleted in mutant extracts. A band of protease activity is also present in the prestained molecular mass markers (arrowhead), which serves as an internal control in these experiments. (B) Coomassie blue–stained denaturing polyacrylamide gel showing equivalent loading of larval brain extracts (three mutant brains are a roughly equivalent amount to one wild-type brain). (C) *Drosophila* IX-14 cleaves *Drosophila* Dm0 lamin in vitro. In vitro transcribed and translated proteins were mixed and incubated for 60 min at 29°C (IX-14 and lamin alone are in the first two lanes). The cleavage of lamin was detected by immunoblotting with a mAb generated against the NH_2-terminal head region (arrowhead). The addition of zinc at 2, 5, or 10 mM enhanced the cleavage reaction, whereas the addition of the 1,10-phenanthroline zinc chelator inhibited the cleavage of lamin by the IX-14 protease (asterisks).

in the cytoplasm, often as unusual ring-like structures (Fig. 7 B). A control transfection with EGFP alone localized throughout both the nucleus and cytoplasm. From these experiments we concluded that the IX-14 protein localized predominantly in the cytoplasm of fly and human cells.

Two protein sequences for the human orthologue possibly representing alternatively spliced forms have been submitted: CAC42883–version 1 and CAC42882–version 2 (Fig. 4 B). These forms differ in their NH_2-terminal regions (upstream of the residues VINK) and by the presence of a 37–amino acid sequence in the COOH-terminal half of version 2 found in all the other eukaryotic orthologues so far (between the residues EDTG:RQML). We generated an antibody to amino acids 327 to 629 of HsIX-14.v1 (downstream of the catalytic motif). As this region is fully present in both predicted human versions, the antibody should recognize the two forms if they indeed both exist. Fig. 8 A shows a typical staining pattern observed with the $HsIX\text{-}14^{327\text{-}629}$ antibody in HeLa cells. We observed unusual ring-like structures similar to those seen with the EGFP-tagged protein. These striking structures were also observed in two other human transformed cell lines, Jurkat and CF-PAC (unpublished data). These structures were observed in all interphase cells, and although their size remained fairly constant (<1 μm in diameter), the number of the structures varied on a cell to cell basis. Z-series of sections through cells showed that these structures were located in the lower third of the cells. Because the ring-like structures were dispersed in mitosis in all cell types examined, we believe that the localization (and/or activity) of IX-14 may be regulated during the cell cycle.

Although proteases are found in diverse structures within cells, this particular localization did not resemble any of the usual protease-containing complexes, e.g., 26S proteasome, the related COP9–signalosome complex, lysosomes, or aggresomes. Nonetheless, we performed colocalization immunofluorescence with antibodies to IX-14 and proteasome core subunits α5 and β5i, signalosome subunit Cgn3, chaperone protein Hsc70, and markers for Golgi, mitochondria, and lysosomes. We observed no significant colocalization between IX-14 and any of these proteins (unpublished data). However, numerous transformed cells contain invadopodia, which are believed to be important for extracellular matrix degradation and cellular migration (Bowden et al., 1999, 2001; Baldassarre et al., 2003; Buccione et al., 2004). Invadopodia resemble in size and distribution the structures labeled by the IX-14 antibody. As no proteins exclusive to invadopodia have yet been identified, definitive colocalization was not possible. However, we detected limited colocalization with markers shown to label invadopodia (e.g., phosphotyrosine, cortactin, and Dynamin 2), suggesting that these cytoplasmic ring-like structures very likely are invadopodia.

A role for IX-14 in cell migration

If IX-14 were involved in cell migration, as suggested by the invadopodia-like localization, one might predict that the protein should localize to regions of cells actively involved in migration. Thus, we examined the localization in stationary and migrating human macrophages (Fig. 8, B and C). Fig. 8 B showed that punctate, at times ring-like, cytoplasmic IX-14 structures were observed in cultured human macrophages (in the example shown, the cell is stationary). The morphology of macrophages is dramatically altered as they migrate. In the two examples shown, the IX-14 protein is strikingly mobilized from internal structures to the leading edge of cells (Fig. 8 C). This extraordinary relocalization of IX-14 protein suggests a very intimate involvement of this protein in cell migration.

Given a possible role for this protein in cell migration, we examined primordial germ cell migration in wild-type and *IX-14* mutant *Drosophila* embryos (for review see Santos and Lehmann, 2004). After being the first cells to form very early in embryogenesis, primordial germ cells are passively carried along the dorsal side of the embryo in close association with the posterior midgut primordium. As this primordium invaginates, the germ cells are carried to the interior of the embryo. After this, they actively migrate away from the midgut toward

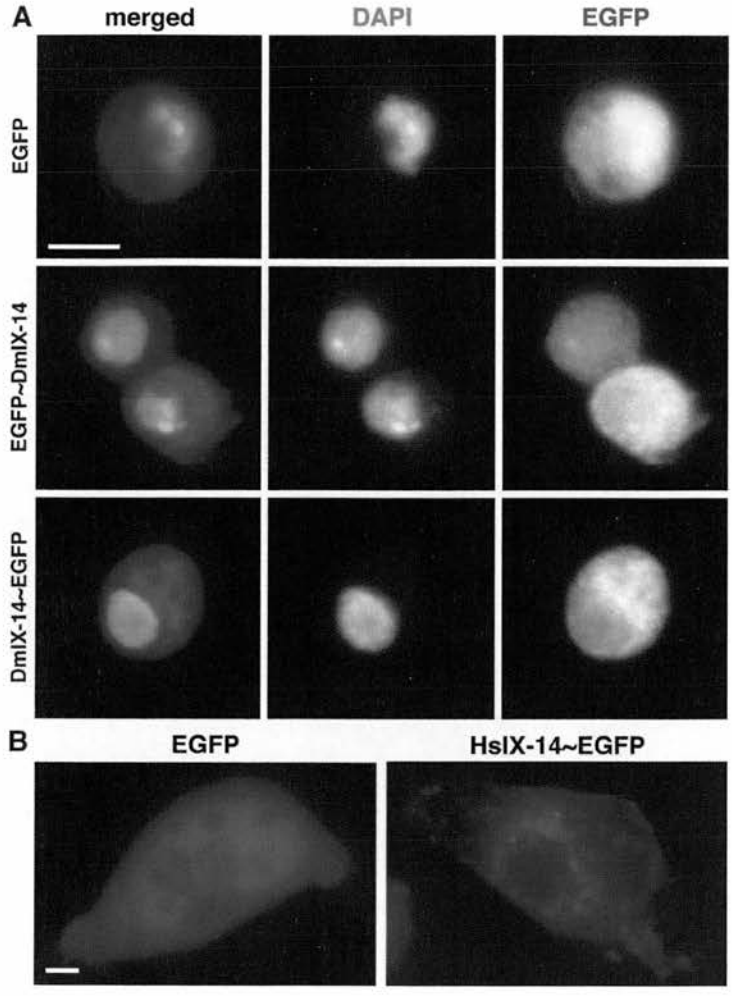

Figure 7. **Localization of GFP-tagged IX-14 in *Drosophila* S2 and HeLa cells.** (A) *Drosophila* S2 cells transiently transfected with constructs expressing EGFP vector only (top) and DmIX-14 tagged at the NH_2 (middle) and COOH termini (bottom). EGFP, green; DAPI, red. DmIX-14 tagged with EGFP at either end appears to be concentrated in cytoplasmic foci, in contrast to EGFP alone, which shows diffuse localization throughout the cytoplasm and nucleus. Bar, 5 μm. (B) HeLa cells transiently transfected with constructs expressing EGFP vector only (left) or HsIX-14 tagged at the COOH terminus (right). EGFP alone is localized diffusely throughout both nucleus and cytoplasm, HsIX-14~EGFP is localized to cytoplasmic ring-like structures. Bar, 5 μm.

the adjacent mesoderm where they associate with somatic gonadal precursor cells. These clusters of cells further migrate and coalesce into gonads later in embryogenesis. Using Vasa as a marker for primordial germ cells, we examined embryos both before and after the migration phases. As shown in Fig. 9, germ cells in both wild-type (Fig. 9 A, top) and mutant (Fig. 9 B, top) embryos are similarly dispersed at the stage before active migration. However, a dramatic difference is seen in embryos at the later stage of gonad coalescence, with gonads visible in wild type (Fig. 9 A, bottom), but not in the mutation (Fig. 9 B, bottom). Mutant larvae then lack gonads (unpublished data). Therefore, the IX-14 protease is playing a role in cell migration, as well as in mitosis, in *Drosophila*.

Discussion

Drosophila IX-14 mutations cause a variety of defects in chromosome, spindle, and nuclear envelope structure during mitosis. Here, we have shown that the *IX-14* gene encodes a novel metalloprotease that is highly conserved in metazoa. Because of its homology to leishmanolysin, we suggest that the core of the IX-14 protease should structurally resemble that of leishmanolysin. In both *Drosophila* and human cells, the metalloprotease is concentrated in cytoplasmic organelles that we believe correspond to invadopodia. In recognition of the homology and intracellular distribution, we have termed the IX-14 enzyme invadolysin.

Three lines of evidence point to invadolysin activity as being crucially involved in the mitotic structural defects observed in *Drosophila IX-14* neuroblasts: (1) The mRNA for the *IX-14* gene is absent from larval tissues of two independently generated mutations, both of which have identical phenotypes; (2) dsRNA-mediated depletion of the IX-14 protein in cultured cells mimics the specific spindle and centrosome defects initially observed in the animal; and (3) in zymography experiments, mutant larval brains lack protease activity that is present in wild-type tissues.

Our analysis of the phenotype of *IX-14* mutant alleles of *Drosophila* revealed that lamin (both Dm0 and C) and otefin proteins are present in elevated amounts in mutant neuroblasts. This finding suggests that invadolysin or one of its downstream targets normally promotes the turnover of these nuclear envelope proteins. In fact, cleavage may be due to invadolysin itself, as we have shown that the enzyme can cleave *Drosophila*

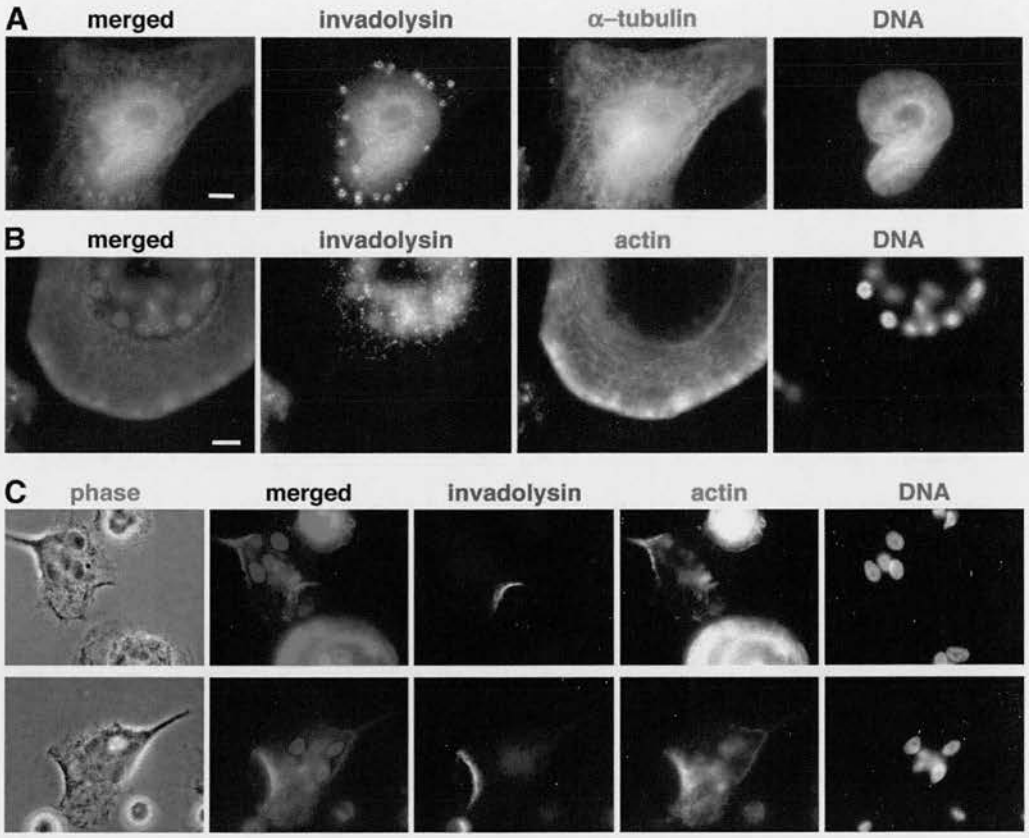

Figure 8. **Localization of IX-14/invadolysin in human cells.** (A) HsIX-14 localization in HeLa cells, detected with a rabbit antibody generated to HsIX-14 (amino acids 327–629). HsIX-14, green; α-tubulin, red; DAPI, blue. The HsIX-14 staining is seen as discrete ring-like structures in the cytoplasm of interphase cells, in addition to a nuclear pool of the protein. This staining pattern becomes more diffuse in mitosis, and is similar in Jurkat and CF-PAC cells (not depicted). Bar, 5 μm. (B) HsIX-14 localization in normal stationary human macrophages cultured in vitro. HsIX-14, green; rhodamine-phalloidin/actin, red; DAPI blue. Bar, 5 μm. (C) HsIX-14 localization in normal migrating human macrophages cultured in vitro. HsIX-14, green; rhodamine-phalloidin/actin, red; DAPI, blue. Note that all of the IX-14/invadolysin has now strikingly relocalized to the leading edge of the cells.

lamin Dm0 in vitro. Many previous papers have demonstrated that lamina dynamics in mitosis are regulated by reversible phosphorylation by Cdk1:cyclin B and that the proteins are reused at nuclear envelope reformation during telophase (Gant and Wilson, 1997). Thus, although the mechanism and timing of the invadolysin-dependent nuclear envelope turnover has yet to be determined, the phenomenon is important because it reveals previously unsuspected complexities of nuclear envelope dynamics during the cell cycle. Identification of other invadolysin substrates, e.g., ones essential for chromosome condensation and spindle assembly, will also illuminate further details of these mitotic rearrangements.

The IX-14 gene encodes a novel metalloprotease

Sequence analysis of the *IX-14* gene suggested that it encodes a novel conserved zinc-metalloprotease with sequence homology to leishmanolysin and to orthologues that we have identified in a range of metazoan species. Leishmanolysin is a major cell surface protease that is required for *Leishmania's* parasitic activity. It has been extensively studied due to its pathogenic role in leishmaniasis (Russell and Wilhelm, 1986; Yang et al., 1990; Connell et al., 1993; Xu and Liew, 1995; McGwire and Chang, 1996; Yao et al., 2003), and has also recently been shown to enhance migration of *Leishmania* through extracellular matrix (McGwire et al., 2003).

Like leishmanolysin, invadolysin has the conserved residues of the metzincin protease "HEXXHXXG[X]$_N$H" motif. This motif has been characterized in detail by mutational analysis of the three conserved histidine (which coordinate the zinc ion) and glutamic acid residues, which are absolutely required for catalytic activity (McMaster et al., 1994; Macdonald et al., 1995; McGwire and Chang, 1996). We additionally noted the conserved spacing of 14 cysteines among leishmanolysin and the orthologues described in this paper. Molecular modeling studies revealed that the framework of the higher eukaryotic form of this protein is likely to closely resemble that of leishmanolysin, with differences being confined to surface features that likely mediate interactions with substrates, regulators, and/or other binding partners.

None of the identified invadolysin orthologues has had any functions ascribed to them. Therefore, we propose that the IX-14/invadolysin family is required for cell cycle structural rearrangements, a novel activity for this class of proteases. The Zmpste24

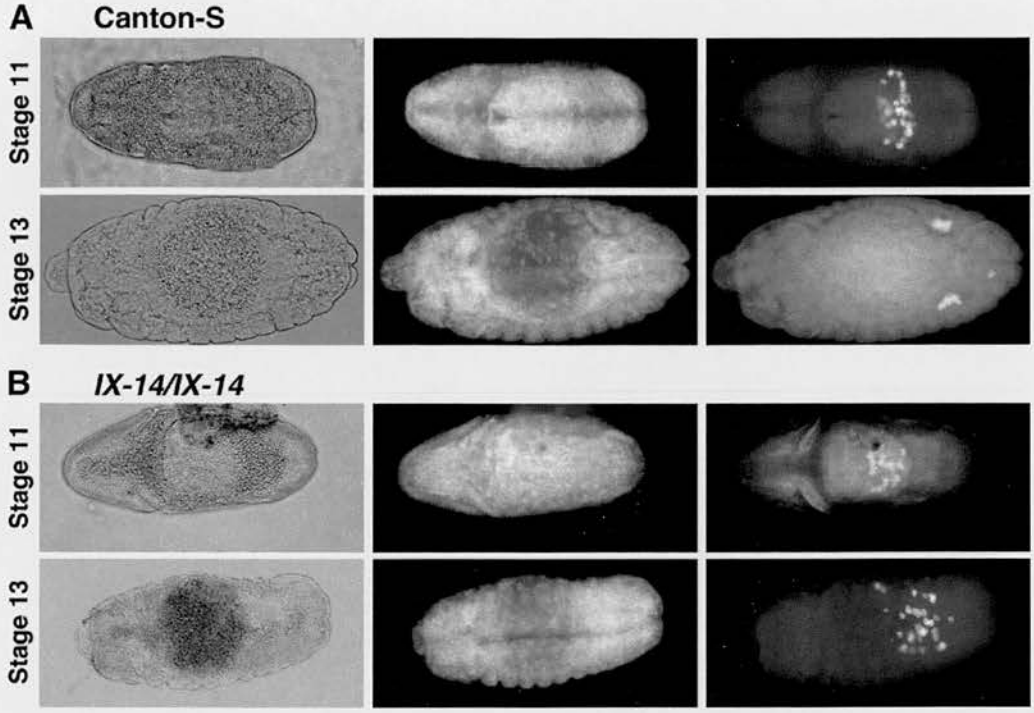

Figure 9. **Germ cell migration defects in *l(3)IX-14* embryos.** All panels are dorsal views of *Drosophila* embryos. Left panels are phase-contrast images, middle panels show DAPI labeling of DNA, right panels show germ cells detected by Vasa antibody. (A) Wild-type Canton S embryos. (top) Stage 10/11, when germ cells are in the middle of passing through the midgut and migrating dorsally. (bottom) Stage 13, when germ cells form two elongated clusters on either side of the embryo. (B) *IX-14* homozygous embryos selected for absence of the Kr-GFP balancer chromosome. (top) Stage 10/11, germ cells appear as in wild-type embryos. (bottom) Stage 13, when the abnormal germ cell migration phenotype is apparent. The germ cells fail to migrate and coalesce into gonads.

metalloprotease in mice (a member of the M48 family of zinc-metalloproteases) has a role in prelamin A cleavage (Pendas et al., 2002). Matrix metalloproteases (MMPs) have been implicated in remodeling of the extracellular matrix (Ishizuya-Oka et al., 2000) and in release of growth factors (Levi et al., 1996). MMPs have been shown to act in some cancers to digest the surrounding extracellular matrix and aid the process of metastasis (Ellerbroek and Stack, 1999; Horikawa et al., 2000; Johansson et al., 2000). Whereas the human genome encodes 24 MMPs, *Drosophila* has only two MMP genes: Dm1-MMP is expressed more specifically during embryonic stages and Dm2-MMP apparently throughout development (Llano et al., 2000, 2002). Few mutations are available to study metalloproteases in a developing organism, although a study on double mutants of the two *Drosophila* MMPs has shown that whereas tissue remodeling is disrupted, embryonic development and larval mitosis are unaffected (Page-McCaw et al., 2003). Thus, no other metalloprotease affects cell proliferation as IX-14/invadolysin does.

Intracellular localization of IX-14 to invadopodia

Although a nuclear pool of invadolysin is detectable in human cells, protein is also localized to the cytoplasm in both fly and human cells, where it is concentrated in unusual ring-like structures. These structures are observed during interphase in all human cultured cells examined, but become dispersed during mitosis, when the protein adopts a more diffuse distribution. We believe the ring-like structures represent invadopodia, cytoplasmic structures that have been proposed to have an important role in cell migration and metastasis. Like invadopodia, the ring-like structures containing invadolysin are localized to the lower third of the cell close to the substratum. They also contain cortactin, paxillin, and dynamin 2, previously shown to be enriched in invadopodia. Intriguingly, dynamin 2, which is also found in invadopodia, has been recently shown to play a role in centrosome cohesion (Thompson et al., 2004), thus tying in with our results linking migration with mitosis.

Strikingly, although invadolysin has a punctate cytoplasmic localization in stationary macrophages, when actively migrating macrophages are visualized, invadolysin becomes strongly concentrated at the leading edge of the cell. How this relocalization occurs will be investigated in living cells, coupled with an analysis of extracellular matrix degradation. Invadolysin appears to be the first specific marker for invadopodia as a discrete cytoplasmic compartment, and, as such, will be a key potential target for drugs designed to limit cell migration.

Analysis of invadolysin mutants identifies a previously unsuspected role for metalloproteases in cell division and development

The *IX-14* mutation in *Drosophila* causes cells to arrest in mitosis with hypercondensed mitotic chromosomes surrounded by poorly condensed chromatin, a phenotype that is clearly dis-

tinct from the chromosome hypercondensation commonly observed in mutations exhibiting mitotic delay (Heck et al., 1993; Theurkauf and Heck, 1999). Invadolysin also appears to have a role in chromosome architecture during interphase because mutations exhibit poorly structured polytene chromosomes and have compromised heterochromatin, as assayed by position effect variegation. The levels of nuclear lamin and otefin proteins are dramatically increased in mutant mitotic cells. One possibility suggested by these results is that invadolysin might regulate interactions between chromatin and the nuclear envelope that are important for gene expression and/or mitotic chromosome condensation. Invadolysin could have a direct role on components such as topoisomerase II or condensin, or the effects we have observed could result from disruption of a novel pathway in which proteolysis plays a role.

In addition, invadolysin has nonchromosomal roles, as both centrosome duplication and/or separation and mitotic spindle formation are aberrant in mutant neuroblasts. Thus, the phenotypes resulting from loss of invadolysin are novel and distinct from other previously described mitotic defects. We have presented evidence that the protein is involved in migration of human macrophages and fly primordial germ cells. Thus the identification and study of this gene has provocatively linked mitosis with cell migration.

A simplistic hypothesis is that different forms of the protein may be important for structural rearrangements during the cell cycle and for cellular migration. Clearly, the generation of reagents recognizing specific forms would be required to address this question. Differential regulation of the expression or localization of these forms could be used during development and/or disease pathogenesis. It is clear from the striking phenotype displayed by *IX-14* mutations that invadolysin illuminates a previously unsuspected pathway essential for cell division and development in metazoa. Future identification of invadolysin substrates will help to clarify the role of this protein and lead to better understanding of the ways in which structural changes during the cell cycle may be coordinated with cell movements.

Materials and methods

Drosophila stocks

The wild-type strain used was Canton S. We received *l(3)IX-14*^{1} from M. Gatti (University of Rome, Rome, Italy); it was originally generated in an ICR-170 screen by A. Shearn (Johns Hopkins University, Baltimore, MD). We generated *l(3)IX-14*^{4Y7} after local hopping a nearly P transposon insertion, *l(3)04017*, obtained from the Bloomington Stock Center.

DAPI staining of *Drosophila* neuroblast squashes and polytene chromosomes

Brains or salivary glands from third instar larvae were processed as described previously (Heck et al., 1993; Loupart et al., 2000) and mounted in Mowiol/glycerol. Fluorescence was observed using a fluorescence microscope (model AX-70 Provis; Olympus) fitted with epifluorescence filters (Chroma Technology Corp.). Digital images were captured (at ~18°C) using a camera (model Orca II; Hamamatsu) with Vysis QUIPS software and processed using Adobe Photoshop 4.0.

Immunofluorescence of third instar larval brains

Analysis of α-tubulin (Sigma-Aldrich), CP190 (provided by W. Whitfield, University of Dundee, Dundee, Scotland), lamin (provided by P. Fisher, State University of New York at Stony Brook, Stony Brook, NY), otefin (provided by Y. Gruenbaum, Hebrew University of Jerusalem, Jerusalem, Israel), cyclin B (provided by J. Raff, University of Cambridge, Cambridge, England), and P~H3 (Upstate Biotechnology) antibodies in third instar larval brains was performed as described previously (Bonaccorsi et al., 2000). BrdU incorporation and subsequent detection by a rat anti-BrdU antibody (Harlan Sera) in larval brains was performed as described previously (Loupart et al., 2000). Imaging was performed as detailed in the previous section.

Immunoblotting

Protein extracts were electrophoresed on Novex SDS-PAGE gels (Invitrogen), and then transferred to nitrocellulose membrane (Schleicher and Schuell). Membranes were rinsed for 5 min with PBS-Tw (PBS + 0.1% Tween 20), and then blocked for 1 h with Safeway dried skimmed milk (5% in PBS-Tw) at RT with shaking. Primary and secondary antibody incubations were performed in PBS-Tw for 1 h at RT with shaking, with washes of 2 × 3 min, 1 × 15 min, and then 2 × 5 min after each incubation. Chemiluminescent detection of HRP-conjugated secondary antibody was performed using ECL reagents from Amersham Biosciences, according to the manufacturer's instructions.

Northern blotting

Northern blots were performed as described in Sambrook et al. (1989). Total RNA was prepared from homogenized third instar larvae using the RNeasy RNA extraction kit (QIAGEN). 10 μg of total RNA per lane was electrophoresed on a 1% agarose gel. RNA was transferred to nylon membrane by capillary action with 20× SSC overnight. RNA was subsequently UV-cross-linked to the membrane using a Strata-linker (Stratagene). Hybridization of ^{32}P-dCTP (AP Biotech)–labeled probes at a specific activity of at least 10^6 counts per milliliter was performed at 65°C overnight as described in Church and Gilbert (1984). The HighPrime kit (Boehringer) was used for all random primer labeling. Autoradiography was done at −80°C using XAR-5 film (Kodak).

dsRNA-mediated interference

dsRNAi was performed on *Drosophila* S2 cells as described previously (Clemens et al., 2000; Vass et al., 2003), using 15 μg/ml of double stranded IX-14 RNA per 2 ml of cells at 10^6 cells/ml.

Immunofluorescence of *Drosophila* S2 and HeLa cultured cells

S2 cells were grown on either Permanox Chamber Slides (Lab-Tek) for the RNAi experiments or on poly-L-lysine coverslips in 6-well plates for the EGFP-fusion detection using a rabbit anti-GFP antibody (Molecular Probes). HeLa cells were grown on coverslips in 6-well plates for transfection with EGFP fusion constructs. For immunofluorescence, cells were fixed with 4% PFA in PBS for 3 min, permeabilized in PBS + 0.5% Triton X-100 for 1 min, and washed 2 × 10 min incubations in PBTx. The cells were blocked for 1 h in 3% BSA in PBS at RT. Primary antibody incubation was overnight at 4°C in 0.3% BSA in PBS. Cells were washed 3 × 5 min in PBTx, followed by secondary antibody incubation for 1 h at 37°C (secondary antibodies incubated separately). Final washes were 3 × 5 min in PBTx, with the penultimate wash containing 0.1 μg/ml DAPI, and the coverslips were mounted in Mowiol-glycerol. Imaging was performed as detailed in the section DAPI staining of *Drosophila* neuroblast squashes and polytene chromosomes.

Detection of protease activity by zymography

Zymogram gels (Novex) containing casein as a substrate were used for all zymography. Wandering third instar larvae were dissected in 1× EBR. Brains were transferred to 50 μl of chilled EBR, and then homogenized for ~30–60 s with a hand-held homogenizer. 50 μl of 2× Tris-glycine gel sample buffer (Novex) plus 1 mM DTT was added, and the samples were incubated for 10 min at RT. Samples (without boiling) were loaded onto 12% Tris-Glycine Zymogram gels and electrophoresed at 125 V constant, generally for 3–4 h, at least until the dye front had run off the gel. After electrophoresis, gels were rinsed in renaturing buffer (2.5% Triton X-100) for 30 min, equilibrated in Developing buffer (Novex) for 30 min, and incubated overnight at 37°C in Developing buffer. Gels were stained with Colloidal Coomassie blue (Sigma-Aldrich) to visualize the casein in the gel.

in vitro proteolysis of lamin by invadolysin

375 ng of Lamin in T7-7 vector, IX-14 in pOT2 vector, or GFP control vector was added to one 24-μl aliquot of the RTS 500 *Escherichia coli* Circular Template kit (Roche). Each expression aliquot was incubated in a water bath at 30°C for 1 h. 10 μl of IX-14 was mixed with 1 or 4 μl of lamin or GFP before being incubated in a water bath at either 29 or 37°C for

15 min, 50 min, or 1 h. In some cases, the incubation was with $ZnCl_2$ or $ZnSO_4$ or the zinc chelator 1,10-phenanthroline. After the reaction, samples were boiled at 100°C for 5 min in SDS-PAGE sample buffer. Lamin was detected after blotting to nitrocellulose using an mAb generated to the *Drosophila* NH_2-terminal head region (amino acids 22–28).

Macrophage isolation and culture

Macrophages were isolated from normal human blood following the procedure of Giles et al. (2001). After isolation, the mononuclear cells were plated at 4×10^6/ml in Iscoves' modified Dulbecco's medium (with L-glut and 25 mM Hepes) onto glass coverslips in 12-well tissue culture plastic plates for 1 h. Adherence to the glass coverslips was used to enrich for the monocytes out of the lymphocytes/monocytes mix (lymphocytes do not attach). After settling, the plates were washed in Hank's Balanced Salt Solution (without divalent cations) to remove nonadherent lymphocytes, and then 2 ml of Iscoves' modified Dulbecco's medium + 10% autologous serum was added and the cells were cultured at 37°C, 5% CO_2, for 5 d. After 5 d, the cells were washed again to remove any nonadherent cells and fixed in 3% PFA at RT for 20 min. After washes in PBS, 50 mM NH_4Cl was added to the wells for 15 min. Coverslips were permeabilized in 0.1% Triton X-100 for 4 min. After washes, the cells were blocked in 10% heat-inactivated human serum and processed for immunofluorescence as usual.

Detection of germ cells

For the examination of appropriately staged embryos, Canton S wild-type and 4Y7/TM3 (Kr:GFP) flies were allowed to lay embryos on yeasted red wine concentrate agar plates either overnight or for 3-h collections, which were then aged until the desired stage. Embryos were washed and dechorionated in 50% bleach in ddH_2O for 4 min and rinsed. Homozygous 4Y7/4Y7 embryos were hand selected (fluorescence microscopy) by virtue of lacking the Kr-GFP expression pattern (visible after stage 9; Casso et al., 2000). The selected embryos were fixed in PFA, permeabilized by heptane, devitellinized by methanol, and rehydrated as described previously (Theurkauf and Heck, 1999). After a block in 1% BSA in PBS for 1 h, rabbit Vasa antibody (provided by P. Lasko, McGill University, Montreal, Canada) was used as 1:500 in PBS + 0.3% Triton X-100 overnight at 4°C. Alexa-594–conjugated secondary antibody was used as 1:500 in PBSTx for 2 h at RT. 4×15 min PBSTx washes were performed before and after antibody incubations. DAPI at 0.1 μg/ml DAPI was included in the penultimate wash. Embryos were mounted with Vectashield and imaged as detailed in the section DAPI staining of *Drosophila* neuroblast squashes and polytene chromosomes.

Online supplemental material

Further details on TUNEL labeling of larval brains, dsRNA-mediated interference in S2 cells, and cultured cell transfections (*Drosophila* and HeLa) are provided online. Online supplemental material is available at http://www.jcb.org/cgi/content/full/jcb.200405155/DC1.

We would like to thank Allen Shearn and Maurizio Gatti for enthusiastically encouraging our progress in this project. Marie-Louise Loupart, Alison Wilkie, Liping Lu, Lynne Cursiter, Sophie Lecomte, and Tina Volaki are all to be acknowledged for technical and intellectual contributions during honors and other projects. We are grateful to the following individuals for generous gifts of antibody: Paul Fisher, Yoshef Gruenbaum, Paul Lasko, Mark McNiven (Dynamin, Mayo Clinic, Rochester, NY), Jordan Raff, and Will Whitfield. Victor Simossis was instrumental in generating the T-COFFEE alignment. M. Heck thanks Susette Mueller (Georgetown University, Washington, DC) for suggesting the examination of macrophages and Ian Dransfield (University of Edinburgh, Edinburgh, UK) for the culturing of macrophages.

Brian McHugh was supported by a Prize Studentship and a Prize Fellowship from the Wellcome Trust. Research in the Heck laboratory is supported by a Senior Research Fellowship in the Biomedical Sciences from the Wellcome Trust.

Submitted: 26 May 2004
Accepted: 4 October 2004

References

Baldassarre, M., A. Pompeo, G. Beznoussenko, C. Castaldi, S. Cortellino, M.A. McNiven, A. Luini, and R. Buccione. 2003. Dynamin participates in focal extracellular matrix degradation by invasive cells. *Mol. Biol. Cell.* 14:1074–1084.

Bhat, M.A., A.V. Philp, D.M. Glover, and H.J. Bellen. 1996. Chromatid segregation at anaphase requires the barren product, a novel chromosome-associated protein that interacts with topoisomerase II. *Cell.* 87:1103–1114.

Bonaccorsi, S., M.G. Giansanti, and M. Gatti. 2000. Spindle assembly in *Drosophila* neuroblasts and ganglion mother cells. *Nat. Cell Biol.* 2:54–56.

Bowden, E.T., M. Barth, D. Thomas, R.I. Glazer, and S.C. Mueller. 1999. An invasion-related complex of cortactin, paxillin and PKCmu associates with invadopodia at sites of extracellular matrix degradation. *Oncogene.* 18:4440–4449.

Bowden, E.T., P.J. Coopman, and S.C. Mueller. 2001. Invadopodia: unique methods for measurement of extracellular matrix degradation in vitro. *Methods Cell Biol.* 63:613–627.

Buccione, R., J.D. Orth, and M.A. McNiven. 2004. Foot and mouth: podosomes, invadopodia, and circular dorsal ruffles. *Nat. Rev. Mol. Cell Biol.* 5:647–657.

Casso, D., F. Ramirez-Weber, and T.B. Kornberg. 2000. GFP-tagged balancer chromosomes for *Drosophila melanogaster*. *Mech. Dev.* 91:451–454.

Church, G.M., and W. Gilbert. 1984. Genomic sequencing. *Proc. Natl. Acad. Sci. USA.* 81:1991 1995.

Clemens, J.C., C.A. Worby, N. Simonson-Leff, M. Muda, T. Maehama, B.A. Hemmings, and J.E. Dixon. 2000. Use of double-stranded RNA interference in *Drosophila* cell lines to dissect signal transduction pathways. *Proc. Natl. Acad. Sci. USA.* 97:6499–6503.

Coelho, P.A., J. Queiroz-Machado, and C.E. Sunkel. 2003. Condensin-dependent localisation of topoisomerase II to an axial chromosomal structure is required for sister chromatid resolution during mitosis. *J. Cell Sci.* 116:4763–4776.

Connell, N.D., E. Medina-Acosta, W.R. McMaster, B.R. Bloom, and D.G. Russell. 1993. Effective immunization against cutaneous leishmaniasis with recombinant bacille Calmette-Guerin expressing the *Leishmania* surface proteinase gp63. *Proc. Natl. Acad. Sci. USA.* 90:11473–11477.

Edgar, B.A., and C.F. Lehner. 1996. Developmental control of cell cycle regulators: a fly's perspective. *Science.* 274:1646–1652.

Ellerbroek, S.M., and M.S. Stack. 1999. Membrane associated matrix metalloproteinases in metastasis. *Bioessays.* 21:940–949.

Fogarty, P., S.D. Campbell, R. Abu-Shumays, B.S. Phalle, K.R. Yu, G.L. Uy, M.L. Goldberg, and W. Sullivan. 1997. The *Drosophila* grapes gene is related to checkpoint gene chk1/rad27 and is required for late syncytial division fidelity. *Curr. Biol.* 7:418–426.

Gant, T.M., and K.L. Wilson. 1997. Nuclear assembly. *Annu. Rev. Cell Dev. Biol.* 13:669–695.

Gatti, M., and B.S. Baker. 1989. Genes controlling essential cell-cycle functions in *Drosophila melanogaster*. *Genes Dev.* 3:438–453.

Giles, K.M., K. Ross, A.G. Rossi, N.A. Hotchin, C. Haslett, and I. Dransfield. 2001. Glucocorticoid augmentation of macrophage capacity for phagocytosis of apoptotic cells is associated with reduced p130Cas expression, loss of paxillin/pyk2 phosphorylation, and high levels of active Rac. *J. Immunol.* 167:976–986.

Glover, D.M., M.H. Leibowitz, D.A. McLean, and H. Parry. 1995. Mutations in aurora prevent centrosome separation leading to the formation of monopolar spindles. *Cell.* 81:95–105.

Heck, M.M.S., A. Pereira, P. Pesavento, Y. Yannoni, A.C. Spradling, and L.S.B. Goldstein. 1993. The kinesin-like protein KLP61F is essential for mitosis in *Drosophila*. *J. Cell Biol.* 123:665–679.

Horikawa, T., T. Yoshizaki, T.S. Sheen, S.Y. Lee, and M. Furukawa. 2000. Association of latent membrane protein 1 and matrix metalloproteinase 9 with metastasis in nasopharyngeal carcinoma. *Cancer.* 89:715–723.

Hudson, D.F., P. Vagnarelli, R. Gassmann, and W.C. Earnshaw. 2003. Condensin is required for nonhistone protein assembly and structural integrity of vertebrate mitotic chromosomes. *Dev. Cell.* 5:323–336.

Ishizuya-Oka, A., Q. Li, T. Amano, S. Damjanovski, S. Ueda, and Y.B. Shi. 2000. Requirement for matrix metalloproteinase stromelysin-3 in cell migration and apoptosis during tissue remodeling in *Xenopus laevis*. *J. Cell Biol.* 150:1177–1188.

Jager, H., A. Herzig, C.F. Lehner, and S. Heidmann. 2001. *Drosophila* separase is required for sister chromatid separation and binds to PIM and THR. *Genes Dev.* 15:2572–2584.

Johansson, N., M. Ahonen, and V.M. Kahari. 2000. Matrix metalloproteinases in tumor invasion. *Cell. Mol. Life Sci.* 57:5–15.

Krause, S.A., M.-L. Loupart, S. Vass, S. Schoenfelder, S. Harrison, and M.M.S. Heck. 2001. Loss of cell cycle checkpoint control in *Drosophila* Rfc4 mutants. *Mol. Cell. Biol.* 21:5156–5168.

Levi, E., R. Fridman, H. Miao, Y. Ma, A. Yayon, and I. Vlodavsky. 1996. Matrix metalloproteinase 2 releases active soluble ectodomain of fibroblast growth factor receptor 1. *Proc. Natl. Acad. Sci. USA.* 93:7069–7074.

Llamazares, S., A. Moreira, A. Tavares, C. Girdham, B.A. Spruce, C. Gonzalez, R.E. Karess, D.M. Glover, and C.E. Sunkel. 1991. Polo encodes a pro-

tein kinase homolog required for mitosis in *Drosophila*. *Genes Dev.* 5:2153–2165.

Llano, E., A.M. Pendas, P. Aza-Blanc, T.B. Kornberg, and C. Lopez-Otin. 2000. Dm1-MMP, a matrix metalloproteinase from *Drosophila* with a potential role in extracellular matrix remodeling during neural development. *J. Biol. Chem.* 275:35978–35985.

Llano, E., G. Adam, A.M. Pendas, V. Quesada, L.M. Sanchez, I. Santamaria, S. Noselli, and C. Lopez-Otin. 2002. Structural and enzymatic characterization of *Drosophila* Dm2-MMP, a membrane-bound matrix metalloproteinase with tissue-specific expression. *J. Biol. Chem.* 277:23321–23329.

Loupart, M.-L., S.A. Krause, and M.M.S. Heck. 2000. Aberrant replication timing induces defective chromosome condensation in *Drosophila* ORC2 mutants. *Curr. Biol.* 10:1547–1556.

Macdonald, M.H., C.J. Morrison, and W.R. McMaster. 1995. Analysis of the active site and activation mechanism of the *Leishmania* surface metalloproteinase GP63. *Biochim. Biophys. Acta.* 1253:199–207.

McGwire, B.S., and K.P. Chang. 1996. Posttranslational regulation of a *Leishmania* HEXXH metalloprotease (gp63). The effects of site-specific mutagenesis of catalytic, zinc binding, N-glycosylation, and glycosyl phosphatidylinositol addition sites on N-terminal end cleavage, intracellular stability, and extracellular exit. *J. Biol. Chem.* 271:7903–7909.

McGwire, B.S., K.P. Chang, and D.M. Engman. 2003. Migration through the extracellular matrix by the parasitic protozoan *Leishmania* is enhanced by surface metalloprotease gp63. *Infect. Immun.* 71:1008–1010.

McMaster, W.R., C.J. Morrison, M.H. MacDonald, and P.B. Joshi. 1994. Mutational and functional analysis of the *Leishmania* surface metalloproteinase GP63: similarities to matrix metalloproteinases. *Parasitology.* 108: S29–S36.

Murray, A.W. 2004. Recycling the cell cycle: cyclins revisited. *Cell.* 116:221–234.

O'Farrell, P.H., B.A. Edgar, D. Lakich, and C.F. Lehner. 1989. Directing cell division during development. *Science.* 246:635–640.

Page-McCaw, A., J. Serano, J.M. Sante, and G.M. Rubin. 2003. *Drosophila* matrix metalloproteinases are required for tissue remodeling, but not embryonic development. *Dev. Cell.* 4:95–106.

Pendas, A.M., Z. Zhou, J. Cadinanos, J.M. Freije, J. Wang, K. Hultenby, A. Astudillo, A. Wernerson, F. Rodriguez, K. Tryggvason, and C. Lopez-Otin. 2002. Defective prelamin A processing and muscular and adipocyte alterations in Zmpste24 metalloproteinase-deficient mice. *Nat. Genet.* 31:94–99.

Pflumm, M.F., and M.R. Botchan. 2001. Orc mutants arrest in metaphase with abnormally condensed chromosomes. *Development.* 128:1697–1707.

Russell, D.G., and H. Wilhelm. 1986. The involvement of the major surface glycoprotein (gp63) of *Leishmania* promastigotes in attachment to macrophages. *J. Immunol.* 136:2613–2620.

Sambrook, J., E.F. Fritsch, and T. Maniatis. 1989. Molecular Cloning: A Laboratory Manual. Cold Spring Harbor Laboratory Press, Cold Spring Harbor, NY. 7.39–7.52.

Santos, A.C., and R. Lehmann. 2004. Germ cell specification and migration in *Drosophila* and beyond. *Curr. Biol.* 14:R578–R589.

Schlagenhauf, E., R. Etges, and P. Metcalf. 1998. The crystal structure of the *Leishmania major* surface proteinase leishmanolysin (gp63). *Structure.* 6:1035–1046.

Shearn, A., T. Rice, A. Garen, and W. Gehring. 1971. Imaginal disc abnormalities in lethal mutants of *Drosophila*. *Proc. Natl. Acad. Sci. USA.* 68: 2594–2598.

Sibon, O.C.M., V.A. Stevenson, and W.E. Theurkauf. 1997. DNA-replication checkpoint control at the *Drosophila* midblastula transition. *Nature.* 388: 93–97.

Steffensen, S., P.A. Coelho, N. Cobbe, S. Vass, M. Costa, B. Hassan, S.N. Prokopenko, H. Bellen, M.M.S. Heck, and C.E. Sunkel. 2001. A role for *Drosophila* SMC4 in the resolution of sister chromatids in mitosis. *Curr. Biol.* 11:295–307.

Sunkel, C., and D.M. Glover. 1988. polo, a mitotic mutant of *Drosophila* displaying abnormal spindle poles. *J. Cell Sci.* 89:25–38.

Theurkauf, W.E., and M.M.S. Heck. 1999. Identification and characterization of mitotic mutations in *Drosophila*. *In* Methods in Cell Biology. Vol. 61. C.L. Rieder, editor. Academic Press, Inc., San Diego, CA. 317–346.

Thompson, H.M., H. Cao, J. Chen, U. Euteneuer, and M.A. McNiven. 2004. Dynamin 2 binds gamma-tubulin and participates in centrosome cohesion. *Nat. Cell Biol.* 6:335–342.

Vass, S., S. Cotterill, A.M. Valdeolmillos, J.L. Barbero, E. Lin, W.D. Warren, and M.M. Heck. 2003. Depletion of rad21/Scc1 in *Drosophila* cells leads to instability of the cohesin complex and disruption of mitotic progression. *Curr. Biol.* 13:208–218.

Whitfield, W.G.F., M.A. Chaplain, K. Oegema, H. Parry, and D.M. Glover. 1995. The 190 kDa centrosome-associated protein of *Drosophila melanogaster* contains four zinc finger motifs and binds to specific sites on polytene chromosomes. *J. Cell Sci.* 108:3377–3387.

Xu, D., and F.Y. Liew. 1995. Protection against leishmaniasis by injection of DNA encoding a major surface glycoprotein, gp63, of *L. major*. *Immunology.* 84:173–176.

Yang, D.M., N. Fairweather, L.L. Button, W.R. McMaster, L.P. Kahl, and F.Y. Liew. 1990. Oral *Salmonella typhimurium* (AroA-) vaccine expressing a major leishmanial surface protein (gp63) preferentially induces T helper 1 cells and protective immunity against leishmaniasis. *J. Immunol.* 145: 2281–2285.

Yao, C., J.E. Donelson, and M.E. Wilson. 2003. The major surface protease (MSP or GP63) of *Leishmania* sp. Biosynthesis, regulation of expression, and function. *Mol. Biochem. Parasitol.* 132:1–16.